THE IMPACT AND ROLE OF SYNTHETIC CHEMISTRY IN ORGANIC CONJUGATED MATERIALS SCIENCE

A Dissertation
Presented to
The Academic Faculty

by

Rylan Michael Webster Wolfe

In Partial Fulfillment
of the Requirements for the Degree
Doctor of Philosophy in the
School of Chemistry & Biochemistry

Georgia Institute of Technology
August 2018

THE IMPACT AND ROLE OF SYNTHETIC CHEMISTRY IN ORGANIC CONJUGATED MATERIALS SCIENCE

Approved by:

Dr. John R. Reynolds, Advisor
School of Chemistry & Biochemistry
Georgia Institute of Technology

Dr. Stefan A. France
School of Chemistry & Biochemistry
Georgia Institute of Technology

Dr. Shannon K. Yee
School of Mechanical Engineering
Georgia Institute of Technology

Dr. Carlos A. Silva
School of Chemistry & Biochemistry
Georgia Institute of Technology

Dr. Seth R. Marder
School of Chemistry & Biochemistry
Georgia Institute of Technology

Date Approved: July 18, 2018

To my Family, Friends, Cat, and Coralie

"Take your time. Have a seat on a rock or a log bench. The trail has no particular destination, so walk as far as you like and then return."

-Great Smoky Mountains National Park Sign

ACKNOWLEDGEMENTS

There are countless people to thank for my successes in life, for I certainly would not have arrived here on my own. There is neither enough time nor enough pages to adequately express my gratitude. This abridgement will serve as a substitute.

A special thank you to my parents for fostering my curiosity and always being supportive. A very special thank you to Dr. Coralie Richard for everything.

I would like to thank Dr. Reynolds for accepting me into his group, for granting me considerable freedom in my choice of projects, and for his continued patience. I would like to thank Dr. Yee for taking the risk of accepting a synthetic chemist into his group and trusting my project direction. I would also like to thank Dr. Marder for serving as a scientific co-advisor on many projects.

I would like to thank the members of the Reynolds group, past and present, for being a home away from home. Specifically, in no particular order, I would like to thank: Dr. Toan Pho, for endless discussions about chemistry and coffee; Dr. Natasha Teran, for upholding the ideals of rigorous chemistry and correcting my English; Dr. Kin Lo, for staying in the group while I finished my PhD and the occasional beer; Dr. Caroline Grand, for laughing at all of my jokes; Dr. Hayden Black, for his enthusiasm about chemistry; Dr. Justin Kerszulis; for always filling the silence; Linda Nhon, for being an excellent mentee and putting up with my long-winded responses that avoided directly answering any of her questions; and Thomas Marchandier, for teaching me the newest French slang. Likewise, I would like to thank the members of the Yee group for welcoming a newcomer to the

group, and especially Dr. Akanksha Menon for trudging through the insoluble, intractable world of NiETT with me.

I must also thank my undergraduate advisor Seth Rasmussen, and the Rasmussen group members Ryan Schwiderski and Sean Evenson, for teaching me synthetic chemistry. And a thank you to my high school chemistry teacher, Scott Weigum, for encouraging my interest in chemistry.

I would like to thank Aaron McKee and Aida Demissie, for years of laughs, cheaper rent, and dog ownership; Matt Cooper, for the best free beer and barbeque in Atlanta; Dr. Stephen Shiring, for Seinfeldian conversations and miniature train rides; Camille Barchers, for helping me find the best Blanco; Anthony Coulter, for the Elizabethan theatre experience and humor to match; and DFB, for hours of entertainment and stress relief.

And finally, all the people at Grand Challenges and LEAD – Dr. Wes Wynens, Dr. Jeff Davis, Stacey Doremus, Alison Southern, and Stephen Steppe – for running an excellent program, feeding the coffee habits of graduate students, making Tuesday and Thursday mornings enjoyable, and bringing wonderful people into my life – Muaz Rushdi, Hommood Alrowais, Hailey Bureau, Brandon Sharp, Ross Beppler, T.J. LaGrow, and many others.

TABLE OF CONTENTS

LIST OF TABLES

LIST OF FIGURES

LIST OF SYMBOLS AND ABBREVIATIONS

A	Ampere
Å	Angstrom
ACN	Acetonitrile
ACS	American Chemical Society
AF	Annealed Film
AP	Annealed Powder
BHT	Butylated Hydroxytoluene
BTI	Bithiophene Imide
CAS	Chemical Abstract Services
CV	Cyclic Voltammetry
°C	Degree Celsius
Da	Dalton
DC	Direct Current
DCM	Dichloromethane
DMF	Dimethylformamide
dmit	1,3-Dithiole-2-thione-4,5-dithiolate
DMSO	Dimethyl Sulfoxide
DPV	Differential Pulse Voltammetry

DSC	Differential Scanning Calorimetry
DTG (Chapter 4)	Dithienogermole
DTG (Chapter 7)	Differential Thermal Gravimetry
Equiv.	Equivalent
ε_r	Relative Dielectric Constant
Et_2O	Diethyl Ether
EtOAc	Ethyl Acetate
ETT	EtheneTetraThiolate
eV	Electron Volt
Fc/Fc^+	Ferrocene-Ferrocenium
HMPA	Hexamethylphosphoramide
HPLC	High Pressure Liquid Chromatography
ICP-MS	Inductively Coupled Plasma – Mass Spectrometry
ICP-OES	Inductively Coupled Plasma – Optical Emission Spectroscopy
m/m	Mass by Mass
MALDI	Matrix Assisted Laser Desorption Ionization
MeOH	Methanol
NBS	*N*-Bromosuccinimide
NiETT	Nickel Ethenetetrathiolate
NiTTO	Nickel Tetrathiooxalate

OAc	Acetate
OPV	Organic Photovoltaic
OTE	Organic Thermoelectric
OTTLE	Optically Transparent Thin Layer Electrode
PF	Pristine Film
PP	Pristine Powder
PTFE	Poly(Tetrafluoroethylene)
PVDF	Poly(vinylidene difluoride)
Rf	Retention Factor
RP	Reverse Phase
S	Siemens
S	Seebeck Coefficient
SEC	Size Exclusion Chromatography
σ	Conductivity
SS	Solid State
TEA	Tetraethyl Ammonium
TEC	Thermoelectric Cooler
TEG	Thermoelectric Generator
TGA-MS	Thermogravimetric Analysis – Mass Spectroscopy
THF	Tetrahydrofuran

TPD	Thienopyrroledione
TTO	TetraThioOxalate
USP	United States Pharmacopeia
UV-Vis-NIR	Ultra-violet – Visible – Near Infra-red
v/v	Volume by Volume

SUMMARY

This dissertation covers broad aspects of synthetic chemistry in organic electronics, from novel molecules to known monomers, from photovoltaics to thermoelectrics, from oxidized “3D” molecules to oxidation control in nickel coordination polymers. It begins with a brief introduction to organic electronics and thermoelectrics and a chapter-by-chapter overview of the impact of rigorous synthetic chemistry. A detailed explanation of proper Stille cross-coupling protocols, polymer purification, and nontraditional experimental methods used in this dissertation follows in Chapter 2. Chapter 3 describes a new synthetic pathway to thienopyrroledione monomers, a common component in donor-acceptor photovoltaic polymers. Principles of green chemistry and waste reduction highlight the need to optimize reactions conditions while increasing the utility of the available materials. Chapter 4 presents a new class of materials, dithienospirogermoles or germanium cruciforms, and their optoelectronic properties with a focus on oxidation level and triplet generation. Chapter 5 begins with an overview of nickel-sulfur square-planar complexes and the development of oligomeric coordination compounds of nickel for use as stable n-type organic thermoelectrics. The synthesis of poly(nickel ethenetetrathiolate) (NiETT) through careful selection of reaction conditions leads to reproducible properties in insoluble oligomers. In Chapter 6, a NiETT material is investigated through mass spectroscopy coupled thermogravimetric analysis to elucidate structural changes upon annealing. Chapter 7 concludes the thesis with the synthetic optimization and testing of a structural analog of NiETT, poly(nickel tetrathiooxalate).

CHAPTER 1. INTRODUCTION

The goal of this introduction is to give a brief overview of the history and more recent developments of organic electronics and their possibilities. The history and significance of each undertaking is described in its own chapter. As this thesis presents and concludes many things based on thermoelectric performance, a brief description of the basics of thermoelectrics is given. Finally, each chapter is introduced from a standpoint of a synthetic chemist's role and contribution to the development of each aspect of the field.

1.1 Organic Electronics – History, Highlights, and Outlook

The field of organic electronics is often traced back to the unintended Ziegler-Natta polymerization of acetylene into a film. The high conductivity of the doped polyacetylene film led to the 2000 Nobel Prize in Chemistry for Heeger, MacDiarmid, and Shirakawa.[1] The field of π-conjugated materials has roots even farther back in the synthesis of polypyrrole[2] and polyaniline.[3,4] A account of the early developments of the field is given in previous Reynolds Group dissertations by Frank Arroyave,[5] Caroline Grand,[6] and Natasha Teran.[7]

The most economically successful and well-known product of the organic electronics field is the organic light emitting diode (OLED). OLEDs in smartphones and other displays represented a $16 billion USD market in 2016, with an expected market of $42 billion USD in 2020.[8] However, the scope of research in organic electronics is much broader than just OLEDs in active displays. Other subfields include organic photovoltaics (OPV),[9–13] organic thermoelectrics (OTE)[14–19], electrochromics,[20] organic thin film transistors (OTFT)

and sensors,[21–25] nonlinear optics (NLO),[7] and interfaces with biological materials.[26,27] The materials developed in this thesis are directed towards OPV and OTE applications.

The typical benefits attributed to organic electronics are their low-cost and abundant materials (carbon, nitrogen, oxygen, sulfur), their low-temperature, large-area processing techniques amenable to flexible substrates, and their biological compatibility.[28–31] This thesis explores one benefit of organic electronics – the ability to modify materials at the molecular level to influence material properties at the macroscopic scale through electronics, solubility, morphology, etc.

1.2 General Introduction to Concepts of Organic Thermoelectrics

Materials presented in Chapters 5, 6, and 7 are evaluated based on their thermoelectric performance. This section provides a brief introduction to the principles behind thermoelectric behavior and the metrics of performance of thermoelectrics. Thermoelectrics can be divided into two categories, thermoelectric generators (TEGs) and thermoelectric coolers (TECs). Their underlying operation principles are similar – TEGs generate electricity from a heat source, TECs act as a heat pump consuming electricity. The two modes of operation are depicted in Figure 1.1.

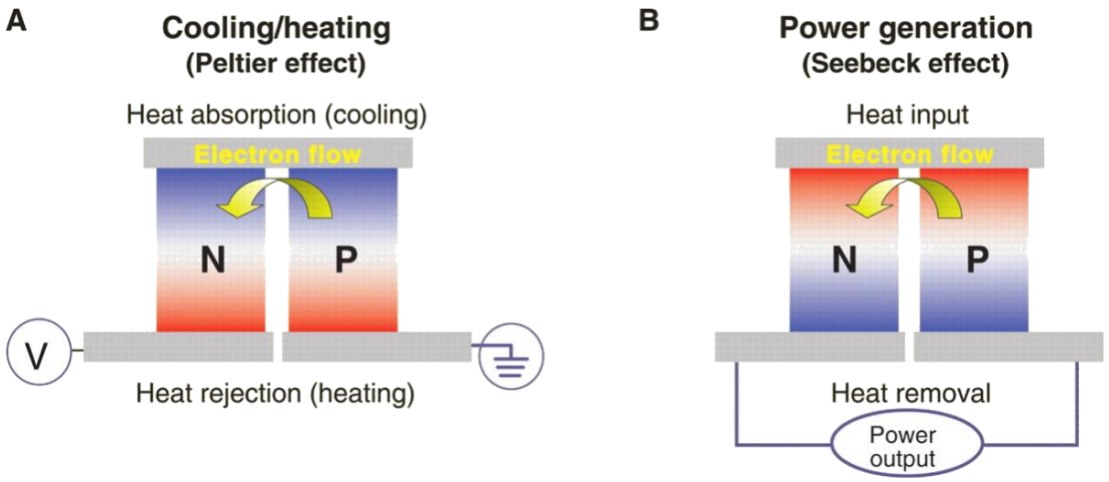

Figure 1.1 – TE heat engines A) When current is run across a TE junction, it heats or cools through the Peltier effect, depending on the direction of the current flow B) When heat flows across the junction, electrical current is generated through the Seebeck effect From Bell, L. E. *Science* 2008, *321* (5895), 1457–1461[32] Reprinted with permission from AAAS

Compared to steam-based power generation and vapor-compression cooling, thermoelectrics have no moving parts and require low maintenance. However, due to their material and construction costs and their low efficiency, thermoelectrics operate in niche, usually luxury, market segments. Current implementations include deep space missions, wine refrigerators, and climate controlled automobile seats.[32]

TEGs operate via the Seebeck effect – a temperature difference across a material produces a potential difference. Alternatively, TECs operate via the Peltier effect – current flow through a junction between two materials produces a heating or cooling effect. The figure of merit for thermoelectric materials, zT, is defined by $zT = S^2\sigma T/k$, where S is the Seebeck coefficient (μV/K), σ is the electrical conductivity (S/cm), k is the thermal conductivity (W/m-K), and T is the absolute temperature (K). When thermal conductivity is not measured, the power factor, $S^2\sigma$ (μW/m-K^2), is reported instead. Optimization of thermoelectric performance involves increasing electrical conductivity (to reduce Joule

heating and parasitic losses), increasing thermopower or Seebeck coefficient (to increase the potential generated from a temperature differential), and decreasing thermal conductivity (to minimize parasitic heat flow and maintain the temperature difference between the hot and cold reservoirs).

Electrical conductivity originates from the distribution and mobility of electrons in the material. The Seebeck coefficient originates from an asymmetry in the distribution and mobility of hot and cold electrons. The thermal conductivity results from the distribution and mobility of electrons and phonons in the material. Due to the underlying relationship between electrical conductivity, Seebeck coefficient, and thermal conductivity, optimizing one factor will have a negative effect on the other two. For example, an increase in electrical conductivity will be accompanied by a decrease in the Seebeck coefficient and an increase in the thermal conductivity.

The materials studied in Chapters 5, 6, and 7 have undefined structures, and any simultaneous improvements to electrical conductivity and Seebeck coefficient should not be viewed as a violation to these concepts. The targeted properties of the studied NiETT and NiTTO materials were electrical conductivities greater than 10 S/cm and Seebeck coefficients greater than 100 μV/K to yield materials with power factors above 10 μW/m-K^2. Future iterations and developments must target power factors above 100 μW/m-K^2.

1.3 Impact of Synthetic Chemistry

As with many disciplines, cross-field collaboration is incredibly important and allows for new viewpoints, disruptions, and gains. This is particularly true for organic electronics which spans from chemical physics/theory, synthetic chemistry, device

engineering, device physics. No one role can be deemed "more important," however, this thesis introduction will focus on the synthetic chemists' impact and role.

Chapter 2 is traditional reserved for experimental methods and synthetic protocols. Here, it covers two techniques that are not common to many synthetic chemists – electrochemical synthesis and analysis by bulk electrolysis. It provides a practical guide to the setup and running of either experiment. A large section of Chapter 2 is dedicated to the Stille cross-coupling reaction for conjugated polymers. This was written in response to a perceived lack of thoroughness in reporting the synthesis, purification, and purity of conjugated polymers. As synthesis is often a means to an end, proper protocols are easily forgotten and ignored. The creation of high-quality, reliable materials and protocols is a strength of a synthetic chemist.

Chapter 3 continues the theme of synthetic chemistry in some application-focused field. The final goal of many syntheses is to have the material for characterization and device testing. The first synthesis is rarely optimized for efficiency of steps, overall yield, or environmental friendliness. Subsequent syntheses follow the path of least resistance or the path of highest chance of success. That is, they repeat the published literature procedure. Chapter 3 reexamines the synthesis of thienopyrroledione by adapting historical techniques and decreasing the environmental impact of synthesis. Expanding the material for the current challenges ahead by expanding the selection of sidechains. The result is one fewer synthetic steps, maintenance of yield, and the use of fewer harsh or toxic materials. A range of "new" materials became available to the research group that were subsequently used in other studies.

Chapter 4 combines the field's interest in fullerene replacements with our group's experience in dithienogermole chemistry. The result is a 3-dimensional system consisting of two conjugated halves with orthogonal π-systems. They are joined around a spirobicyclic germole center. The goal of this project was to study the electronics of an orthogonal pi-system in comparison to its planar analog. Initial characterizations indicate that spirobicyclic germoles have low fluorescent quantum yields, fast singlet-triplet intersystem crossing, and non-independent pi-systems. This class of molecules previously unexplored is worthy of more focused studies.

Chapter 5 switches from the traditional purely organic conjugated systems to square-planar nickel complexes and oligomers with organic ligands in the study of n-type materials for organic thermoelectrics. The benefit of nickel complexes is their intrinsic conductivity, that is, they are charge conductors at a doping level that is stable to ambient exposure. This is compared to doped n-type conjugated polymers and their related dopants, which are not air-stable. However, the nickel oligomers are insoluble, intractable powders that are inherently difficult to characterize. Reported synthetic protocols vary as much as the reported thermoelectric properties. Despite the differences, materials were being compared equally across reports. Chapter 5 details the synthetic care taken to create a reproducible synthesis of NiETT in terms of thermoelectric properties and material constitution. Once a baseline was established, one variable – counter ion, nickel equivalents, or oxidation level – was modified across a family of polymers. This allowed us to look for subtle variations in behavior, composition, and properties to further investigate 1) what these materials are 2) their formation mechanism and 3) what aspects

make them work better. These standardized conditions are now openly reported in the literature and awaiting reproduction.

Chapter 6 continues the work on NiETT away from synthesis and towards device processing. Annealing films was known to increase performance. From thermogravimetric analysis and our noses, we knew that some compound was off-gassing from the film. Mass spectroscopy coupled to thermogravimetric analysis allowed us to investigate exactly what was being evolved at each temperature stage. Knowing the off-gas and the end composition of the material allowed us to construct a more thorough picture of the pre-annealed material structure. From this structure, we hypothesize synthetic methods to avert these detriments or additional ways to increase performance.

Chapter 7 explores an isomer of NiETT known as NiTTO. Again, the insolubility has plagued the field in its quest to determine the true structure of the material of interest. Research groups have hypothesized both structures as well as an interconversion between the two. Having developed a controlled synthesis of NiETT, with some level of confidence of its structural nature and composition, we turned towards a controlled synthesis of NiTTO. With no ambiguity as to the identity of the material, we can compare our NiETT, our NiTTO, and the literature reports of potential NiTTO. Here, a rigorous synthetic process was required to fully understand the material of interest.

CHAPTER 2. EXPERIMENTAL METHODS

Chapter 2 covers experimental methods of uncommon techniques that were learned through colleagues, group lore, books, chemistry blogs, trial, and many errors. The aim is to collect this information in one location and provide the fullest account of research methods for those looking to reproduce experiments in this thesis. Literature procedures provide sufficient reaction information for straightforward or common procedures but often fail to provide enough information for difficult reactions with nuances. This responsibility for faithful reporting conclusions, data, and methods falls on all authors.[33,34] As Derek Lowe highlights in a 2009 *In The Pipeline* post, there exists an expectation of success depending on the publication. A *Journal of Organic Chemistry (JOC)* procedure is expected to be successful or more accurate than a *Tetrahedron* procedure, a patent procedure with spectroscopic information is more reliable than without, and procedures from obscure journals are to be used at your own risk.[35]

The lack of detail in synthetic procedures can be partly remediated by experience, or "chemical intuition."[36] If not, the procedure may get a reputation for not working.[37–41] The "Replication Crisis" has gained attention in psychology and medical trials recently.[42,43] In a survey of 106 chemists, a majority reported that 70-90% of work is reproducible, but over 80% report having failed to reproduce another's results and 60% have failed to reproduce their own results. However, the reproduction of old results doesn't lead to high impact publications or new funding sources.[44]

There exist some notable exceptions to this phenomenon. *Organic Syntheses* is an open access journal that publishes synthetic procedures only after they have been

reproduced twice in laboratory of a member of the Board of Editors. Explicit care is taken to ensure all parts of the procedure are clear, unambiguous, and reported in full detail. An editorial in *Organic Syntheses* suggests the movement of experimental procedures to the supporting information has reduced the amount of care and detail in published procedures.[45] The Phil Baran group runs a blog named *Open Flask* that provides additional insight into their published procedures and the progression of scientific thought.[45] Another attempt at crowdsourcing the checking and reproducing of difficult procedures was *Blog Syn* run briefly in 2013.[46] Unfortunately, funding and the transient nature of doctoral students in academic laboratories made the venture short lived. Their testing and initial failed reproduction of benzylic oxidation with 2-iodoxybenzoic acid (IBX) led to a response from the original authors, the Baran Group. Together, Blog Syn and the Baran Group ran additional experiments leading to the discovery that hydrated IBX was the active oxidant.

This chapter covers experimental techniques on purity determination and purification of materials, quantitative electrochemistry and bulk electrolysis, and nuances when working with insoluble, intractable materials.

2.1 Obtaining High-Purity Conjugated Polymers and Discrete Molecules

Purity, n. – the state of being unmixed with any other matter.[47]

In a section about purity and purification, it is worth discussing what is "pure," as the required purity is often dependent on the application. For example, 24 karat gold is considered "pure gold" at 999 fineness. However, gold is also available at 9999, 99999, and 999999 fineness, corresponding to 1 ppm, 1 ppb, and 1 ppt[48] impurity levels

(mass/mass – units should always be defined in parts-per-notation for clarity). In synthetic chemistry, the American Chemical Society (ACS) and United States Pharmacopeia (USP) have set standards for reagents to qualify as either ACS grade or USP grade. However, this has been complicated by each chemical supplier inventing its own terminology to market its inventory. As a rule of thumb, reagent and technical grades or ACS grade is sufficient for all procedures presented in this thesis, unless further purification is specified. Preparations for inductively coupled plasma/optical emission spectroscopy (ICP-OES) analysis were not performed with trace metal certified nitric acid, and a control sample was run as a standard.

When reporting the preparation of a material, the publishing journal sets the requirement for acceptable levels of purity. The ACS journals *JOC* and *Organic Letters* have extensive guidelines for proving identity and purity available online.[49,50] Identity should not be confused with purity, and each is confirmed through different means. Identity of a material is supported by proton and carbon nuclear magnetic resonance (^{1}H NMR and ^{13}C{^{1}H} NMR) spectroscopy, elemental analysis (EA), and high-resolution mass spectroscopy (HRMS). A certain level of purity is not required for publication in *JOC* or *Organic Letters* as long as the purity is faithfully documented. Both *JOC* and *Organic Letters* consider these characterizations as measures of purity: high resolution ^{1}H and ^{13}C{^{1}H} NMR spectra (high resolution is generally defined as sufficient signal to noise such that peaks with 5% of the intensity of the largest signal are identifiable), quantitative high-performance liquid chromatography (HPLC) traces in two different solvent systems with reported stationary phase, solvent, and detector type, and combustion analysis (EA) for carbon, hydrogen, and nitrogen within 0.4% of calculated values.

The guidelines importantly recognize that one technique alone is insufficient to confirm purity and that certain techniques are inappropriate for certain impurity classes. For example, if an impurity is an inorganic salt, clean NMR spectra are not sufficient evidence of purity. Likewise, a UV-Vis-NIR detector on an HPLC cannot quantify impurities that do not absorb light in that region or that are obscured by the mobile-phase absorption.

The guidelines make two additional observations about purity. First, on the 0.4% tolerance in combustion analysis data: "The need to include fractional molecules of solvent or water in the molecular formula to improve the fit of the data usually reflects incomplete purification of the sample."[50] And second, on mass spectrometry and purity: "HRMS data may be used to support a molecular formula assignment but cannot be used as a criterion of purity."[49]

This section focuses on the importance of monomer purity and catalyst purity on the final material, and methods for obtaining high-purity materials.

2.1.1 *Purity Considerations for Stille Cross-Coupling Reactions*

The Migita-Kosugi-Stille,[51] or commonly Stille,[52] cross-coupling reaction is widespread in synthetic chemistry for its ability to form aromatic C-C bonds with high selectivity and functional group tolerance.[52,53] The Stille reaction has been utilized by the organic electronics field to form extended conjugated systems for photovoltaics, light emitting diodes, field effect transistors, and sensors.[54,55] The primary drawback of Stille couplings is the stoichiometric use of toxic organostannanes.[56–61] This section aims to review the Stille coupling and use that knowledge to inform purification attempts.

The general catalytic cycle of the Stille cross-coupling reaction is shown in Figure 2.1, which follows the typical cross-coupling catalytic cycle: oxidative addition, transmetallation, and reductive elimination. An understanding of this cycle is vital for understanding potential impurities and how to prevent or remove them.

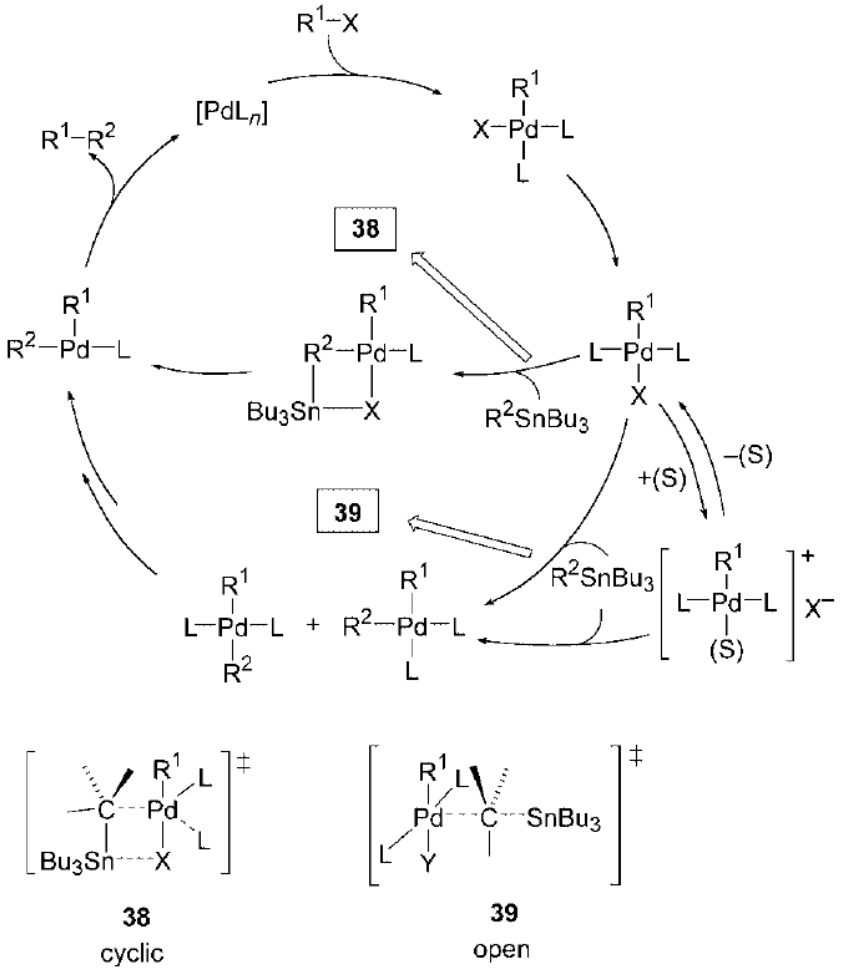

Figure 2.1 – Stille cross-coupling mechanism. Reprinted with permission from ref [53]. Copyright 2004 John Wiley and Sons.

The use of coordinating or non-coordinating solvents, conventional or microwave heating,[62] and copper or fluoride salts as additives[63,64] are covered by other reports[54] and

will not be covered here. Much work has been put into understanding the mechanism and transition states of the catalytic cycle.[52,53,65]

In the field of organic photovoltaics, synthetic chemistry is typically a means to an end, that is, to create a new molecule or polymer and test its material properties. Significant work is invested into developing a new highest-performing material. If a material does not perform well enough, it will be abandoned completely or lost in low-impact publications. Without a thorough understanding of the purity of a material, it is impossible to draw correct conclusions about the material's performance. A positive or negative affect on the material's performance may be incorrectly attributed to the material itself, such as the effect of ambient atmosphere on doping of poly(3-hexyl thiophene) (P3HT) OTFTs[66] or the unintended addition of plasticizers when using plastic labware.[67]

2.1.1.1 Monomer Purity and Stoichiometric Balance

A special form of the Carother's equation describes the obtainable degree of polymerization in a step-growth polycondensation reaction based on monomer conversion and monomer stoichiometric balance.[68] Assuming 100% monomer conversion, a 1% imbalance limits the degree of polymerization to 199; a 2% imbalance limits the degree of polymerization to 99, and a 5% imbalance limits the degree of polymerization to 39. Stoichiometric imbalances can arise from several lapses: the presence of non-reactive impurities in the monomers, the loss of monomer functional groups, the presence of impurities in the palladium catalyst, and the presence or use of palladium(II) as a catalyst.

The molecular weight and dispersity of polymers is well known to have an effect on the overall performance of the material in organic photovoltaics.[69–75] The ideal

molecular weight for each polymer, morphology, and application may be different or may not be known, so “low” and “high” molecular weights are relative terms for each situation. The unifying goal is to achieve reproducible molecular weights from batch-to-batch and to avoid molecular weight limitations from poor polymerization protocols.

Monomer balance, in conjunction with monomers and catalysts of verified purity and proper polymer purification, allows for a thorough study of molecular weight effects. This was demonstrated by Wei You and coworkers in a study of an alternating polymer for organic photovoltaics. The authors note the purification of both monomers through multiple recrystallizations and the purification of the palladium catalyst before polymerization. Using stoichiometric ratios of 1:1.000, 1:1.025, 1:1.050, and 1:1.100, the obtained number-average molecular weight was 71.4, 55.2, 36.5, and 18.3 kg/mol, respectively.[74] Alternatively, the molecular weight can be blindly improved by varying the monomer stoichiometry, as was done in a study by Guillermo Bazan and coworkers. [62] The authors use stoichiometric monomer ratios (bromide:tin) of 1:1.00, 1:1.05, 1:1.10, and 1:1.15 to obtain number average molecular weights of 22, 34, 31, and 18 kg/mol, respectively. This is claimed to “streamline” the achievement of a higher molecular weight polymer from tin monomers that are “difficult to fully purify” despite the tin monomer purity being “confirmed by multinuclear NMR spectroscopy, mass spectrometry and elemental analysis.” The observed optimal balance (1:1.05) is only valid for a single batch of tin monomer; whereas ensuring the purity of the tin monomer, although time consuming, keeps the optimal balance at 1:1. The adjustment of monomer ratio to increase molecular weight also obscures other issues with the polymerization that should be addressed (and

are addressed in this chapter), namely monomer purity, catalyst purity, the use of triphenylphosphine as a ligand, the use of mass spectrometry as a confirmation of purity.

The choice of organotin group used to complete the Stille coupling also affects the final material. The two most common trialkyltins for Stille couplings are trimethyl and tributyl. They have synthetic and safety trade-offs. Trimethyltin species react faster[76] and are more likely to be solids that can be recrystallized. Trimethyltin species are more likely to transfer a methyl group instead of the aryl group during transmetallation[76] and are more toxic.[59] Tributyltin species react more slowly and are more likely to be oils that require more time consuming purification techniques. Tributyltin species are less likely to transfer a butyl group during transmetallation and are less toxic.

2.1.1.2 Catalyst Choice and Purification

As every bond formed during the Stille coupling proceeds through the palladium catalyst, the purity and choice of catalyst are important to consider. The reliability of the Stille reaction and the commercial availability of catalysts and ligands have removed the burden of understanding the reaction mechanisms at play from the average chemist. In a 2016 *Chemical and Engineering News* article Victor Snieckus of Queen's University, Ontario quipped, "Chemists today don't make catalysts – they buy, open the bottle, and let the genie do its magic."[77] Palladium catalysts are commercially available in two oxidation states, palladium(0) and palladium(II).

Two common forms of palladium(II) are palladium(II) acetate ($Pd(OAc)_2$) and palladium(II) chloride ($PdCl_2$). While their ambient stability is desirable, using palladium(II) as a catalyst has disadvantages. Palladium(II) species need to undergo a

reduction to palladium(0) to begin the Stille catalytic cycle. This is achieved through a homocoupling of organotin monomers,[78] consuming two reactive groups, or through a ligand oxidation.[79] A 3-5% palladium(II) catalyst loading could create a 1.5-3% monomer stoichiometric deficiency. In discrete molecule synthesis, this creates difficult to remove impurities and decreases yield. In polymer synthesis, this creates a deviation from a true alternating copolymer and lowers the obtained molecular weights.

Palladium(II) acetate has an additional caveat. Despite commercial suppliers marketing $Pd(OAc)_2$ as a molecule in the monomeric form, three forms are known: $Pd_3(OAc)_6$, $Pd_3(OAc)_6(NO_2)$, and polymeric $[Pd(OAc)_2]_n$. The form affects reactivity in cross-coupling reactions and in formation of palladium precatalysts.[80,81]

Common commercial sources of palladium(0) are tetrakis(triphenylphosphine) palladium(0), $Pd(PPh_3)_4$, and tris(dibenzylideneacetone) dipalladium(0), Pd_2dba_3, or its chloroform adduct, $Pd_2dba_3 \bullet CHCl_3$. Due to their instability to oxygen,[82] palladium(0) catalysts should be kept in an inert atmosphere below 0 °C, such as a glovebox with a freezer or a desiccator in a standard laboratory freezer. All handling of palladium(0) should be conducted in a glovebox.

$Pd(PPh_3)_4$ has four phosphine ligands and does not need an additional ligand to function. It also has a clear visual indicator of when the catalyst is starting to go bad – the canary yellow color will fade to orange. Excess triphenylphosphine is a known inhibitor of the Stille catalytic cycle.[63] A simple depiction of the catalytic cycle implies $Pd(PPh_3)_4$ must dissociate two ligands to become PdL_2 before undergoing oxidative addition. This suggests that a drawback to $Pd(PPh_3)_4$ is an excess of ligand; however, the effect of excess ligand is

dependent on solvent, additive, and substrate.[63,76] The use of triphenylphosphine as a ligand is discouraged due to exchange reactions and phosphonium salt formation discussed in the next section.

The other source of palladium(0), Pd_2dba_3, is difficult to determine purity by visual inspection. Samples may appear black or purple and dull or lustrous. Typical impurities in Pd(0) catalysts include elemental palladium nanoparticles, palladium(II) and excess ligand, which can lead to improper or unknown catalyst loading, side reactions, and retardation of the reaction. All Pd_2dba_3 catalyst should be purified upon receipt from the manufacturer and stored for no longer than two months before use. One investigation into the purity of Pd_2dba_3 as received from suppliers found variations from 64% to 92% purity compared to ~99% of freshly purified or synthesized samples.[83]

2.1.1.3 Ligand Selection

Ligands play a significant role in the reactivity, stability, and solubility of the palladium species. They affect aryl vs. alkyl transfer rates, overall reaction rate, catalyst stability, the requirement or effectiveness of additives. The mechanism of the catalytic cycle may change based on the conditions;[53] it is therefore difficult to isolate effect of the ligand from the solvent system, reaction temperature, reaction substrates, and additives.[53,54,64,65,76]

The chosen ligand should be highly electron donating to stabilize the catalyst and prevent formation of palladium black and sterically bulky to accelerate reductive elimination.[84] Thus, triaryl phosphines are common ligands in Stille couplings due to their ambient stability and commercial availability. Triphenylphosphine is often used only as

the preformed catalyst, $Pd(PPh_3)_4$. Tri(*o*-tolyl)phosphine and Tri(*o*-anisyl)phosphine are common ligands used in conjunction with Pd_2dba_3. Their greater steric bulk near the phosphorous atom increases reductive elimination rates.[84] However, dibenzylideneacetone may not dissociate completely from the metal,[53,83] and Pd_2dba_3 will complete the catalytic cycle sans ligand, but with lower stability.[76,85] Tri(*o*-tolyl)phosphine is the ligand used in this thesis. Bidentate phosphines are rare in Stille couplings, as are trialkylphosphines, with the exception of the bulky tri(tert-butyl)phosphine.[76,84] Two other ligands, triphenylarsine and tri(2-furyl)phosphine show significant rate improvements in Stille reactions, but these ligands increase alkyl transfer rates in certain conditions.[65,76]

Triphenylphosphine is known to undergo phenyl-aryl and phenyl-methyl exchange from the oxidative addition product $ArPd(PPh_3)_2X$ to $PhPd(PPh_3)(PPh_2Ar)X$. Triphenylarsine and tri(2-furyl)phosphine also undergo rapid aryl exchange.[86–88] Triphenylphosphine is also known to undergo reductive elimination from the oxidative addition palladium complex to form a phosphonium salt. Oxidative addition of the phosphonium salt back to palladium(0) can result in either the aryl group or a phenyl group transfer to the palladium.[89] In discrete molecules, this leads to impurities that are difficult to remove and reduced yields. In polymers, this will result in the capping of one end of a chain and lower molecular weights. It also results in the scrambling of the desired alternating structure.

Scrambling of the alternating structure, or incidences of homocoupling, is not desirable due to the increase in energetic disorder[73,90] and potential misinterpretation of results. Homocoupling defects are detractors of power conversion efficiency in both discrete molecule and polymeric systems.[91,92]. A recent study on homocoupling defects in

diketopyrrolopyrrole polymers (via direct arylation) noted a pronounced long wavelength absorption on purposeful increasing of homocoupling defects. Without measures to decrease homocoupling, long wavelength absorptions are often taken to be a result of aggregation, leading to significant misinterpretation of film and solution absorption spectra.[93]

More care should be dedicated to ligand and catalyst selection in organic electronic polymers. There is much benefit in understanding the reaction mechanisms and catalytic cycle.

2.1.1.4 Importance of Post-Polymerization Purification

Proper synthetic techniques and care will reduce the prevalence of impurities and defects while maximizing molecular weight. However, attention should still be given to purification of the polymer after the reaction to obtain the highest quality polymer possible – free of catalyst and other reaction byproducts, insoluble material, and grease. Impurities are classified as intrinsic (i.e. a part of the molecule or polymer) or extrinsic (i.e. an undesired addition to the molecule or polymer).

For both molecular and polymeric systems, the removal of intrinsic and extrinsic impurities is important in reducing charge recombination centers.[90] In Stille polymerizations, common extrinsic impurities include soluble and insoluble palladium,[94] phosphines and phosphine oxides, trialkyltin halides, tetraorganotins, and halides.[95,9697] Direct arylation and Suzuki polymerizations add the presence of alkali salts, often potassium or cesium.[95] Intrinsic impurities include homocoupling or other structural

defects, low molecular weight oligomers, high dispersity samples, insoluble polymer, and residual tins or bromines at the end of chains.[97]

Extrinsic impurities can often be removed by exploiting the differential solubility or polarity of the impurities. Typical purification protocols for discrete molecules, such as column chromatography, will effectively remove residual catalyst, ligand, and inorganic impurities. Conjugated polymers are not often subjected to column chromatography during purification, and therefore other methods, such as precipitation and Soxhlet extraction, are required. Soxhlet extraction also reduces intrinsic impurities by removing low molecular weight oligomers and insoluble polymeric material. Residual polymerization functional groups are most easily removed during the reaction through end-capping.[98,99]

Other intrinsic impurities, such as homocoupling or other structural defects, are difficult to remove from both discrete molecules and polymers. Careful purification is required for discrete molecules. The transfer of a methyl group over the more electron rich aryl group during transmetallation results in methylated impurities. In a dithienosilole-based molecular donor, Leong et al. observe a decrease in photovoltaic performance (6.5% to 3.0%) in samples containing less than 1% of the methyl transfer contaminant due to increased recombination.[100] Homocoupling defects or methyl transfer defects are extremely difficult to detect and remove from polymeric materials. The utmost care should be taken during polymerization to avoid these defects.

Other difficult to remove impurities include grease and plasticizers that may result from laboratory greases[101] or from using solvents stored in plastic wash bottles. These plasticizers can act as additives and change the morphology, film forming, and

performance of materials.[67] Teflon tape should be used in place of grease on ground glass joints when seizing is probable. Bare glass joints are acceptable in many situations when the joint is room temperature or isothermal throughout the reaction. Solvents used for polymer purification should not be taken from plastic wash bottles. It is much easier to keep a polymer uncontaminated than to remove grease from a contaminated polymer.

2.1.1.5 Final Polymer Purity Determination

Relative molecular weight for conjugated polymers is often determined by gel permeation chromatography (GPC) against narrow dispersity polystyrene standards. Molecular weight results should be presented for all polymers in publications. Preferably chromatograms are included in the supporting information to indicate whether a polymer is monomodal in molecular weight distribution. While a vital characterization tool, GPC gives no indication of polymer purity. Important techniques to evaluate purity include mass spectrometry, nuclear magnetic resonance spectroscopy, elemental analysis by combustion analysis, and trace element analysis by inductively coupled plasma coupled mass spectroscopy. Each technique provides a unique slice of purity information.

Elemental analysis gives the broadest picture of purity. As it combusts an entire sample of material, it accounts for extrinsic and intrinsic impurities. It is also the least descriptive, and potentially the least sensitive account of purity. Components of less than 0.3% m/m cannot be detected by combustion analysis. Halogens must be present above 0.5% m/m for detection. Combustion analysis of carbon, hydrogen, nitrogen, and sulfur are considered accurate and precise within 0.3%, and publication expectations are within 0.4% of theoretical values. Thus, combustion analysis is capable of detecting insufficiently

dried (solvent contaminated) polymer, significant degrees of homocoupling, and the presence of inorganic or non-polymer impurities. However, it is weak at determining what impurities are present – other techniques must be incorporated.

The sensitivity of elemental analysis to homocoupling defects or monomer ratio depends on the elemental content of the monomers. The sensitivity to end-group analysis is dependent on molecular weight. The sensitivity to residual solvent or inorganics is dependent only on the mass percent of residuals. Polymers should be held to the same purity considerations as discrete molecules. Values outside of 0.4% of theoretical require further purifications.

Thermogravimetric analysis is useful in determining if volatile impurities, such as solvent or surface moisture, are present. These manifest as mass losses between 25 – 150 °C (depending on the solvent) that stabilize before true decomposition of the polymer begins. Residual solvent that is not removed from the polymer after 24 hours under high vacuum can often be removed in a vacuum oven with gentle heating or by precipitating the polymer again. This should be performed before sending materials to elemental analysis, as residual solvent will skew results.

Trace impurities of catalyst, ligand, and other inorganic materials should be quantified in all new materials. For trace analysis of impurities, ICP-MS is required. Typical detection limits are parts per billion or parts per trillion. Complete destruction of the organic matrix (polymer) and dissolution of impurities as aqueous soluble compounds is required before analysis. Aqua regia or concentrated nitric acid alone is ineffective for some polymers. A reliable method is to first dehydrate the matrix in concentrated sulfuric

acid at elevated temperatures. Microwave vessels work especially well due to their ability to withstand elevated temperatures and pressures. The destroyed matrix was much easier to oxidize with concentrated nitric acid at elevated temperatures. Impurities of interest are palladium, tin, bromine, and phosphorus for Stille polymerizations. Alkali metals and boron are of interest for direct arylation and Suzuki polymerizations.

Mass spectroscopy gives an absolute molecular weight of the polymer, and high resolution techniques can assist in defining if the polymer is truly alternating, end capped, or containing bromine.[97,99,102] Soft ionization techniques are required, such as matrix-assisted laser desorption ionization (MALDI), to avoid fragmentation of the polymer chain.

Polymer ^{1}H NMR spectroscopy is a powerful characterization technique when used properly. Broader signals than molecular species are expected due to polymer chain conformations and molecular weight distributions; however, "conjugated polymer" should not be an excuse for lack of ^{1}H NMR characterization.[103] Tetrachloroethane-d_2 is a practical solvent due to its high solubilizing power for conjugated polymers, higher boiling point than chloroform (145 °C versus 61 °C), and a usually innocent residual solvent signal at 6.0 ppm. Long delay times between acquisitions may be necessary for polymers or viscous solutions to prevent signal saturation and to obtain quantitative NMR results. T1 (spin-lattice) relaxation should be experimentally measured using an inversion recovery pulse sequence to verify the integration results can be treated quantitatively. NMR spectroscopy has been used to estimate absolute molecular weight, end-capping efficiency, monomer incorporation ratios.[99,104] ^{1}H NMR spectroscopy is not sensitive to inorganic materials or impurities lacking protons.

2.1.2 *Stille Polymerization Procedure*

Typical purification protocols for discrete molecules, such as column chromatography, will effectively remove residual catalyst and ligand. Conjugated polymers are not often subjected to column chromatography during purification, and thus other methods are required. Here is presented a complete conjugated polymer guide for polymerization by Stille cross-coupling with a palladium catalyst. From preparation to purification, it attempts to thoroughly detail all steps taken during the reaction to maximize molecular weight and minimize potential impurities or defects. It is based on experience, laboratory lore, and literature readings.

Purification of Pd_2dba_3 catalyst should be performed upon receipt or before use. If the catalyst has not been purified within the last two months, it should be purified again. The purity can be roughly tested by ^1H NMR spectroscopy. From a pure sample, dissociation of the free ligand dba indicates decomposition of the palladium complex to palladium black. We use the thorough procedure reported by Zalesskiy and Ananikov[83] with some modifications detailed below.

An impure sample or sample of unknown purity is dissolved in a minimum amount of purified chloroform. (Presence of hydrochloric acid, a decomposition product of chloroform, facilitates the decomposition of Pd_2dba_3. Chloroform is washed with water to remove hydrochloric acid and any ethanol stabilizer, dried over anhydrous calcium chloride, distilled from phosphorous pentoxide, and degassed by sparging with argon before use.) Palladium black nanoparticles are removed by filtration. Zalesskiy and Ananikov note most particles were between 60 – 200 nm (0.06 – 0.2 μm) with a minority

between 10-20 nm. Removal of these particles is not possible with fine or very fine glass frits (0.9 – 2.5 μm). Filtration through a typical 0.45 μm syringe filter will remove agglomerates of nanoparticles but may pass a significant amount. A 0.2 μm syringe filter is recommended as a first pass to remove large agglomerates that may otherwise clog smaller filters. Removal of smaller particles can be done through an inorganic filter, such as an anopore (aluminium oxide) filter. Whatman Anotop 0.02 μm inorganic filters are used to remove nanoparticles as small as 20 nm. The process is tedious and should be performed in glovebox to limit sample exposure to atmosphere. The inorganic filters are rinsed and reused until they clog, due to cost. Centrifugation has also been reported as a method to remove palladium black from solution.[94]

The excess ligand is now removed from the sample. The chloroform solution is concentrated (not above 40 °C, as this induces decomposition) to a near saturated solution. Degassed acetone (4× volume) is added, and the mixture is stored under argon in a freezer (~ –20 °C) overnight. The shiny, purple crystals of $Pd_2dba_3 \bullet CHCl_3$ are collected by filtration and washed with cold acetone. Drying under high vacuum gives the desired catalyst in >99% purity by ^1H NMR spectroscopy.

The importance of the purity of monomers has been well established in previous sections. At least 99% monomer purity should be obtained for effective polymerizations. Purity can be confirmed by high resolution ^1H and $^{13}C\{^1H\}$ NMR spectroscopy and HPLC (see Section 2.1.3.2 for details on HPLC purification of 4,4-bis(2-ethylhexyl)-2,6-bis(trimethylstannyl)germolo[3,2-*b*:4,5-*b*']dithiophene). Crystalline monomers are best purified by column chromatography once followed by one or two recrystallizations. Oil or liquid monomers, especially tins, often require additional purification. Performing a Stille

polymerization with an oily monomer without HPLC purification should be considered a waste of time and resources.

The reaction solvent is purified directly before use. Toluene is obtained from a solvent purification system, which utilizes argon-sparged, HPLC-grade toluene passed through two alumina columns and kept under positive argon pressure. The water content can be tested before use by Karl Fischer coulometric titration but is usually below 1 ppm. Alternatively, a sodium benzophenone still or drying over activated ("molecular sieves can be [activated] by heating at between 300 – 350 °C for several hours … preferably under vacuum, then cooling in a desiccator")[105] 3Å or 4Å molecular sieves will give sufficiently dry toluene.[106] Chlorobenzene or dimethylformamide should be purified and dried by the appropriate means.[105,107] Removing impurities that may coordinate to palladium, such as dimethylamine from dimethylformamide, is more important than obtaining absolute dryness.[108] Any solvent purification system storing dimethylformamide should have a final isocyanate column to scrub amines from the solvent before dispensing.

The reaction solvent is degassed by one of three techniques – sparging, vacuum degassing, or freeze-pump-thaw. Testing for dissolved oxygen is intensive and not performed; therefore, degassing is performed thoroughly. Sparging is often considered a rough degassing technique and is recommended for large volumes and non-volatile solvents. Vacuum degassing is performed by applying a high vacuum to the solvent until it is rapidly boiling. The vacuum is removed, and the flask is backfilled with an inert gas. The process is repeated. Vacuum degassing is extremely effective at removing oxygen from nonpolar solvents.[109] Freeze-pump-thaw is the most time consuming process of the three, but it is considered the most thorough and effective.

The setup of reaction glassware can be easily overlooked. Proper drying of glassware and standard air-free techniques are to be used at all times. Grease, whether hydrocarbon, siloxane, or poly(tetrafluoroethylene) (PTFE), should not be used on any parts or joints. If seizing of joints is a concern, use a minimal amount of an insoluble PTFE grease, such as Krytox. PTFE tape may also be used in a thin layer on the upper third of the ground glass joint to prevent seizing and allow for a sufficient glass-glass seal to form. A stir bar with sufficient power to vortex the entire solution, even when viscous or in a high aspect ratio piece of glassware (i.e. Schlenk tube), should be used.

Solid monomers not strongly affected by static electricity are directly added into the reaction flask. Oils, tacky solids, and static monomers are best weighed into a clean, dry vial and quantitatively transferred to the reaction flask using an inert solvent, such as DCM, hexanes, or toluene. Avoid chloroform unless stabilizers and hydrochloric acid have been carefully removed. The transfer solvent is removed under high-vacuum. Organotin monomers are to be weighed in a fume hood.

With the monomers in the reaction vessel, do not add catalyst directly to the reaction mixture. This is especially important if using Pd_2dba_3 or other soluble palladium source without phosphine ligands. In a separate flask or vial, dissolve the catalyst and ligand in a small amount of reaction solvent before transferring to the reaction flask. This process allows for the formation of the phosphine-palladium complex before exposure to the reactive substrates[55,83] and prevents the palladium catalyst from partially dissolving in and beginning to react with oily or liquid monomers.

Immerse the flask in a preheated oil bath, in order to rapidly bring the reaction to the desired temperature. Once the reaction is at a stable temperature, the reaction vessel is either left under continuous positive argon pressure or sealed off completely. The reaction is run for the desired time, which may be as short as ten minutes for microwave heating[62] or as long as five days for conventional heating.[103,110,111]

While the efficiency and extent of end-capping is not easily determined or fully understood, end-capping is recommended for all polymerizations as a method to reduce residual tin and bromine end-groups.[98,99,102,112] In Stille couplings with equivalent monomer stoichiometry, a tin (i.e. 2-(tributylstannyl)thiophene) and a bromide (i.e. 2-bromothiophene) end-capping reagent must be used sequentially. The first end-capping reagent is used in excess, and the second end-capping reagent must be in excess beyond that of the first. The tin end-capping is performed first to minimize the required amount of organotin. The reaction is run for an additional four to twelve hours for each end-capping process. After extended polymerization times (i.e. five days), the amount of active palladium catalyst may be diminished.[55] Fresh palladium catalyst and ligand (amount at user discretion, but suggested 10–20% of original loading) may be added at this stage to facilitate the end-capping reaction.

After polymerization and end-capping, the reaction is cooled to ~60 °C. Additional reaction solvent is added to fully dissolve the polymer at this stage. Scavenging for palladium and other impurities is performed at this stage. Diethyldithiocarbamic acid diethylammonium salt (CAS: 2391-78-8) is used as the palladium scavenger and, if present, crown ethers are used for alkali salts (18-crown-6 for K, 15-crown-5 for Na, 12-crown-4 or 9-crown-3 for Li).[95,103] The reaction is stirred for at least one hour before

precipitation into a non-solvent, often methanol. Do not use solvents from wash-bottles for precipitation. The solution is precipitated while warmed and with excess solvent to prevent trapping of impurities in the polymer matrix. If the polymer does not precipitate in methanol, 10-20% v/v water may encourage precipitation. The polymer is collected by filtration onto a 0.45 μm filter or directly into a cellulose Soxhlet thimble (double-walled thimbles have an effective particle retention of 1 μm and are stable to 120 °C). The stir bar from the reaction may be added to the Soxhlet thimble. This allows for agitation of the thimble without disassembling the setup during extraction in the event of thimble clogging.

Another literature source reports scavenging with diethyldithiocarbamic acid sodium salt (CAS: 20624-25-3) in a well stirred biphasic mixture to reduce residual palladium(II).[97] This was found to be more effective than substrate-based palladium scavengers. The mechanism of action is the complexation of residual palladium(II) with the dithiocarbamate. This results in a stable palladium(II) complex that remains in the methanolic solution upon polymer precipitation. Both salt forms are expected to function effectively as the chelating agent is the same, and the palladium(II) is not extracted into the aqueous phase.[113] The diethylammonium salt has the benefit of not requiring a biphasic mixture.

Soxhlet extraction is performed sequentially with methanol, acetone, hexanes, and dichloromethane for most conjugated polymers for organic photovoltaics. Each extraction is performed for 24 hours or until the extraction runs colorless, whichever is longer. ACS grade solvents are suitable for washing solvents. HPLC grade solvent is recommended for the final extraction. Chloroform (free of HCl) is the typical solvent for final extraction.

Remaining lower solubility material can be extracted with hot chlorobenzene (note the stable temperature range of cellulose thimbles).

Methanol extraction removes residual catalyst, residual ligand, bithiophene, and scavengers.[97] Acetone continues this process and removes monomeric and low oligomeric material. Hexanes and dichloromethane remove material with lower than desired molecular weights. Tetrahydrofuran, ethyl acetate, and other solvents may be used as washing or final extraction solvents based on final material solubility. Until familiar with the solubility and behavior of the polymer, do not discard the hexanes or dichloromethane Soxhlet fractions. Do not use any grease on the Soxhlet setup. Unless the polymer is oxidatively unstable, the extractions are performed in atmosphere. The reactions may be performed under inert atmosphere, but the intense pressure fluctuations caused by Soxhlet cycling may cause issues in Schlenk lines. Do not use insoluble material left behind in the Soxhlet thimble (often significant palladium black remains in the thimble) unless further purification is performed.

The desired fraction (chloroform for this example) is concentrated to minimum volume. If desired, column chromatography can be run on the sample using a ~4" column of 1:1:1 v/v silica, alumina, and celite. Higher molecular weight material will be retained more strongly on the column, so elute thoroughly or use a recycling column. This effectively removes polar inorganic contaminants and insoluble materials. Concentrate again to a minimum volume

Precipitate the Soxhlet fraction or column fraction in the strongest solvent possible, often acetone or tetrahydrofuran. Methanol is the least effective solvent at this stage, as the

polymer has already been precipitated once into methanol. The polymer is collected on a 0.45 μm filter and dried thoroughly (at least one full day under high vacuum). Residual solvent will affect elemental analysis.

If chloroform and chlorobenzene do not fully extract the polymer, the Soxhlet thimble should be removed, cut up, and dissolved in boiling chlorobenzene and filtered through a 0.45 μm syringe filter into the strongest possible precipitating solvent. If precipitation does not take place in strong solvent, 10% v/v methanol will induce it. Polymers not soluble in room temperature chloroform should be precipitated at least twice at this stage.

All polymers should pass elemental analysis within 0.4% and have trace metal analysis performed by ICP-MS for palladium, bromine, tin, and phosphorus. If the polymer fails elemental analysis, ensure removal of solvent by thermogravimetric analysis, and reprecipitate if necessary. If trace impurities analysis indicates significant residual trace elements, use appropriate method for removing the particular impurity, or report that value faithfully in the literature.

At all times, do not use plastic labware or grease when working with purified polymers. Use glass syringes or glass pipettes in place of plastic syringes. Avoid solvents stored in plastic containers.

2.1.2.1 Polymer Synthesis Case Study

A recent study[114] investigated a polymer synthesized through two common palladium-ligand combinations, Pd_2dba_3/P(*o*-tolyl)$_3$ (resulting in Polymer 1, P1) and

$Pd(PPh_3)_4$ (resulting in Polymer 2, P2), discussed in Section 2.1.1.2. (P1 and P2 are my designations.) The intent of the study was valid; however, the polymers were synthesized under completely different conditions with poorly controlled and reported procedures. The relevant discrepancies are described below as a guide and a warning.

P1 used a 6 mol% palladium loading (relative to the stoichiometry of one monomer) with a palladium:ligand ratio of 1:3. P2 used a 5 mol% palladium loading with a palladium:ligand ratio of 1:4. The purity of neither catalyst was confirmed before use, and the procedure implies the catalysts were stored under different conditions ($Pd(PPh_3)_4$ in a glovebox and Pd_2dba_3 not in a glovebox). Despite the catalyst systems being remarkably similar, two vastly different solvent systems were used. P1 was synthesized in chlorobenzene (a non-coordinating solvent) at 140 °C, and P2 was synthesized in a 5:1 (v/v) toluene:dimethylformamide (dimethylformamide is a coordinating solvent) mixture at "reflux". No indication was made about the degassing procedure of either solvent system, nor the dryness of the toluene:dimethylformamide mixture. The reaction temperature and solvent coordination are well known to affect the catalyst stability and probability of defects in the catalytic cycle.

The polymerization of P1 was run for 48 hours before cooling to room temperature and dropwise addition to methanol. P2 was run for 32 hours with an additional 12 or 24 hours for end-capping (the procedure is vague) before cooling to room temperature and being poured into methanol. The difference in end-capping procedure will affect the residual amount of tin and bromine that is still attached to the polymer chain.[98] The dropwise versus rapid precipitation may affect the entrapment of impurities in the polymer matrix. Both polymers were subjected to Soxhlet extractions in methanol, acetone, and

hexanes. P1 was extracted into dichloromethane. P2 was extracted with dichloromethane then extracted into chloroform. Both were precipitated into methanol, collected by filtration, and dried. Unsurprisingly the molecular weights (M_n) of P1 and P2 were considerably different at 12.4 and 22.6 kg/mol, respectively. No elemental analysis or trace metal analysis was recorded for either polymer.

The authors measured the monomer ratio by ^{1}H NMR spectroscopy. Deviation from the monomer feed ratio of 1:1 is indicative of homocoupling, aryl transfer, or another defect in the catalytic cycle. In P1, the organotin monomer was measured as more prevalent in a ratio of 1:0.97. In P2, the bromide monomer was measured as more prevalent in a ratio of 1:1.1. ^{1}H NMR signals are quantitative and can be accurate to within 1% if proper precautions are taken. Integrations are affected by signal-to-noise ratios, saturation effects, peak-shape, integration range, and the baseline and phasing algorithms used during data processing. The authors fail to provide verification of proper relaxation times to avoid saturation or appropriate integration windows against the peaks of interest full width at half-maximum. No information is given about the inclusion of ^{13}C satellite peaks, which account for 1% of the total integration. A lenient estimation of accuracy yields integrations ±5%. With no protocol provided for NMR spectroscopy, a conservative estimate of integration accuracy is ±10%. The measured ratios of 1:0.97 and 1:1.1 are therefore indistinguishable from 1:1 and each other.

No connection of incorporation ratio to catalytic cycle, palladium and ligand combination, or solvent system was made by the authors. “The reported findings clearly demonstrates the critical importance of choosing the right catalyst to prepare high performing [donor-acceptor] copolymers and preventing from misreading corresponding

photovoltaic performance when an incompetent catalyst is employed." However, the authors and reviewers missed the incompetent employment of the catalyst and provide no useful information for selecting the critically important catalyst.

2.1.3 *Purification Techniques Utilized in this Thesis*

When purifying materials, it is extremely useful to know the expected by-products and impurities, thereby facilitating separations and selecting the appropriate method for purification. An otherwise difficult chromatographic separation can be simplified by changing workup conditions or exploiting solubility differences.

2.1.3.1 Example #1 – Tosylate Workup with Lithium Bromide

Compound 3.6 was synthesized by the nucleophilic attack of a thiophene imide on di(ethylene glycol) monomethyl ether tosylate (See Figure 3.27). Chromatographic separation of the product from the thiophene imide starting material and potassium carbonate was easily performed. However, separation of the product from excess di(ethylene glycol) monomethyl ether tosylate proved difficult as the retention factors were nearly identical in all solvent systems. To ease separation, the mechanism of the reaction was reviewed – the tosylate undergoes nucleophilic displacement due to the weak basicity of the leaving group and the stronger basicity of the imide conjugate base. A nucleophile that is strong enough to displace tosylate but weak enough to not displace the imide would ease separation – if the nucleophile converted the remaining di(ethylene glycol) methyl ether to a material with a substantially different retention factor than Compound **3.6**. Bromide satisfied these constraints. Stirring the completed reaction with lithium bromide converted the excess tosylate to 1-(2-bromoethoxy)-2-(2-methoxyethoxy)ethane, which

elutes much sooner on silica gel than Compound **3.6**. The excess lithium bromide and lithium tosylate are removed during aqueous workup or by column chromatography.

2.1.3.2 Example #2 – Preparatory Reverse Phase(RP)-HPLC for Stannylated Monomers

The carbon-tin bond is weak (209-238 kJ/mol)[60,115] compared to carbon-carbon, (Me_3C-CH_3), (343-363 kJ/mol)[116,117] or carbon-silicon, (Me_3Si-CH_3), (374 kJ/mol).[116] Aryl-trialkyltin bonds undergo protodestannylation by mineral acids and acidic silica gel. When 99.9% purity is required for polymerization, any amount of destannylation is unacceptable. Reverse phase (RP) chromatography is amenable to organotin purification. Due to limited solubility in "low eluting power" solvents (water, acetonitrile) for RP, gravity and flash column chromatography are inefficient at separating monofunctionalized and difunctionalized monomers. High performance liquid chromatography with a preparatory RP column and UV-Vis detector (diode array and two individual wavelength channels) is employed to obtain sufficiently pure tin monomers. An effective elution solvent is acetonitrile mixed with acetone or mixed with tetrahydrofuran (THF). An initial purification must be run on the organotin, as RP-HPLC does not detect non-absorbing species and will not remove many inorganic impurities. Suggested purification for all tin species after a traditional aqueous workup is to dissolve in hexanes and wash with methanol. Hexanes and methanol are partially miscible. A 2:1 v/v ratio of hexanes to methanol is found to work well. This aids in removing polar tin byproducts not removed during aqueous workup.

The following is an example of RP-HPLC purification on bis(2-ethylhexyl)-2,6-bis(trimethylstannyl)germolo[3,2-*b*:4,5-*b*']dithiophene (DTG-$SnMe_3$). The peak

absorbances of DTG-$SnMe_3$ are at 241 and 345 nm, the higher energy absorbance is obscured by the common RP-HPLC solvent acetone (UV cutoff 330 nm). Using a mixture of acetonitrile (UV cutoff 190 nm) and THF (UV cutoff 212 nm) allows for both absorbances to be monitored. The THF must be stabilizer free, including butylated hydroxytoluene (BHT) (UV maximum 278 nm). Unstabilized THF is susceptible to peroxide formation and should not be left on the column or exposed to atmosphere for extended periods of time. The highest concentration of DTG-$SnMe_3$ that gives acceptable separation during chromatography is ~50 mg/ml in 60:40 acetonitrile:acetone or acetonitrile:THF. Because DTG-$SnMe_3$ is poorly soluble in acetonitrile, the compound is first dissolved in THF or acetone then diluted to the appropriate concentration and volume with acetonitrile. The monotin impurity is present at ~10 mol%. After purification, analytical HPLC reports >99% purity.

2.1.3.3 Example #3 – Size Exclusion Chromatography for Molecular Systems

Multiple Stille couplings to one core molecule, as in the creation of a branched or star shaped system, presents challenges to impurity identification and removal. If each of the four cross-coupling sites has a 95% chance of correct completion, the crude yield will be at most 81% $((95\%)^4)$. An increase in reaction defects or incompletion will result in an exponential decrease in yield. In the coupling of 2,2',6,6'-tetrakis(trimethylstannyl)-4,4'-spirobi[germolo[3,2-*b*:4,5-*b*']dithiophene] (4.4) to bithiophene or benzothiadiazole-bithiophene, core molecules having undergone 2, 3, and 4-fold Stille couplings are observed by mass spectroscopy. Although mass spectroscopy could not quantify the impurities, it is essential in identifying their presence.

2,2',6,6'-tetrakis(3,5'-dihexyl-[2,2'-bithiophen]-5-yl)-4,4'-spirobi[germolo[3,2-*b*:4,5-*b*']dithiophene] (**4.5**) was successfully purified and separate less substituted impurities by traditional column chromatography, albeit with losses due to UV-photo-instability. Column chromatography was unable to separate 2,2',6,6'-tetrakis(7-(3,5'-dihexyl-[2,2'-bithiophen]-5-yl)benzo[*c*]thiadiazol-4-yl)-4,4'-spirobi[germolo[3,2-*b*:4,5-*b*']dithiophene] from its trisubstituted impurity due to low polarity differences between the two molecules. Due to the presence of two hexyl sidechains per arm, this class of molecules is not able to be crystallized or separated by solubility differences. The molecular difference most effective in separating these two molecules is hydrodynamic radius by size exclusion chromatography. Bio-Beads S-X1, a polystyrene matrix with 1% crosslinking by divinylbenzene, is suitable for molecular weights from 600 – 14,000 daltons. THF is an appropriate eluent for swelling the beads and solubilizing the sample. As with all SEC, the larger hydrodynamic radius of the tetrasubstituted product prevents diffusion into the small pores of the swollen matrix compared to the trisubstituted impurity. The band of tetrasubstituted product is retained less strongly and eluted first. Through SEC, the product was successfully isolated from impurities which could not have been otherwise removed by traditional chromatographic techniques.

2.1.3.4 Example #4 – Purification of Light, Acid, and Oxygen Sensitive Materials

The all donor 2,2',6,6'-tetrakis(3,5'-dihexyl-[2,2'-bithiophen]-5-yl)-4,4'-spirobi[germolo[3,2-*b*:4,5-*b*']dithiophene] degrades by simultaneous exposure to light and oxygen. It is more susceptible to ultraviolet light and acidic silica gel. The degradation products are unknown, but the color changes from red-orange to brown and is accompanied by a loss of solubility in most solvents. Column chromatography is performed in the

absence of light wrapping the column in aluminum foil. Bands of insoluble material are "burned" on silica gel columns when illuminated with longwave UV (365 nm). Similar spots were left on TLC plates when visualizing with longwave or shortwave UV (254 nm) or upon standing in ambient light. Therefore, TLC plates are developed immediately in light-excluding TLC jars after spotting with no exposure to UV light prior to developing. Two-dimensional TLC plates are not visualized with UV light between developments. The methods above for exclusion of light during purification and analysis are sufficient for obtaining 4.5.

The planar analog, 2,6-bis(3,5'-dihexyl-[2,2'-bithiophen]-5-yl)-4,4-bis(2-ethylhexyl)-germolo[3,2-*b*:4,5-*b*']dithiophene (**4.6**) is less stable to light, oxygen, and acidic silica gel. The reaction also yielded the homocoupled product, 6,6'-bis(3,5'-dihexyl-[2,2'-bithiophen]-5-yl)-4,4,4',4'-tetrakis(2-ethylhexyl)-2,2'-bi[germolo[3,2-*b*:4,5-*b*']dithiophene], which was not separable from 4.6 using hexanes on silica gel. Due to the small quantity of material to be purified and the small difference in retention factor in hexanes, preparatory TLC plates are employed using n-pentane as an eluent. The plates are neutralized by developing in 5% triethylamine in pentane, drying under a stream of nitrogen, and developing again in 100% pentane. Spotting of the plate is performed in the absence of as much ambient light as possible. The plates are developed using 100% pentane in a chamber excluding light and purged with argon. The desired product is successfully separated from the impurity in this manner. A "burn" mark is strongly visible along the baseline. Loading of the plate is best performed under complete exclusion of air and light.

2.2 Electrochemical Synthesis of Bis(tetraethylammonium) Tetrathiooxalate (TEA_2TTO)

Electrochemical processes are prevalent on the industrial scale; however, chemical synthesis dominates chemistry on the laboratory scale. The use of electrochemical reactions reemerges when chemical attempts have failed.[118] Electrochemical reactions are also of interest in flow[119–121] and green[118,122,123] chemistries, as it provides a constant source of oxidation or reduction power without the consumption of chemical reagents. The chemical synthesis of bis(tetraethylammonium) tetrathiooxalate (TEA_2TTO) has not been reliably accomplished through reduction of carbon disulfide and the synthesis must be performed electrochemically (See Section 7.2.1).

2.2.1 *Electrochemical Cell Setup*

The electrochemical synthesis of TEA_2TTO is achieved through the dimerization of carbon disulfide in the presence of a tetraethylammonium supporting electrolyte in cold acetonitrile. See 7.2 for the standard reaction protocol. This section details the specifics of equipment and processes to reliably synthesize TEA_2TTO.

2.2.1.1 Electrolyte Selection

Tetrathiooxalate is believed to be an intermediate in the synthesis of dmit (See Section 5.2). In order to prevent the degradation of TTO to dmit, the reaction must be effectively stopped at that stage. Dmit is thermodynamically accessible at the reduction potential employed during synthesis; therefore, TTO must be kinetically trapped as an insoluble species. Effective cations are tetraethylammonium and

tetraphenylphosphonium.[124] The anion must undergo oxidation at the counter electrode. Bromide and iodide will undergo oxidation to tribromide or triiodide under the reaction conditions. Tetraethylammonium bromide is recommended as the electrolyte. The concentration of electrolyte is maximized to reduce solution resistance and joule heating. The solubility limit of tetraethylammonium bromide in warm acetonitrile is ~0.6 M. Experimentally, 0.5 M is acceptable at reaction temperatures of –10 °C to 0 °C.

The oxidation products of tetraethylammonium bromide react with products in the working compartment to form a black deposit at the joining frit. An unexplored method to alleviate this concern is the use of an anion that once oxidized is either insoluble or gaseous. Such an anion has not yet been identified.

2.2.1.2 Electrochemical Cell

The reaction is convenient to perform in an electrochemical H-cell separated by a fine-porosity glass frit. This limits diffusion between the compartments but will inevitably clog as the compartments react at that interface. The compliance voltage between the working and counter electrode is high due to their separation and cleaning an H-cell frit is tedious and requires complete disassembly of the apparatus. An H-cell remains the recommended cell design despite these concerns. Both chambers of the electrochemical cell were fitted with rubber stoppers modified to accommodate necessary intrusions.

Stirring is accomplished with an adjustable-speed mechanical stirrer with a half-moon impeller inserted through the working compartment stopper. The slowest speed vigorously disturbed the mercury surface. An additional Variac (variable autotransformer) was added in series to further drop the supplied voltage to the motor. Stirring should be

performed at the slowest speed possible that does not result in a current drop from the deposition of TEA_2TTO on the mercury pool. We found the ideal speed to be slower than one revolution per minute.

2.2.1.3 Inert Atmosphere

To facilitate an inert atmosphere and prevent unwanted oxidation by atmospheric exposure, rigorous protocols were applied to keep the working compartment solution degassed. The acetonitrile was thoroughly degassed by sparging with argon or vacuum degassing before creation of the electrolyte solution and briefly sparged with argon afterwards (to minimize loss of solvent and precipitation of electrolyte). When assembling the electrochemical cell, an argon sparge line was introduced through the working compartment stopper to provide continuous sparging. Before the reduction was started, the sparge line was removed from solution and transitioned to a purge line to maintain a blanket of argon above the solution. Carbon disulfide was not degassed prior to use due to its high vapor pressure.

2.2.1.4 Cooling

To ensure precipitation of the TEA_2TTO intermediate, the reaction is kept between –10 °C and 0 °C. Maintaining sub-zero temperatures can be achieved using ice-salt or ice-acetone mixtures. To reduce consumption of sodium chloride or generation of acetone waste, an immersion cooler capable of temperatures as low as –90 °C in an isopropanol bath was used. The isopropanol bath provided a thermal reservoir for maintaining reaction temperature as well as additional space for pre-cooling electrolyte solutions and cold storage of product.

2.2.1.5 Alternative Cell Setup

Breitzer and Holloway[125] have reported an electrochemical cell for the synthesis of TEA_2TTO consisting of one standard beaker, mercury pool electrode, platinum mesh counter electrode, and a cellulose Soxhlet thimble. The thimble acts as the compartment separator and salt bridge. The entire setup is performed in one beaker without a reference electrode which simplifies the reaction setup and reduces the distance between the working and counter electrode. However, the thimble does not adequately contain the tribromide byproduct in my reproduction. The close proximity between the two compartments results in rapid destruction of product. An ultrafine glass frit may be suitable to reduce diffusion while maintaining electrode proximity.

2.2.2 *Working, Counter, and Reference Electrode Selection*

The choice of electrode is vital for the electrochemical reaction. Mercury is a particularly useful working electrode as it is a conductive liquid that can form a large surface area electrode. The amount of current that can be passed, and therefore the rate of the reaction, is partially dependent on the surface area of the electrode. Literature reports insist the working electrode must be mercury for the electrochemical reaction to occur, and no reports of other electrodes are known.[125–128] In our tests, the reduction did not proceed on platinum grid electrodes.

The counter electrode may be any number of conductive materials as long as the surface area is sufficiently large to handle the current passed by the working electrode. A platinum mesh basket is used in this experiment. Coiled sheets of 310 stainless steel, a zinc block, and platinized grids all allow current to flow and the reduction of carbon disulfide

to occur, but all have issues preventing their use in place of a platinum mesh. The stainless steel corrodes on exposure to tribromide. The zinc block is surface passivated, presumably due to tribromide, and then ineffective. The platinized grid contains insufficient surface area, and the reaction is very slow.

The Ag/Ag^+ electrode used as a reference electrode in Chapter 4 is not appropriate for this reaction. The potentiostat was unable to attain the desired reduction potential when using Ag/Ag^+ as a reference. Additionally, the Vycor frit was rapidly fouled to an impermeable state. Ag/AgI was previously used by Reynolds et al.[127] Ag/AgCl[129] is used in this experiment. The electrode is separated from the working compartment by a coarse porosity frit – this prevents solids from fouling the reference but does not impede the diffusion of reaction by-products into the reference compartment. The reference potential of the Ag/AgCl electrode drifts as the reaction proceeds. Maintenance of a constant current once the reaction is established accounts for this drift.

2.2.3 *3-Electrode Potentiostat Power Supply or DC Power Supply*

The power source must be DC and able to obtain the necessary reduction potential. For control, ease, and troubleshooting purposes, a 3-electrode potentiostat is recommended when first attempting this synthesis. In this experiment, a PAR 273 potentiostat is used. The rated compliance voltage between working and counter electrodes is 100 V. (NB: The PAR 273 is capable of delivering 1 A at 100 VDC, far above the lethal current. Follow proper safety precautions.) If the potentiostat is unable to reach the required reduction potential versus reference, the *iR* drop is the culprit. This is mediated by increasing the

electrolyte concentration, decreasing the reduction potential versus reference, or cleaning the H-cell frit. Techniques are available for measuring and accounting for *iR* drop.[130]

Traditional DC power supplies can be used, but caution must be taken to not apply too much potential. Without a reference electrode, the working electrode serves as the reference electrode, and potentials should be reported versus mercury pool. In my attempts with either a 125V or 18V DC power supply, both sources were successful in driving the reaction. The potential was gradually increased until the telltale formation of tribromide was visible at the counter electrode. Minor adjustments to the potential were made from that point based on rate and observed decomposition. DC power supplies are more compact than a potentiostat and much less expensive; therefore, it is convenient to place inside a hood with corrosive chemicals.

2.2.4 *Material Collection and Electrolyte Replacement*

Previous reports of monomer preparation use a batch preparation technique. Continuous collection is desirable. This is done manually by pipetting with a large bore pipet (a normal glass pipet with the tip broken off) or a volumetric pipet. This method works well with minimal stirring as large crystals form on the surface of the mercury. Applying rapid suction at the surface of the mercury effectively draws the product into the pipet with mercury and electrolyte. The mercury settles inside the pipet and is returned to the mercury pool. The slurry of product is collected in a vial or centrifuge tube kept cold in the cooling bath. The product settles out rapidly, and the electrolyte is returned to the reaction. No degradation of TEA_2TTO is observed during collection if the material was maintained below 0 °C.

With mechanical stirring, continuous collection is done from the bulk of the solution instead of at the electrode surface, as the TEA_2TTO crystals are much smaller and are suspended by stirring. A glass tube (pipet barrel) with a 90° bend and flared scoop facing into the direction of stirring/fluid motion will passively collect TEA_2TTO crystals in the flared base. Connection to a peristaltic pump pulls a slurry of product and electrolyte out of the reactor. This process also avoids any mercury as long as the base is kept at the surface or above the mercury electrode. The suspension is pumped to 10ml syringe barrel and wide bore needle place through an entry port in the working compartment stopper. The syringe is equipped with a glass wool plug at the bottom that captures the product and returns the electrolyte to the working compartment. A cone of argon is beneficial to reduce exposure to atmosphere and the product is kept cool due to a continuous supply of chilled electrolyte slurry. A fluoropolymer peristaltic tubing is recommended as it must be compatible with acetonitrile, alkylammonium halide salts, and carbon disulfide.

2.2.5 *Purification of Air-Sensitive, Mercury-Contaminated TEA_2TTO*

Bulk or continuous collection of TEA_2TTO yields a crude product contaminated with electrolyte, acetonitrile, mercury, carbon disulfide, and dmit. Rough purification is performed immediately upon collection, as continued exposure to carbon disulfide and oxygen will result in decomposition products. Keeping the product below 0 °C limits the degradation even when exposed to atmosphere. Upon warming to room temperature, TEA_2TTO is immediately placed under high vacuum to remove carbon disulfide. Washing with cold acetonitrile removes any remaining carbon disulfide and most electrolyte. Rough purification is also obtained by sonication in degassed ethanol.

Further purification is performed by recrystallization from methanol. This effectively removes remaining mercury and remaining electrolyte. Slow cooling gives orange crystals. An alternative precipitation method is to dissolve TEA_2TTO in thoroughly degassed deionized water. Any mercury is filtered off at this time. Precipitation is induced with degassed acetone. Electrolyte remains soluble in the water-acetone mixture.

2.2.6 *Cleaning Mercury and Mercury-Contaminated Glassware*

Mercury and potentially mercury oxides and $Hg(dmit)_2$ are removed and isolated from glassware before the traditional cleaning process. Metallic mercury should be worked with in a secondary container at all times with a mercury absorbent or sulfur powder nearby. Two filtrations of all wash materials were performed to collect and remove mercury from the waste stream. If contaminated with carbon disulfide, the waste is treated as P-list waste.

2.3 Quantitative Electrochemistry by Bulk Electrolysis

The basics of cyclic voltammetry and electrochemistry are discussed elsewhere.[131,132] Quantitative electrochemistry by bulk electrolysis is utilized in Chapter 4 to determine the number of electrons transferred during an oxidation process based on Faraday's law.[133,134] The Randles–Sevcik[135] equation provides another method of determining electron count only if the diffusion coefficient is known. In chemically and electrochemically reversible systems with fast electron transfer processes, the ideal peak-to-peak separation from anodic to cathodic current is 57 mV for a one-electron process.[132] While this value is rarely obtained experimentally, a value from a well-behaved system (i.e. ferrocene) can be used in its place.[136]

These alternative methods fail when the electron-transfer process involves one electron, but the molecule contains multiple isoelectronic redox sites. Bulk electrolysis provides a method of electron counting independent of the electron transfer process and amenable to overlapping redox peaks. Bulk electrolysis is the oxidation (or reduction) of the entire population of a species (i.e. $A \rightarrow A^+$ quantitatively) in solution. This is facilitated by a large working electrode surface area in a stirred solution. This prevents mass transport from limiting the rate of the electrolysis. With a known solution concentration, the number of electrons transferred at a given potential is calculated.

2.3.1 *Cell Design*

The electrochemical cell for bulk electrolysis has these desired features: multi-compartment, minimal volume, stirring, easy cleaning, and inert electrodes. The working, counter, and reference electrodes are separated by a fine porosity or Vycor glass frit. This prevents diffusion of oxidized species between electrodes and the contamination of the reference electrode. A coarse glass frit was found to provide unacceptably high rates of analyte transport between the working and counter electrode compartments.

The overall volume is kept to a minimum. Thus, the overall amount of charge to pass during an experiment is kept to a minimum, assuming equal concentrations. The rate of electrolysis is kept high, as the electrode's double-layer volume to overall solution volume ratio is kept high. The volume must be large enough to prevent evaporation losses from disturbing the cell. The electrochemical cell, particularly the working compartment, benefits from stirring that suspends TEA_2TTO off of the mercury pool but does not froth the mercury pool or otherwise cause it to become discontinuous.

The working electrode is composed of a high surface area, inert, conductive material. Acceptable electrodes are the same as those used in cyclic voltammetry – platinum, gold, or graphite carbon as a mesh or foam are recommended. Platinum is preferred because it is easily cleaned in sulfuric acid or by flame. The specifications for the working electrode also apply for the counter electrode. The counter electrode is ideally designed to *capacitively* store the entire charge required to be passed. That is, all faradaic currents at the working electrode are preferred to be non-faradaic at the counter electrode. Otherwise degradation of solvent, electrolyte, or a sacrificial reagent occurs at the counter electrode. The reference electrode is stable with minimal drift over the time of the experiment. An Ag/Ag^+ electrode separated by a Vycor frit fulfills these requirements. The solvent and electrolyte are selected based on the solubility of the analyte and its redox products and the required electrochemical window.

2.3.2 *Experimental Protocol*

Quantitative electrochemistry by bulk electrolysis is not well described in literature. A more general term, coulometry, applies here, but is avoided as much coulometry is dedicated to inorganics, electrogravimetry, and constant-current references. Reports of electron count in electrochemistry are often based on peak current height comparisons[137] or assumed diffusion coefficients.[138] One *J. Ed. Chem.* article details the quantitative electrolysis of a confined volume using an optically transparent thin-layer electrode (OTTLE). The experimental setup was not used here, but the theory and principles are useful to review.[139]

Before starting on quantitative electrochemistry, the analyte is confirmed to be well-behaved under normal cyclic voltammetry conditions. The oxidation potential(s) are noted versus ferrocene to give a stable oxidation potential reference. With a large and separated working and counter electrodes, *iR* drop and scan speed become an issue. Slow scan speeds mediate *iR* drop by lowering current flow, but the large surface area of the electrode increases current flow. Only an acceptable cyclic voltammogram on ferrocene is needed in the bulk cell to begin experiments. This avoids unnecessary consumption of analyte.

From the cyclic voltammogram, the $E_{1/2}$ of the process of interest is determined. The Nernst equation dictates the overpotential needed to drive the electrochemical process based on the initial concentration of analyte and degree of reaction completion. These variables are adjusted such that the overpotential does not interfere with other redox processes. For example, a 10^{-6} M analyte concentration oxidized to 99% will require a 0.18 V overpotential. The current will fall off exponentially with time and is dependent on the electrode area and rate of stirring. Typical electrolysis run times are 30-60 minutes.

To begin the experiment, a known amount of analyte is introduced into the working compartment containing solvent and electrolyte. The potentiostat is set to the appropriate voltage beyond $E_{1/2}$. The potential is held until a stable current is obtained. The potential is reversed to at least the opposite voltage beyond $E_{1/2}$ in the opposite direction. Returning to 0 V versus reference is often suitable. The potential is once again held until a stable current is obtained. This process may be repeated until evaporation, electrolyte decomposition, or material decomposition prohibits accurate data collection. The procedure is repeated on a blank sample to determine the influence of background processes.

2.3.3 *Data Analysis*

Several processes are occurring during the electrolysis that contribute to the total measured charge passed – oxidation of analyte, non-faradaic processes, oxidation of impurities, movement of the oxidized analyte to the counter electrode for reduction and back to the working electrode (i.e. double oxidation), and movement of reactive species generated at the counter electrode (i.e. solvent or electrolyte decomposition to oxidized or unoxidized analyte resulting in double oxidation or complete decomposition (no oxidation). Only the first, complete oxidation of the analyte is desired. The other processes are minimized through experimental setup or accounted for during data processing.

The blank experiment yields a current that rapidly decreases to a negligible amount. This charge is a result of non-faradaic processes (i.e. electrode double layer charging). The amount of charge is extrapolated back to time zero using a linear regression of the final portion (~2.5 – 5%) of the experiment. This number will vary based on the electrochemical setup, solvent, electrolyte, electrodes, and analyte. The number should be standardized across an experiment and reported faithfully. The slight increase in charge from the extrapolated time zero and time final is accounted for in the experiment analysis and is therefore neglected here.

The analyte electrolysis yields a higher current that more slowly decreases to an often non-negligible amount. The amount of charge is extrapolated back to time zero using a linear regression of the final portion (~2.5 – 5%) of the experiment. This accounts for unwanted processes that are assumed to occur at a constant rate for the entire experimental time, and accounts for the neglected processes from the blank experiment. This is an

acceptable estimate due to the rapid initial current drop-off. The non-faradaic charge is subtracted from the extrapolated analyte charge at time zero to give the desired value – that is, the charge passed as a result of the analyte's oxidation.

CHAPTER 3. THIENOPYRROLEDIONE (TPD): IMPROVING REACTIONS TO EXPAND UTILITY AND REDUCE WASTE

3.1 Introducing Thienopyrroledione

While new donor polymers,[140–142] such as poly[(5,6- difluoro-2,1,3-benzothiadiazol-4,7-diyl)-*alt*-(3,3‴-di(2-octyldodecyl)-2,2′; 5′,2″; 5″,2‴-quaterthiophen-5,5-diyl) (PCE-11) and its analogs,[111,143] and non-fullerene acceptors[10,144,145] are pushing to ever higher efficiencies, it is important to revisit the synthetic cost of production and end goal of these materials – low cost sensors or devices,[146–148] and additive manufacturing or high-throughput printing.[146,149,150] The cost and effort put into new materials with slightly higher performances was highlighted by Po et al.[151] An exceptional material with the ideal characteristics, may have a higher "cost" of production through synthetic complexity and waste disposal that off-sets its performance increase. This chapter serves to emphasize the need to evaluate the "cost" of synthesis and to suggest that an environmentally-friendlier route does not have to come at some other expense. In fact, a more concise synthesis can create possibilities, as demonstrated with thieno[3,4-*c*]pyrrole-4,6-dione (TPD).

TPD has found a role as a useful acceptor moiety for organic electronic polymers due to several important characteristics: (1) The imide functionality provides a strong electron withdrawing, or electron deficient, characteristic to the monomer, (2) the imide nitrogen provides a convenient location to append a side chain, (3) the monomer is regiosymmetric, and (4) the thiophene ring facilitates cross-coupling reactions.[104,152]

Downfalls of the first TPD polymer syntheses were an eight step monomer synthesis which required a primary amine to install the sidechain and a degree of polymerization of eight by Ullmann coupling.[104] Leclerc and coworkers have addressed the first half of the monomer synthesis[153] and advanced direct arylation polymerization conditions.[154,155] However, the early selection of the sidechain by an amine precursor and harsh imide formation conditions remain as drawbacks in the synthesis.

The electron withdrawing imide moiety of TPD makes it a compelling monomer in polymers for organic thin film transistors (OTFTs) and organic photovoltaics (OPVs). Copolymers of TPD and dithieno[3,2-*c*:2',3'-*e*]azepine-4,6-dione (commonly bithiophene imide or BTI) with thiophene were studied for OFETs[156,157] with the number of thiophene units affecting the resulting material significantly.[158] These polymers would later give OPV donor polymers with exceptional fill factors approaching 80%.[159] Copolymers of TPD with silolo[3,2-b:4,5-b']dithiophene (DTS) and germolo[3,2-b:4,5-b']dithiophene (DTG) have been studied as OPV materials.[110,160] TPD may benefit from the availability of the imide carbonyl and the thiophene sulfur to participate in non-bonding interactions.[161]

Many of these studies use TPD as an innocent bystander, that is, TPD is rarely the independent variable being modified. Instead, TPD remains as a constant between polymers in a study. While other repeat units have been extensively modified via their sidechains,[162] TPD monomers are almost exclusively limited to alkyl chains due to the requirement of an amine precursor in the typical synthesis. Few other chains (oligoether[163], aryl[164], and alkoyl substituents[165,166]) have been synthesized. These studies have demonstrated the versatility of TPD, but its use remains limited with respect to other nitrogen-based acceptors. For example, on acceptors such as diketopyrrolopyrrole[167] and

isoindigo,[168] (Figure 3.1, Green Box), the sidechain is installed after core construction allowing for rapid, late-stage modifications. Other common acceptors have no option for sidechains at all (Figure 3.1, Blue Box). TPD is one of the acceptors that has a sidechain, but it must be installed early in the synthesis (Figure 3.1, Red Box). Studies that do investigate the sidechain of TPD find significant reason to study them further.[169]

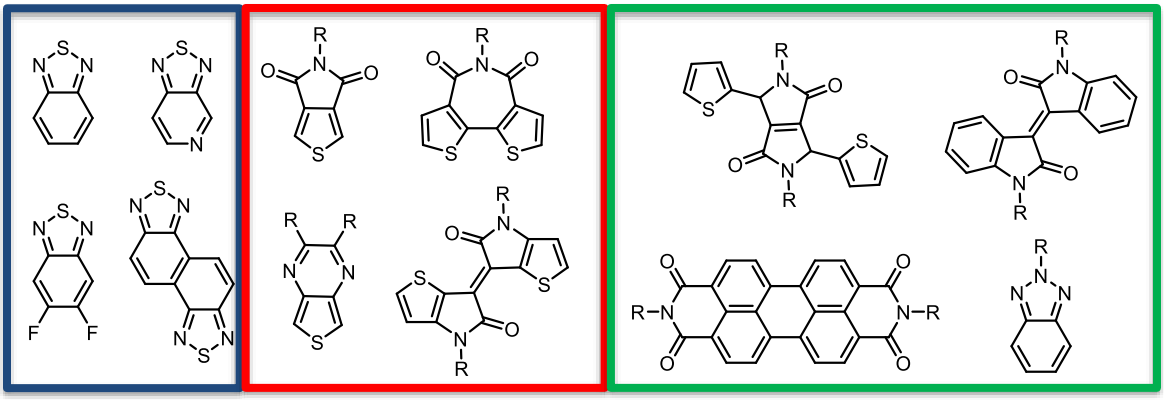

Figure 3.1 – Common electron-deficient monomers used in donor-acceptor polymers. Blue box: Monomers with no sidechain functional points. Red box: Monomers with side chains that are chosen before the final synthesis step. Green box: Monomers with sidechains that are typically installed in the final synthesis step

3.2 Original Syntheses of Phthalimide and Thienopyrroledione

In the search for a cleaner synthesis of thienopyrroledione (H-TPD, Figure 3.2) from 3,4-thiophene dicarboxylic acid, the benzene analog (phthalimide, Figure 3.2) was used as a guide. The synthesis of phthalimide is well established, having been reported by Noyes and Porter and verified independently by Clarke and Bishop in 1922.[170] In their procedure, 500 grams of phthalic anhydride is reacted with two equivalents of aqueous ammonia (aqueous ammonia serves as a convenient source of ammonia as the equilibrium between ammonia and ammonium hydroxide heavily favors ammonia[171]). The mixed amide-acid intermediate is heated until it becomes a homogenous melt near 300 °C. At this point, pure

phthalimide will begin subliming from the reaction mixture. The crude product is considered analytically pure upon cooling, or it can be purified by trituration with cold water. The authors caution that at large scales, a capture device for ammonia is warranted. A final note from the manuscript references previous reports of the diammonium dicarboxylate salt of phthalic acid being heated through the same procedure to give phthalimide.[172] This began the conception of a new synthesis for the unfunctionalized TPD.

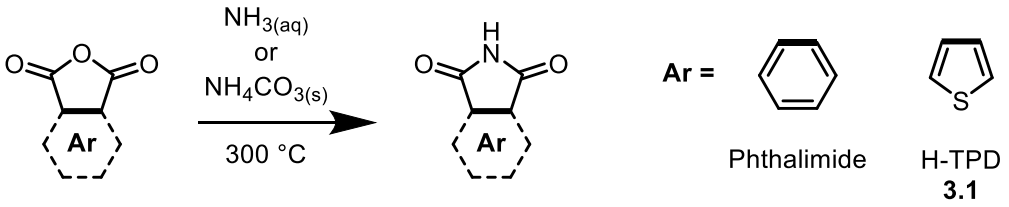

Figure 3.2 – Synthetic route to phthalimide and thienopyrroledione (H-TPD) using aqueous ammonia or ammonium carbonate, the appropriate anhydride, and heat

Compound **3.1** was first reported in 1954 by Sice in a study of thenoic acid absorption bands.[173] The anhydride was converted to the imide through "the usual method" of treatment with aqueous ammonia.[170]

The most commonly reported syntheses of substituted TPDs do not utilize **3.1** as an intermediate; instead, a primary amine is reacted with the anhydride. The anhydride is prepared from the commercially available 3,4-thiophene dicarboxylic acid. This synthesis is outlined in Figure 3.3. From the diacid, the anhydride is formed through a reaction with excess acetic anhydride. Using acetic anhydride as the solvent requires approximately 100 equivalents that are not recovered. The by-product, acetic acid, can be fractionally distilled from excess acetic anhydride[105] However, the inexpensive price of acetic anhydride prevents the reasonable chemist from recovering the excess acetic anhydride.

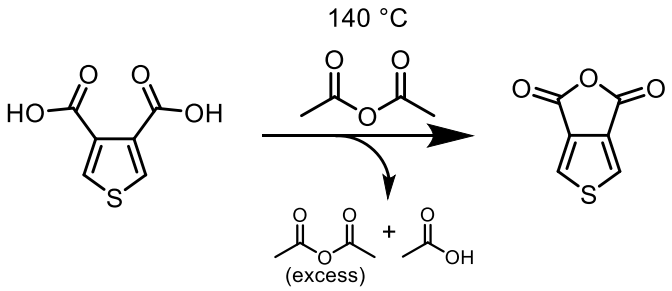

Figure 3.3 – Conversion of 3,4-thiophene dicarboxylic acid to the anhydride in excess acetic anhydride at reflux

The anhydride requires minimal, if any, purification before conversion to the substituted TPD as shown in Figure 3.4. In toluene, the anhydride undergoes ring-opening with a slight excess of a primary amine yielding the mixed amide-acid. Some procedures call for a nucleophile enhancer, such as dimethylaminopyridine (DMAP), to facilitate the reaction. The mixed amide-acid must be collected and washed before continuing with the imide formation, otherwise unreacted amine will react with thionyl chloride, forming a sufinylamine, or with oxalyl chloride, forming an ethanediamide.

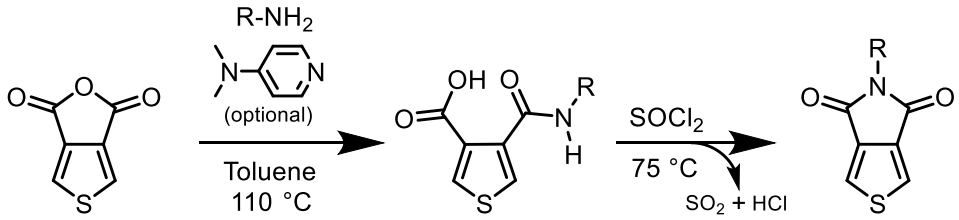

Figure 3.4 – Formation of imide, completing the TPD monomer, using a primary amine to generate an intermediate which is ring closed with thionyl chloride

The mixed amide-acid is ring closed into an imide using thionyl chloride as the reagent and solvent. The generation of the acyl chloride allows for ring-closure and imide formation. The excess reagent can be recovered by distillation at this stage but is usually quenched out of convenience. At larger reaction scales, large volumes of sulfur dioxide and hydrochloric acid are produced and must be treated before venting to the environment. 100 mL of thionyl chloride quenched with water will generate 31 liters of sulfur dioxide

(assuming an ideal gas) and require 154 grams of potassium hydroxide to neutralize the hydrochloric acid. When possible, quenching with an alcohol to generate the *O*,*O*-dialkylsulfite is preferred to releasing sulfur dioxide.[174] Ethanolic potassium hydroxide is good for this procedure, but incompatible with the imide. Storing thionyl chloride reagent for later TPD ring closings requires a proper container lid and seal, as these chemicals are highly corrosive to rubber septa and unlined caps. The desired functionalized TPD is isolated by column chromatography on silica gel.

With the side chain installed, and the imide formed, the monomer is ready for direct arylation polymerizations.[154,155,175] For Stille cross-coupling polymerization, the brominated species is required. Bromination is typically achieved after heating at 55 °C in 3:1 concentrated sulfuric acid to trifluoroacetic acid with three to four equivalents of NBS. This creates significant amounts of bromine fumes which must be quenched before discharge to the environment.

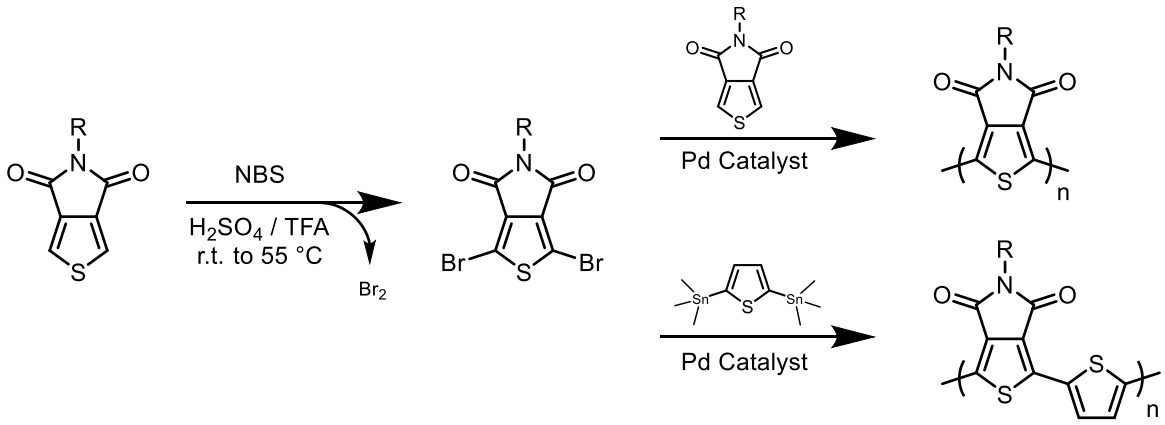

Figure 3.5 – Bromination of TPD using NBS as a bromine source in a strong acid mixture. This prepares the monomer for a wider range of cross-coupling reactions. Homopolymers and Copolymers are accessible by DHAP. Copolymers are accessible by Stille

The clear downside in this synthetic route is the requirement of a primary amine to install the side chain in an early stage. Common side chains include n-octyl[103,110,160] and 2-hexyldecyl[159,176] for solubility. Octylamine is commercially available. 2-hexyldecylamine is not and requires its synthesis from 2-hexyldecan-1-ol shown in Figure 3.6. A Mitsunobu reaction with diisopropyl azodicarboxylate and triphenylphosphine attaches the alcohol directly to phthalimide. Then, as in the Gabriel amine synthesis, treatment with hydrazine releases the amine.

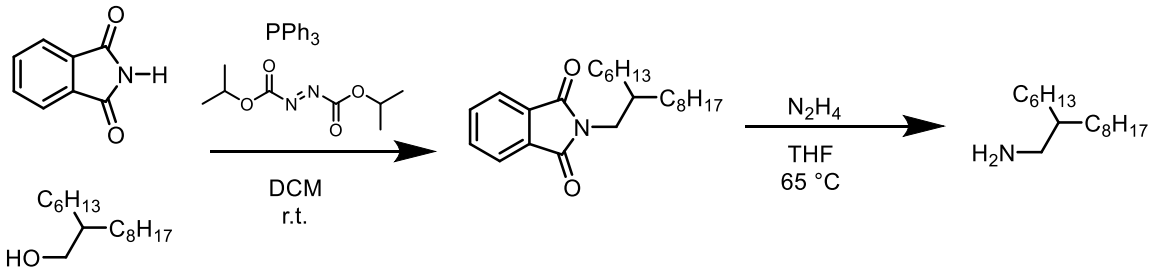

Figure 3.6 – Representative Mitsunobu coupling of 2-hexyldecan-1-ol to phthalimide before liberation of the amine with hydrazine

To circumvent this cumbersome step, compound **3.1** is the ideal target. However, early reports of TPD report difficulties of its synthesis.[104] The unsubstituted thiophene imide remained out of the literature for over 50 years, before the synthesis of its brominated analog was reported by Griffini et al. in 2011, shown in Figure 3.7.[177] The synthesis follows a similar path as previous TPD syntheses with the exception of bromination occurring before the anhydride formation. The brominated anhydride is converted to the mixed acid/amide using three equivalents of ammonia from a methanol solution. Ring closure is accomplished using carbonyldiimide (CDI) and triethylamine. While this route gives the desired unsubstituted imide, the continued use of excess reagents and dry ammonia prevent the widespread adoption of the synthesis. Functionalization of H-TPD-Br_2 is achieved by deprotonation with sodium hydride and quenching with an electrophile. This limits the reaction to exclusively the dibromide as a substrate, as sodium hydride can deprotonate with the thiophene α-position.

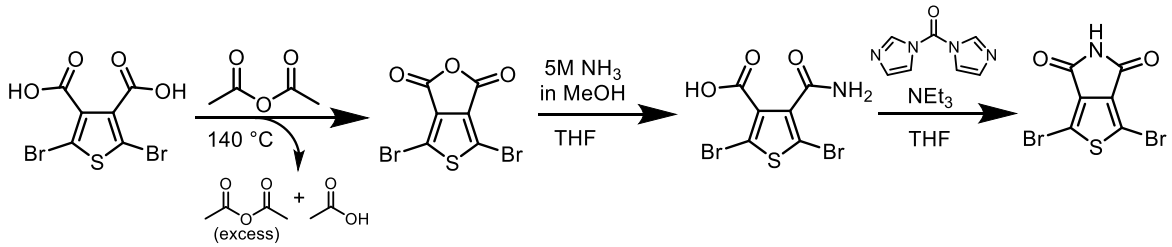

Figure 3.7 – An alternative route to the unfunctionalized, brominated TPD monomer unit

A related route bypassing the anhydride was investigated by Beaupré et al.[178] during the synthesis of furan analogs of TPD. Formation of the diacid chloride from the reaction of oxalyl chloride on 3,4-thiophene dicarboxylic acid gives a reactive intermediate that can directly form the imide through reaction with a primary amine (Figure 3.8). My attempts at this reaction gave unsatisfactory yields compared to the longer route and was abandoned – an indication that chemists will still use dangerous reagents if the yields are higher and more consistent. Additional synthetic attempts from the diacid chloride were made with anilines to create a series of N-aryl TPDs. Again, the reaction is successful, but the setup to create and then isolate the diacid chloride from highly corrosive reagents is cumbersome.

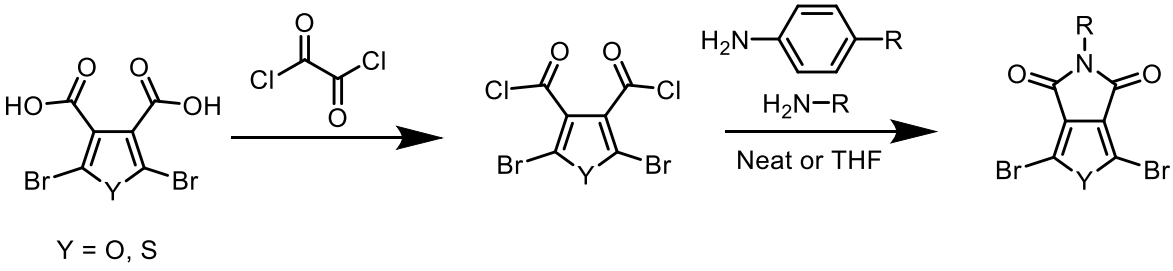

Figure 3.8 – Attempt at direct imide formation through diacid chloride

I begin the refinement of the TPD synthesis starting with 3,4-thiophene dicarboxylic acid, which is commercially available. The first syntheses of the diacid required a four-step synthesis starting from thiophene (shown in Figure 3.9). Tetrabromination of thiophene, followed by selective cleaving of the 2,5 bromines with

zinc gives 3,4-dibromothiophene. Conversion to the thiophene-3,4-dicarbonitrile requires potassium cyanide. Alternatively, lithium-halogen exchange on 3,4-diiodothiophene can be quenched with dry ice to give the diacid.[173] Leclerc and coworkers have previously reported an efficient two-step process to generate the diacid using the Gewald thiophene synthesis, the Sandmeyer reaction for removal of the amine, and hydrolysis of the esters.[153] Therefore my focus was shifted to final steps of monomer preparation which still consumed considerable time and reagents.

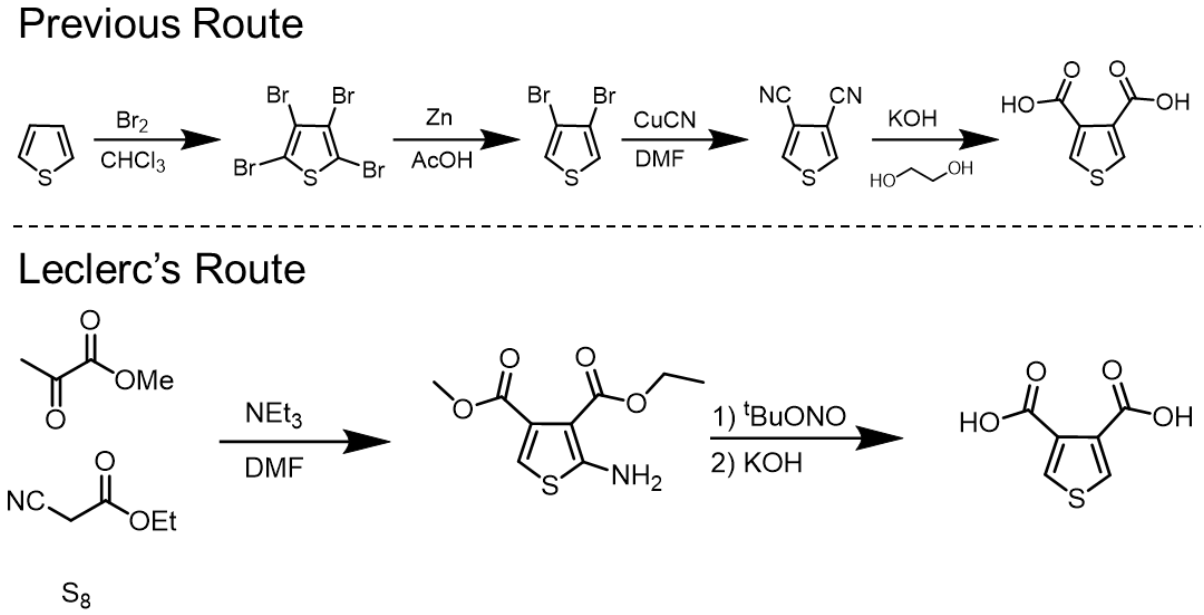

Figure 3.9 – Comparison of old and new syntheses to dicarboxylic acid

3.3 Synthesis of Unsubstituted TPD

3.3.1 *Reaction Setup, Purification, and Analysis of H-TPD*

Our synthetic route was inspired by the original synthesis of H-TPD using aqueous ammonia with thiophene-3,4-dicarboxylic anhydride.[173] However, we were especially interested in avoiding the anhydride. The note by the authors in Organic Syntheses[170] led

us to attempt the creation of **3.1** directly from the dicarboxylic acid. The reaction with hypothesized intermediates is shown in Figure 3.10. The proposed mechanism results in the formation of the anhydride with a closely associated molecule of ammonia immediately acting upon the anhydride to form the mixed amide-acid. Ring closure is thermally driven on to give **3.1**.

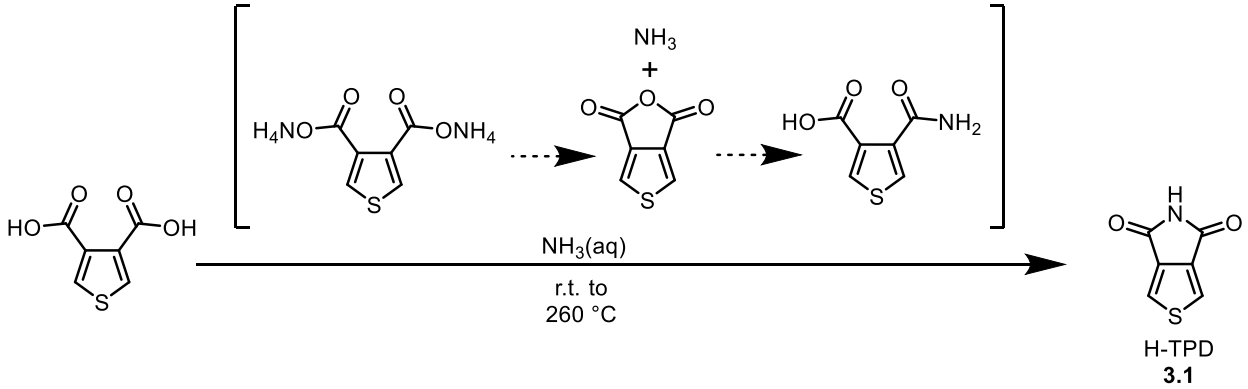

Figure 3.10 – Improved reaction of 3,4-thiophene dicarboxylic acid to the unsubstituted thienopyrroledione (3.1) with proposed reaction intermediates above

The diacid was fully dissolved in minimal concentrated aqueous ammonia. Excess ammonia and water were removed by gentle heating or rotary evaporation to give a white solid. Complete conversion to the diammonium salt was confirmed by ^{1}H NMR spectroscopy shown in Figure 3.11. After treatment with ammonia, the carboxylic acid proton (H_c, δ=13.0 ppm) disappears, and a signal indicative of an ammonium cation (H_b, δ = 7.1 ppm) appears. The solid was then heated, neat, to 260 – 280 °C. At the typical reaction scale of ten millimole, the reaction does not become a homogeneous melt as previously described. Instead, product was observed directly subliming from the reaction flask. The crude product slowly sublimed from the reaction and deposited around the neck of the round bottom flask and in the condenser. After cooling the reaction setup to room temperature, the product was collected by scraping the solids from the sides of the flask

and condenser. When mechanical removal was impractical, acetone or acetonitrile were used in conjunction with sonication to collect the product.

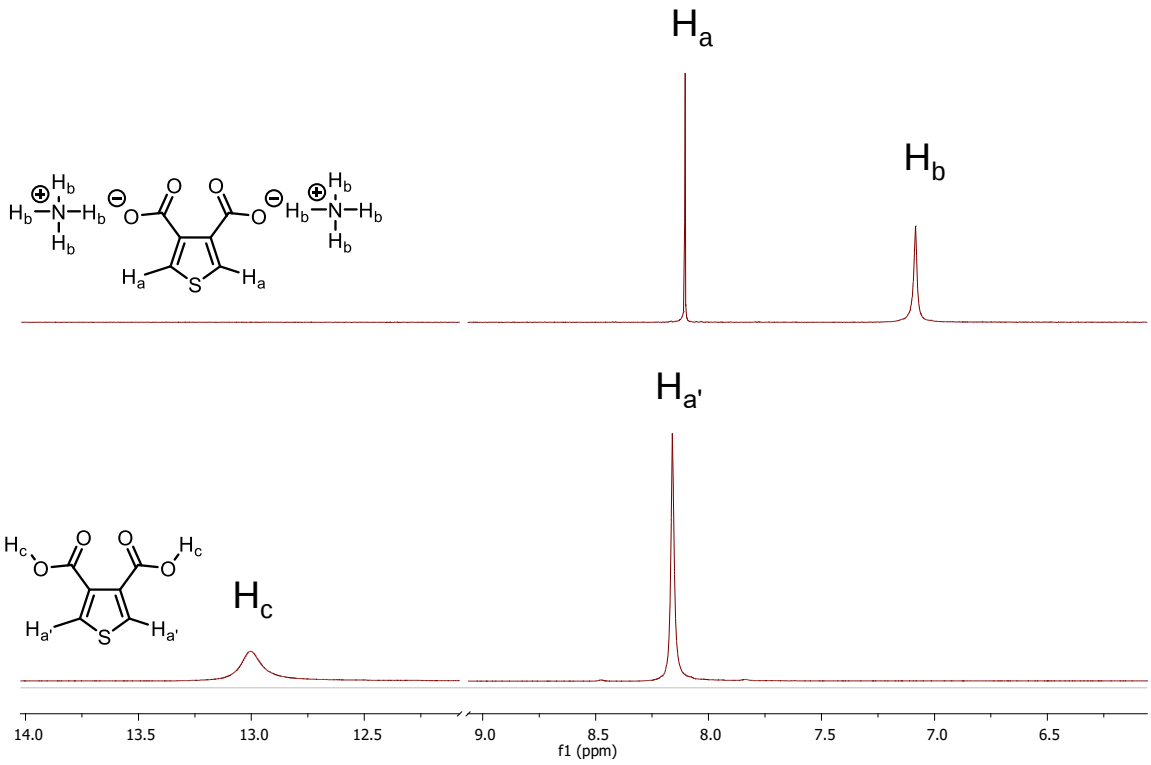

Figure 3.11 – ^{1}H NMR Spectra of the 3,4-thiophene diammonium carboxylate (top) and dicarboxylic acid (bottom) in DMSO-d_6

The reaction is independent of the reaction apparatus if the following requirements are met. The glassware reaches temperatures approaching 300 °C. The thermometer should be able to measure to 400 °C; the Keck clips should be metal or not used at all – polyacetal Keck clips will melt; the ground glass joints should be protected with PTFE tape – most laboratory greases will not withstand 300 °C temperature. The condenser should be sufficiently long to cool exit gasses and deposit TPD completely. A high surface area condenser is not recommended, as it will be very difficult to mechanically remove the low solubility H-TPD product afterwards. If the condenser is too long or has a sufficiently large heatsink attached (metal clamp), water will not escape the reaction and continually drip

back into the reaction flask. This can be prevented with a Dean Stark apparatus. Heating rates and times are flexible – the product is stable at high temperatures – provided loses due to sublimation are prevented.

3.3.2 *Common Impurities during Imide Formation*

While the phthalimide procedure obtains pure product directly from the reaction, this reaction on thiophene has several impurities that are beneficial to remove before continuing the synthetic route. Common impurities are the starting material or its ammonium salt, the mixed amide-acid intermediate, and thiophene-3-carboxamide from thermal decarboxylation of the intermediate.

The impurities can be removed through recrystallization, sublimation, or trituration. Trituration in water is the recommended purification technique due to its simple procedure and low hazardous waste generation. The ammonium salt is highly soluble in water and can be easily removed with minimal loss in yield. Acetonitrile effectively solubilizes thiophene-3-carboxamide while acting as a suitable recrystallization solvent for the imide. However, the required volume of acetonitrile may become prohibitive as the scale of the reaction is increased. Sublimation generates no additional hazardous waste but requires a multizone furnace or other specialized apparatus.

A Kugelrohr was found to be the most convenient apparatus for temperature control and separation. With the Kugelrohr furnace set at 140 – 160 °C and at ~10 mbar, thiophene-3-carboxamide sublimes into the chilled bulb. It fluoresces a violet color under 365 nm light. The product sublimes to the intermediate bulb, cleanly subliming from the crude material but depositing before the chilled bulb. It fluoresces a cyan blue color under 365

nm light. Unreacted starting material, intermediate salts, and/or decomposition products do not sublime from the crude chamber under these conditions.

3.3.3 *Unsuccessful Reaction Conditions*

Working at elevated temperatures with a material that sublimes readily is not convenient. Several other reaction setups were attempted to ease the reaction procedure.

1. Direct conversion of the diacid to the imide was attempted in a laboratory microwave to give more effective control over outgassing and temperature. While release of water and ammonia byproducts can be effectively managed with the pressure-venting sequence, sublimation was a concern in the microwave vial. This method was not found to be more convenient than the traditional synthesis.
2. The reaction was attempted in a sublimation apparatus at atmospheric pressure. The temperature difference between the sand bath and the condenser causes convection currents to form in the reaction chamber. This method was not successful.

3.3.4 *Bromination of H-TPD*

With the unfunctionalized H-TPD in hand, the focus shifted to bromination. The unfunctionalized, brominated TPD (**3.2**) was desired as some side chains contain functional groups that would not survive the harsh bromination conditions shown in Figure 3.12. However, the electron withdrawing imide moiety increases the required driving force for the reaction. While the bromination of 3,4-thiophene dicarboxylic acid is known under less harsh conditions (AcOH and Bromine),[177] the doubled molecular weight (153 to 311 Da) increase the temperature required for sublimation of the imide, and the bromides decrease the thermal stability.

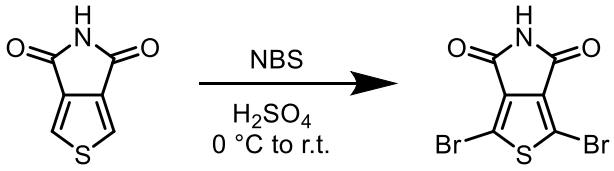

3.1 **3.2**

Figure 3.12 – Bromination of the unfunctionalized imide avoiding the use of trifluoroacetic acid

To avoid optimizing the reaction for each sidechain, or exposing sidechains to harsh brominating agents, I developed new conditions for brominating the unfunctionalized imide. Heating was not an option due to the observed hydrolysis reaction. Thus, a sufficiently strong driving force needed to be applied at room temperature or below. Sulfuric acid was observed to give the proper solubility and polarity. Four equivalents of NBS in cold concentrated sulfuric acid gave the pure, desired product after quenching over ice. The reaction can be monitored by TLC on standard silica gel plates in 10% ethyl acetate in dichloromethane after quenching an aliquot. The use of trifluoroacetic acid was avoided in this way.

3.3.5 *Unsuccessful Bromination Conditions*

Bromination conditions which did not require strong acids were desired. Polar solvents were investigated due to their ability to stabilize the Wheland intermediate. No suitable alternative to sulfuric acid was found. A list of unsuccessful reactions is given below:

1. Glacial acetic acid ($\varepsilon_r = 6.5$) and liquid bromine. The imide was not soluble in acetic acid at 55 °C, and ^{1}H NMR spectroscopy indicated only starting material. The imide appears to hydrolyze when heating to 100 °C.

2. Glacial acetic acid (ε_r = 6.5) and liquid bromine at 110 °C in sealed microwave vial. No material, starting material or otherwise, was recovered.
3. Liquid bromine (ε_r = 3.1)[179] as solvent and reagent at 55 °C. The imide was poorly soluble in bromine. ^{1}H NMR spectroscopy indicated ~6% conversion to any brominated species by imide proton integration.
4. Concentrated sulfuric acid (ε_r = 8.6) and liquid bromine at 50 °C. Bromine is not miscible with sulfuric acid. ^{1}H NMR spectroscopy detects thiophene-3-carboxamide indicating hydrolysis and decomposition of the imide is occurring.
5. Concentrated sulfuric acid (ε_r = 8.6), trifluoroacetic acid (ε = 8.6), and *N*-bromosuccinimide at 55 °C. Destruction of the imide during the reaction or the workup was observed.
6. THF (ε_r = 7.6) and *N*-bromosuccinimide at reflux. No bromination occurred. The starting material was recovered quantitatively.
7. Dimethylformamide (ε_r = 36.7) and *N*-bromosuccinimide. At 0 °C, no reaction occurred. At 80 °C, no material was recovered.

3.4 Side Chain Selection and Expansion

3.4.1 *Bringing N-Functionalized Acceptor Sidechains to TPD*

Functionalization of both **3.1** and **3.2** was desired with a single set of reaction conditions. The literature procedure for functionalizing TPD using sodium hydride in tetrahydrofuran[165] was unsuccessful in my hands. Seeking milder general conditions potentially useful for all TPD derivatives, I employed potassium carbonate in dimethylformamide (DMF) – a procedure adapted from the alkylation of isoindigo.[180]

Because DMF readily solubilized the TPD imides and all sidechain precursors used in this study at room temperature, functionalization reactions were run at room temperature. Heat was not required to drive reactions forward, and all attempts at heating were unsuccessful. The expanded selection of side chains is shown in Figure 3.13.

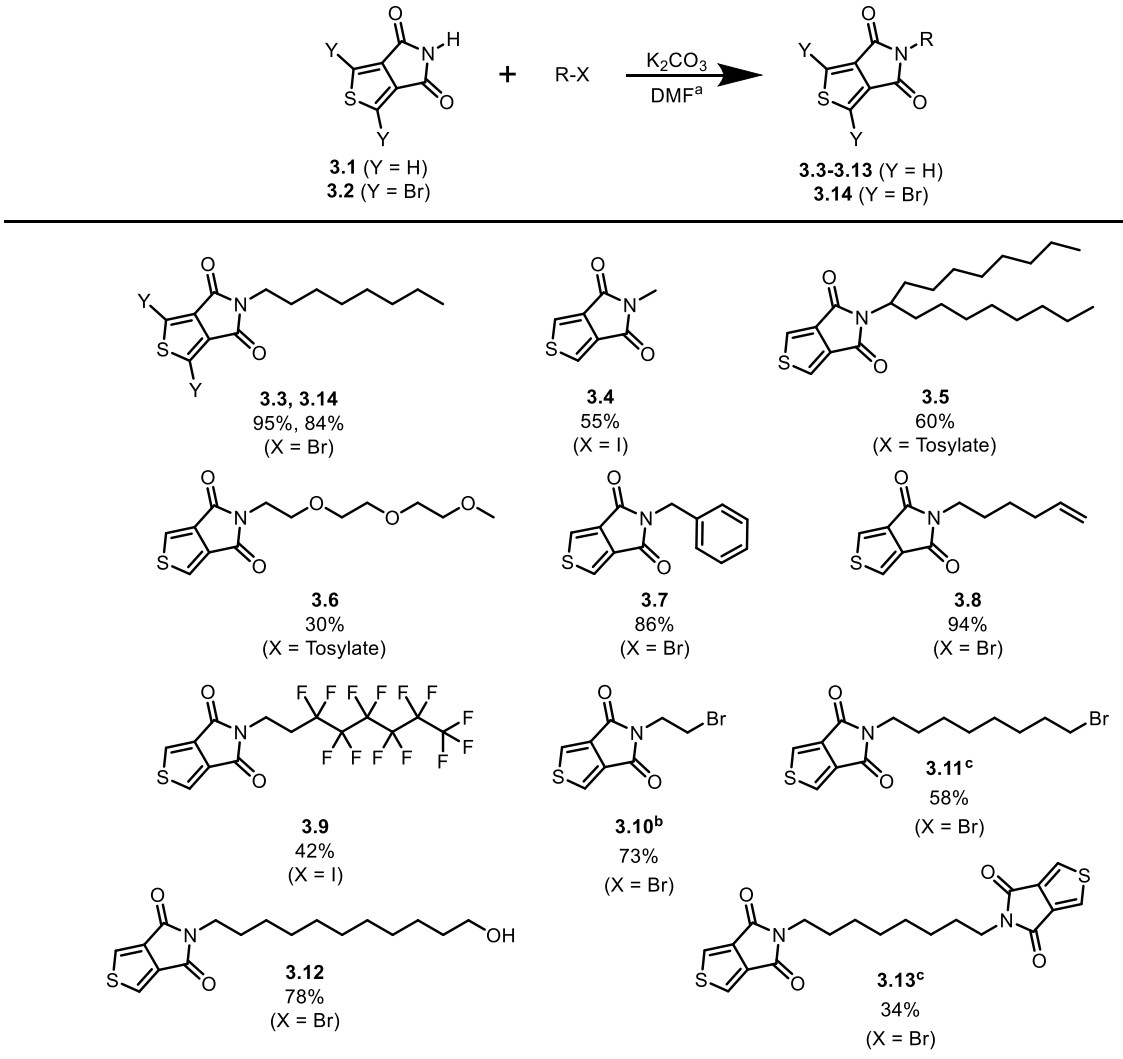

Figure 3.13 – Primary functionalization of 3.1 and 3.2. [a]Isolated yields are shown. Unoptimized reaction conditions: Imide (1.0 equiv.), R-X (1.5 equiv.), K_2CO_3 (2.0 equiv.), DMF (0.1 M), r.t. [b]Formation of dimer not observed [c]1.0 equiv. of 1,8-dibromooctane used, forming 3.11 and 3.13 in the same reaction. 92% overall conversion of 3.1 to products 3.11 and 3.13

To show these reaction conditions were viable for the most common TPD monomers, I first repeated the synthesis of primary and secondary alkyl chains. These were synthesized using halides (1-bromooctane, **3.3, 3.14**) or tosylates (9-tosylheptadecane, **3.4**) as leaving groups, eliminating the need for an amine synthesis, as is required for 5-(2-hexyldecyl)thienopyrrole-4,6-dione using the commercially available 2-hexadecan-1-ol[181]. This especially simplified the synthesis of the methyl derivative (**3.4**). Where methyl iodide is an easily handled liquid, methylamine is a gas at room temperature and is a DEA List I chemical.[182]

Sterics of the electrophile affected the reaction success. Reactions at primary, secondary, and benzylic (**3.7**) carbons proceeded without issue. We were unable to extend these conditions to a tertiary electrophile, tert-butyl bromide. Heating at 50 °C or 100 °C overnight did not promote product formation. When using 1,8-dibromooctane as an electrophile, the stoichiometry was set to allow both mono (**3.11**), and disubstitution, (**3.13**). Interestingly, dimer formation was not seen when using 1,2-dibromoethane as an electrophile, even when **3.10** was reacted with excess imide.

The choice of sidechain has a dramatic impact on the final properties and uses of the TPD derivatives. Oligoether chains (**3.6**) have been investigated previously to produce amphiphilic materials, but the ether chains are particularly susceptible to bromination. They are postulated to affect dielectric constant in conjugated polymers[183,184] and have been used in Langmuir–Blodgett deposition techniques.[163] The yield of **3.6** was reduced by difficulty in chromatographic separation from the tosylate electrophile. Treating the reaction with excess lithium bromide quenches any remaining tosylate starting material and eases purification significantly. Perfluoroalkyl chains are popular for improving n-type

mobilities[185] and for their solubility in perfluorinated solvents.[186] To avoid special conditions often required for attaching perfluoroalkyl chains, electron deficient 1H,1H,2H,2H-perfluorooctyl chains were used in this study to give (**3.9**) in satisfactory yield.

3.4.2 *Post installation modification*

The mild reaction conditions allow for sidechains that would normally react or decompose under the previous reaction conditions. Specifically, **3.8**, **3.11**, and **3.12** present latent functionality end-groups that are useful for post polymerization functionalization or for diversifying monomer units, Figure 3.14. **3.11** was functionalized to the nitrile derivative (**3.15**), useful for increasing dielectric constant,[187] to the azido derivative (**3.16**), useful for cross-linking to make thermally stable, solvent resistant films,[188] and to a pyridyl group (**3.17**), useful for creating conjugated polyelectrolytes for fluorescence sensing systems,[189] electrochromic films,[190] interlayers in OPV,[191] and for thermoelectrics.[192] Hydrosilylation with Karstedt's catalyst gave a siloxy terminated alkyl chain (**3.18**) that has been shown to reduce π -π stacking distances and increase mobility in solution cast films of isoindigo-based molecules.[193]

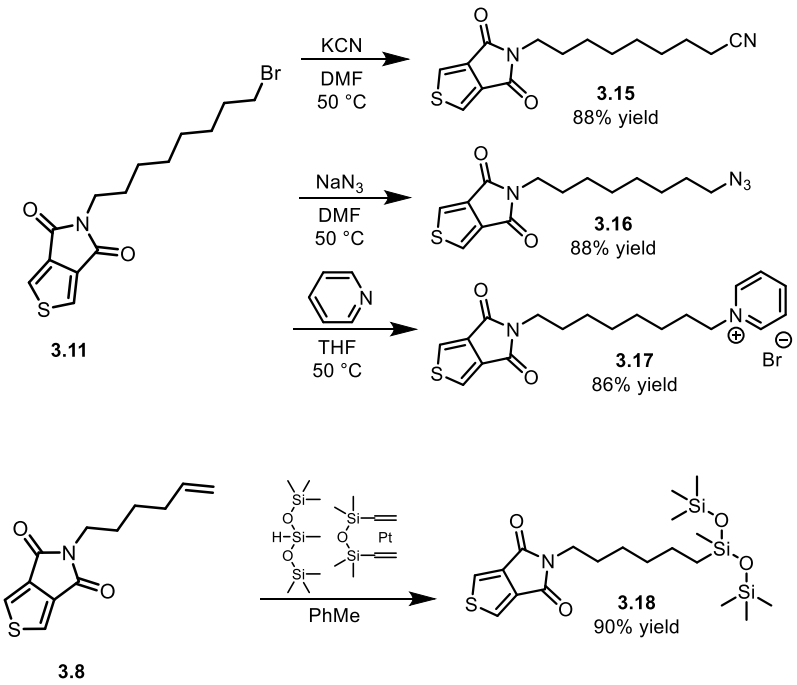

Figure 3.14 – Post functionalization modifications to sidechains on TPD

3.4.3 *PhenylTPDs through Chan-Lam Coupling*

Aryl *N*-functionalization of TPD is challenging due to the lower solubility of the resulting TPDs and the need to purchase or synthesize custom anilines as precursors. By using Chan-Lam couplings, as shown in Figure 3.15, completed with boroxines (dehydrated boronic acid rings), I arrived at arylated TPD (**3.19**) without the need for anilines.

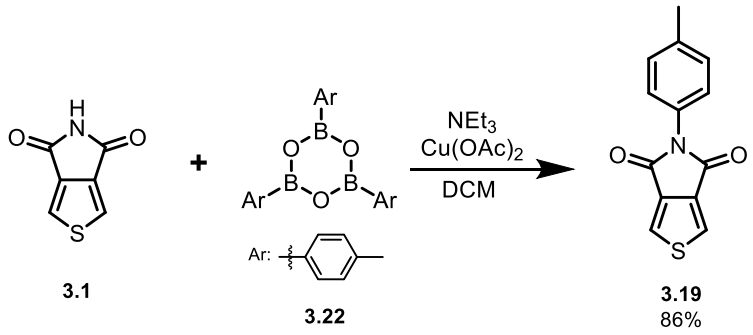

Figure 3.15 – Chan-Lam coupling of an aryl boroxine to the imide of TPD using mild conditions

3.5 Porting of Reaction Conditions to Other Thiophene Imides

We have extended our conditions to the synthesis of unfunctionalized dithieno[3,2-*c*:2',3'-*e*]azepine-4,6-dione (commonly known as 2,2'-bithiophene-3,3'-dicarboximide or BTI) (**3.21**) as illustrated in Figure 3.16. The synthesis of BTI suffers the same drawbacks of TPD preparation – excess corrosive reagents, early sidechain installation, and sidechain installation via amine precursor.

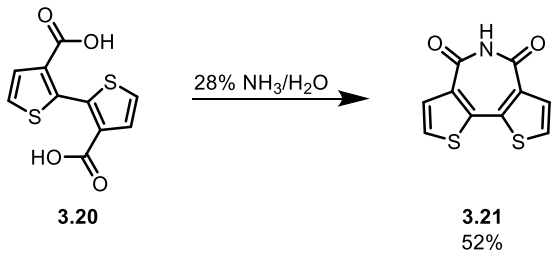

Figure 3.16 – Synthesis of a bridged thiophene imide resulting in the synthesis of the common OPV acceptor moiety, BTI

Initial reaction attempts again employed the Kugelrohr for its temperature control and ease of running the reaction under reduced pressure if needed. As with **3.1**, conversion to the diammonium salt was very easily obtained. The dried powder was collected by rotary evaporation before the next step. Compound **3.21** did not form using the Kugelrohr under atmospheric conditions or the traditional setup used for **3.1**. The reaction temperature was

pushed to 300 °C, the upper limit of the Kugelrohr. This lead to a char forming in the reaction vessel and unknown decomposition products. From these reactions, it was concluded that **3.21** is not stable under atmospheric conditions at the temperatures required for the molecule to form or sublime. This was later confirmed during melting point analysis of **3.21,** during which it melts and decomposes at 250 °C.

To avoid exposure to atmosphere and to lower the temperature of sublimation, Kugelrohr sublimation at ~10 mbar was attempted. Slowly increasing the temperature appeared to give similar results as the sublimation of **3.1**: a forefront material of off-white powder with light blue fluorescence is 2,2'-bithiophene-3-carboxylic acid; middle section of yellow powder with light green fluorescence was suspected to be **3.21**; and the reaction vessel retained an off-white or black powder that fluoresces a light violet color, the unreacted starting material. However, the suspected **3.21** was not stable to methanol or mildly basic aqueous conditions. ^{1}H NMR spectroscopy indicated complete hydrolysis back to **3.20** after exposure to aqueous base (0.1M KOH). The reduced pressure reaction was yielding the anhydride, but not the imide. From these experiments, it was hypothesized that the anhydride may be an intermediate in the formation of the imide. In the case of **3.1** under atmospheric conditions, the liberated ammonia is present to react with the formed anhydride. Under partial vacuum, the liberated ammonia is unable to react with the formed anhydride.

Knowing that BTI is unstable at the temperatures required for sublimation at atmospheric pressure, and that the amide does not form at temperatures reached at sub-atmospheric pressures, a different reaction protocol was devised. To reach the desired reaction temperatures without decomposition under atmospheric pressure, the new protocol

had to involve an inert atmosphere. To encourage the movement of the imide away from the starting material (beyond relying on solely the thermal gradient), a flow-through apparatus was desired. A tube furnace with a thermal gradient and light flow of argon met these criteria and was employed.

Heating the diammonium salt at 240 °C with a flow of 15 mL/min of argon gave a mixture of the anhydride and **3.21**. The presence of the anhydride was confirmed by 1H NMR spectroscopy using a literature preparation of the anhydride.[156] This indicated that the reaction conditions allowed for the formation of the imide, but there continues to be a deficiency of ammonia in the reaction chamber. Compound **3.21** was separated from the anhydride by ring-opening the anhydride on silica gel and eluting the stable imide with ethyl acetate. While this reaction provided **3.21**, the loss in yield associated with the anhydride was undesirable.

To increase the availability of ammonia and ensure conversion of the anhydride to the imide, the flow of argon was bubbled through concentrated aqueous ammonia before entering the tube furnace apparatus. In this way, the environment always had an available supply of ammonia for imide formation, and **3.21** was the majority product with only traces of anhydride.

3.6 The Impact of this Work Through the Lens of Green Chemistry Principles

Synthetic chemistry, especially in organic electronics, is heavily directed towards the development of new structures for particular properties and applications. Work is focused on obtaining the end product; however, more and more focus is being applied to renewable feedstocks and safer chemical transformations. This effort is highlighted by the Twelve

Principles of Green Chemistry.[194] Initial development and testing of organic electronic materials in an academic laboratory typically require less than one gram of polymer material for a complete study. As research moves from material development to processing conditions, an increase demand for material arises. The stochiometric generation of tin waste from Stille couplings and 100-fold excesses of thionyl chloride no longer are viable reaction conditions. This section will outline the impact the reactions described in this chapter have on the safety concerns and waste generation in the manufacture of TPD.

In a review of common conjugated polymers for organic photovoltaics, Po *et al.* evaluated the synthetic complexity of repeat units based on number of synthetic steps, overall yields, purification requirements, and the use of hazardous materials.[151] TPD and BTI score remarkably well despite typical syntheses requiring a number of hazardous reagents[104,165,177] Their analysis does not take into account the Gabriel synthesis of amine precursors, which requires diisopropylazidodicarboxylate (DIAD) and hydrazine. The authors were making the point that poly(3-hexylthiophene), despite its lower performance, is superior to many other "designer" polymers that require multiple syntheses and purifications steps to get to viable monomers. However, the traditional goal of synthesis in an organic electronics laboratory is to create the final product for further testing. The synthetic route is a means to an end. Replication of that material follows the reported literature synthesis as the path of least resistance. This project attempts to optimize the syntheses of a common OPV monomer, TPD, to limit the time and resources consumed while simultaneously expanding the sidechain functionality. Six of the twelve Principles of Green Chemistry[194] have been implemented while simultaneously expanding the utility of TPD by

I. Preventing waste: It is better to prevent waste than to treat or clean up waste after it has been created.

II. Maximizing atom economy: Synthetic methods should be designed to maximize the incorporation of all materials used in the process into the final product.

III. Using less hazardous chemical syntheses: Wherever practicable, synthetic methods should be designed to use and generate substances that possess little or no toxicity to human health and the environment

V. Using safer solvents and auxiliaries: The use of auxiliary substances (e.g., solvents, separation agents, etc.) should be made unnecessary wherever possible and innocuous when used.

VI. Designing for energy efficiency: Energy requirements of chemical processes should be recognized for their environmental and economic impacts and should be minimized. If possible, synthetic methods should be conducted at ambient temperature and pressure.

VIII. Reducing unnecessary derivatization: Unnecessary derivatization (use of blocking groups, protection/ deprotection, temporary modification of physical/chemical processes) should be minimized or avoided if possible, because such steps require additional reagents and can generate waste.

The creation of one mole of 1,3-dibromo-5-(2-hexyldecyl)thieno[3,4-*c*]pyrrole-4,6-dione final product using reported yields and reagents in the literature (Figure 3.17)[104,195] and the reported yields and reagents in this chapter (Figure 3.18) is used as an illustration of the benefits of the newly developed reaction conditions. When estimating conditions for scaled-up reactions, the reagents used scale linearly, while the amount of solvent or workup auxiliaries is unlikely to scale linearly and is more difficult to estimate. Piccinno et al. suggest a 20% reduction in solvent used when transition from laboratory to pilot scale.[196] In this example, both reagents and solvents are both estimated on a linear scale, while auxiliaries are mentioned but not calculated.

The traditional route requires six synthetic steps, one with cooling to 0 °C, and the other five with heating from 65 – 140 °C. The new route achieves the same material in just four steps with only one step requiring the addition of heat. (Principle I, III, VI).

Both routes begin with the 2-hexyldecan-1-ol and 3,4-thiophene dicarboxylic acid. The traditional route requires 3.5 moles of the alcohol for one mole of final product. The new route requires 2.0 moles. Both routes require approximately 2.0 moles of 3,4-thiophene dicarboxylic acid. Given the expense of these starting materials, any reduction in waste comes with significant cost benefits. (Principle I, II).

The traditional route uses phthalimide (3.89 mol), triphenylphosphine (3.89 mol), DIAD (3.89 mol), acetic anhydride (9.3 L), and thionyl chloride (34 L) of which no atoms remain in the final material. The new route uses *p*-toluenesulfonyl chloride (1.98 mol), triethylamine (3.97 mol), trimethylamine hydrochloride (0.20 mol), and potassium carbonate (2.38 mol) of which no atoms remain in the final material. (Principle II, VIII).

The traditional route requires three aqueous workups and extractions (Step 1, 3, 6), three recrystallizations (Step 3, 5, 6), and three chromatographic separations on silica gel (Step 1, 5, 6). In contrast, the new route requires one aqueous workup and extraction (Step A), zero recrystallizations, and two chromatographic separations on silica gel (Step A, D). Trituration or filtration are sufficient purification techniques for Step B and C. The traditional route generates the hazardous byproducts acetic acid (Step 3), hydrochloric acid and sulfur dioxide (Step 5), and bromine (Step 6). The new route generates only bromine as a hazardous byproduct (Step D). (Principle I, V).

The new route brings a significant reduction in the amount of required reagents and solvents, notably the complete removal of thionyl chloride (OPCW Schedule III Chemical)[197] and trifluoroacetic acid (an environmentally persistent chemical). (Principle I, III).

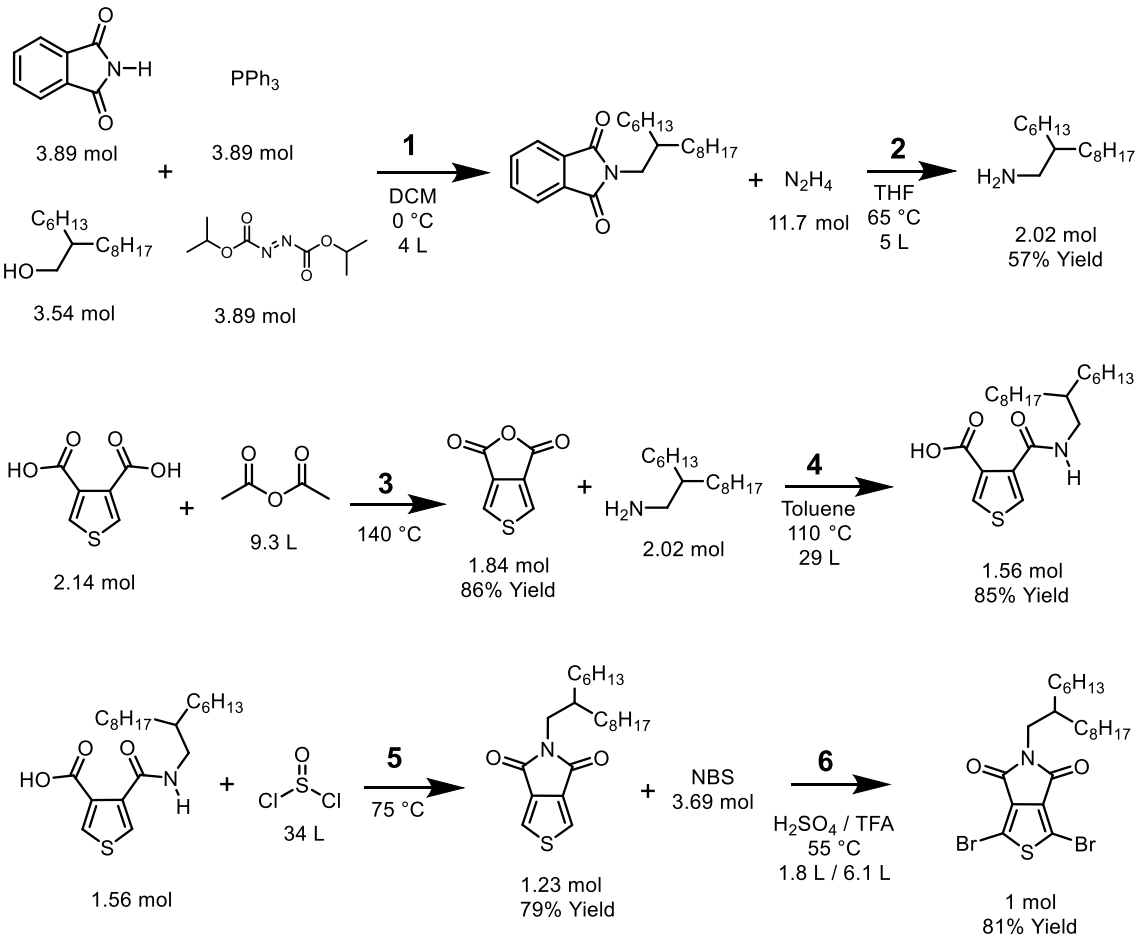

Figure 3.17 – Synthetic requirements for one mole of 1,3-dibromo-5-(2-hexyldecyl)thieno[3,4-*c*]pyrrole-4,6-dione using literature procedures

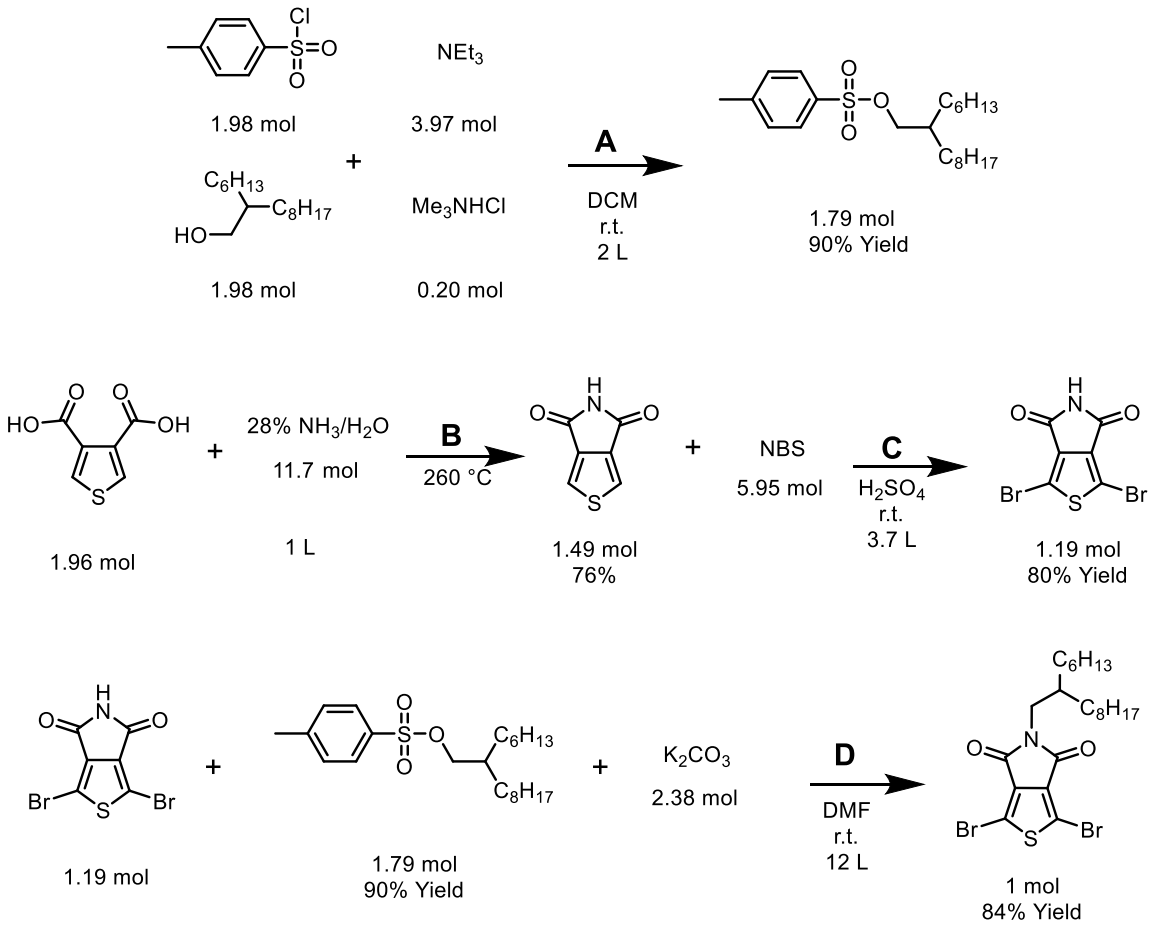

Figure 3.18 – Synthetic requirements for one mole of 1,3-dibromo-5-(2-hexyldecyl)thieno[3,4-*c*]pyrrole-4,6-dione using the chemistry developed in this thesis

3.7 Overview of Work Facilitated through this Reaction

The benefit of green chemistry has no impact if the procedures are not implemented. Post-doctoral researchers, graduate students, and visiting scholars within the Reynolds Group have utilized this chemistry to create functionalized TPD monomers for fundamental studies which would have otherwise been synthetically challenging to achieve.

Dr. Bing Xu has synthesized a family of TPD-based polymers with straight chain functionality with the corresponding nitrile terminated derivates. Through the traditional

TPD synthesis, an α-amino alkane nitrile is required. The synthesis from literature reports starting with commercially available 1,4-dibromobutane is presented in Figure 3.19. Nucleophilic attack with potassium cyanide gives a statistical ratio unsubstituted, monosubstituted, and disubstituted products.[198] After isolation by distillation, the remaining bromide is converted to an azide in high yield.[199] The azide is reduced to the amine with triphenylphosphine via the Staudinger reaction.[199] The predicted yield of the amine is 41% with 16% atom economy. The predicted yield of the functionalized TPD using reported literature yields[104] is 24% across six steps with 23% atom economy.

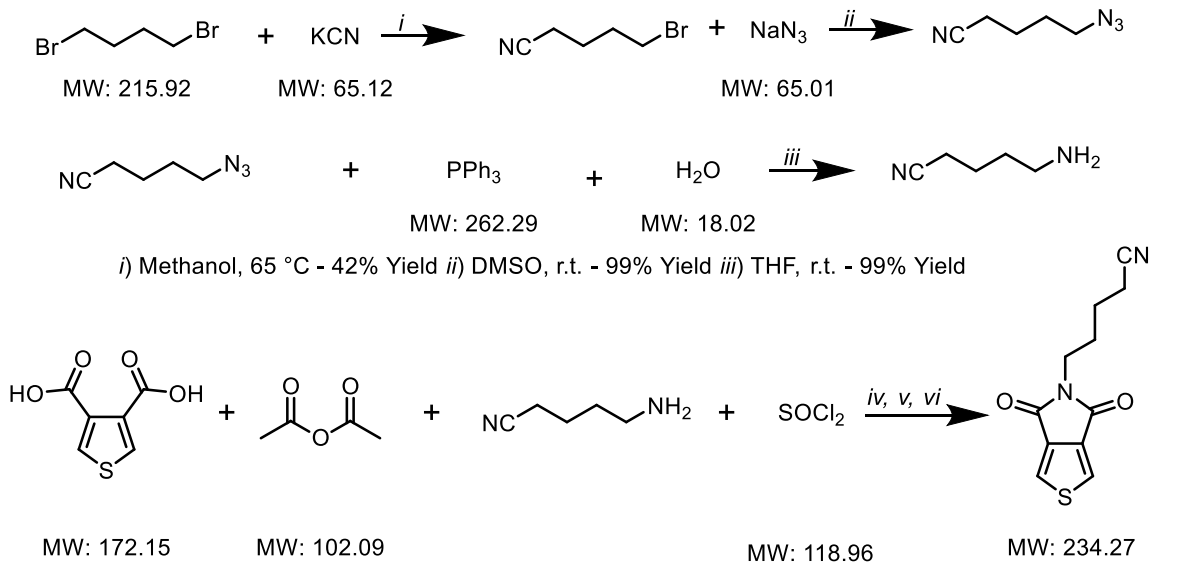

Figure 3.19 – Synthesis of the required amine precursor and final synthesis of 5-(5-nitrilopentyl)thieno[3,4-*c*]pyrrole-4,6-dione

The monomer can be prepared from the same starting materials through just three reactions demonstrated in this thesis, Figure 3.20. These reactions give a predicted overall yield of 39 to 62% (estimated using yields of **3.1**, **3.11**, **3.13**, and **3.15**) with an atom economy of 39%. The simultaneous increase in atom economy and overall yield across

three fewer steps illustrates the benefit of these reactions beyond the reduced generation of hazardous waste and safer reagents.

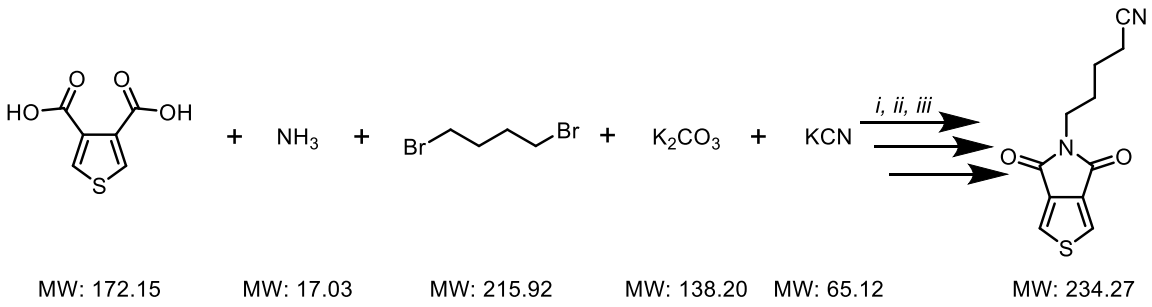

i) Neat, 240 °C - 76% Yield *ii*) DMF, r.t. - 58 to 92% Yield *iii*) DMF, 50 °C - 88% Yield

Figure 3.20 – Atom economy analysis of 5-(5-nitrilopentyl)thieno[3,4-*c*]pyrrole-4,6-dione utilizing three sequential reactions presented in this thesis

Graduate students Brian Schmatz and Abigail Advincula have utilized this chemistry in a project to understand minimally functionalized electron deficient monomers in OPV polymers. The traditional synthetic route of TPD requires methylamine as a reagent. Methylamine (b.p. –6 °C) must be purchased as a pressurized gas or in solution and has the added detriment of being a DEA List I chemical precursor because of its use in the manufacturing of methamphetamine.[182] The alternative route described in this thesis uses methyl iodide (b.p. 42 °C), a liquid under ambient conditions with no legal restrictions on purchasing.

Visiting scholars Jungho Lee and Kyu Cheol Lee from the lab of Professor Changduk Yang at Ulsan National Institute of Science and Technology have directly utilized **3.11** and **3.16** for investigation of thermally stable polymer films. Installing an alkane sidechain with a terminal bromide group using an amine functionality requires an aminoalcohol starting material, Figure 3.21. The availability of these starting materials varies based on the length of the alkane chain. One example beginning with the widely available γ-aminobutyric acid

is shown in Figure 3.21. Hydrogenation of the carboxylic acid is achieved with a silica-supported rhodium/molybdenum oxide catalyst under high pressure.[200] Hydrobromic acid converts the alcohol to the desired terminal bromide.[201] Alternatively, terminal dibromides of carbon chain length two through ten are commercially available.

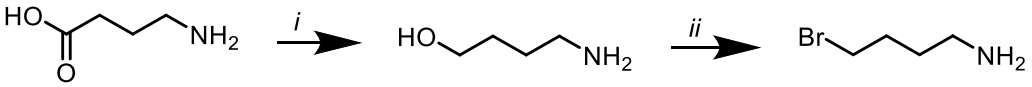

i) Rh-MoO_x/SiO_2, 5M H_2SO_4, H_2 8 MPa, 50 °C *ii*) HBr, Benzene, 80 °C

Figure 3.21 – Synthesis of a primary amine with a terminal bromide from aminobutyric acid

3.8 Conclusions and Outlook

Chapter 3 details the modification of the synthesis of TPD using procedures adapted from the synthesis of phthalimide. These conditions provide two benefits. The first is the one-step conversion of the diacid to the unfunctionalized imide. The second is the use of less toxic and less corrosive chemicals to effect the transformation. The final result is a procedure that is preferable in its sense of required chemicals, atom economy, overall yield, and potential applications of the final products.

The chapter also presents the first exploration of the diverse array of side-chains that have can be appended to TPD. The ability to append previously inaccessible side-chains to TPD represents the potential impact to the field of conjugated polymers containing TPD. Initial work detailed in Section 3.7 foreshadows the possibilities facilitated by this chapter. As this work focused solely on monomer syntheses, the creation and evaluation of TPD containing conjugated polymers with application specific side-chains is a wide open field.

3.9 Collection of Synthetic Writeups and Experimental Data

Solution NMR spectra were collected on Varian Mercury Vx (300 MHz ^{1}H, 75 MHz ^{13}C{^{1}H}), Bruker Avance III (376.5 MHz ^{19}F), or Bruker Avance III-HD (700 MHz ^{1}H, 176 MHz ^{13}C{^{1}H}). Spectra were processed using MestReNova v6.0 and referenced to residual protonated solvent signals ($CDCl_3$: ^{1}H 7.26 ppm, ^{13}C 77.16; CD_2Cl_2: ^{1}H 5.32 ppm, ^{13}C 54.00 ppm; DMSO-d_6: ^{1}H 2.50 ppm, ^{13}C 39.52 ppm). The ^{19}F spectrum is not referenced to an internal solvent signal. The solvent peak used as the internal reference is labeled in each spectrum as its deuterated parent solvent. Accurate mass spectra were collected by the Bioanalytical Mass Spectrometry Facility at Georgia Tech on either a MicroMass AutoSpec M (EI) or a Micromass Quattro LC (ESI). Elemental analyses were carried out by Atlantic Microlabs on a PerkinElmer 2400 II analyzer (CHN) and a Carlo Erba 1108 analyzer (S). Melting points were collected on a MEL-TEMP apparatus with digital thermometer at a 10 °C/min heating rate and are reported uncorrected.

3,4-Thiophene dicarboxylic acid was purchased from Frontier Scientific and used without further purification. Heptadecan-9-ol,[202] 9-heptadecyl 4-toluenesulfonate,[202] 3,6,9-trioxadecyl 4-toluenesulfonate[203], and 3,3'-bithiophene dicarboxylic acid[156] were synthesized according to literature procedures. Silica gel (60 Å, 230-400 mesh) was purchased from Sorbtech (Norcross, GA). All other reagents were purchased from commercial suppliers and used without further purification.

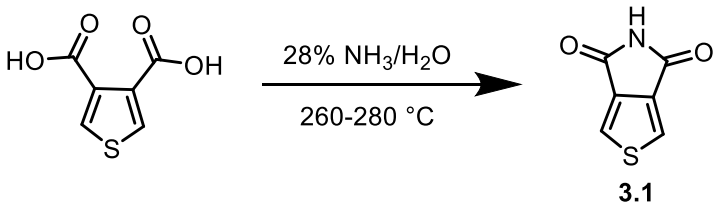

Figure 3.22 – Synthesis of thieno[3,4-*c*]pyrrole-4,6-dione (3.1)

Thieno[3,4-*c*]pyrrole-4,6-dione (3.1): Compound **3.1** has been previously synthesized by a different route.[173] A modified and more thorough account is given here. To a 50 mL 1-neck RBF was added 3,4-thiophene dicarboxylic acid (3.44 g, 20 mmol) and H_2O (2-3 mL). Small pieces of glass were added as boiling stones. Concentrated aqueous ammonia (28%/14.8M, ~10 equiv.) was added slowly. The flask was heated gently to dissolve starting material, then to a boil until all H_2O and NH_3 were driven off. A white, crystalline material remained. ^1H NMR spectroscopy indicated complete conversion to the diammonium salt. A short (3-4") air-condenser was attached to the flask (use PTFE tape). In a sand bath, the flask was heated to 260 – 280 °C for 3-4 hours. During this time, the reaction became a homogenous melt, and product began to sublime to the top of the flask and into the condenser. Heating was continued until all material had sublimed. Solids were collected using excess hot acetonitrile (low solubility). Insoluble materials were filtered off. The solution was cooled in a –20 °C freezer to precipitate a beige solid. The precipitate was collected and washed with H_2O, then cold ACN. Drying under high vacuum gave the title compound (2.3g, 76%) as a beige solid, which can be used in subsequent reactions without further purification.

For obtaining high purity material, the product can be purified in multiple ways:

- Trituration or recrystallization in hot ACN
- Sublimation under vacuum (~10 mbar) at 160 °C.

- Brief sonication in H_2O effectively removes starting material

^{1}H NMR (300 MHz, DMSO-d_6): δ 11.25 (bs, 1H), 8.26 (s, 2H). ^{13}C{^{1}H} NMR (75 MHz, DMSO-d_6): δ 163.29, 137.16, 127.32. HRMS (EI) *m/z* calculated for $C_6H_3NO_2S$ $[M]^+$ 152.9885; found 152.9881 EA: Anal. Calcd for $C_6H_3NO_2S$ (%): C, 47.05; H, 1.97; N, 9.15; S, 20.93. Found (%): C, 47.08; H, 2.15; N, 9.23; S, 20.69.

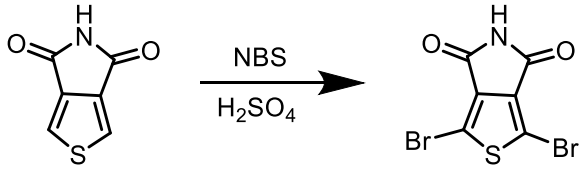

3.1 **3.2**

Figure 3.23 – Synthesis of 1,3-dibromothieno[3,4-*c*]pyrrole-4,6-dione (3.2)

1,3-Dibromothieno[3,4-*c*]pyrrole-4,6-dione (3.2): Compound **3.2** has been previously synthesized by a different route.[177] An alternate procedure from **3.1** is given here. **3.1** (710 mg, 4.6 mmol) was added to conc. H_2SO_4 (11 mL, 0.4M) at 0 °C. NBS (3.3 g, 18.5 mmol, 4.0 equiv.) was added in one portion. The reaction was stirred for 30 min at 0 °C, then 3 hours at r.t. The reaction was poured onto a large excess of ice-water. The precipitated solid was collected on a nylon filter, washed with a large excess of H_2O, then 1:1 H_2O:MeOH. The material can be used without further purification or can be recrystallized from acetonitrile. Typical yields obtained were between 70-80%

^{1}H NMR (300 MHz, DMSO-d6): δ 11.57 (bs, 1H). ^{13}C{^{1}H} NMR (75 MHz, DMSO-d6) δ 161.01, 135.96, 112.53. HRMS (EI) *m/z* calculated for $C_6HBr_2NO_2S$ $[M]^+$ 308.8095; found 308.8098 EA: Anal. Calcd for $C_6HBr_2NO_2S$ (%): C, 23.18; H, 0.32; N, 4.50; S, 10.31; Br, 51.39. Found (%): C, 23.43; H, 0.52; N,4.54; S, 10.23; Br, 51.25.

3.9.1 *General Procedure for Reaction of a Thiophene Imide with an Electrophile*

To a reaction vessel charged with a thiophene imide (**3.1** or **3.2**) (1.0 equiv.) and K_2CO_3 (2.0 equiv.) was added dry dimethylformamide to make a 0.1 M solution of the imide. The electrophile (1.5 equiv.) was introduced in one portion. The reaction was stirred at room temperature overnight, or until starting material is not present by TLC (10% EtOAc:DCM). The reaction was gravity filtered through a conical paper funnel (25 µm particle retention) with the aid of DCM or $CHCl_3$ and then concentrated. The resulting material was dissolved in a suitable solvent (often DCM), filtered again to remove insoluble material, and concentrated. Further purification is described separately.

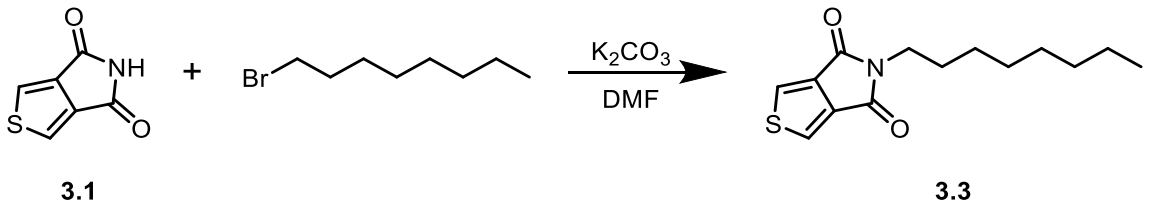

3.1 **3.3**

Figure 3.24 – Synthesis of 5-octylthieno[3,4-*c*]pyrrole-4,6-dione (3.3)

5-Octylthieno[3,4-*c*]pyrrole-4,6-dione (3.3): Compound **3.3** has been previously synthesized by a different route.[104] The reaction was performed on a 1.0 mmol scale following the given procedure with 1-bromooctane as the electrophile. The crude material was subjected to column chromatography (silica gel, 1:1 DCM:Hexanes) to give 252 mg (95%) of a white, crystalline solid.

^{1}H NMR (300 MHz, $CDCl_3$): δ 7.80 (s, 2H), 3.60 (t, *J*=7.2 Hz, 2H), 1.63 (p, 2H), 1.39 – 1.15 (m, 10H), 0.92 – 0.80 (m, 3H). $^{13}C\{^1H\}$ NMR (75 MHz, $CDCl_3$): δ 162.81, 136.80, 125.60, 38.63, 31.91, 29.30 (2C), 28.61, 27.01, 22.76, 14.23. HRMS (EI) *m/z* calculated for $C_{14}H_{19}NO_2S$ $[M]^+$ 265.1137; found 265.1132. EA: Anal. Calcd for $C_{14}H_{19}NO_2S$ (%):

C, 63.37; H, 7.22; N, 5.28; S, 12.08. Found (%): C, 63.41; H, 7.05; N, 5.19; S, 12.03. Melting Point (°C): 121 – 122 (Lit. 120 – 121).[104]

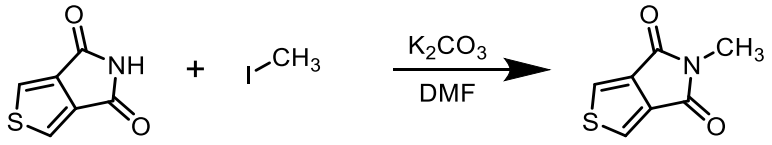

3.1 **3.4**

Figure 3.25 – Synthesis of 5-methylthieno[3,4-*c*]pyrrole-4,6-dione (3.4)

5-Methylthieno[3,4-*c*]pyrrole-4,6-dione (3.4): The reaction was performed on a 1.0 mmol scale following the given procedure with methyl iodide as the electrophile. Column chromatography (silica gel, 0-5% Et_2O:$CHCl_3$) gave 92 mg (55%) of a white, crystalline solid.

^1H NMR (300 MHz, $CDCl_3$) δ 7.79 (s, 2H), 3.07 (s, 3H). $^{13}C\{^1H\}$ NMR (75 MHz, $CDCl_3$) δ 162.73, 136.58, 125.70, 24.42. HRMS (ESI) *m/z* calculated for $C_7H_5NO_2S$ $[M + H]^+$ 168.0114; found 168.0113. EA: Anal. Calcd for $C_7H_5NO_2S$ (%): C, 50.29; H, 3.01; N, 8.38; S, 19.18. Found (%): C, 50.29; H, 3.06; N, 8.33; S, 19.02. Melting Point (°C): 149 – 151.

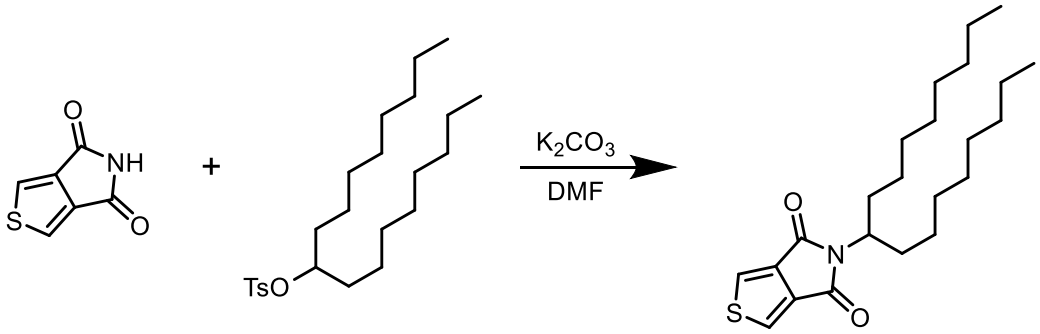

3.1 **3.5**

Figure 3.26 – Synthesis of 5-(heptadecan-9-yl)thieno[3,4-*c*]pyrrole-4,6-dione (3.5)

5-(Heptadecan-9-yl)thieno[3,4-*c*]pyrrole-4,6-dione (3.5): Compound **3.5** has been previously synthesized by a different route.[153] The reaction was performed on a 1.0 mmol

scale following the given procedure with 9-heptadecanyltosylate as the electrophile. Column chromatography (silica gel, 0-20% EtOAc:DCM) failed to separate the tosylate starting material from the product. To ease purification, the crude product was stirred with LiBr (1.0 mmol) in DMF (0.2M) to convert excess tosylate to the bromide. Conversion of the tosylate and stability of the imide were monitored by TLC and confirmed by ^{1}H NMR spectroscopy. Column chromatography (silica gel, 10% EtOAc:90% DCM) gave 236 mg (60%) of a waxy solid.

^{1}H NMR (300 MHz, $CDCl_3$) δ 7.77 (s, 2H), 4.10 (hept, *J* = 5.3 Hz, 1H), 2.14 – 1.92 (m, 2H), 1.74 – 1.54 (m, 2H), 1.38 – 1.10 (m, 24H), 0.85 (t, *J* = 6.7 Hz, 6H). ^{13}C{^{1}H} NMR (75 MHz, $CDCl_3$) δ 163.19, 136.59, 125.40, 52.86, 32.40, 31.96, 29.59, 29.43, 29.36, 26.80, 22.78, 14.24. HRMS (EI) *m/z* calculated for $C_{23}H_{37}NO_2S$ $[M]^+$ 391.2545; found 391.2538. Melting Point (°C): 46 – 47 (Lit. 40 – 42).[153]

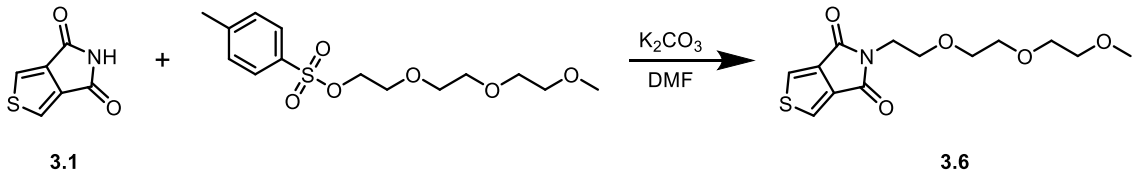

3.1 3.6

Figure 3.27 – Synthesis of 5-(2-(2-(2-methoxyethoxy)ethoxy)ethyl)-thieno[3,4-*c*]pyrrole-4,6-dione (3.6)

5-(2-(2-(2-Methoxyethoxy)ethoxy)ethyl)-thieno[3,4-*c*]pyrrole-4,6-dione (3.6): The reaction was performed on a 1.0 mmol scale following the given procedure with 2-(2-(2-methoxyethoxy)ethoxy)ethyltosylate as the electrophile. Column chromatography (silica gel, 0-10% EtOAc:DCM) gave a colorless oil (90 mg, 30%). Purification may have been simplified by using LiBr during workup, see **3.5**.

^{1}H NMR (300 MHz, $CDCl_3$) δ 7.79 (s, 2H), 3.82 – 3.75 (m, 2H), 3.70 – 3.63 (m, 2H), 3.63 – 3.41 (m, 8H), 3.30 (s, 3H). $^{13}C\{^{1}H\}$ NMR (75 MHz, $CDCl_3$) δ 162.47, 136.54, 125.73, 71.89, 70.58, 70.56, 70.08, 67.81, 59.03, 37.63. HRMS (EI) *m/z* calculated for $C_{13}H_{17}NO_5S$ $[M]^+$ 299.0827; found 299.0830. EA: Anal. Calcd for $C_{13}H_{17}NO_5S$ (%): C, 52.16; H, 5.72; N, 4.68; S, 10.71. Found (%): C, 52.02; H, 5.71; N, 4.57; S, 10.60.

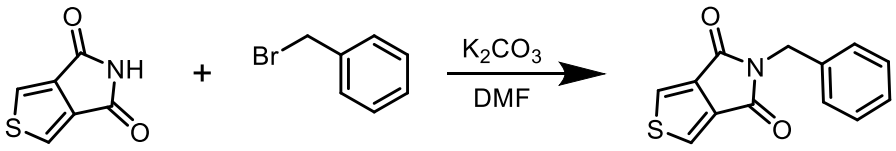

3.1 **3.7**

Figure 3.28 – Synthesis of 5-benzylthieno[3,4-*c*]pyrrole-4,6-dione (3.7)

5-Benzylthieno[3,4-*c*]pyrrole-4,6-dione (3.7): The reaction was performed on a 1.0 mmol scale following the given procedure with benzylbromide as the electrophile. Column chromatography (silica gel, 100% DCM) gave 210 mg (86%) of a white, crystalline solid.

^{1}H NMR (300 MHz, CD_2Cl_2) δ 7.85 (s, 2H), 7.41 – 7.25 (m, 5H), 4.76 (s, 2H). $^{13}C\{^{1}H\}$ NMR (75 MHz, CD_2Cl_2) δ 162.74, 137.18, 137.04, 129.10, 128.77, 128.20, 126.43, 42.36. HRMS (EI *m/z* calculated for $C_{13}H_9NO_2S$ $[M]^+$ 243.0354; found 243.0349. EA: Anal. Calcd for $C_{13}H_9NO_2S$ (%): C, 64.18; H, 3.73; N, 5.76; S, 13.18. Found (%): C, 63.97; H, 3.82; N, 5.79; S, 13.31. Melting Point (°C): 152 – 153.

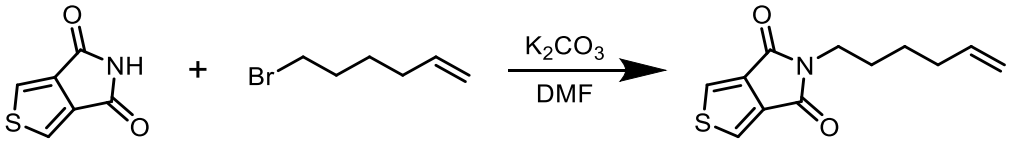

3.1 3.8

Figure 3.29 – Synthesis of 5-(hex-5-en-1-yl)thieno[3,4-*c*]pyrrole-4,6-dione (3.8)

5-(Hex-5-en-1-yl)thieno[3,4-*c*]pyrrole-4,6-dione (3.8): The reaction was performed on a 1.0 mmol scale following the given procedure with 6-bromohex-1-ene as the electrophile. Column chromatography (silica gel, 100% DCM) gave 222 mg (94%) of a white, crystalline solid.

^{1}H NMR (300 MHz, $CDCl_3$) δ 7.80 (s, 2H), 5.78 (ddt, *J* = 16.9, 10.2, 6.7 Hz, 1H), 5.18 – 4.80 (m, 2H), 3.62 (t, *J* = 7.3 Hz, 2H), 2.09 (qt, *J* = 7.3, 1.3 Hz, 2H), 1.79 – 1.53 (m, 3H), 1.54 – 1.32 (m, 2H). ^{13}C{^{1}H} NMR (75 MHz, $CDCl_3$) δ 162.76, 138.40, 136.77, 125.64, 114.99, 38.41, 33.39, 28.04, 26.22. HRMS (EI) *m/z* calculated for $C_{12}H_{13}NO_2S$ $[M]^+$ 235.0667; Found 235.0665. EA: Anal. Calcd for $C_{12}H_{13}NO_2S$ (%): C, 61.25; H, 5.61; N, 5.95; S, 13.63. Found (%): C, 61.46; H, 5.61; N, 5.97; S, 13.78. Melting Point (°C): 98 – 99.

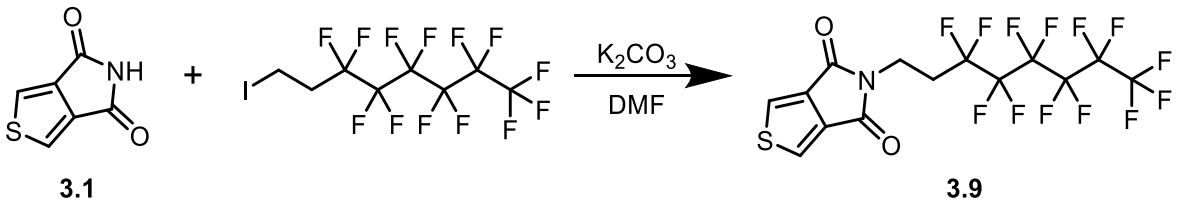

Figure 3.30 – Synthesis of 5-(3,3,4,4,5,5,6,6,7,7,8,8,8-tridecafluorooctyl)thieno[3,4-*c*]pyrrole-4,6-dione (3.9)

5-(3,3,4,4,5,5,6,6,7,7,8,8,8-Tridecafluorooctyl)thieno[3,4-*c*]pyrrole-4,6-dione (3.9): The reaction was performed on a 1.0 mmol scale following the given procedure with 1,1,1,2,2,3,3,4,4,5,5,6,6,7,7,8,8-heptadecafluoro-10-iododecane as the electrophile. Column chromatography (silica gel, 100% DCM) gave 207 mg (42%) of a white solid.

^{1}H NMR (300 MHz, $CDCl_3$) δ 7.87 (s, 2H), 3.97 (t, *J* = 7.3 Hz, 2H), 2.62 – 2.38 (m, 2H). 13C{^{1}H} NMR (176 MHz, $CDCl_3$) δ 162.01, 136.25, 126.50, 30.70, 30.67, 30.64, 29.85, 29.58, 29.46, 29.33. Note: This carbon spectrum was not ^{19}F decoupled. ^{19}F couples with ^{13}C. Additional peaks could not be marked with certainty. HRMS (EI) *m/z* calculated for $C_{14}H_6F_{13}NO_2S$ $[M]^+$ 498.9912; Found 498.9911. EA: Anal. Calcd for $C_{14}H_6F_{13}NO_2S$ (%): C, 33.68; H, 1.21; F, 49.47; N, 2.81; S, 6.42. Found (%): C, 36.29; H, 1.60; F, 46.03; N, 2.97; S, 6.21. Melting Point (°C): 96 – 98.

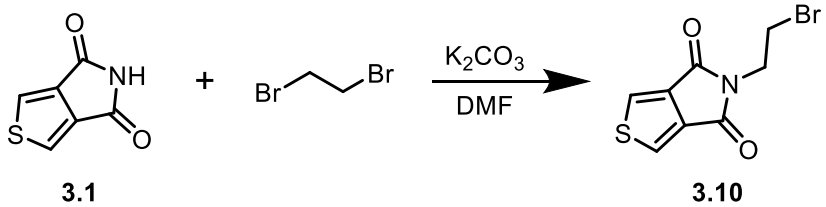

Figure 3.31 – Synthesis of 5-(2-bromoethyl)-thieno[3,4-*c*]pyrrole-4,6-dione (3.10)

5-(2-Bromoethyl)-thieno[3,4-*c*]pyrrole-4,6-dione (3.10): The reaction was performed on a 1.0 mmol scale following the given procedure with 1,2-dibromoethane as the electrophile. A substoichiometric amount of dibromoethane (94 mg, 0.5 mmol, 0.5 equiv.) was used to

encourage dimer formation. Dimer formation was not observed by TLC or NMR spectroscopy. Column chromatography (silica gel, 100% DCM) gave 190 mg (73%, calculated with imide as limiting reagent and represents a low estimate) of a white, crystalline solid.

^{1}H NMR (300 MHz, $CDCl_3$) δ 7.87 (s, 2H), 4.04 (t, *J* = 6.7 Hz, 2H), 3.58 (t, *J* = 6.7 Hz, 2H). $^{13}C\{^{1}H\}$ NMR (75 MHz, $CDCl_3$) δ 162.13, 136.25, 126.43, 39.79, 28.11. HRMS (EI) *m/z* calculated for C8H6BrNO2S [M]+ 258.9303; found 258.9294. EA: Anal. Calcd for C8H6BrNO2S (%): C, 36.94; H, 2.33; N, 5.39; S, 12.33. Found (%): C, 36.95; H, 2.33; N, 5.26; S, 12.34. Melting Point (°C): 142 – 143.

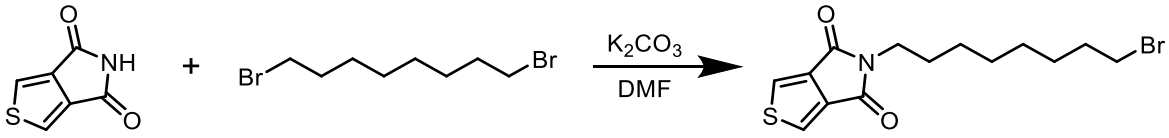

3.1 **3.11**

Figure 3.32 – Synthesis of 5-(8-bromooctyl)-thieno[3,4-*c*]pyrrole-4,6-dione (3.11)

5-(8-Bromooctyl)-thieno[3,4-*c*]pyrrole-4,6-dione (3.11): The reaction was performed on a 2.0 mmol scale following the given procedure with 1.0 equiv. of 1,8-dibromooctane used to allow for formation of dimer. Column chromatography (silica gel, 100% DCM, Rf = 0.33) gave 396 mg (58%, overall conversion with **3.13** was 92%) of a white, crystalline solid.

^{1}H NMR (300 MHz, $CDCl_3$) δ 7.80 (s, 2H), 3.60 (t, *J* = 7.4 Hz, 2H), 3.39 (t, *J* = 6.8 Hz, 2H), 1.83 (p, *J* = 7.1 Hz, 2H), 1.71 – 1.55 (m, 2H), 1.48 – 1.36 (m, 2H), 1.36 – 1.23 (m, 6H). $^{13}C\{^{1}H\}$ NMR (75 MHz, $CDCl_3$) δ 162.78, 136.75, 125.64, 38.51, 34.12, 32.85, 29.07, 28.71, 28.52, 28.17, 26.83. HRMS (EI) *m/z* calculated for $C_{14}H_{18}BrNO_2S$ $[M]^+$ 343.0242;

found 343.0236. EA: Anal. Calcd for $C_{14}H_{18}BrNO_2S$ (%): C, 48.84; H, 5.27; N, 4.07; S, 9.31. Found (%): C, 49.01; H, 5.24; N, 4.04; S, 9.42. Melting Point (°C): 77 – 78.

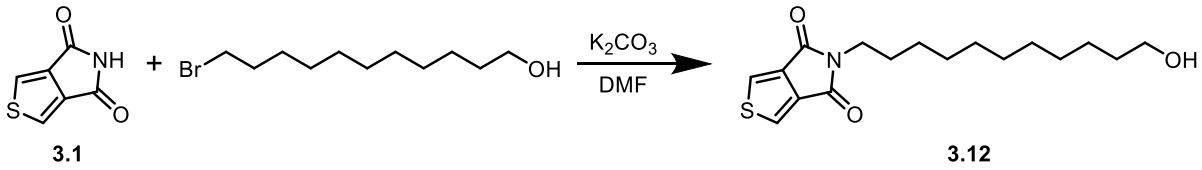

3.1 3.12

Figure 3.33 – Synthesis of 5-(11-hydroxyundecyl)thieno[3,4-*c*]pyrrole-4,6-dione (3.12)

5-(11-Hydroxyundecyl)thieno[3,4-*c*]pyrrole-4,6-dione (3.12): The reaction was performed on a 0.36 mmol scale following the given procedure with 11-Bromo-1-undecanol as the electrophile. Column chromatography (silica gel, 10% MeOH:$CHCl_3$) gave 90 mg (78%) of a white solid.

^{1}H NMR (300 MHz, $CDCl_3$) δ 7.80 (s, 2H), 3.67 – 3.52 (overlapping triplets, 4H), 1.70 – 1.47 (m, 4H), 1.40 – 1.15 (m, 14H). $^{13}C\{^1H\}$ NMR (75 MHz, $CDCl_3$) δ 162.81, 136.71, 125.65, 63.12, 38.58, 32.90, 29.61, 29.52 (2C), 29.46, 29.24, 28.54, 26.92, 25.82. HRMS (ESI) *m/z* calculated for $C_{17}H_{26}NO_3S^+$ Calc. $[M + H]^+$ 324.1628; found 324.1628. EA: Anal. Calcd for $C_{17}H_{25}NO_3S$ (%): C, 63.13; H, 7.79; N, 4.33; S, 9.91. Found (%): C, 63.24; H, 7.86; N, 4.20; S, 9.82. Melting Point (°C): 116 – 117.

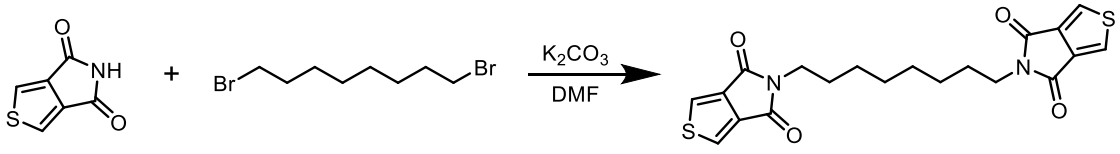

3.1 3.13

Figure 3.34 – Synthesis of 5,5'-(octane-1,8-diyl)bisthieno[3,4-*c*]pyrrole-4,6-dione (3.13)

5,5'-(Octane-1,8-diyl)bisthieno[3,4-*c*]pyrrole-4,6-dione (3.13): The reaction was performed on a 2.0 mmol scale following the given procedure with 1.0 equiv. of 1,8-

dibromooctane used to allow for formation of dimer. Column chromatography (silica gel, 100% DCM to elute **3.11** then 10% Et_2O:DCM) gave 143 mg (34%, overall conversion with **3.11** was 92%) of a white, crystalline solid.

^{1}H NMR (300 MHz, $CDCl_3$) δ 7.80 (s, 4H), 3.60 (t, *J* = 7.3 Hz, 4H), 1.62 (p, *J* = 6.9 Hz, 4H), 1.37 – 1.22 (m, 8H). $^{13}C\{^1H\}$ NMR (75 MHz, $CDCl_3$) δ 162.81, 136.79, 125.62, 38.56, 29.20, 28.57, 26.92. HRMS (EI) *m/z* calculated for $C_{20}H_{20}N_2O_4S_2$ $[M]^+$ 416.0865; found 416.0866. EA: Anal. Calcd for $C_{20}H_{20}N_2O_4S_2$ (%): C, 57.67; H, 4.84; N, 6.73; S, 15.39. Found (%): C, 57.42; H, 4.74; N, 6.57; S, 15.12. Melting Point (°C): 206 – 207.

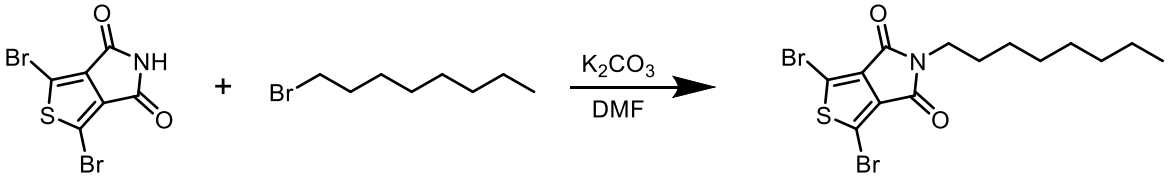

3.2 **3.14**

Figure 3.35 – Synthesis of 1,3-Dibromo-5-octylthieno[3,4-*c*]pyrrole-4,6-dione (3.14)

1,3-Dibromo-5-octylthieno[3,4-*c*]pyrrole-4,6-dione (3.14): Compound **3.14** has been previously synthesized by a different route.[104] The reaction was performed on a 0.50 mmol scale following the given procedure with 1-bromooctane as the electrophile. The obtained crude red oil was passed through a pad of silica with DCM to give beige crystals (202 mg). Further purification (silica gel, 1:1 DCM:Hexanes) yielded 177 mg (84%) of a white, crystalline solid.

^{1}H NMR (300 MHz, $CDCl_3$) δ 3.58 (t, *J* = 7.2 Hz, 2H), 1.69 – 1.55 (m, 2H), 1.43 – 1.15 (m, 10H), 0.87 (t, *J* = 6.7 Hz, 3H). $^{13}C\{^1H\}$ NMR (75 MHz, $CDCl_3$) δ 160.53, 134.92, 113.06, 38.97, 31.91, 29.25, 28.39, 26.93, 22.76, 14.23. HRMS (EI) *m/z* calculated for

$C_{14}H_{17}NO_2SBr_2$ $[M]^+$ 420.9347; found 420.9337. Melting Point (°C): 105 – 106 (Lit. 104 – 105).[104]

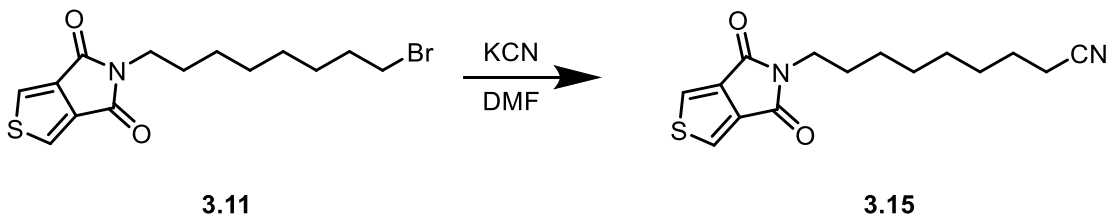

3.11 **3.15**

Figure 3.36 – Synthesis of 5-(9-nitrilononanyl)thieno[3,4-*c*]pyrrole-4,6-dione (3.15)

5-(9-Nitrilononanyl)thieno[3,4-*c*]pyrrole-4,6-dione (3.15): 3.11 (100 mg, 0.29 mmol, 1.0 equiv.) and potassium cyanide (28 mg, 0.44 mmol, 1.5 equiv.) were dissolved in 5 ml DMF. The mixture was heated at 50 °C for 4 hours at which point TLC indicated no starting material remained. The reaction was cooled, poured into 50 mL H_2O, extracted with DCM (3x). The combined organics were washed with H_2O, dried over $MgSO_4$, and concentrated. Residual DMF was removed on high vacuum overnight. Column chromatography (silica gel, 100% DCM, Rf = 0.2) gave 74 mg (88 %) of a white, waxy solid.

^{1}H NMR (300 MHz, $CDCl_3$) δ 7.79 (s, 2H), 3.57 (t, *J* = 7.3 Hz, 2H), 2.30 (t, *J* = 7.1 Hz, 2H), 1.70 – 1.54 (m, 4H), 1.47 – 1.35 (m, 2H), 1.35 – 1.24 (m, 6H). $^{13}C\{^1H\}$ NMR (75 MHz, $CDCl_3$) δ 162.69, 136.62, 125.64, 119.89, 77.16, 38.35, 28.84, 28.64, 28.59, 28.39, 26.70, 25.34, 17.13. HRMS (EI) *m/z* calculated for $C_{15}H_{18}N_2O_2S$ $[M]^+$ 290.1089; found 290.1094. EA: Anal. Calcd for $C_{15}H_{18}N_2O_2S$ (%): C, 62.04; H, 6.25; N, 9.65; S, 11.04. Found (%): C, 62.20; H, 6.22; N, 9.51; S, 10.95. Melting Point (°C): 51 – 52.

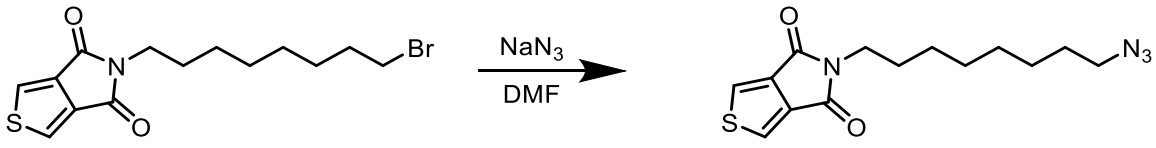

3.11 **3.16**

Figure 3.37 – Synthesis of 5-(8-azidooctyl)thieno[3,4-*c*]pyrrole-4,6-dione (3.16)

5-(8-Azidooctyl)thieno[3,4-*c*]pyrrole-4,6-dione (3.16): 3.11 (100 mg, 0.29 mmol, 1.0 equiv.) and sodium azide (28 mg, 0.44 mmol, 1.5 equiv.) were dissolved in 5 ml DMF. The mixture was heated at 50 °C for 4 hours at which point TLC indicated no starting material remained. The reaction was cooled, poured into 50 mL H_2O, extracted with DCM (3x). The combined organics were washed with H_2O, dried over $MgSO_4$, and concentrated. Residual DMF was removed on high vacuum overnight. Column chromatography (silica gel, 100% DCM, Rf = 0.24) gave 78 mg (88%) of a white, waxy solid.

^{1}H NMR (300 MHz, $CDCl_3$) δ 7.80 (s, 2H), 3.60 (t, *J* = 7.3 Hz, 2H), 3.23 (t, *J* = 6.9 Hz, 2H), 1.73 – 1.49 (m, 4H), 1.43 – 1.20 (m, 8H). $^{13}C\{^1H\}$ NMR (75 MHz, $CDCl_3$) δ 162.77, 136.74, 125.63, 51.54, 38.50, 29.10, 29.09, 28.89, 28.51, 26.82, 26.72. HRMS (EI) *m/z* calculated for $C_{14}H_{18}N_4O_2S$ $[M]^+$ 306.1150; found 306.1156. EA: Anal. Calcd for $C_{14}H_{18}N_4O_2S$ (%): C, 54.88; H, 5.92; N, 18.29; S, 10.46. Found (%): C, 55.14; H, 5.83; N, 18.18; S, 10.37. Melting Point (°C): 44 – 45.

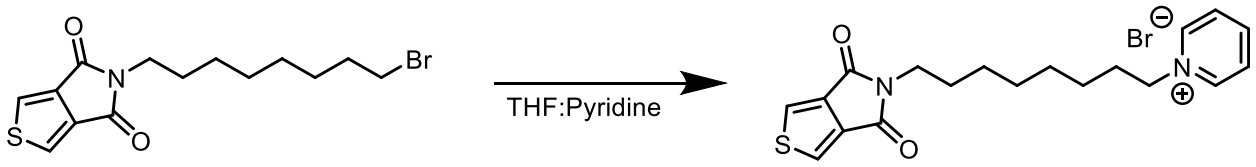

3.11 **3.17**

Figure 3.38 – Synthesis of 1-(8-(4,6-dioxothieno[3,4-*c*]pyrrol-5-yl)octyl)pyridinium bromide (3.17)

1-(8-(4,6-Dioxothieno[3,4-*c*]pyrrol-5-yl)octyl)pyridinium bromide (3.17): 3.11 (85 mg, 0.25 mmol, 1.0 equiv.) was dissolved in 1:1 THF:pyridine (6 mL). The mixture was heated at 65 °C for 3 hours at which point TLC indicated no starting material remained (100% DCM). The reaction was cooled and concentrated to a beige solid. The crude product was dissolved in H_2O and washed with $CHCl_3$ (3x). The combined organics were back extracted with H_2O. The organics were dried over $MgSO_4$ and concentrated to give ~8 mg (0.03 mmol) of starting material indicating ~90% conversion. The combined aqueous washes were concentrated to 90 mg (86%) of a pale beige solid.

^{1}H NMR (300 MHz, CD_2Cl_2) δ 9.51 (d, *J* = 5.7 Hz, 2H), 8.55 (t, *J* = 7.8 Hz, 1H), 8.14 (t, *J* = 7.0 Hz, 2H), 7.86 (s, 2H), 4.95 (t, *J* = 7.4 Hz, 2H), 3.52 (t, *J* = 7.3 Hz, 2H), 2.02 (p, *J* = 7.2 Hz, 2H), 1.56 (p, *J* = 7.1 Hz, 2H), 1.45 – 1.16 (m, 8H). ^{13}C{^{1}H} NMR (75 MHz, CD_2Cl_2) δ 162.98, 145.76, 145.51, 136.93, 128.85, 126.20, 62.16, 38.52, 32.20, 29.17, 29.10, 28.64, 26.96, 26.20. HRMS (ESI) *m/z* calculated for $C_{19}H_{23}N_2O_2S^+$ Calc. $[M - Br]^+$ 343.1475; found 343.1475. EA: Anal. Calcd for $C_{19}H_{23}BrN_2O_2S$ (%): C, 53.90; H, 5.48; N, 6.62; S, 7.57. Found (%): C, 53.63; H, 5.55; N, 6.51; S, 7.68. Melting Point (°C): 188 – 189.

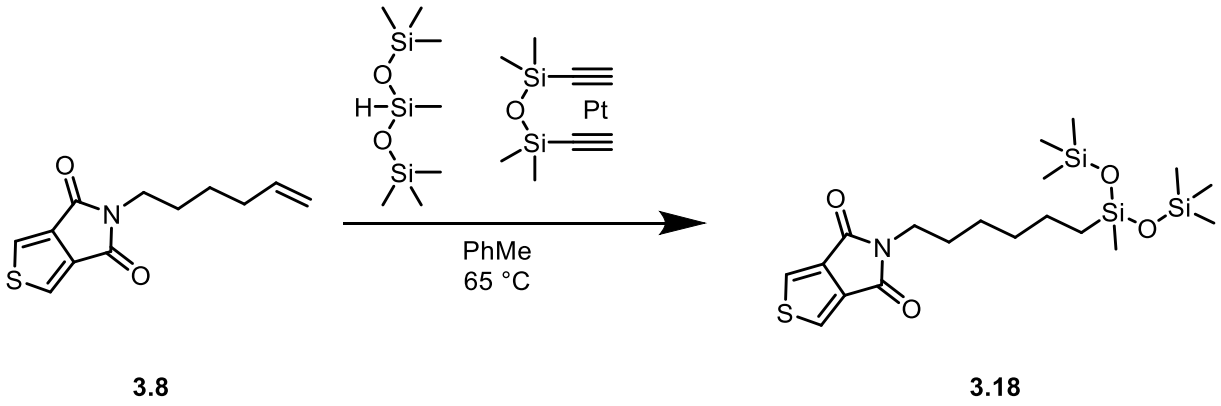

3.8 **3.18**

Figure 3.39 – Synthesis of 5-(6-(1,1,1,3,5,5,5-heptamethyltrisiloxan-3-yl)hexyl)thieno[3,4-*c*]pyrrole-4,6-dione

5-(6-(1,1,1,3,5,5,5-Heptamethyltrisiloxan-3-yl)hexyl)thieno[3,4-*c*]pyrrole-4,6-dione (3.18): 3.8 (71 mg, 0.30 mmol, 1.0 equiv.) was dissolved in dry toluene (3 mL). 1,1,1,3,5,5,5-Heptamethyltrisiloxane (0.2 mL, 2.3 equiv.) and platinum(0)-1,3-divinyl-1,1,3,3-tetramethyldisiloxane (Karstedt's Catalyst, 2 wt.% in xylenes, 0.17 mL, 5 mol% Pt) were added by syringe through a septum. The reaction was heated at 65 °C for 6 hours. TLC indicated starting material after 2 hours and no starting material after 6 hours. Reaction was concentrated to a brown oil and directly chromatographed (silica gel, 100% DCM, Rf = 0.44) to give a light brown, waxy solid. 123 mg (90%).

^{1}H NMR (300 MHz, $CDCl_3$) δ 7.80 (s, 2H), 3.61 (t, 2H), 1.69 – 1.59 (m, 2H), 1.39 – 1.22 (m, 6H), 0.48 – 0.38 (m, 2H), 0.07 (s, 18H), -0.02 (s, 3H). ^{13}C{^{1}H} NMR (75 MHz, $CDCl_3$) δ 162.81, 136.83, 125.58, 38.68, 32.97, 28.62, 26.78, 23.14, 17.71, 2.02, -0.16. HRMS (EI) *m/z* calculated for $C_{19}H_{35}NO_4SSi$ $[M]^+$ 457.1595; found 457.1596. EA: Anal. Calcd for $C_{19}H_{35}NO_4SSi_3$ (%): C, 49.85; H, 7.71; N, 3.06; S, 7.00. Found (%): C, 49.66; H, 7.91; N, 2.86; S, 6.71.

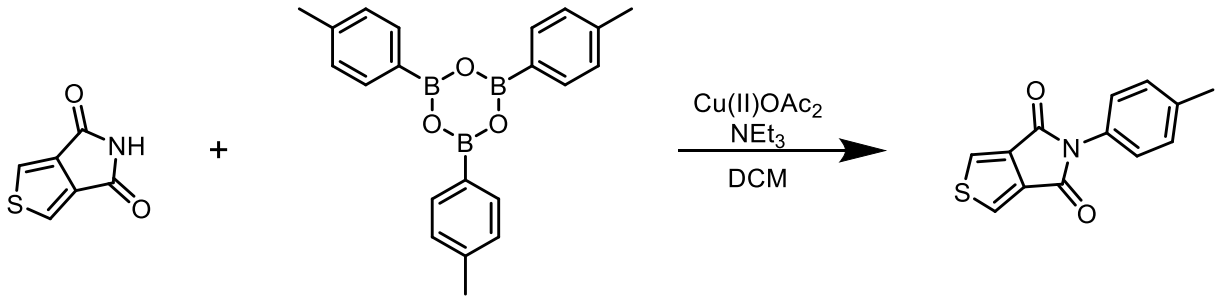

3.1 3.22 3.20

Figure 3.40 – Synthesis of 5-(*p*-tolyl)thieno[3,4-*c*]pyrrole-4,6-dione (3.20)

5-(*p*-Tolyl)thieno[3,4-*c*]pyrrole-4,6-dione (3.20): A reaction vessel was charged with **3.1** (115 mg, 0.75 mmol, 1.0 equiv.), triethylamine (0.23 mL, 1.5 mmol, 2.0 equiv.), anhydrous copper(II) acetate (137 mg, 0.75 mmol, 1.0 equiv.), **3.22** (178 mg, 0.5 mmol, 2.0 equiv. of boronic acid), and dry dichloromethane (10 mL). The reaction was stirred at r.t. and monitored by TLC (product has Rf of 0.4 in 100% DCM, imide visualized in 10% Et_2O:DCM). After 36 hours, the reaction was quenched by pouring into H_2O. The mixture was extracted with DCM (3x). The combined organics were washed with H_2O, then brine, and dried over $MgSO_4$, and concentrated. Column chromatography (silica gel, 100% DCM) gave 156 mg (86%) of a white, crystalline solid.

^{1}H NMR (300 MHz, CD_2Cl_2) δ 7.96 (s, *J* = 0.8 Hz, 2H), 7.36 – 7.28 (m, 2H), 7.27 – 7.19 (m, 2H), 2.41 (s, 3H). $^{13}C\{^1H\}$ NMR (75 MHz, $CDCl_3$) δ 161.84, 138.61, 136.34, 129.92, 129.32, 126.71, 126.62, 21.38. HRMS (EI) *m/z* calculated for $C_{13}H_9NO_2S$ $[M]^+$ 243.0354; found 243.0353. EA: Anal. Calcd for $C_{13}H_9NO_2S$ (%): C, 64.18; H, 3.73; N, 5.76; S, 13.18. Found (%): C, 64.28; H, 3.83; N, 5.61; S, 13.08. Melting Point (°C): 246 – 248.

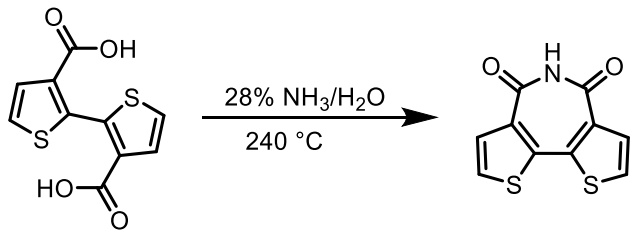

3.23

Figure 3.41 – Synthesis of dithieno[3,2-*c*:2',3'-*e*]azepine-4,6-dione (BTI) (3.23)

Dithieno[3,2-c:2',3'-*e*]azepine-4,6-dione (BTI) (3.23): Synthesized in a similar fashion as **3.1** with equipment and procedure modifications. 2,2'-bithiophene-3,3'-dicarboxylic acid was treated with 28% ammonium hydroxide. After heating to dryness, the solid ammonium salt was placed on a small piece of aluminum foil (10 mm × 10 mm). The aluminum foil boat was slid into a 20 mm diameter glass tube lined with aluminum foil. Heating tape was wrapped around the glass tube to create a temperature gradient at least 200 mm in length. The temperature at the starting material was maintained at 240 – 260 °C for 8 hours. A continuous flow of argon (15 mL/min) was passed through the tube during the reaction. To prevent anhydride formation, the argon was bubbled through 28% ammonium hydroxide. An exit bubbler of hydrochloric acid was used to scrub the exiting gas. After 8 hours, the aluminum foil lining was removed and pure **3.23** can be directly collected as yellow crystals (62 mg, 50%). Major impurities could include decarboxylated starting material (which can be removed by sublimation at 100 °C, <500 mTorr) and the anhydride (which can be removed by passing the crude material through a pad of silica gel in 100% EtOAc. **3.23** has an Rf of 0.8 in 100% EtOAc).

^{1}H NMR (700 MHz, $CDCl_3$) δ 8.50 (s, 1H), 7.76 (d, *J* = 5.4 Hz, 2H), 7.29 (d, *J* = 5.4 Hz, 2H). $^{13}C\{^{1}H\}$ NMR (176 MHz, $CDCl_3$) δ 159.66, 139.97, 132.39, 131.17, 125.15. HRMS (EI) *m/z* calculated for $C_{10}H_6NO_2S_2^+$ Calc. $[M + H]^+$ 234.9762, Found 234.9765. Melting Point (°C): 247 – 250 (melts, sublimes decomposition products).

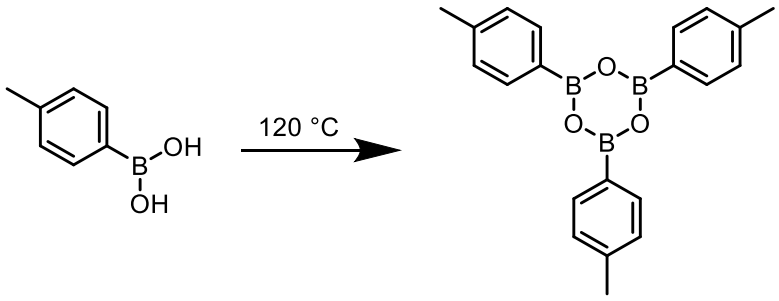

3.22

Figure 3.42 – Synthesis of 2,4,6-tri-*p*-tolylboroxine (3.22)

2,4,6-Tri-*p*-tolylboroxine (3.22): From a commercial bottle of *p*-tolylboronic acid, both boroxine and boronic acid species are present by ^{1}H NMR spectroscopy. The free acid is only slightly soluble in $CDCl_3$, so a quantitative comparison is not practical. Dehydration was performed in an open Erlenmeyer flask placed a standard laboratory oven (~120 °C) for six hours.[204] The resulting material was fully soluble in $CDCl_3$ and the ^{1}H NMR spectrum shows no free acid. **3.22** was stored in a desiccator until use to prevent hydrolysis back to the boronic acid.

Boroxine: ^{1}H NMR (300 MHz, $CDCl_3$) δ 8.13 (d, *J* = 7.9 Hz, 6H), 7.32 (d, *J* = 7.6 Hz, 6H), 2.45 (s, 9H). $^{13}C\{^{1}H\}$ NMR (75 MHz, $CDCl_3$) δ 143.08, 135.85, 128.92, 22.09.

Boronic acid: ^{1}H NMR (300 MHz, $CDCl_3$) δ 7.63 (d, *J* = 7.9 Hz, 2H), 7.23 (d, *J* = 7.6 Hz, 2H), 2.39 (s, 3H).

CHAPTER 4. ELECTRONICS OF SPIROBICYCLIC (CRUCIFORM) GERMANIUM COMPOUNDS

4.1 Introduction

Many conjugated polymers and discrete molecules used in organic photovoltaics are one-dimensional conductors.[205] The plane of π-conjugation – and therefore the dimensionality of charge transport – is one-dimensional. The design of conjugated materials as 1-D follows from the "rule" for aromaticity and π-π overlap, namely that the σ-framework is planar, so the orthogonal π-orbitals overlap. However, planarity is not a strict requirement for π-conjugation – helicenes and fullerenes demonstrate non-planar, overlapping π-networks.[206]

Fullerenes have long been the primary acceptor used in organic photovoltaics due to their isotropic charge transport and multi-reduction stability.[207] However, their low contribution to photogenerated charges and their thermal instability[208] have pushed the field to develop non-fullerene acceptors (NFAs).[13,145] Many of these structures attempt to mimic the 3-D structure and isotropic transport of fullerenes.[209–212]

The concept of a 3-D structure was of interest, but star-shaped structures[211,213,214] tend to have poor electronic communication through the central sp^3-hybridized atom. An alternative structural motif, the spirobicyle, provides another route to 3-D structures. The most notable spirobicylic molecule used in organic electronics today, 2,2′,7,7′-tetrakis-(*N*,*N*-di-4-methoxyphenylamino)-9,9′-spirobifluorene (spiro-MeOTAD), is widespread as a hole transport material in perovskite solar cells.[215] The non-planar, 3-D structure was

targeted to increase intermolecular interactions and the thermal stability of the amorphous films.

Carbon-centered spirobiheterocyclic systems, including spirobifluorene[216–218] and spirobi[cyclopentadithiophene],[137,219–221] have been studied in organic electronics as hole transport materials, non-planar NFA cores, and donor materials in organic photovoltaics. An obvious synthetic modification was the replacement of the carbon core with other Group 14 elements. Travelling down the periodic table in Group 14, the electronegativity drops, and the atomic orbitals become more diffuse. The number of systems studied, and the synthetic methods also change.

The silicon-based system, spirobi[silolodithiophene], had been previously synthesized.[222,223] The original report on spirobi[silolodithiophene] included a successful attempt at spirobi[germolodithiophene] and an unsuccessful attempt at spirobi[stannolodithiophene].[223] Our interest was to transition the cruciform system to a germanium core, in-line with our group's previous history in the development of dithienogermole as a monomer in organic photovoltaics.[110,160] Concurrently, Ohshita et al. developed spirobiheterocycles based on germolodithiophene for singlet oxygen sensitization.[224,225] Beyond dithienogermoles, germanium has been used as a cruciform center in alternative structures for charge transport applications.[226,227] Non-spirocyclic (excluding dithienogermole based polymers) structures have been investigated as donor materials in organic photovoltaics[228] and as precursors to polygermanes.[229]

Heterocycles containing the final two elements in Group 14, tin and lead, are rarely found in organic electronics. Stannoles have been incorporated into discrete

molecules[230,231] and polymers[232] for their unique electronic behavior.[233] Lead(II) is more stable than lead(IV) due to the "inert pair effect," making plumboles rare and unstable.[234,235]

Chapter 4 presents synthetic developments to the spirobi[germolodithiophene] core that prepare the molecule for Stille couplings. After coupling to bithiophene, the resulting molecule consists of orthogonal sexithiophene moieties centrally fused by a spirobigermole. The planar analog was synthesized to elucidate the effect of the spirobigermole core. Electrochemistry and absorption spectroscopy determined the planar analog undergoes two one-electron oxidations while the cruciform complex can support four one-electron oxidations. An equilibrium exists between two radical cations across two arms and one dication localized on one arm in the germanium cruciform.

4.2 Core Synthesis Methods

From previous literature[103,110,236] and experience synthesizing dithienogermole(DTG)-based compounds, the germanium cruciform core was designed along a similar synthetic route. A synthetic overview is given in Figure 4.1. Compound **4.2** and the silole analog have been previously synthesized, with subsequent conversion of the silole to the tetrabromo-and tetraiodo-molecules in good yield (>80%). The authors report 82% yield on the spirobi[silolodithiophene] but only 32% yield on **4.2**, which may have discourage additional experiments.[223] This work reports increased yields of **4.2** and successful conversion in high yield to the tetrahalide (**4.3**) and tetratin (**4.4**) molecules in preparation for Stille cross-coupling.

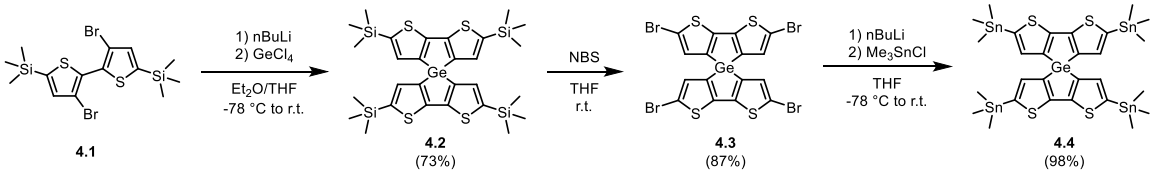

Figure 4.1 – Synthesis of key intermediate germanium cruciform core molecules

Planar versions of DTG have previously been synthesized from **4.1**[110] and the unprotected 3,3'-dibromobithiophene[236] with no difference in yield. (Most literature yields are around or below 50%, indicating a space for improvement in the cyclization reaction.) The protected version is used in this synthesis to decrease the potential for deprotonation at the α-position and to increase solubility of the product. Lithium-halogen exchange followed by quenching with germanium tetrachloride yields spirobigermole **4.2**. Compound **4.2** is amenable to traditional column chromatography on silica gel in hexanes. The compound is soluble in hexanes but slow to dissolve. If loaded on the column before being completely dissolved, the product will slowly leach onto the column and disrupt separation. Extended exposure on acidic silica gel begins protodesilylation. The trisubstituted impurity trails slightly behind the desired tetrasubstituted product. Compound **4.2** is efficiently isolated from deprotected impurities by slow evaporation from hexanes to yield X-ray quality crystals. A repeated synthesis by Thomas Marchandier gave 70% yield.

A known impurity that reduces yield is shown in Figure 4.2a. This impurity has only been reported when attempting to form the stannole cruciform.[223] Although unconfirmed, the related impurity suspected to decrease the obtained yields of planar DTGs is shown in Figure 4.2b. The impurity in 4.2a was isolated from the reaction workup (Compound **4.2**) as a hexanes insoluble product. The identity of the impurity was assigned by comparison of ^{1}H NMR shifts with the stannole impurity.[223] The occurrence of the

impurity is more evident in lower yielding formation reactions. Identifying reaction conditions to limit formation of the by-product is a worthwhile endeavor.

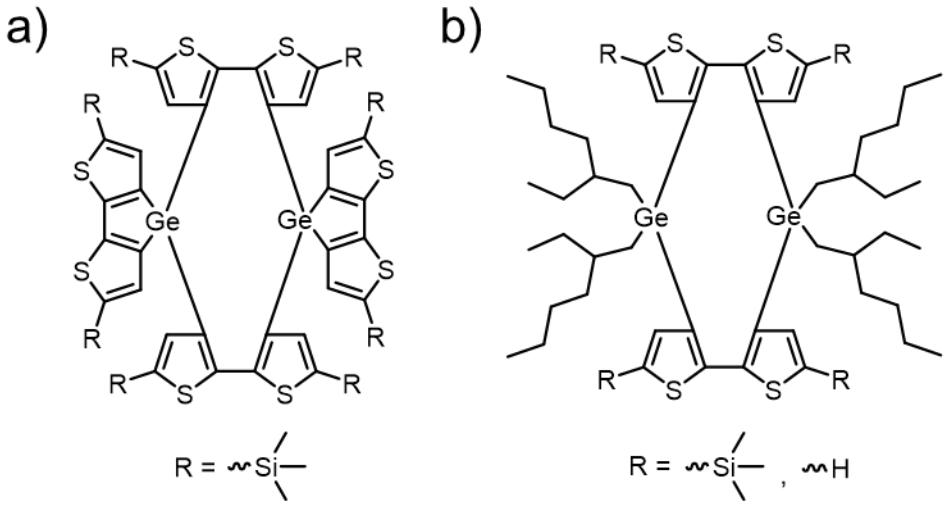

Figure 4.2 – Known and isolated impurity from germanium cruciform formation reaction (a), and suspected impurity formed during dithienogermole formation reaction (b)

The unfunctionalized, unprotected spirobi[germolodithiophene] core was of interest. Compound **4.2** was subjected to deprotection by lithium-halogen exchange and hydrochloric acid treatment. Both gave highly insoluble material which was not easily analyzed or purified by sublimation. Cyclization of unprotected **4.1** likewise yielded an insoluble material.

Conversion of **4.2** to **4.3** was adapted from a procedure for the bromination of 2,6-dibromo-4,4-bis(2-ethylhexyl)germolo[3,2-*b*:4,5-*b'*]dithiophene.[237] Previous halogenations on spirobi[silolodithiophene]s used elemental bromine and iodine monochloride.[223] The bromination of **4.2** occurs rapidly at room temperature. Compound **4.2** is soluble in THF and **4.3** is insoluble, allowing the reaction to be easily monitored by the formation of a yellow precipitate. The precipitate typically forms between 30 and 90

minutes after addition of NBS. The reaction should not be stirred for longer than four hours and never overnight. Extended reaction times result in the disappearance of the yellow precipitate and no recovery of **4.3**. After quenching with water, the yellow precipitate is isolated by filtration and washing with water and a 1:1 mixture of water:methanol to remove succinimide. Compound **4.3** has low solubility in chloroform, THF, and toluene, so a ^{13}C NMR spectrum was not obtained. Attempts at dissolution in DMSO or by heating in chloroform or dichlorobenzene resulted in the destruction of the compound. The mass spectrum of **4.3** was particularly convoluted with many unidentifiable species. The reactivity of this compound (likely with itself) results in many byproducts during analysis techniques and Stille coupling attempts. The level of purity was not a concern as elemental analysis and ^{1}H NMR spectroscopy indicated an acceptable level of purity and conversion to **4.4** was near quantitative.

A crystal structure of **4.3** was obtained successfully by slow evaporation of a dilute dichlorobenzene solution, Figure 4.3. The mother liquor was created by saturating a solution of dichlorobenzene at room temperature, then filtering through a 0.45 μm syringe filter. No heat was added to increase solubility. The loosely capped vial was kept in an undisturbed cabinet with complete exclusion of light. The small distance between adjacent bromine atoms and their quasi-columnar formation opens possible studies on treatment of single crystals of **4.3**.[238,239]

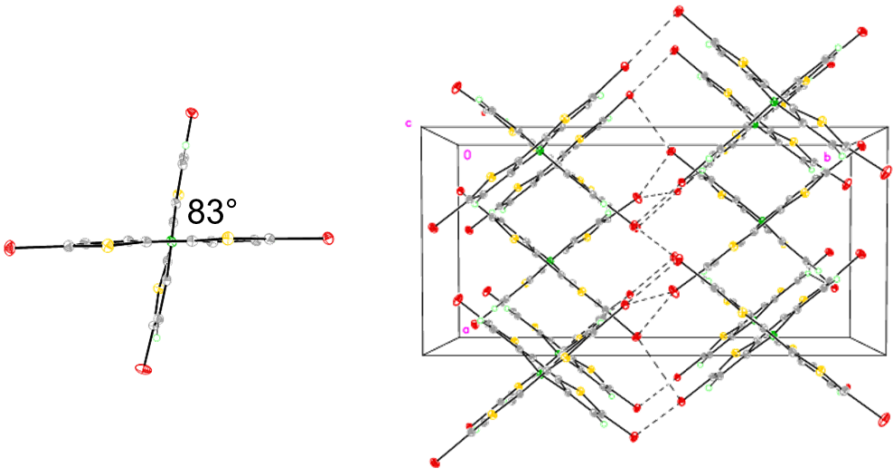

Figure 4.3 – Single crystal structure and crystal unit cell of Compound 4.3. The angle between "orthogonal" π-faces is 83°. Dashed lines indicate Br – Br separations of 3.28, 3.87, and 4.86 pm.

Attempts at Stille couplings with **4.3** resulted in dark red color formation and highly insoluble products, assumed to be from homocoupling. The instability of **4.3** was previously noted in its synthesis, in heating for NMR spectroscopy and or single crystal growth, and in its mass spectrum with coupled species present. Stille cross coupling is not recommended for bromide functionalized dithienogermoles. Others have reported poor yields from other bromides.[224,225]

Tetralithiation by lithium-halogen exchange had been previously demonstrated on spirobi[silolodithiophene]s.[223] Solubility and stability during lithiation was still a concern for spirobi[germolodithiophene]. Despite low solubility of **4.3** cold THF, the lithiation was successful and quenching with trimethyltin chloride yielded **4.4**. The forest-green solid obtained after a standard workup is dissolved in hexanes and washed with methanol (See Section 2.1.3.2) to give a purity acceptable in Stille couplings.

4.3 Four-fold Stille Coupling to Give Extended Germanium Cruciforms

With the core molecules obtained, Stille couplings were attempted to append thiophene extensions with solubilizing alkyl groups. This would lend increased solubility, longer wavelength absorption, and the potential for more π-π overlap. Thiophene, bithiophene, and terthiopene were originally planned. Due to stability and purification difficulties, only the bithiophene version, **4.5**, was isolated pure for further characterization.

The synthesis of the extended germanium cruciform, **4.5**, was synthesized by Stille cross-coupling with 5-bromo-3,5'-dihexyl-2,2'-bithiophene, Figure 4.4. An unsuccessful alternative route through cruciform formation as a final step is also shown. Compound **4.5** was synthesized in moderate yield which was reduced by light instability. The pure compound was isolated after column chromatography as a tacky red solid which was stable under inert atmosphere.

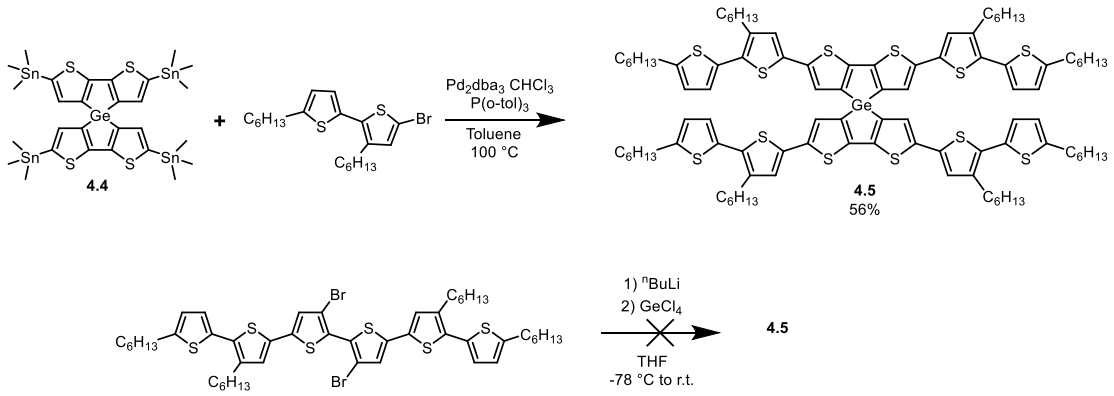

Figure 4.4 – Synthetic attempts at extended germanium cruciform systems

The planar analog, 2,6-bis(3,5'-dihexyl-[2,2'-bithiophen]-5-yl)-4,4-bis(2-ethylhexyl)-germolo[3,2-*b*:4,5-*b*']dithiophene, **4.6**, was also synthesized by Stille cross-coupling, Figure 4.5. A milder set of conditions (lower temperature in a coordinating

solvent) were attempted due to stability concerns. Compound **4.6** was isolated as an orange oil by preparatory TLC in low yield, 22%, due to multiple purification attempts by traditional column chromatography. Compound **4.6** exhibits a greater instability to silica gel and UV light compared to **4.5**.

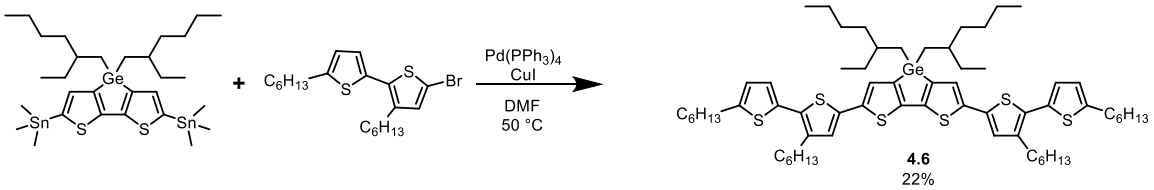

Figure 4.5 – Stille cross-coupling to give the planar analog of the germanium cruciform

4.4 Extended Germanium Cruciform Molecular Properties

The germanium cruciform, **4.5**, and the planar analog, **4.6**, are compared in terms of optical transitions, redox behavior, and optical absorptions of oxidized solutions. Where appropriate, the properties of sexithiophene are provided as a reference. Because **4.5** is a tacky red material and **4.6** is an oil, device-level data was not pursued.

4.4.1 *Light Absorption and Emission*

The normalized absorption and fluorescence spectra of **4.5** and **4.6** obtained in dichloroethane are shown in Figure 4.6. Both molecules exhibit an absorption maximum near that of sexithiophene (λ_{max} 436 nm, 50,000 M^{-1} cm^{-1}).[240] Compound **4.5** (λ_{max} 470 nm, 80,000 M^{-1} cm^{-1}) exhibits a slight redshift in absorption maximum compared to **4.6** (λ_{max} 463 nm, 34,500 M^{-1} cm^{-1}). The redshift is potentially due to the electron donating characteristics of the aromatic groups over alkyl groups attached through germanium. One noticeable feature is the absorption of **4.5** at 366 nm, which is not present in **4.6**. The

fluorescence spectra of **4.5** (λ_{max} 540 nm) and **4.6** (λ_{max} 555 nm) are similar in energy and features.

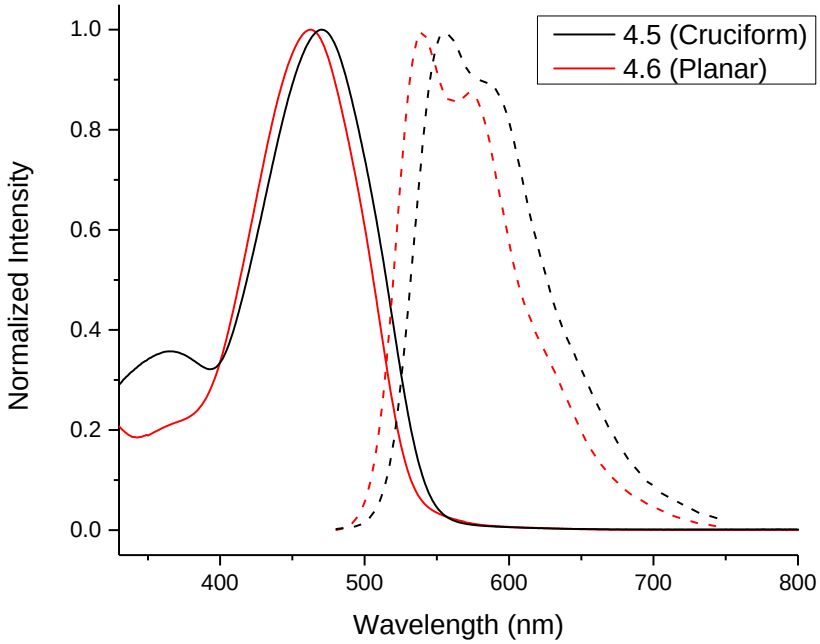

Figure 4.6 – Absorption (solid) and fluorescence (dashed) spectra of 4.5 (black) and 4.6 (red)

Absolute quantum yields were obtained for **4.5** (Φ_{fl} = 0.10) and **4.6** (Φ_{fl} = 0.35) in dichloroethane. Relative quantum yields (Φ_{fl} = 0.97, 9,10-diphenylanthracene) in THF for **4.2** (Φ_{fl} = 0.09) and **4.3** (Φ_{fl} = 0.11) were taken by Dr. Sarah Chi in the Perry group. The low quantum yields may indicate efficient intersystem crossing in germanium cruciform. Fluorescence lifetime measurements were attempted on **4.5**. The lifetimes are on the order of, or below, the detection limit of the instrument (1 nanosecond), which agrees with transient absorption experiments on **4.2** that show a decay in the excited singlet state absorption ($\tau \sim 510$ ps) with a subsequent rise of what is assumed to be the triplet state

absorption ($\tau \sim 580$ ps). Non-cruciform germanium compounds demonstrate higher absolute quantum yields and longer fluorescence lifetimes.[241]

4.4.2 *Electrochemistry*

Both compounds were evaluated by electrochemistry to estimate ionization potential. Compound **4.5**, Figure 4.7a, shows two reversible, overlapping oxidation waves with $E_{1/2}$ (determined by CV anodic-cathodic peak average and DPV oxidation scan peak) at 0.20 V and 0.39 V versus Fc/Fc^+ (–5.1 eV versus Vacuum)[242] corresponding to –5.3 eV as an estimate for the ionization potential. Compound **4.6**, Figure 4.7b, shows two reversible, well resolved oxidation waves with $E_{1/2}$ at 0.18 V and 0.39 V versus Fc/Fc^+, corresponding to –5.3 eV as an estimate for the ionization potential. In comparison, α-sexithiophene has two oxidation processes at 0.52 V and 0.67 V versus Fc/Fc^+ corresponding to –5.6 eV as an estimate for the ionization potential.[240]

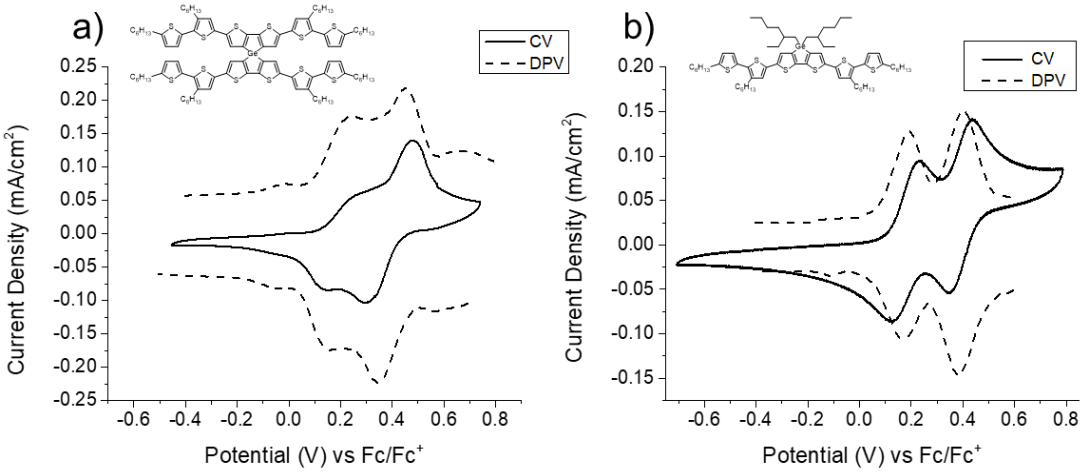

Figure 4.7 – Electrochemistry of 4.5 (a) and 4.6 (b). Cyclic voltammetry (solid) and differential pulse voltammetry (dashed) are shown for both compounds.

4.4.3 *Quantitative Electrochemistry*

Intuition suggests each oxidation wave in **4.6** consists of one electron, resulting in the radical cation and dication species, respectively. Transferring that logic to **4.5**, each wave consists of two electrons (one occurring on each half of the molecule) for each oxidation wave. The equivalent cathodic peak heights in **4.6** supports an equal charge passed for each process. However, the first oxidation wave in **4.5** is not well defined and the two waves are asymmetric in size. The potential for electronic communication between the two halves of **4.5** warrants a more thorough investigation of the oxidation processes. The amount of charge passed under each peak was determined by coulometry.

Electrochemical setup and data processing is described in Chapter 2. The electrochemistry of **4.5** is discussed first. The concentration of analyte in the electrochemical cell was ~3×10^{-5} M in 3 mL total volume. With $E_{1/2}$ at 0.20 V, and the applied voltage at 0.25 V, the Nernst equation predicts 88% conversion to the oxidized species for the first oxidation processes. The second oxidation was held at 0.46 V, predicting 94% conversion. Given the number of electrons transferred per mole must be a whole number, these conversions are suitable. The reduction potentials are far more negative than $E_{1/2}$, and full conversion to the neutral species is expected. (Note: the charge passed during reduction is never expected to exceed the charge passed during oxidation). Example coulometric plots (Q versus t) are shown in Figure 4.8. The final 20 seconds of each run was used for linear regression analysis back to time zero. Points A and D represent the charge passed (not adjusted for background) during complete oxidation of **4.5** (oxidation at 0.46 V and reduction to neutral). Points B and C represent charge passed at the first oxidation wave (0.25 V and reduction to neutral).

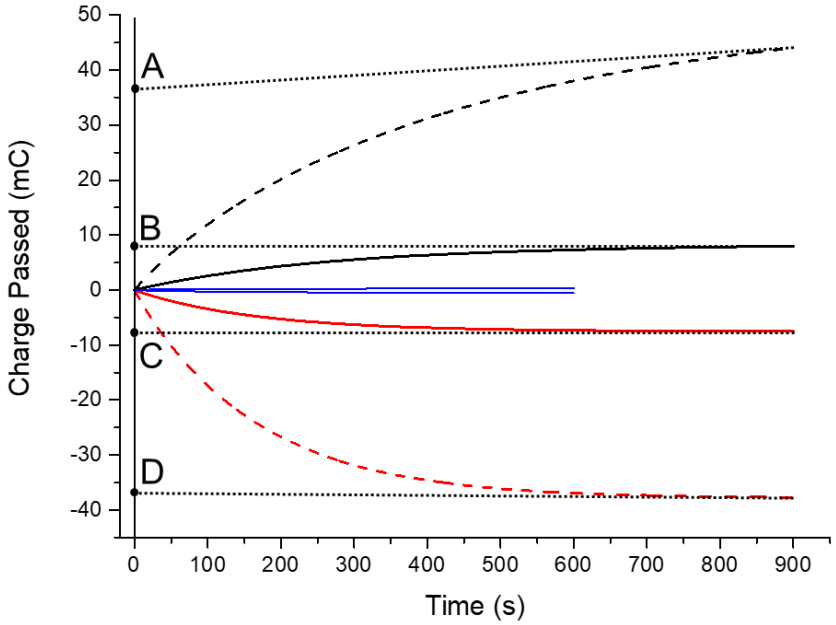

Figure 4.8 – Coulometry plots of 4.5: oxidation at 0.25 V (black, solid) and corresponding reduction to neutral at -0.20 V (red, solid), oxidation at 0.46 V (black, dashed) and corresponding reduction to neutral at -0.20 V (red, dashed), background scans at 0.46 V and -0.20 V (blue, solid). Linear regression plots (black, dotted) are traced to time zero

Multiple experiments were performed at each potential. After six to eight runs were performed on one sample, a reduction in charge passed was observed due to decomposition of the material. Figure 4.9 shows the average and standard deviation for coulometric measurements on **4.5**. One electron is passed during the first oxidation process. This is contrary to the expected two electrons as detailed above. Four electrons are passed when holding at the higher potential (one electron in the lower potential process and three in the higher potential process).

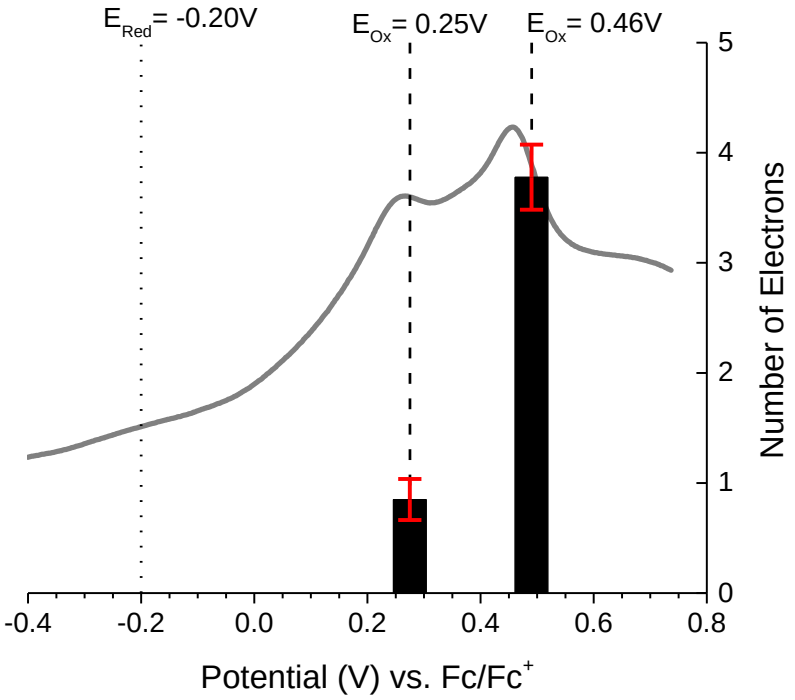

Figure 4.9 – Quantitative electrochemistry results for 4.5 against a DPV background to indicate potential.

The first oxidation is assigned to one half of the cruciform molecule, as it is equipotential to the first oxidation in **4.6**. The oxidation of the other half of the cruciform is affected by this first oxidation. These data support, but do not confirm, that the first radical cation is delocalized across both halves of the cruciform or exerts an electronic influence across the entire molecule. Electrochemistry has inherent factors that skew the observed potential versus true IP, and one should not take electrochemically derived values as absolute.[243] The shift of the second removed electron from **4.5** to a higher potential, but not the fourth removed electron, is interesting. If that first electron is partially delocalized, the second oxidation appears to cease that delocalization. The result being that the second oxidation is more difficult, but once performed, the 3rd and 4th oxidations occur at the expected potentials.

Compound **4.6** depicts a 1:2 ratio of charge between the two oxidation waves, Figure 4.10. This leads to the conclusion that one electron is passed under each oxidation. The required dilution ($1x10^{-8}$ mol) on a small volume (<5 mL) is presumed to have caused a measurement error, such that the number of electrons does not correspond to a whole number. Based on electrochemistry and electron pair resonance studies of sexithiophene[240,244] and the precise 1:2 ratio of the obtained data, it is within reason to assume one electron is passed under each oxidation wave. This is further supported by doping studies performed in Section 4.4.4.

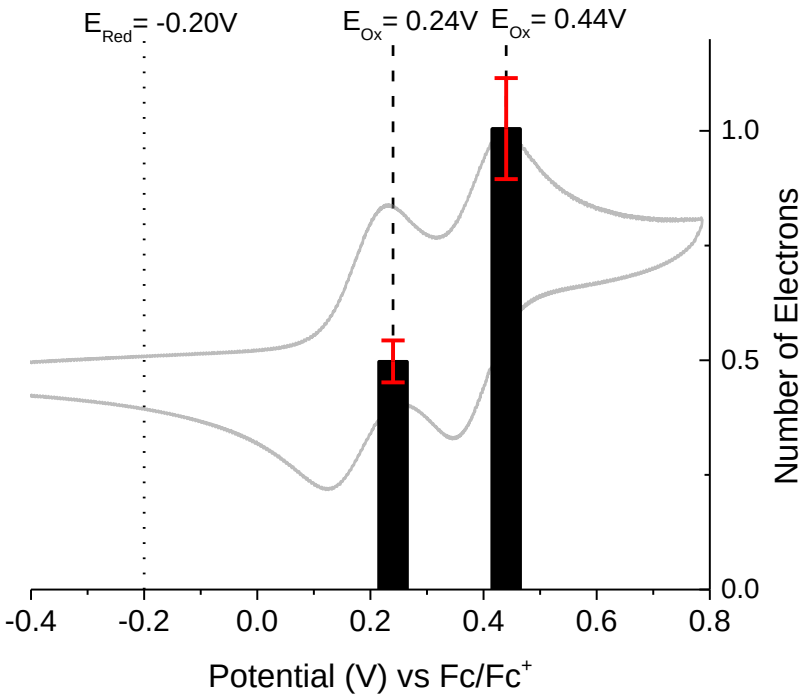

Figure 4.10 – Quantitative electrochemistry results for 4.6 against a CV background to indicate potential.

4.4.4 *Analysis of Oxidized Species by UV-Vis Spectroscopy*

A spectroscopic method was implemented to elucidate the species generated during oxidation. Bulk chemical oxidation for spectroscopy was preferred to bulk electrochemical

oxidation or optically transparent thin-layer electrode (OTTLE) techniques due to stoichiometric conversion to the species of interest using strong dopant. Tris(4-bromophenyl)ammoniumyl hexachloroantimonate (Magic Blue) was used as a chemical dopant (oxidation potential 0.70 V vs Fc/Fc^{+}).[245]

Stoichiometric equivalents of Magic Blue from 0 to 4 were investigated for **4.5**, Figure 4.11a-c. From neutral absorption to 1.0 equiv., the neutral absorbance decreases to approximately half its original absorption. Two longer wavelength absorptions, characteristic of a radical cation (RC),[244] appear and increase in intensity. The near half decrease in neutral absorbance intensity with no shift in energy suggests no significant delocalization occurs across the two halves. Continuing to 2.0 equiv. of Magic Blue, the neutral absorption is nearly completely removed. The radical cation absorptions remain but do not grow in intensity, and the dication (DC) absorption begins to grow in. This is attributed to an equilibrium between the dication-neutral and radical cation-radical cation pairs in solution. The agrees with electrochemistry results suggesting the second neutral-to-oxidized process occurs at the same potential as the oxidized-to-doubly oxidized process. From 2.0 equiv. to 4.0 equiv., the dication peak continues to grow as the radical cation disappears. No additional oxidation occurs beyond 4.0 equiv., confirming the four-electron count from quantitative electrochemistry.

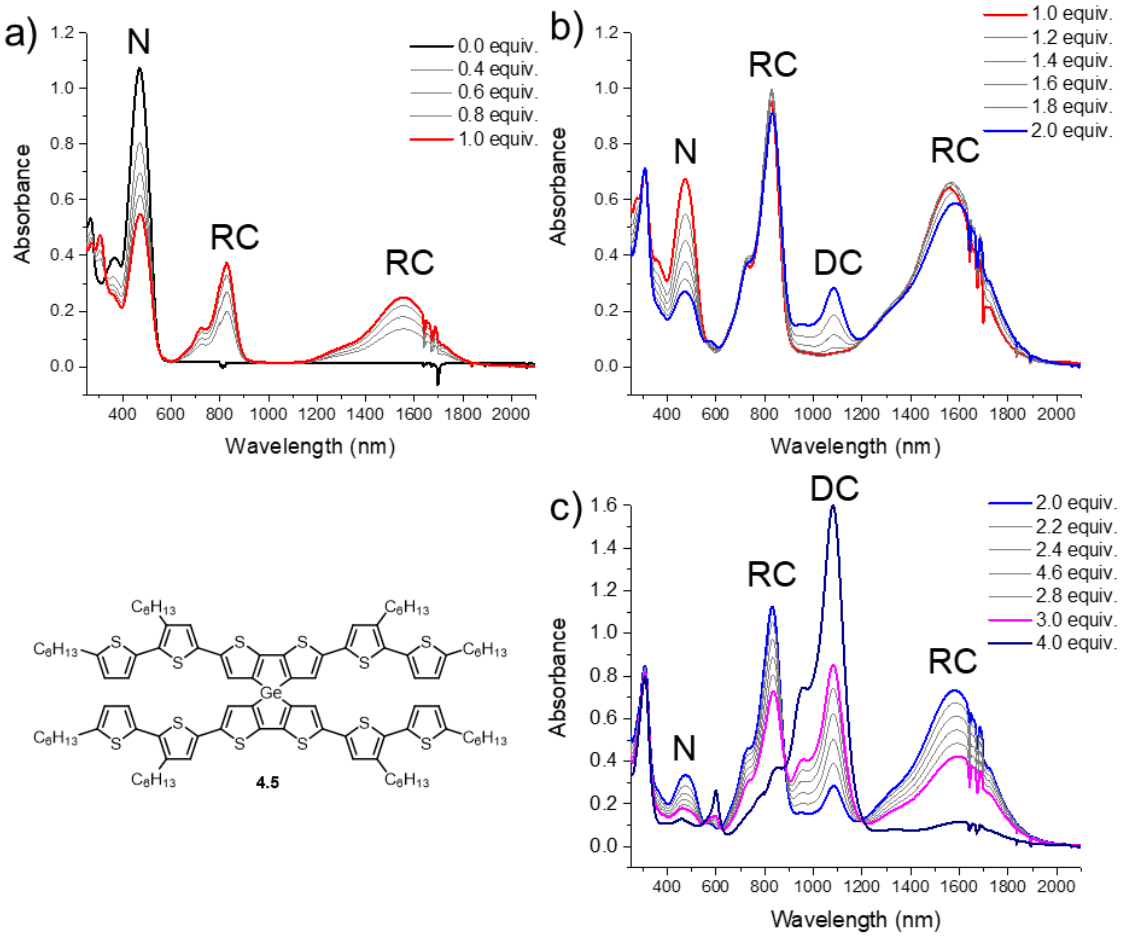

Figure 4.11 – UV-Vis spectra of Compound 4.5 doped with Magic Blue. a) Stoichiometric equivalents 0.0 – 1.0, b) stoichiometric equivalents 1.0 – 2.0, c) stoichiometric equivalents 2.0 – 4.0.

Stoichiometric doping with Magic Blue of **4.6** tells a similar story, Figure 4.12. In substoichiometric equivalents, the neutral absorbance decreases completely by 0.8 equiv., accompanied by the growth of a radical cation absorption at longer wavelengths. The beginning of the dication absorption before 1.0 equiv. is attributed to inaccuracies in concentration of stock solutions, not an equilibrium. Beyond 1.0 equiv., the radical cation absorbance disappears as the dication continues to increase in intensity. The radical cation is quenched by 1.6 equiv., which agrees with the 0.8 equiv. required for complete neutral absorbance quenching. No change in absorption occurs above 2.0 equiv. This is consistent

with two one-electron oxidations occurring sequentially, as in the quantitative electrochemistry experiment.

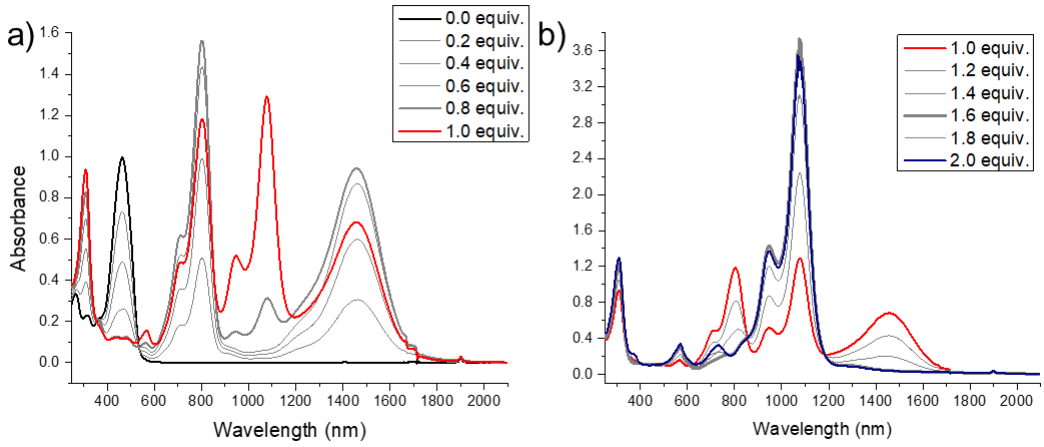

Figure 4.12 – UV-Vis spectra of Compound 4.6 doped with Magic Blue. a) Stoichiometric equivalents 0.0 – 1.0, b) stoichiometric equivalents 1.0 – 2.0.

4.5 Conclusions and Outlook

A three-dimensional extended spirobi[germolodithiophene] was synthesized by four-fold Stille cross-coupling. The first oxidation behavior and UV-Vis absorption is nearly indistinguishable from the planar analog; however, the second oxidation behavior indicates an equilibrium between the dication and the bis(radical cation). This energetic equivalence is supported by quantitative electrochemistry. While compounds **4.5** and **4.6** were not solids, not tested in devices, and not stable to ambient conditions, the emphasis of the study was the electronics of germanium cruciforms. The first oxidation on one arm of **4.5** clearly affects the oxidation of the second arm, as evidenced by electrochemistry and spectroscopic doping studies. Further experiments to investigate the electronics of partially oxidized **4.5** are warranted.

The rapid intersystem crossing and low singlet quantum yield is attributed to the rigid cruciform structure and germanium center. These may be useful in studying triplet processes in organic photovoltaics and as singlet fission materials.[246–248] The core species are stable solid that allow for experiments to be performed in the solid state.

The future of this project is best split into three directions. From an applications standpoint, the final material should be modified so that it is a solid. This can be done by reducing the number of hexyl solubilizing chains, albeit at the expense of solubility and ease of purification. A solid product can also be obtained by the addition of benzothiadiazole moieties in the arms. This has the added benefit of moving the absorption maximum to a longer wavelength through the creation of a donor-acceptor molecule. This work has been undertaken by Thomas Marchandier.

The second direction is the more thorough investigation of the excited and oxidized states of the germanium cruciform. Electron pair resonance spectroscopy can be implemented to determine the relationship and equilibrium between radical cation and dication species during the second oxidation of the cruciform. Ultrafast laser spectroscopy can be used to identify the rate of intersystem crossing.

The third direction is the expansion to silole and cyclopentadiene cruciform analogs. The comparison of germanium containing molecules to their silicon and carbon derivatives is a continued interest in the group and wider field. The synthesis of silicon and carbon cruciforms will allow for direct investigation of the role of germanium in the properties of the molecule.

4.6 Synthetic Writeups and Experimental

4.6.1 *Instrumentation and General Methods*

Solution NMR spectra were recorded on a Varian Mercury Vx (300 MHz ^{1}H, 75 MHz ^{13}C). Spectra were processed using MestReNova v6.0 and referenced to residual protonated solvent signals ($CDCl_3$: ^{1}H 7.26 ppm, ^{13}C 77.16). Accurate mass spectra were collected by the Bioanalytical Mass Spectrometry Facility at Georgia Tech on a Bruker AutoFlex III (MALDI-TOF). Elemental analyses were carried out by Atlantic Microlabs on a PerkinElmer 2400 II analyzer (CHN) and a Carlo Erba 1108 analyzer (S). Absorption spectra were recorded on a Varian Cary 5000 Scan UV-Vis-NIR spectrophotometer in dichloroethane. Fluorescence spectra were recorded on a HORIBA Fluorolog in dichloroethane at 298 K. Absolute quantum yields were determined on a Hamamatsu Quantaurus-QY absolute PL quantum yield spectrometer in dichloroethane at 298 K. Electrochemistry (differential pulse voltammetry (DPV) and cyclic voltammetry (CV) were obtained on a Princeton Applied Research (PAR) 270A potentiostat in dichloroethane with 0.1 M supporting electrolyte (Bu_4NPF_6) using a platinum button working electrode, platinum flag counter, and Ag/Ag^+ reference. The reference was calibrated with ferrocene the day of each experiment and all potentials are referenced versus Fc/Fc^+. Melting points were collected on a MEL-TEMP apparatus with digital thermometer at a 10 °C/min heating rate and are reported uncorrected.

The X-Ray crystal structure was obtained by Dr. Khalil A. Abboud and Ashley C. Felts. X-Ray intensity data were collected at 100 K on a Bruker **DUO** diffractometer using MoKα radiation (λ = 0.71073 Å) and an APEXII CCD area detector.

Raw data frames were read by program SAINT[1] and integrated using 3D profiling algorithms. The resulting data were reduced to produce hkl reflections and their intensities and estimated standard deviations. The data were corrected for Lorentz and polarization effects and numerical absorption corrections were applied based on indexed and measured faces. The structure was solved and refined in *SHELXTL2014*, using full-matrix least-squares refinement. The non-H atoms were refined with anisotropic thermal parameters and all of the H atoms were calculated in idealized positions and refined riding on their parent atoms. Each half of the molecule joined at Ge1 is planar and the dihedral angle between the two planes is 83.0(1). In the final cycle of refinement, 4614 reflections (of which 4285 are observed with $I > 2\sigma(I)$) were used to refine 226 parameters and the resulting R_1, wR_2 and S (goodness of fit) were 2.28%, 5.45% and 1.099, respectively. The refinement was carried out by minimizing the wR_2 function using F^2 rather than F values. R_1 is calculated to provide a reference to the conventional R value but its function is not minimized.

Dibromobis(2-ethylhexyl) germane[249,250] and 4,4-bis(2-ethylhexyl)-2,6-bis(trimethylstannyl)germolo[3,2-*b*:4,5-*b'*]dithiophene (not purified by HPLC)[110,250] were prepared according to literature procedures. 5-bromo-3,5'-dihexyl-2,2'-bithiophene was prepared by treating 3,5'-dihexyl-2,2'-bithiophene with NBS in chloroform. All reactions were performed under inert (argon) conditions using standard Schlenk techniques. THF and toluene were obtained from an MBraun Solvent Purification System with alumina columns. DMF (EMD DriSolv) was stored over activated 3Å molecular sieves and sparged with argon before use. Silica gel (60 Å, 230-400 mesh) was purchased from Sorbtech

(Norcross, GA). All other reagents were purchased from commercial suppliers and used without further purification unless otherwise specified.

4.6.2 *Synthesis of Chapter 4 Compounds and Precursors*

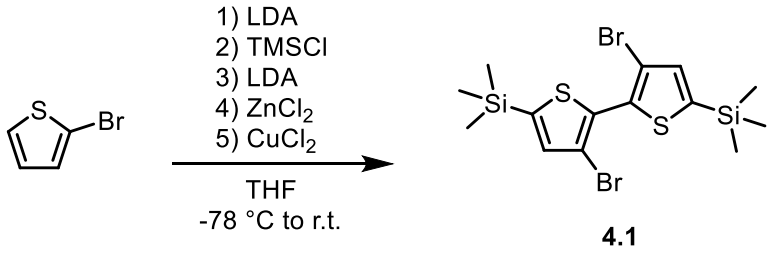

Figure 4.13 – Synthesis of 4.1 from 2-bromothiophene

3,3'-dibromo-5,5'-bis(trimethylsilyl)-2,2'-bithiophene (4.1): The reaction was carried out using a modified literature procedure.[251,252] THF (500 mL) containing 2-bromothiophene (19.4 g, 119 mmol, 1.0 equiv.) was cooled to –78 °C. Lithium diisopropylamide (LDA) (59.5 mL, 2.0 M in THF, 119 mmol, 1.0 equiv.) was added dropwise over 30 min, and the reaction was stirred for 60 min. Trimethylsilylchloride (12.9 g, 119 mmol, 1.0 equiv.) was added dropwise, and the reaction was stirred for 30 min. LDA (65.5 mL, 2.0 M in THF, 130.9 mmol, 1.1 equiv.) was added dropwise over 30 min., and the reaction was stirred for 30 min. Zinc chloride (16.2 g, 119 mmol, 1.0 equiv.) was added in one portion, and the reaction was stirred for 30 min. Copper(II) chloride (16.0g, 119 mmol, 1.0 equiv.) was added in one portion, and the reaction was allowed to warm to r.t. overnight with stirring. The reaction was diluted with hexanes (300 mL) and filtered through a Celite plug before being concentrated to a brown solid. The crude material was subjected to column chromatography (silica gel, 100% hexanes) to give a faint green solid. Recrystallization from ethanol yielded faint blue crystals (20 g, 43 mmol, 72%).

^{1}H NMR (300 MHz, $CDCl_3$): δ 7.15 (s, 2H), 0.34 (s, 18H). $^{13}C\{^{1}H\}$ NMR (75 MHz, $CDCl_3$): δ 143.06, 137.15, 134.06, 113.07, -0.23.

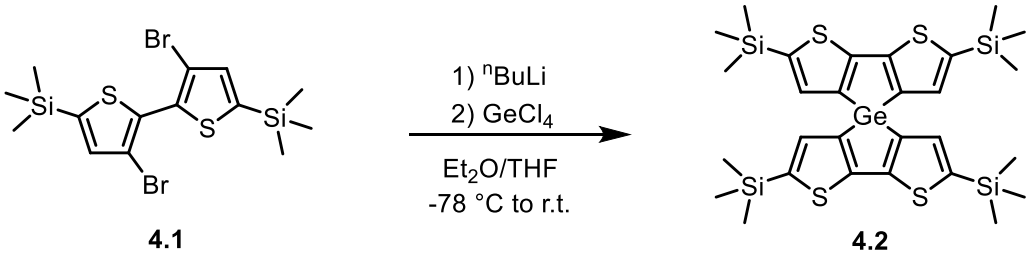

4.1 **4.2**

Figure 4.14 – Cyclization of 4.1 to give spirobi[germolodithiophene], 4.2

2,2',6,6'-tetrakis(trimethylsilyl)-4,4'-spirobi[germolo[3,2-*b*:4,5-*b*']dithiophene] (4.2): The reaction was carried out using a modified literature procedure for 4,4-bis(2-ethylhexyl)-2,6-bis(trimethylsilyl)germolo[3,2-*b*:4,5-*b'*]dithiophene.[110] To a solution of *n*BuLi (16.8 mL, 2.5 M in hexanes, 42 mmol, 2.1 equiv.) in Et_2O (300 mL) at –78 °C was added **4.1** (9.368 g, 20 mmol, 1.0 equiv.) in THF (50 mL). The resulting solution was stirred at –78 °C for 2.5 hrs. before the dropwise addition of germanium tetrachloride solution (2.145 g, 10 mmol, 0.5 equiv.) in Et_2O (30mL). The mixture was stirred for 30 min. before being allowed to warm to r.t. overnight. The reaction was poured into 0.25 M $NaHCO_3$ and extracted three times with hexanes. The combined organics were washed with brine, dried over $MgSO_4$, and concentrated to give a crystalline solid. Column chromatography (silica gel, 100% hexanes) gave the title compound as an off-white crystalline solid (5.0 g, 73%). NMR agrees with the previous report.[223]

^{1}H NMR (300 MHz, $CDCl_3$): δ 7.09 (s, 4H), 0.31 (s, 36H). $^{13}C\{^{1}H\}$ NMR (75 MHz, $CDCl_3$): δ 153.97, 142.31, 138.25, 137.00, 77.16, 0.18. Anal. Calcd for $C_{28}H_{40}GeS_4Si_4$ (%): C, 48.75; H, 5.84; S, 18.59. Found (%): C, 48.73; H, 5.94; S, 18.39. HRMS (MALDI-TOF) Calc. [M+] 690.0302, Found 690.0269. Melting Point: 347 °C, decomposition.

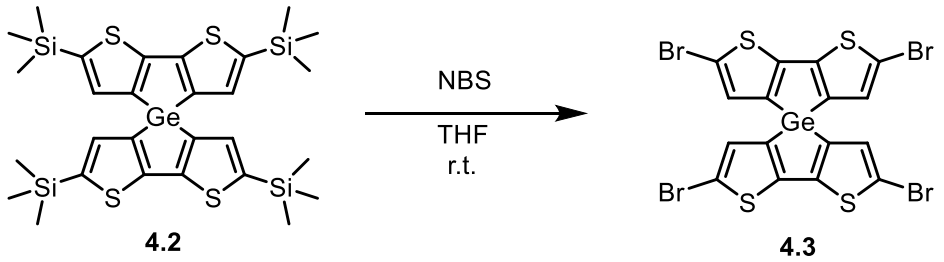

4.2 4.3

Figure 4.15 – Simultaneous deprotection and bromination of 4.2 to give the tetrahalide 4.3

2,2',6,6'-tetrabromo-4,4'-spirobi[germolo[3,2-*b*:4,5-*b*']dithiophene] (4.3): The reaction was carried out using a modified literature procedure for 2,6-dibromo-4,4-bis(2-ethylhexyl)germolo[3,2-*b*:4,5-*b'*]dithiophene.[237] To a solution of **4.2** (1.38 g, 2.0 mmol, 1.0 equiv.) in THF (20 mL), *N*-bromosuccinimide (1.50 g, 8.4 mmol, 4.1 equiv.) was added in one portion. The mixture was stirred at r.t. for 4 hours during which time a yellow precipitate formed. The reaction was poured into a large excess of cold water (100 mL), and the yellow precipitate was collected by vacuum filtration onto a 20 µm nylon filter. The yellow solid was washed thoroughly with water followed by a 1:1 methanol:water mixture, leaving behind **4.3** as a pale-yellow solid which was dried under high vacuum overnight (1.21 g, 87%).

^{1}H NMR (300 MHz, $CDCl_3$): δ 6.93 (s). $^{13}C\{^{1}H\}$ NMR (75 MHz, $CDCl_3$) δ 148.84, 133.42, 132.13, 112.96. Anal. Calcd for $C_{16}H_4Br_4GeS_4$ (%): C, 26.81; H, 0.56; Br, 44.60; S, 17.89. Found (%): C, 26.94; H, 0.36; Br, 44.34; S, 17.84. HRMS (MALDI-TOF) Calc. [M+] 713.5141, Found 713.5154. Melting Point: 325 °C, decomposition.

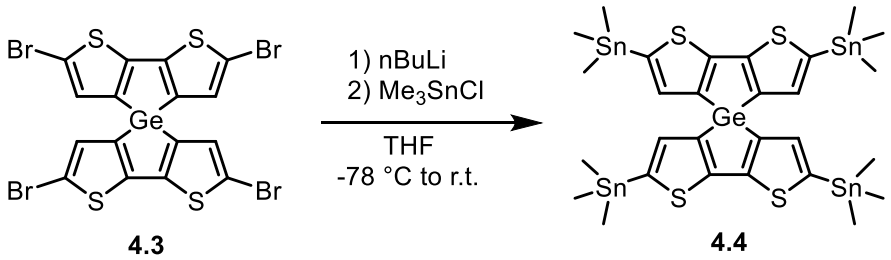

4.3 **4.4**

Figure 4.16 – Stannylation of 4.3 by lithium-halogen exchange and quenching with Me_3SnCl

2,2',6,6'-tetrakis(trimethylstannyl)-4,4'-spirobi[germolo[3,2-*b*:4,5-*b*']dithiophene] (4.4): Compound **4.3** (143.3 mg, 0.20 mmol, 1.0 equiv.) in THF (30 mL) was cooled to –78 °C and stirred for 30 min. to ensure complete dissolution. ^{n}BuLi (0.40 mL, 2.5 M in hexanes, 1.0 mmol, 5.0 equiv.) was added dropwise over 15 min. The mixture was allowed to stir for 30 min. before the dropwise addition of Me_3SnCl (1.2 mL, 1.0 M in hexanes, 1.2 mmol, 6.0 equiv.). The reaction was stirred for 1 hr. at –78 °C, warmed to r.t., and allowed to stir for 1 hr. The reaction was poured into 0.25 M $NaHCO_3$ and extracted with hexanes three times. The combined organics were washed with water, then with MeOH. The MeOH wash was back extracted once with fresh hexanes. The combined hexanes were dried over $MgSO_4$ and concentrated to a green and white, crystalline solid which was used without further purification. (200 mg, 98%).

^{1}H NMR (300 MHz, $CDCl_3$): δ 7.04 (s, 4H), 0.35 (s, 36H). HRMS (MALDI-TOF) Calc. [M+] 1057.7313, Found 1057.7294.

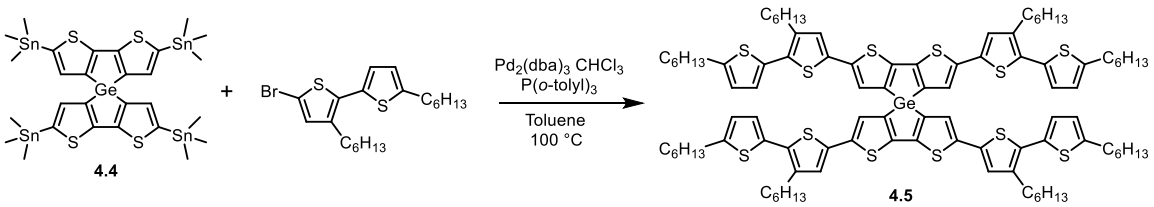

Figure 4.17 – Synthesis of spirobi[germolodithiophene] 4.5 by four-fold Stille coupling

2,2',6,6'-tetrakis(3,5'-dihexyl-[2,2'-bithiophen]-5-yl)-4,4'-spirobi[germolo[3,2-*b*:4,5-*b*']dithiophene] (4.5): A known amount of **4.4** (55 mg, 0.052 mmol, 1.0 equiv.) in a pre-tared vial was transferred to a flame dried Schlenk tube with a minimal amount of DCM, which was removed under light vacuum before drying completely under high vacuum. 5-bromo-3,5'-dihexyl-2,2'-bithiophene (173 mg, 0.4 mmol, ~7.5 equiv.), $Pd_2dba_3 \cdot CHCl_3$ (1.2 mg, 5mol% Pd per **4.4**), and P(*o*-tol)$_3$ (1.6 mg, 10mol% per **4.4**, 2:1 L:Pd loading) were added to the Schlenk tube with a stir bar. (Note Section 2.1 for proper modifications to this procedure, such as 3:1 L:Pd loading, premixing ligand-catalyst, and not adding palladium directly to liquid monomer). The tube was subjected to three evacuation-backfill cycles with argon. Toluene (5mL), degassed by four freeze-pump-thaw cycles, was added by syringe. The reaction was heated to 100 °C overnight. TLC analysis (5% DCM:Hexanes) showed residual bromide starting material, bromide homocoupling, and yellow-orange spots that turned red upon exposure to light and atmosphere (product). The reaction was poured into 0.25 M $NaHCO_3$ and extracted three times with DCM. The combined organics were washed with brine, dried over $MgSO_4$, and concentrated to a red oil that slowly solidified to a tacky solid. A repeat reaction using 90 mg of **4.4** with identical conditions was performed. The combined crude materials were subjected to column chromatography (silica gel, 5% DCM:hexanes) with light excluded as much as possible by using aluminum foil around the column. 137 mg (56% combined yield) of a tacky red solid was recovered.

^{1}H NMR (300 MHz, $CDCl_3$): δ 7.08 (s, 4H), 6.98 (s, 4H), 6.90 (d, *J* = 3.6 Hz, 4H), 6.71 (dt, *J* = 3.6, 0.9 Hz, 4H), 2.80 (t, *J* = 7.6 Hz, 8H), 2.75 – 2.65 (m, 8H), 1.75 – 1.57 (m, 16H), 1.44 – 1.25 (m, 48H), 0.97 – 0.83 (m, 24H). ^{13}C{^{1}H} NMR (75 MHz, $CDCl_3$): δ 146.93, 146.43, 139.77, 139.36, 136.34, 134.19, 133.32, 130.59, 126.50, 126.09, 125.62, 124.52, 31.81, 31.71, 30.62, 30.28, 29.49, 29.37, 28.96, 22.77, 22.73, 14.26, 14.24. Note: One alkyl carbon signal cannot be resolved due to overlapping peaks in the ^{13}C spectrum. Anal. Calcd for $C_{96}H_{120}GeS_{12}$ (%): C, 66.60; H, 6.99; S, 22.22. Found (%): C, 66.63; H, 7.13; S, 21.99. HRMS (MALDI-TOF) Calc. [M+] 1730.5250, Found 1730.5195.

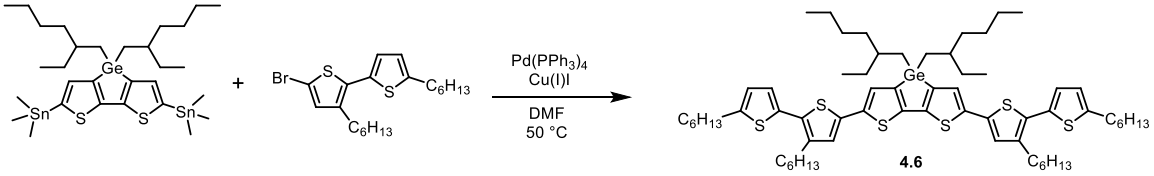

Figure 4.18 – Synthesis of planar analog 4.6 by Stille coupling

2,6-bis(3,5'-dihexyl-[2,2'-bithiophen]-5-yl)-4,4-bis(2-ethylhexyl)-germolo[3,2-*b*:4,5-*b*']dithiophene (4.6): A known amount of 4,4-bis(2-ethylhexyl)-2,6-bis(trimethylstannyl)germolo[3,2-*b*:4,5-*b'*]dithiophene (126.6 mg, 0.160 mmol, 1.0 equiv.) in a pre-tared vial was transferred to a flame dried Schlenk tube with stir bar with a minimal amount of DCM, which was removed under light vacuum. 5-bromo-3,5'-dihexyl-2,2'-bithiophene (199 mg, 0.481 mmol, 3.0 equiv.) was added to the Schlenk tube, and the two monomers were held under vacuum for 2 hours, then subjected to 3 evacuation-backfill cycles with argon. The monomers were dissolved in dry, argon sparged DMF (~5 mL). In a separate dry vial, copper(I) iodide (3.1 mg, 0.016 mmol, 10 mol% Cu per tin compound), tetrakis(triphenylphosphine)palladium(0) (9.3 mg, 0.008 mmol, 5 mol% Pd per tin compound) were dissolved in a minimal amount of dry, argon sparged DMF. The catalysts were transferred to the reaction by syringe. The reaction was heated to 50 °C for 24 hrs.

The reaction was poured into 0.25 M $NaHCO_3$ and extracted three times with hexanes. The combined organics were washed with water, dried over $MgSO_4$, and concentrated to a red-brown oil. A short plug (silica gel, 100% hexanes) removed starting materials and catalyst residues. The resulting red oil was further purified on preparatory TLC plates (20 cm × 20 cm, 1000 μm, 100% *n*-pentane) pretreated with triethylamine in *n*-pentane (5% v/v) and washed by developing once with 100% *n*-pentane. After loading the plates with minimal light exposure, the plates were developed with complete light exclusion under an inert atmosphere. An orange band at R_f ~0.4 was separated from a red band at R_f ~0.25. The red band was identified as the dimer of dithienogermole flanked by bithiophenes (6,6'-bis(3,5'-dihexyl-[2,2'-bithiophen]-5-yl)-4,4,4',4'-tetrakis(2-ethylhexyl)-2,2'-bi[germolo[3,2-*b*:4,5-*b*']dithiophene]). The orange band was concentrated to an orange oil affording **4.6** (39 mg, 22%).

^{1}H NMR (300 MHz, $CDCl_3$) δ 7.09 (s, 2H), 6.93 (bs, 4H), 6.73 (d, J = 3.6 Hz, 2H), 2.82 (m, 4H), 2.77 – 2.67 (m, 4H), 1.79 – 1.61 (m, 12H), 1.44 – 1.13 (m), 0.94 – 0.77 (m). Residual pentane prevented accurate integrations of alkyl region. HRMS (MALDI-TOF) Calc. [M+] 1128.4892, Found 1128.4891.

CHAPTER 5. OPTIMIZATION OF POLY(NICKEL ETHENETETRATHIOLATE) REACTION CONDITIONS

5.1 NiS_4 Complexes: History and Applications

The field of conducting nickel coordination compounds grew from the merging of two fields: conducting metallic salts – such as Magnus' Green Salt (tetraammineplatinum(II) tetrachloroplatinate(II), $[Pt(NH_3)_4][PtCl_4]$)[253,254] and Krogmann's Salt (Dipotassium tetracyanoplatinate(II) bromide trihydrate, $K_2[Pt(CN)_4]Br_{0.3}\bullet 3H_2O$)[255] – and conducting organic radical salts – such as tetrathiafulvalene tetracyanoquinodimethane (TTF-TCNQ).[256,257] The one-dimensional metal characteristics of the platinate chains originates from overlapping d_z^2 orbitals, but the material undergoes a metal-to-semiconductor transition above 70 K.[258] Radical organic salts were also found to have quasi one-dimensional metal behaviour due to the parallel stacks of planar π-systems.[259] These typically undergo a metal-to-insulator transition upon cooling due to a Peierel's distortion (also called a Peierel's transition).[257] Notable exceptions are bis(tetramethyltetraselenafulvalene) $[(TMTSF)_2X]$[260,261] and bis(ethy1enedithiolo)tetrathiafulvalene $[(BEDT\text{-}TTF)_2X]$[262,263] salts, whose superconductivity at low temperatures is attributed to multidimensional conduction through strong interchain electronic interactions.

The search for multidimensional metal systems increased interest in nickel-sulfur coordination complexes, especially bis(dithiolenes). These materials form mixed valence systems, with close π-π spacing, and short sulfur-sulfur or nickel-sulfur interstack

connections.[257,264] For example, the crystals of partially oxidized tetrabutylammonium bis(2-thioxo-1,3-dithiol-4,5-dithiolato)nickelate(II) ($[NBu_4]_2[Ni(dmit)_2]_7$) show conductivities from 1-10 S/cm at 300 K with low anisostropy.[257] Great interest was supplied to combining concepts of nickel bis(dithiolenes) with TTF-like ligand extensions or counterions. The core ligands for these coordination complexes are described in the following section.

5.1.1 *Common Dithiolene Ligands for Square Planar Nickel(II) Complexes*

Figure 5.1 shows common dithiolene-based ligands that take square planar geometries with nickel(II). This allows for the interchain interactions (Ni-S, S-S, π-π) associated with multidimensional conductivity.[264] Crystals and compacted powders of these complexes are often intrinsic conductors, meaning they require no doping or oxidation-reduction reaction to be conductive in ambient conditions.[265]

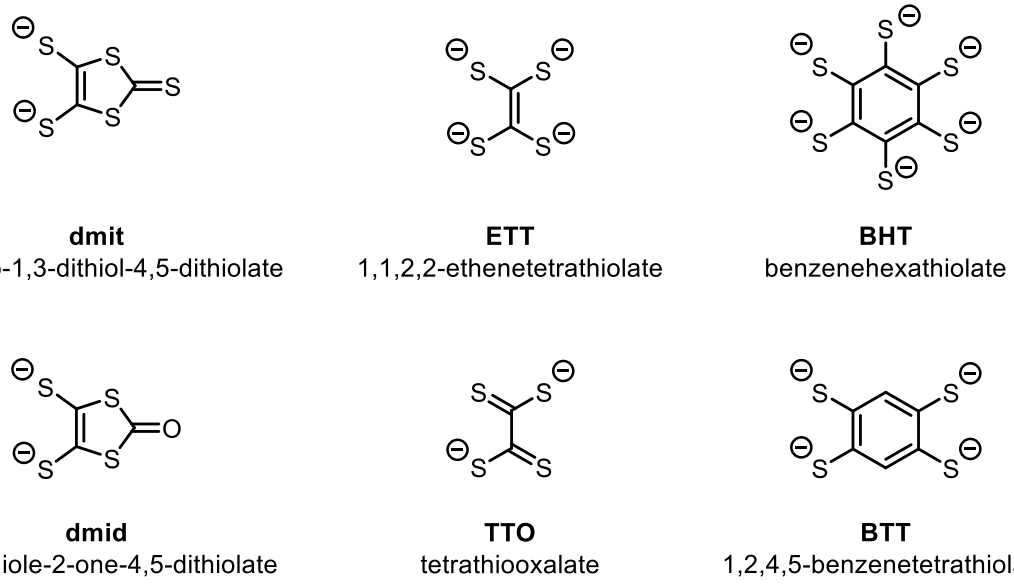

Figure 5.1 – Common dithiolene ligands for square planar nickel(II) complexes and their abbreviations

5.1.1.1 Bidentate Dithiolene Ligands

The two most common bidentate ligands are dmit (1,3-dithiole-2-thione-4,5-dithiolate) and dmid (1,3-dithiole-2-one-4,5-dithiolate). Extensive studies are published on dmit and its transformations.[258,266] Daoben Zhu and coworkers have studied complexes of $Ni(dmid)_2$.[267,268]

The naming convention for dmit came from "trithione" as suggested by Böttcher and Lüttringhaus for 1,2-dithiole-3-thiones. 1,3-Dithiole-2-thione was then shortened to "isotrithione." Thus 1,3-dithiole-2-thione-4,5-dithiolate is dimercaptoisotrithione (dmit). This nomenclature spawned the related ligand names dmid (1,3-dithiole-2-one-4,5-dithiolate) and dsit (1,3-dithiole-2-thione-4,5-diselenolate). These remain widespread in the literature to this day.[266,269]

Figure 5.2 details the synthesis and interconversion between dmit and dmid. Both syntheses are discussed in more detail later in this chapter. The reduction of carbon disulfide electrochemically or by sodium results in the formation of dmit.[266,270–272] Treatment of thiapendione with a nucleophilic base gives dmid. Conversion from alkylated derivatives of dmit to dmid is realized with mercuric acetate, while the reverse conversion is realized with boron sulfide.[266,273]

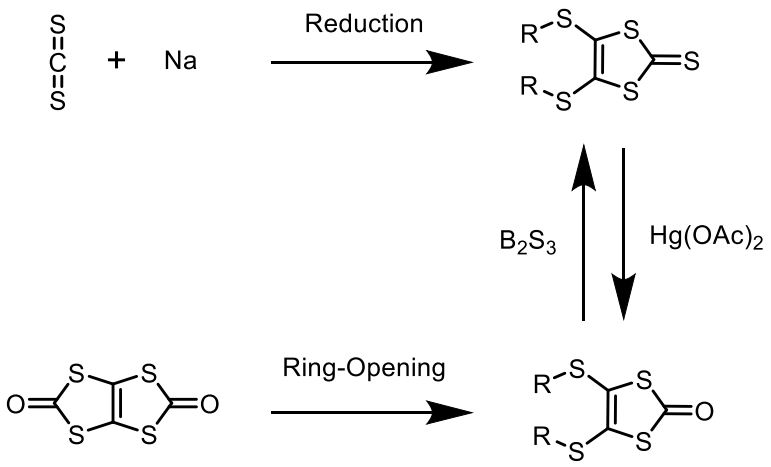

Figure 5.2 – Formation and interconversion of bidentate dithiolene ligands

5.1.1.2 Tetradentate Bis(dithiolene) Ligands

While single crystals of nickel(II) complexes are conductive, it was believed that extending the conductive pathway through multiple nickel centers in metal coordination polymers would allow for increased conductivity beyond the single crystal.[264,274] The simplest structures are realized with bis(dithiolenes) such as 1,1,2,2,-ethenetetrathiolate (ETT) or tetrathiooxalate (TTO).[265,275,276] Aromatic thiolates including benzenetetrathiolate and benzenehexathiolate have also been extensively studied.[277–280]

Coordination polymers of nickel with ETT and TTO are described in more detail in this chapter (ETT), Chapter 6 (ETT), and Chapter 7 (TTO). It is important to note now the similarities and differences between ETT and TTO, Figure 5.3. Both ligands are of the composition C_2S_4, with ETT being $C_2S_4^{4-}$ and TTO being $C_2S_4^{2-}$. In its uncoordinated state, TTO ($C_2S_4^{2-}$) shows considerable C-C single bond character with a near 90° dihedral angle.[264,281] After coordination, the S-C-C-S dihedral angle planarizes, the C-C bond shortens, and the C-S bonds lengthen.[264] The uncoordinated ETT ligand $C_2S_4^{4-}$ has not been experimentally confirmed and is only hypothesized to exist as an intermediate or to exist

as a coordinated ligand acting as that fragment. This highlights the difficulty in assigning specific ETT or TTO character to ligands in discrete complexes. This is especially true in coordination polymers where the oxidation state is not easily determined.

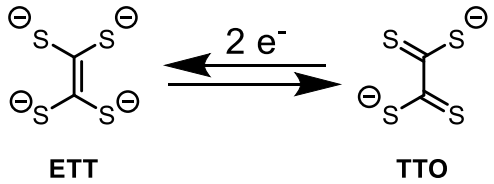

Figure 5.3 – Interconversion of ETT and TTO through a two-electron oxidation-reduction reaction

5.1.1.3 Bimetallic Complexes

Between $Ni(dmit)_2$ and NiETT exists a class of oligonickel materials with a discrete number of nickel centers. Our group has studied both copper[282,283] and nickel species.[284] Others have continued this work with other capping ligands.[285] The low yields and intensive separations required for obtaining these materials discouraged our continued investigation. An alternative route by direct treatment of $Ni(dmit)_2$ with sodium dithionite was reported by Bai et al.[286]

5.1.2 *Organic Thermoelectrics Niche*

Nickel dithiolenes, originally conceived as potential superconductors, also showed a negative thermopower or Seebeck coefficient. The majority work focused on single crystals and pressed pellets. The rise of poly(ethylenedioxythiophene):poly(stryenesulfonate) (PEDOT:PSS) and doped p-type conducting polymers that show appreciable conductivity and high Seebeck coefficients drove the need for a suitable organic n-type thermoelectric material.[18,287] The ambient

stability of nickel dithiolenes, their intrinsic conductivity, and their negative Seebeck coefficient make these materials promising n-type thermoelectrics to explore.

5.2 Nickel(II) Bis(1,3-dithiole-2-thione-4,5-dithiolate) (Ni(II)(dmit)$_2$)

Ni(dmit)$_2$ is a well-studied material that can be synthesized on a large scale through readily available chemicals. The material is a useful entry point to understanding nickel coordination compounds, their solubilities, oxidation states and sensitivity, color changes, reaction behavior. Therefore, Ni(dmit)$_2$ was the first coordination complex targeted.

5.2.1 *Large Scale Synthesis*

The ease of reaction chemistry and inexpensive reagents allows Ni(dmit)$_2$ to be prepared on a multigram scale, which is ideal for rapid material testing and investigation as a precursor to NiETT. Figure 5.4 shows reaction to form the ligand dmit through reduction of carbon disulfide with an alkali metal (both sodium and potassium are used) in cold DMF developed by Hoyer and coworkers[271,288] and reported in English by others.[266] Direct complexation of dmit with nickel(II) is unsuccessful. An alternative route first captures dmit as a tetraethylammonium zinc complex, [TEA]$_2$[Zn(dmit)$_2$] (**5.1**). Destruction of the coordination complex generates the air-stable benzoyl-protected dmit ligand, **5.2**. Direction formation of **5.2** from the sodium salt of dmit is also unsuccessful due to the nucleophilicity of the thiolate anion. Direct formation of **5.2** is observed only at low reaction temperatures (–70 °C).[266] Dmit is regenerated from **5.2** through treatment with methoxide. Ni(dmit)$_2$ is formed by coordination of the regenerated dmit with a nickel(II) source and is precipitated as the bis(tetraethylammonium) salt ([TEA]$_2$[Ni(dmit)$_2$], **5.3**). Through this method, I prepared **5.1** on 65 g scale and **5.3** on a 15 g scale.

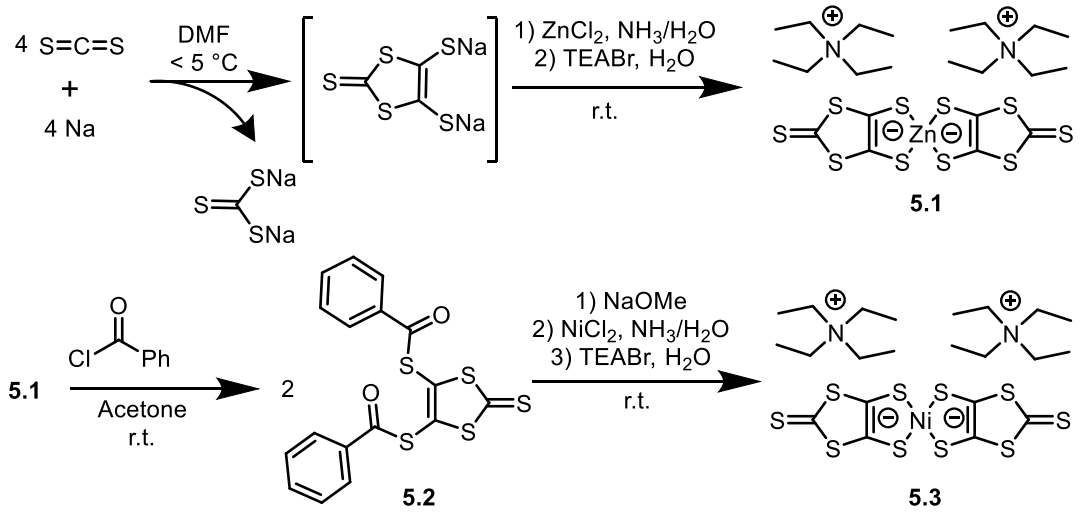

Figure 5.4 – Synthesis of Ni(dmit)$_2$ proceeding through the Zn(dmit)$_2$ intermediate

The reduction of carbon disulfide requires an excess of sodium and exhibits poor atom economy due to the production of trithiocarbonate as a stoichiometric byproduct, with the original mechanism shown in Figure 5.5.[266,270,271,288] Generation of tetrathiooxalate occurs first, followed by nucleophilic attack on carbon disulfide and subsequent ring closure to the 4,5-dithioxo-1,3-dithiolane-2,2-bis(thiolate). Attack at another molecule of carbon disulfide and subsequent elimination generates the byproduct trithiocarbonate and the 2,4,5-trithione. Reduction by two equivalents of sodium yields the desired product, dmit.

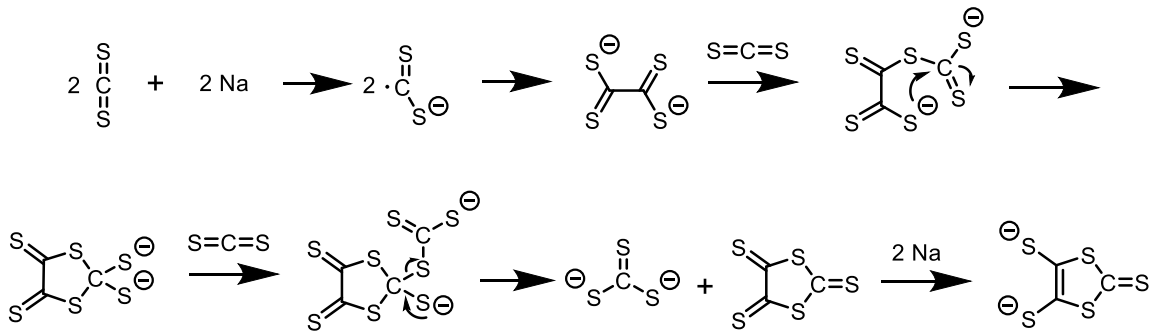

Figure 5.5 – Original proposed reaction mechanism for formation of dmit by the reduction of carbon disulfide

More recently, a modified mechanism, Figure 5.6, was proposed which requires only two equivalents of sodium for five equivalents of carbon disulfide. The increased yield despite using less sodium supports the authors' claim; however, the "disgusting smell" of the filtrate discouraged further isolation and study of byproducts.[272]

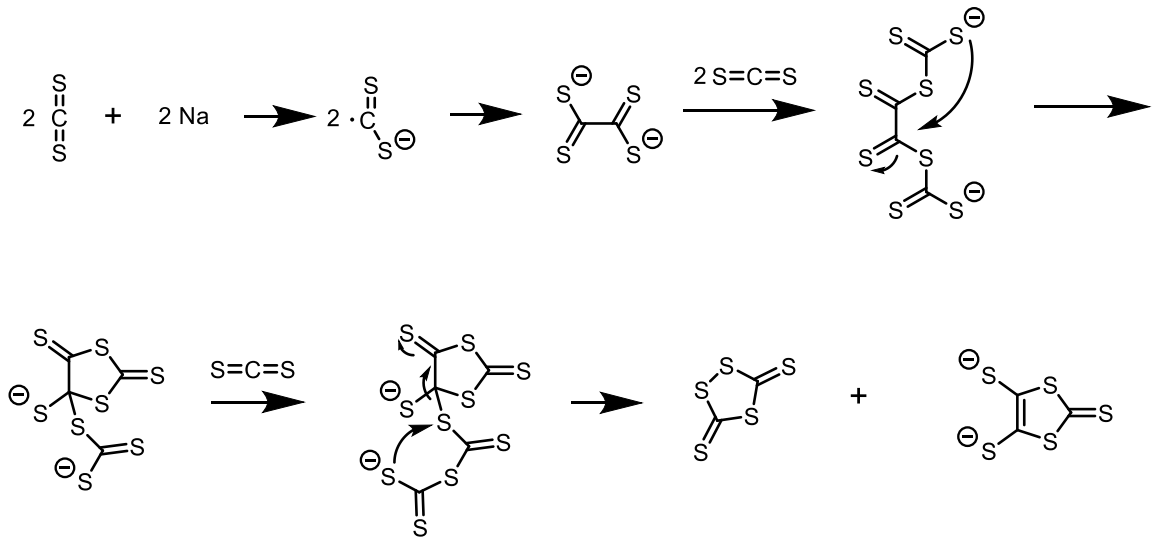

Figure 5.6 – Updated reaction mechanism for formation of dmit utilizing less sodium metal

5.2.2 *Ni(dmit)$_2$ as a Synthesis Test Case for NiETT*

Thin films of **5.1** and **5.3** were cast from acetone and DMSO but were not conductive. This agrees with the only reports of conductive Ni(dmit)$_2$ materials coming from charge transfer single crystals and partially oxidized salts.[258,289] Though these are not

useful thin film thermoelectric materials, **5.3** serves as convenient analog to NiETT when testing reaction conditions and oxidants. The effect of oxidizing agents and the ability to exchange counter ions were particularly useful test reactions. Figure 5.7 shows the counterion exchange reaction using the insolubility of tetraethylammonium tetraphenylborate ($TEABPh_4$) in methanol. The commercial availability of alkali salts of tetraphenylborate from lithium to cesium allow any of the alkali salts of $Ni(dmit)_2$ to be obtained. The sodium salt, **5.4**, was the only material we synthesized.

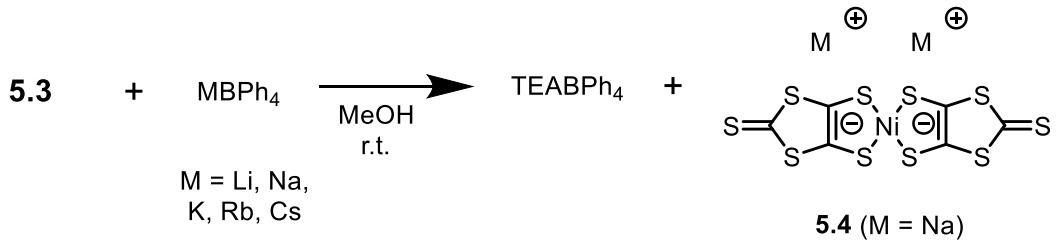

Figure 5.7 – Tetraethylammonium to sodium counterion ion exchange of $Ni(dmit)_2$

The salts of dmit and $Ni(dmit)_2$ are prone to oxidation by atmospheric oxygen. Many procedures, both discrete molecules and oligomers, utilize atmospheric exposure to precipitate a species of mixed or unknown oxidation state. The chemical control over oxidation state was desired, so several oxidants were tested on **5.3** for extent of oxidation and reactivity.

Figure 5.8 summarizes the results of the oxidation tests performed on **5.3** in methanol. Oxidants were tested using two equivalents of oxidant to give $Ni(dmit)_2^0$. Additional tests were run using an excess of each oxidant. No difference was observed between the two tests beyond the color of excess oxidant in some tests. Iodine (a), *p*-benzoquinone (b), tetrachloro-*p*-benzoquinone (chloranil) (c), 2,3-Dichloro-5,6-dicyano-*p*-benzoquinone (DDQ) (d), tris(4-bromophenyl)ammoniumyl hexachloroantimonate

(Magic Blue) (e), and atmospheric oxygen (f) were tested as oxidants. The proton for benzoquinone, chloranil, and DDQ was provided by acetic acid. All oxidants generated a black precipitate upon mixing with a solution of **5.3** in methanol. Iodine rapidly gives a black precipitate that settles out of solution. The complete disappearance of iodine color from using two equivalents qualitatively suggests the complete oxidation of $Ni(dmit)_2^{2-}$ to $Ni(dmit)_2^{0}$. Benzoquinone produced a suspension of black precipitate that settled slower than iodine leaving behind a green colored solution. This suggests the oxidation proceeds at a slower rate, proceeds to a lesser degree, or results in the formation of byproducts. The oxidation potential of *p*-benzoquinone is stronger than iodine, so an incomplete oxidation is counterintuitive. Chloranil also transitions through a green color similar to benzoquinone before a black precipitate forms and settles out of solution. As chloranil is a stronger oxidant than *p*-benzoquinone, the green color is assigned to $Ni(dmit)_2^{1-}$. The tetrachlorination also makes the oxidant more susceptible to nucleophilic attack. DDQ leads to a rapid precipitation and settling of the expected black material. The remaining solution is vibrant red in color suggesting a side reaction is occurring or that DDQ is forming a charge transfer complex with $Ni(dmit)_2$. Magic Blue gives the expected black precipitate rapidly. No color remains in solution even with excess Magic Blue, as the oxidant is slowly consumed in a reaction with methanol. The sample exposed to atmosphere (6) slowly turned green over the course of several hours and forming a small amount of precipitate, suggesting that air is capable of forming oxidation intermediates and end-products. The difficulty in controlling stoichiometry discouraged its use. Iodine was chosen as the ideal oxidant due to its fast reaction, soluble and innocuous byproducts, low concern for side reactions, and its ease of handling.

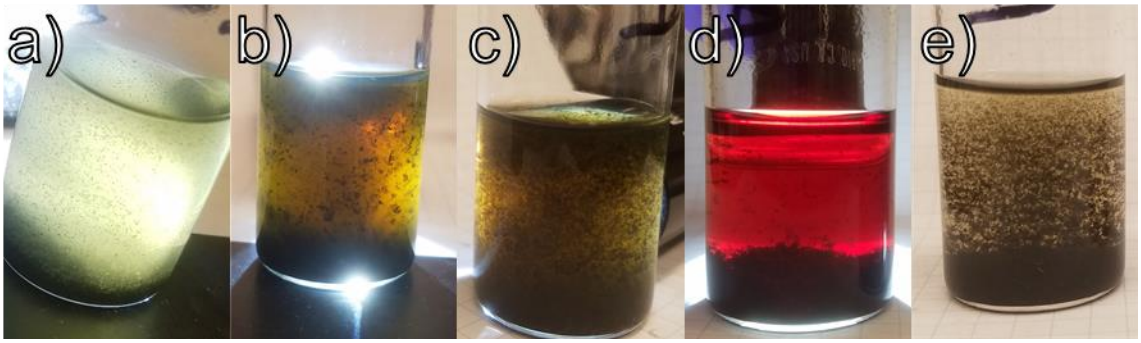

Figure 5.8 – Oxidation tests on 0.01 mmol $[TEA]_2[Ni(dmit)_2]$ in 10 mL methanol with a) iodine, b) benzoquinone, c) chloranil, d) DDQ, and e) Magic Blue. a-d are backlit with a flashlight to emphasize precipitate and solution color.

For conductive single crystals of $Ni(dmit)_2$ salts, a slow diffusion of oxidant or electrocrystallization techniques are typically used. Single crystals of the completely neutral $Ni(dmit)_2^0$ are nonconductive, confirming the need of a controlled and measurable oxidation procedure.[257] To test the stability of **5.1** to oxidation and to determine if oxidizing **5.1** would increase conductivity, an oxidation with iodine on **5.1** was attempted but unsuccessful. Literature reports of oxidization of **5.1** also led to decomposition and polysulfides. Successful oxidation was achieved with sulfuryl chloride at –40 °C or iodine at –50 °C, but the product is not a neutral $Zn(dmit)_2$, but rather oligo(1,3-dithiole-2,4,5-trithione).[266,290]

5.2.3 *$Ni(dmit)_2$ as a Characterization Test Case for NiETT*

Analyzing spectra of polymeric nickel dithiolenes is difficult due to their unknown composition and structure. Here $Ni(dmit)_2$ serves as a well-defined test case for characterizations. Solid state NMR spectroscopy (SS-NMR) was employed to distinguish ETT and TTO from their different carbon nuclei environments. Raman spectroscopy was employed to distinguish ETT and TTO from the nature of C=C, C-S or C=S, and Ni-S bond vibrations.

Results from SS-NMR spectroscopy are shown in Figure 5.9. Figure 5.9 shows the ^{13}C SS-NMR spectrum of **5.3** with C_1 at 217.5 ppm and C_2/C_3 at 141.8 / 139.3 ppm. Signals for all carbons C_1-C_5 were visible in both cross polarization (VACP) and direct polarization (DP) experiments. The dmit carbon shifts agree with reported values in solution of **5.3** (with different counterions) assign C_1 at 216.5 ppm and C_2/C_3 at 137.9 ppm in deuterated DMSO.[291,292] Carbons C_2 and C_3, which are expected to be identical, show two peaks at 141.8 and 139.3 ppm. The splitting of this peak could be attributed to crystal polymorphs (these were analyzed as polycrystalline powders, not single crystals) or distortions in geometry from S-S and M-S interactions in the solid state.[264]

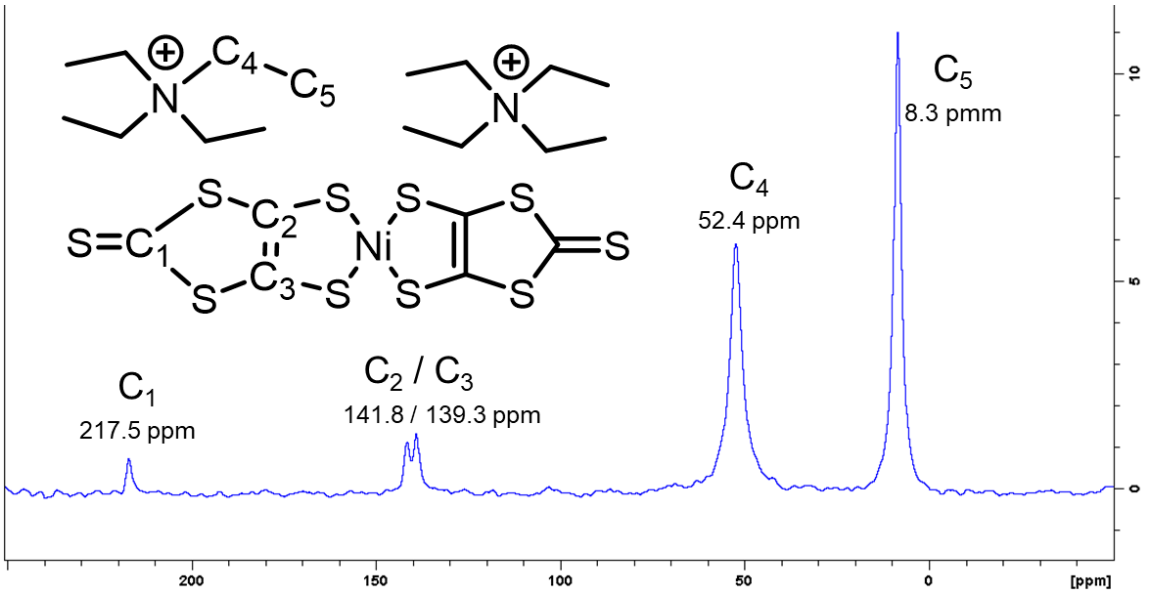

Figure 5.9 – ^{13}C SS-NMR (Variable-Amplitude Cross Polarization (VACP) technique) spectrum of 5.3 with tentative carbon assignments

A ^{13}C SS-NMR experiment was attempted on thiapendione. The absence of hydrogen nuclei prevents the utilization of cross polarization techniques. Direct polarization techniques did not yield a signal. Exceedingly long acquisition times would be required to obtain acceptable signal-to-noise ratios. Therefore, materials with no

hydrogen nuclei – such as Na[NiETT] and Na[NiTTO] in Chapter 7 – will not be suitable for this experiment.

Vibrational spectroscopies are another way to probe the structure and electronics of the nickel coordination center. Compound **5.3** has been previously studied by IR and Raman spectroscopies.[291,293–296] Compound **5.3** was employed to test the usefulness of Raman spectroscopy. Figure 5.10 shows Raman spectra of 5.3 at two laser powers, with tabulated data compared with literature assignments in Table 5.1. The assignments by Pokhodnya et al. focuses on in-plane symmetric A_g modes.[293]

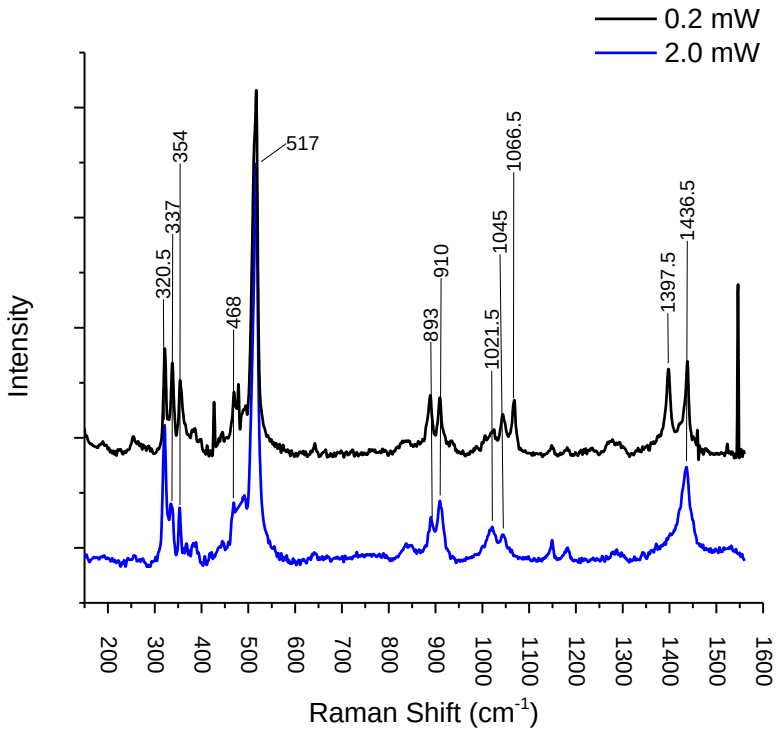

Figure 5.10 – Raman spectra of Compound 5.3 taken at 0.2 mW and 2.0 mW

These assignments are tentative. Mode A (1329 – 1435 cm^{-1}) is assigned to C=C stretching modes. Mode B (1046 – 1052 cm^{-1}) is assigned to the C=S terminal thione stretch. Mode C (907 – 950 cm^{-1}) and is assigned to C-S stretching. Mode D (496 – 521

cm^{-1}) is assigned to in-phase C=C and C-S of the $S_2C=CS_2$ central fragment. Mode E (466 – 488 cm^{-1}) is assigned to C-S stretching associated with the terminal thione. Mode F (351 – 364 cm^{-1}) is assigned to Ni-S stretching. Mode G (323 – 363 cm^{-1}) is assigned to out-of-phase deformation of the two five-member rings of the thiapentalene core coordinated to nickel.

Table 5.1 – Raman shifts (cm^{-1}) of Modes A-H as assigned by Pokhodnya et al. in charged states of $Ni(dmit)_2$.[293] Tabulated Raman shifts from Figure 5.10 and tentative mode assignments

	A	B	C	D	E	F	G
$Ni(dmit)_2^{-2}$	1435	1046	907	521	466	351	323
$Ni(dmit)_2^{-1}$	1403	1052	933	507	478	358	338
$Ni(dmit)_2^{0}$	1329	1051	950	496	488	364	363
Compound 5.3 -2 / -1	1397 1436	1021 1045 1066	910	517	468	354	337 320

With an understanding of nickel coordination reactions, the reactivity of $Ni(dmit)_2$, and the availability of characterization techniques, the focus was shifted to polymeric nickel complexes, such as NiETT.

5.3 Poly(Nickel Ethenetetrathiolate) (NiETT)

The first ligand we studied for metal coordination materials was ethenetetrathiolate (ETT) due to its widespread resurgence in the organic thermoelectrics literature. NiETTs offer advantages in that they: (i) have tunable electronic properties through multiple oxidation states on both the ligand and metal center, (ii) exhibit n-type behavior as evidenced by their negative Seebeck coefficients, and (iii) are stable to ambient conditions without special exclusion of moisture or oxygen. However, NiETTs also have drawbacks associated with their production and processing: (i) the poorly understood synthetic

pathway leads to irreproducible syntheses, (ii) the insoluble nature of the final material limits traditional structural characterization, and (iii) fabrication via solution-based techniques requires the use of an insulating matrix that adversely affects performance. The poorly understood reaction mechanism in the formation of NiETT, and the lack of characterization techniques available for studying the structures of these insoluble complexes, make synthetic optimizations difficult.

5.3.1 *Previous Literature Reports*

Reports of NiETT as an n-type thermoelectric material drove our interest in the material. While its synthesis, conductivity, and thermopower have been studied extensively in the 80's, the paper that brought NiETT to the forefront of recent studies was Sun et al.[297] The published reaction procedure that is described in Figure 5.11 widely followed in subsequent studies. A reactive intermediate of debated structure is generated from the reaction of potassium methoxide on thiapendione. Coordination with a source of nickel(II) gives the unoxidized version of K[NiETT], which must undergo oxidation, often by atmospheric oxygen, to a state useful for thermoelectrics. Recent reports of NiETT thermoelectric performance are given in Table 5.2.

Table 5.2 – Literature Reports of NiETT Thermoelectrics

Polymer	Form	σ (S cm^{-1})	S (μV K^{-1})	PF (μW m^{-1} K^{-2})	Reference
Na[NiETT]	Pellet	40	-75	23	297
K[NiETT]	Pellet	44	-122	66	
Ni[NiETT]	Pellet	6.6	-84	4.7	
Electrochemical NiETT	Film	220	-125	344	298
K(NiETT)	Pellet	8	-67	3.7	299
K(NiETT)	Film	2	-45	0.4	

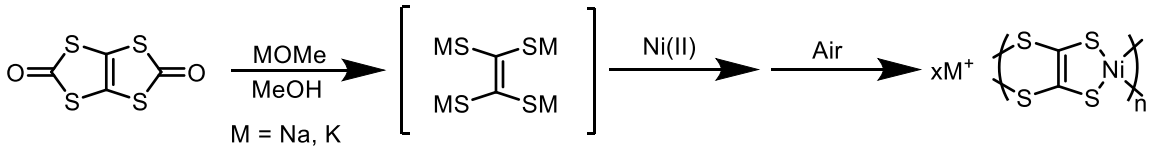

Figure 5.11 – Typical reaction procedure for the synthesis of Na[NiETT] or K[NiETT]

Comparison between literature reports of NiETT is difficult because the procedures vary widely on synthetic conditions, workup, and characterization. Significant variations in performance are seen with the "same" material. Within my own syntheses, I have synthesized NiETT which is non-conductive and NiETT that has a conductivity above 100 S/cm. The appearance, elemental composition, and performance of NiETT experiences significant batch-to-batch variations. With this in mind, the literature procedure was systematically adapted to give a consistent, reproducible material.

5.3.2 *Modifying Literature Procedures with Intent*

The current synthetic reports of NiETT are written such that it is difficult to produce materials with consistent properties. Indeed, the first attempts in our groups at reproducing the K[NiETT] procedure, Figure 5.11, resulted in similar, but inconsistent, conductivity

and thermopower. The synthetic work performed by Dr. Akanksha Menon is more thoroughly described in her Ph.D. thesis.[300] A brief summary of the study is worthwhile to note here on the difficulty of the reported procedure in giving an adequate material.

The reaction was performed in a 250 mL, 24/40, three-neck round bottom flask with attached condenser. Stirring was maintained throughout the procedure with a 1-2" Teflon-coated stir bar at 300 rpm. The reaction was not run under inert atmosphere, but open joints were sealed with septa. A solution of potassium methoxide (1.50 g, 22.2 mmol, Alfa Aesar) in methanol (45 mL, BDH) was prepared. Thiapendione (1.0 g, 4.8 mmol, TCI America) was added in one portion, and the resulting solution was heated at 75 °C for 24 hours. Separately, a solution of nickel(II) chloride hexahydrate was prepared from nickel(II) chloride (0.63 g, 4.8 mmol, Sigma Aldrich) and water (300 mL, deionized). This solution was diluted in 25 mL of methanol before addition to the reaction in one portion. The reaction was heated to reflux for an additional 24 hours. Heating was stopped, and the solution was immediately exposed to air for 30 minutes or 24 hours by removing the condenser and septa from all three necks, while stirring was continued at 300 rpm. During exposure, a black precipitate formed. The K[NiETT] oxidized for 30 minutes yielded NiETT:PVDF composite films with a power factor of 4.6 ± 0.4 μW m^{-1} K^{-2} ($\sigma = 43 \pm 4$ S/cm; $S = -33 \pm 1$ μV/K). The K[NiETT] oxidized for 24 hours yielded composite films with a power factor of 0.40 ± 0.06 μW m^{-1} K^{-2} ($\sigma = 5.2 \pm 0.1$ S/cm; $S = -27 \pm 3$ μV/K).[301] The importance of control over every step of the reaction, especially oxidization, was evident.

In order to address the lack of consistency in material properties, the following parameters from the reaction must be addressed: (1) The reagent source and purity should

be identical, or as close to identical as possible for all reactions. This includes solvent, thiapendione, sodium methoxide, and nickel(II). (2) Addition of each reagent should be performed in a logical, consistent order, such that no unknown interferences are introduced at any point. (3) The oxidation should be done in a manner such that the extent of oxidation/strength of oxidation agent/exposure rate/and *O*-atom transfer can be controlled. (4) The workup should identify and isolate the material of interest while removing as many identifiable impurities as possible. In this section, each of these concerns is systematically addressed to give a consistent, reliable, and scalable reaction procedure.

5.3.3 *Control of Reagent Purity*

Reagent purity is the first requirement for a reliable synthesis. Any effects caused by modifications to the procedure may never be noticed if the reagents used are not of consistent quality from reaction to reaction. Here, purification, storage, and use of each reagent is addressed individually before discussions of best reaction practices.

5.3.3.1 Thiapendione

1,3,4,6-Tetrathiapentalene-2,5-dione, **5.7**, commonly thiapendione, is the precursor to NiETT as the dithiocarbonate cleaves under mild basic conditions. At the time of writing, only one commercial source existed ($900 USD / 25 grams),[300] which can be seen in Figure 5.12a. This material, **5.7-Commercial**, has a strong sulfurous odor. Recrystallization from acetonitrile (ACN) yielded brown crystals with a similar odor, Figure 5.12c. Thiapendione synthesized according to the literature procedure,[273,302] **5.7-House**, yielded off-white needles, Figure 5.12b. We also had a custom supplier who provided **5.7-Custom**, Figure 5.12d, as a beige powder.

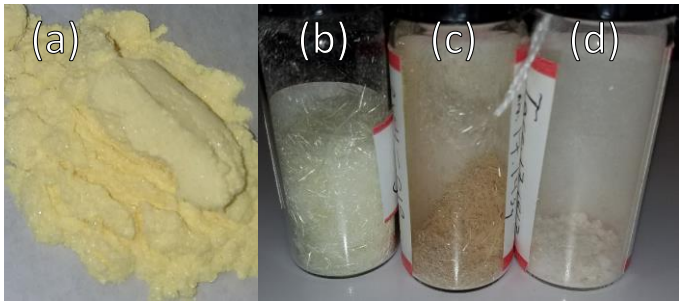

Figure 5.12 – Figure S1. (a) Vibrantly yellow 5.7-Commercial from TCI, (b) 5.7-House synthesized in house and recrystallized from ACN, (c) 5.7-Commercial recrystallized from ACN, (d) Off-white 5.7-Custom as received from the supplier

The synthesis of **5.7** is shown in Figure 5.13. The first step is the creation of the potassium xanthate, **5.5**.[303] Isopropoxide is generated in situ and reacts with carbon disulfide to give *O*-isopropyl potassium xanthate. The reaction with dichloromethylacetate gives the stable precursor, **5.6**. An acid catalyzed ring closure in sulfuric acid yields the final material, 5.7, which can be recrystallized from chloroform or acetonitrile.

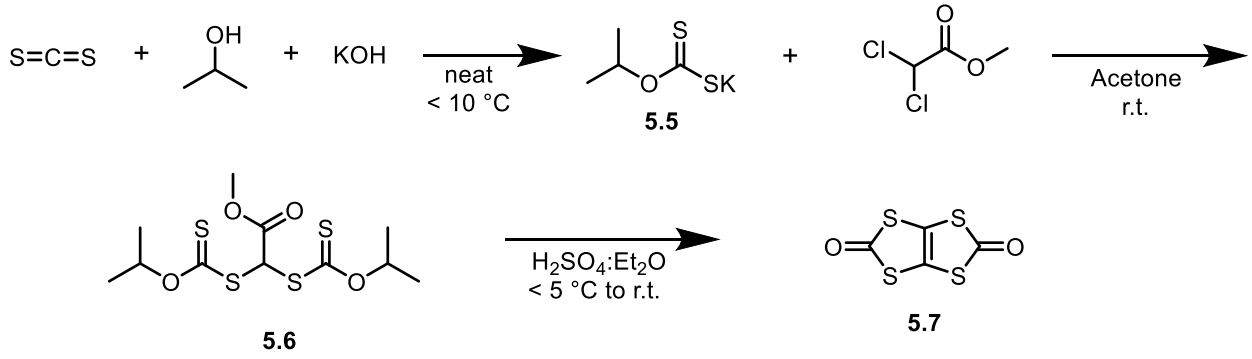

Figure 5.13 – Synthetic scheme showing the synthesis of thiapendione

The discrepancy between the observed forms and colors of **5.7** was a cause of concern when attempting to minimize any variations in synthesis. Elemental analysis, Table 5.3, was performed to confirm the purity. All samples returned acceptable carbon and sulfur values, so the decision of thiapendione supplier was based on visual purity, reaction behavior, and intuition.

Table 5.3 – Elemental compositions of thiapendione 5.7 for NiETT from different sources

Element	Theoretical	Commercial	House	Custom
Carbon	23.07	23.05	22.80	23.04
Sulfur	61.57	61.85	61.29	61.78

5.7-House is the cleanest visually and had the least odor; however, its synthesis was time consuming and may suffer from batch-to-batch variation. **5.7-Commercial** was presumed to be impure due to its color and odor despite returning acceptable elemental values. Attempts at recrystallization from chloroform or acetonitrile did not yield a cleaner looking material, Figure 5.12c. **5.7-Custom** had an intermediate odor and could be recrystallized with no apparent gain in color purity or decomposition behavior Figure 5.14. The only difference is a 1% weight loss change below 100 °C, presumed to be a difference in surface moisture from powder to crystal.

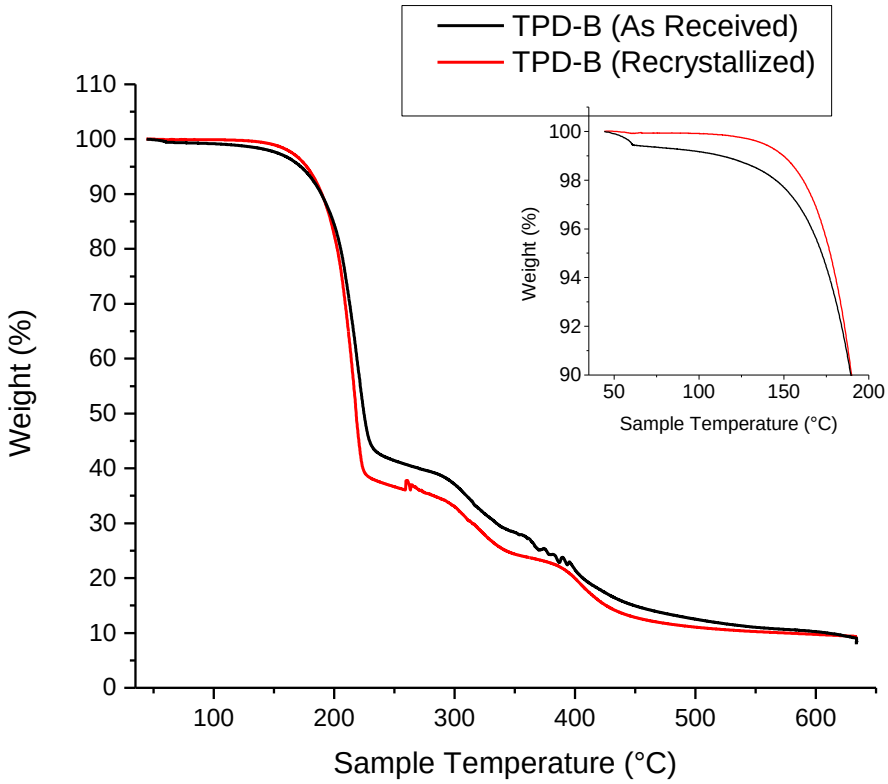

Figure 5.14 – Thermogravimetric analysis of 5.7-Custom as received (black) and after recrystallization from acetonitrile (red).

5.3.3.2 Reaction Solvent

An ideal reaction solvent for NiETT synthesis will solubilize the reaction intermediates and NiETT chain for as high of molecular weight as possible. Two classes of solvents are considered for NiETT – alcoholic and polar aprotic. The bulk of NiETT synthesis is reported in alcoholic solvents. This facilitates the use of alkoxide bases, and conveniently solubilizes the first intermediate. The idealized backbone of NiETT has few degrees of freedom and presumably low solubility in methanol, especially as its oxidation state approaches neutral. Polar aprotic solvents, such as dimethylformamide, dimethyl sulfoxide, and hexamethylphosphoramide, may provide better chain and cation solubility and allow access to higher temperatures.

For this study, methanol was used in all reactions. To obtain a consistent grade of methanol across every reaction, reagent grade methanol was thoroughly dried and degassed prior to use. Drying was achieved using sequential loadings of activated 3Å molecular sieves.[106] Degassing was achieved through sparging with argon for no less than 30 minutes.

To test the strict requirement for dry and degassed methanol, a control experiment using ACS grade methanol with no measures taken to dry or degas the solvent was devised. Reactions were performed in reagent grade (not dried or degassed) methanol with ten equivalents of sodium methoxide (5.037.C) and sodium hydroxide (5.037.A) to simulate the probable and extreme cases of base degradation due to moisture saturated methanol, Table 5.4. No test on oxygen dissolution was devised. While in depth characterizations were not performed on each NiETT powder, no difference in thermoelectric performance – at least that could be directly associated with using hydroxide or methoxide – was observed between the materials. The presence of water or conversion of methoxide to hydroxide does not impede the formation of NiETT. Dried, degassed methanol under an argon atmosphere was used for all reactions to limit unforeseen interferences. Sodium carbonate failed to give conductive NiETT (5.037.B), potentially due to its low solubility in methanol. Sodium carbonate was previously used to generate dmid from thiapendione using a mixture of water and benzene with a phase transfer catalyst. Surprisingly, sodium carbonate does not cleave the remaining carbonyl even after the free thiolates were substituted with propargyl bromide, but sodium methoxide does.[302]

Table 5.4 – Thermoelectric performance of NiETT:PVDF composites with NiETT from methoxide and hydroxide bases in reagent grade methanol. Films are not annealed. [a]Conductivity below detection limit

ETT Synthesis (Base)	σ (S/cm)	S (μV/K)
5.037.C (NaOMe)	5.7 ± 1.8	-36.2 ± 0.7
5.037.A (NaOH)	15.7 ± 2.9	-32.9 ± 2.1
5.037.B (Na_2CO_3)	N/A[a]	N/A[a]

Alternative solvents to methanol include the class of polar, aprotic solvents. It was impractical to test each solvent in a NiETT reaction. The ability to solvate a growing chain of NiETT is the most desired property; therefore, solvents were tested on their ability to suspend or dissolve a premade sample of Na_0[Ni(ETT)]. Dimethyl carbonate, propylene carbonate, dimethylsulfoxide (DMSO), hexamethylphosphoramide (HMPA), *N*-Methyl-2-pyrrolidone (NMP), and 1,3-dimethyl-2-imidazolidinone (DMI) were compared against methanol (MeOH). A few milligrams of NiETT was added to a few milliliters of each solvent. Dimethyl carbonate, propylene carbonate, and DMI did not suspend or dissolve any NiETT even with agitation and heating. These solvents were not tested further.

NMP, DMSO, and HMPA showed some ability to suspend or dissolve NiETT. These tests are documented against a methanol control in Table 5.5. The test with methanol shows no evidence of dissolution or even suspension of NiETT with agitation (crushing with a glass rod) or heating. NMP did not dissolve NiETT at room temperature. Agitation produced a very faint yellow color in solution which did not increase in intensity with heat. NMP is a candidate for trituration when purifying NiETTs. DMSO did not dissolve NiETT at room temperature or with agitation. Heating yielded a faint yellow color in solution similar to that observed with NMP. It is cautioned that DMSO undergoes

disproportionation to dimethyl sulfide and dimethyl sulfone above 90 °C, which could result in unwanted byproducts or side reactions.[304] All NiETT:PVDF composite films are processed from a concentrated suspension in DMSO. DMSO is a candidate for future reaction solvent testing and workup procedures. HMPA immediately showed signs of dissolution of NiETT at room temperature. A yellow-brown color trailed from the NiETT particles. Agitation increased the rate of dissolution and the intensity of color in solution. Gentle heating (~60 °C) produced a dark brown, transparent solution with some NiETT remaining undissolved. HMPA was tested for recovery of the NiETT and as a potential reaction solvent.

Table 5.5 – Solubility of Na_0[Ni(ETT)] in polar, aprotic solvents with agitation and heating (in six dram vials capsule form vials for scale)

	No Agitation No Heating	With Agitation No Heating	With Agitation With Heating
MeOH	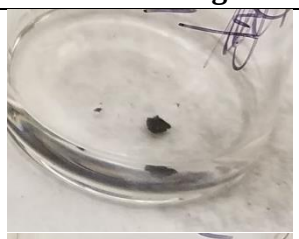	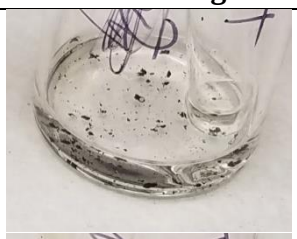	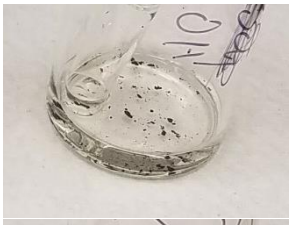
NMP	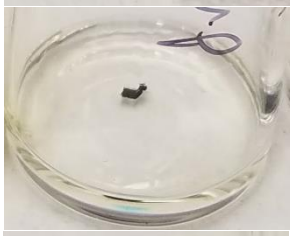		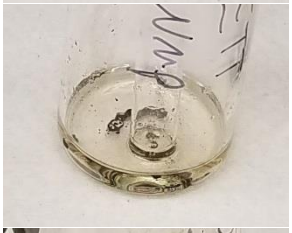
DMSO			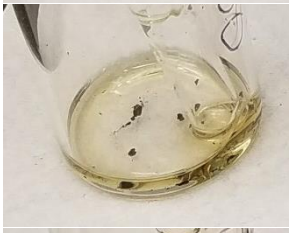
HMPA			

To test whether the NiETT was suspended or dissolved rather than degraded or destroyed when heated with HMPA, as attempt was made to reprecipitate and recover the NiETT. Figure 5.15 shows the precipitation and collection process. To the previously agitated and heated solution of NiETT in HMPA, an excess amount of methanol was added. A yellow brown liquid resulted without visible precipitate settling. Filtration through a 0.2 um nylon-membrane syringe filter collected a black material visually resembling NiETT. The filtrate was a faint yellow color. This suggests that HMPA dissolves NiETT or suspends particles of NiETT effectively, which can be recovered with addition of a poor solvent (methanol). The remaining color in the filtrate is potentially the lowest molecular

weight NiETT chains or reaction byproducts that were not fully removed during workup. Further investigations into HMPA as a reaction solvent or purification method are warranted.

Figure 5.15 – The recovery of NiETT from HMPA by precipitation in methanol and filtration

HMPA was tested as a reaction solvent for NiETT which resulted in an atypical vibrant red solution during Step 1, Figure 5.16b (compare with typical color change in methanol shown in Figure 5.16a and Figure 5.18). This unexpected color change warranted further investigation before continuing NiETT reactions in HMPA.

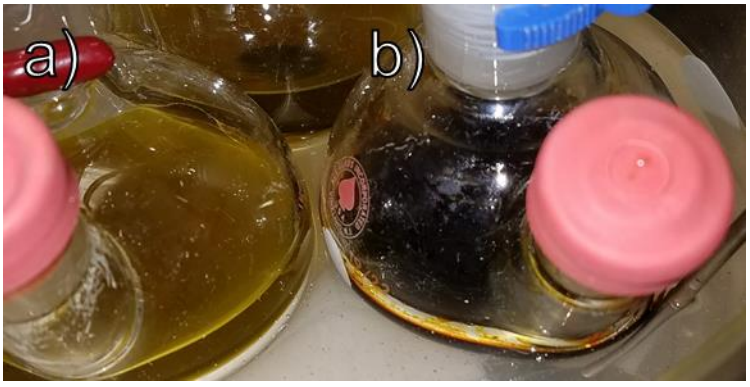

Figure 5.16 – Comparison of reaction color during Step 1 of NiETT synthesis in a) methanol, and b) hexamethylphosphoramide. The red color is most apparent on the sides of the reaction flask

The strong odor of amines from the reagent bottle of HMPA (as HMPA is odorless but releases dimethylamine on degradation) gave a starting point to the investigation.

Figure 5.17 shows a comparison of the behavior of thiapendione in HMPA and other solvents. Thiapendione is soluble in DMSO, resulting in a light-yellow color, Figure 5.17a. A solution of thiapendione in HMPA immediately shows the vibrant red color, Figure 5.17c. Addition of HMPA to thiapendione in DMSO also resulted in the red color, Figure 5.17b. The color change was positively assigned to an amine impurity by adding n-hexylamine to thiapendione in DMSO, Figure 5.17d. HMPA distilled from calcium hydride under high vacuum[105] resulted in an odorless HMPA which dissolves thiapendione with no change in color. Solvents which may be contaminated with amines or other nucleophilic impurities must be rigorously purified before use or avoided completely.

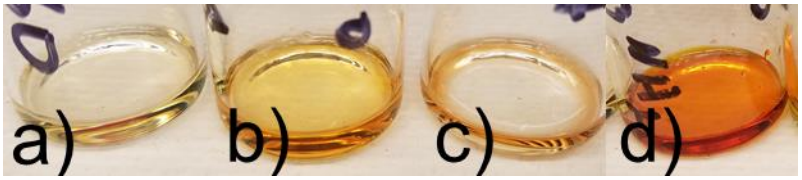

Figure 5.17 – Comparison of thiapendione dissolved in a) DMSO, b) 1:1 DMSO:HMPA, c) HMPA, d) DMSO with *n*-hexylamine

5.3.3.3 Choice and Amount of Nucleophile

While previous trials, Table 5.4, did not indicate a substantial difference in thermoelectric performance between sodium methoxide and sodium hydroxide, sodium methoxide is very soluble in methanol, is synthesized in house under rigorous exclusion of moisture, and is the nucleophile of choice for literature experiments. Therefore, sodium methoxide was used in all optimization experiments. Other nucleophiles, such as hydroxides, amines, and thiols, present future research opportunities.

Despite the relatively low rate of water absorption of methanol in properly sealed vessels[5] and the apparent insensitivity of the nucleophile used (Table 5.4), it was

hypothesized that an excess of methoxide may be required to complete the ring opening in Step 1. To test, reactions with five equivalents (5.033A, 5.034A) or ten equivalents (5.33B, 5.034B) of sodium methoxide were performed under otherwise identical conditions. No significant difference in the conductivity of these films was observed. Within this small sample set, five equivalents of sodium methoxide gave consistently larger thermopower measurements, Table 5.6. This evidence combined with previous trials using wet methanol and sodium hydroxide indicated that a large excess of methoxide was not required to optimize this reaction, and in fact, could diminish Seebeck values. Five equivalents of methoxide were used for all other syntheses in this study.

Table 5.6 – Thermoelectric performance of thin-film composites (4:1 w/w NiETT:PVDF annealed at 160 °C) testing reaction conditions involving methoxide equivalents and Ni(II) addition times and rates

ETT Synthesis	σ (S/cm)	S (μV/K)
5.033A (5 Equiv. NaOMe) (Ni(II) @ 1 hr over 20 hr)	12.1 ± 2.4	-63.6 ± 2.2
5.033B (10 Equiv. NaOMe) (Ni(II) @ 1 hr over 20 hr)	13.5 ± 3.6	-44.5 ± 1.3
5.034A (5 Equiv. NaOMe) (Ni(II) @ 23 hr over 1 hr)	15.6 ± 3.7	-71.8 ± 0.2
5.034B (10 Equiv. NaOMe) (Ni(II) @ 23 hr over 1 hr)	17.8 ± 4.1	-56.2 ± 1.2

5.3.3.4 Choice of Nickel(II) Source

The bulk of the NiETT literature utilizes (presumably, but not specified) anhydrous nickel(II) chloride that is not dissolved prior to addition[297–299,305,306] or purposefully hydrated nickel(II) chloride dissolved in methanol.[301] We prefer to use anhydrous nickel(II) acetate, a salt which has been previously used in conducting nickel-complex syntheses[265,307] and was chosen due to its high solubility and dissolution in anhydrous methanol compared to anhydrous nickel(II) chloride. In addition, the acetate salt was chosen due to its ease of dehydration[308] compared with the chloride.[309] Thermoelectric performance of control reactions using nickel(II) acetate tetrahydrate, anhydrous nickel(II) acetate, anhydrous nickel(II) chloride are reported in Table 5.7. No significant material performance differences were observed. Because it is easily obtained, soluble in methanol, and avoids any unknowns in extent of hydration, anhydrous nickel(II) acetate is used for all other studies.

Table 5.7 – Impact of nickel(II) salt selection on Na[NiETT] thermoelectric properties

ETT Synthesis	σ (S/cm)	S (μV/K)
5.008 ($Ni(II)OAc_2 \bullet 4H_2O$)	67 ± 5	-63 ± 1
5.069 (Anhydrous $Ni(II)OAc_2$)	54 ± 1	-65 ± 4
5.073 (Anhydrous $Ni(II)Cl_2$)	28 ± 2	-69 ± 3

5.3.3.5 Choice of oxidant

Most of the recent NiETT literature[297–299,301,305,306] imply the requirement of oxidation for the precipitation and collection of NiETT. In 5.3.4.3, we provide examples in contrast to those reports. The oxidation of NiETT remains an important reaction process that sets the charge level of the final material. One oxidant, iodine, acts as a mild electron-transfer oxidant with byproducts (I^-, I_3^-, NaI, NiI_2) that are soluble in methanol. With an oxidation potential of +0.54V vs SHE, iodine is more oxidizing than oxygen in a basic aqueous environment ($O_{2(g)} + 2H_2O + 4e^- \rightleftharpoons 4OH^-_{(aq)}$ @ +0.4V) and less oxidizing than oxygen in an acidic environment ($O_{2(g)} + 4H^+ + 4e^- \rightleftharpoons 4H_2O_{(aq)}$ @ +1.23V).[310] By avoiding oxygen-transfer oxidants and atmospheric oxygen, undesired chemical modifications to the Ni-ETT backbone are limited. Additionally, iodine chemical oxidation is performed under continued exclusion of oxygen, thereby limiting any uncontrolled or external oxidation events, and allowing an exact oxidation level to be set and adjusted. In conjunction with oxidation testing on $Ni(dmit)_2$ in 5.2 and previous reports of iodine as an oxidant for NiETTs that obtain conductivities greater than 0.5 S/cm,[276,311] iodine was selected as the oxidant of choice for all reactions.

5.3.4 *Explanation of Reaction Procedures*

Through an intensive, iterative feedback loop of synthetic modification, solid state analysis, thermoelectric performance, and peer discussion, an optimized procedure for the synthesis of NiETT with reproducible thermoelectric properties was developed. The full procedure with experiments and justifications is provided here. The abridged procedure akin to other literature supporting information is given at the end of this section.

5.3.4.1 Addition of Methoxide and Thiapendione

The proposed and followed method for NiETT is to prepare a solution of methoxide and a slurry of thiapendione separately, before adding methoxide to thiapendione. Methoxide is obtained from its storage location inside of the glovebox. One-half of the total volume of methanol to be used is added to make a sodium methoxide solution. Separately, thiapendione is loaded into a flask, and the atmosphere is cycled three times between high-vacuum and argon. The remaining methanol is added to the main reaction flask to give a slurry of thiapendione. The prepared sodium methoxide solution is added to the thiapendione. This procedure has several benefits over the reverse addition: the flask does not need to be opened to atmosphere to add the thiapendione (although that can be done effectively against a positive flow of argon), and the rate of addition can be controlled by cannula, syringe, or syringe pump. Figure 5.18 shows the color evolution of a typical Na[NiETT] reaction before the addition of nickel. After the mixing of the two reagents, a light-yellow color develops immediately (2 min), before darkening (10, 25 min). The reaction transitions through a green-tinted brown (60 min, 120 min) before becoming a constant opaque black (240 min). Beyond the rate of color change, no quantitative data (i.e. elemental analysis or thermoelectric performance) distinguishes NiETT synthesized with thiapendione added as a solid to a solution of sodium methoxide from NiETT synthesized with a solution of sodium methoxide added to a slurry of thiapendione. The removal of atmospheric exposure may be the only reason for the decreased rate of color change.

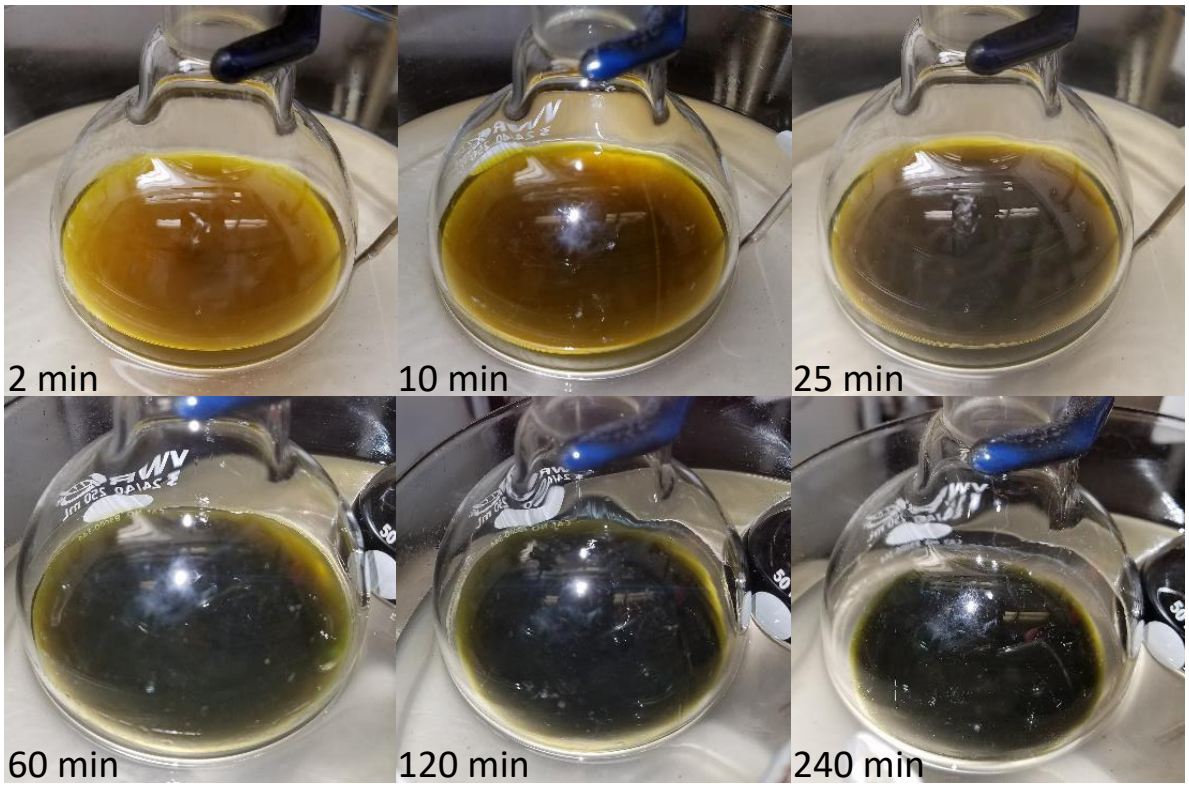

Figure 5.18 – Timed photographs of the representative color change during the reaction of thiapendione with methoxide. A light-yellow color forms immediately upon mixing, quickly darkening to a brown-green, and finally to opaque black within several hours. The reduction in reaction volume is due to aliquot removals and is unrelated to the color change

5.3.4.2 Discussion of Potential Reaction Intermediates

The reaction mechanism and potential intermediates in the formation of NiETT are still under investigation. Early reports concluded ethenetetrathiolate as the reactive intermediate[267,273,275,311,312] with 1,1,2,2-tetrakis(methylthio)ethene resulting from trapping with methyl iodide.[273] The full reaction to Na[NiETT] would follow Figure 5.19.

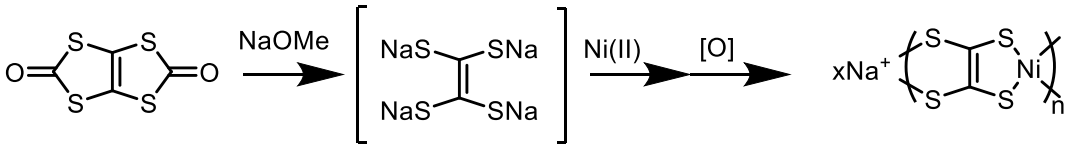

Figure 5.19 – Typical reaction route to Na[NiETT] indicating formation of the tetrathiolate intermediate before coordination to nickel(II) and oxidation

More recent reports that have not focused on reaction conditions and intermediates continue to report ethenetetrathiolate as the reactive intermediate.[297,298,313,314] Others have provided evidence for strictly the formation of dithiolate, and 1,1,2,2-tetrakis(methylthio)ethene is explained through a stepwise reaction.[276,281,302] The stepwise reaction resulting in Na[NiETT] is outlined in Figure 5.20.

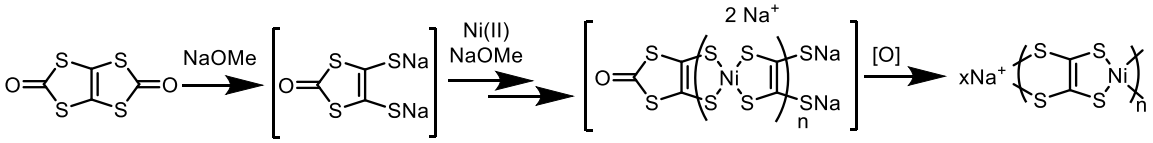

Figure 5.20 – Reaction route to Na[NiETT] through a stepwise coordination with nickel(II) and subsequent ring-opening

Another mechanism is the oxidation of the dithiolate to 4,5-dithioxo-1,3-dithiolan-2-one or its oligomer, Figure 5.21.[281] This intermediate may then coordinated with nickel(II) and continue in a similar fashion as Figure 5.20, or undergo ring opening to form Na_2TTO to give Na[NiTTO] as a final product.

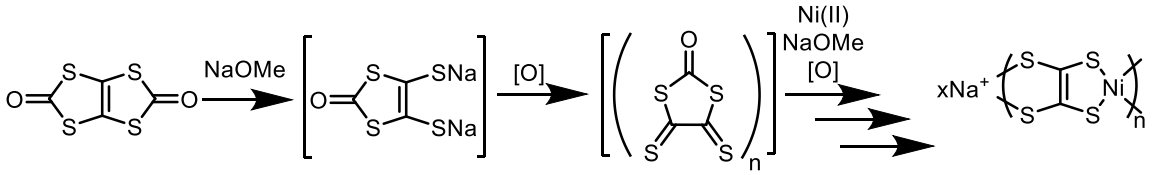

Figure 5.21 – Reaction route to Na[NiETT] through initial oxidation of dithiolate intermediate with subsequent coordination and ring-opening

Another reaction mechanism for the formation of NiETT was suggested by Tkachov et al. in 2017.[281] They show that the dithiolate undergoes disproportionation to tetrathiooxalate in methanol at reflux with the release of carbon monoxide, Figure 5.22.

This transformation has been previously reported for 4,5-bis(methylthio)-1,3-dithio1-2-one[270,315] and thiapendione[316] and is well-supported when UV irradiation is present. Thermally driven disproportionation occurs during pyrolysis at 450 °C and 0.05 torr.[315] Disproportionation in the absence of UV light and disproportionation of the dianion have not been previously reported.

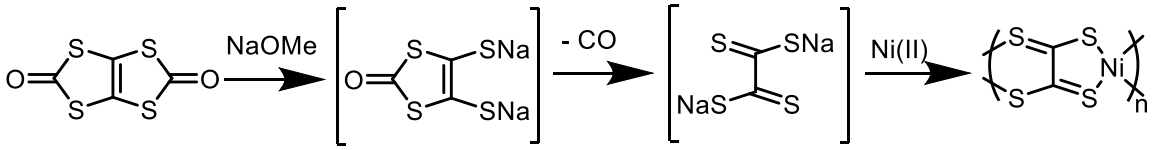

Figure 5.22 – Reaction route to Na[NiTTO] through disproportionation of the dithiolate to give Na_2TTO prior to coordination with nickel(II)

One could imagine dmit also being an accessible precursor to tetrathiooxalate. However, dmit does not undergo the same transformation under UV irradiation. A thermal isomerization happens in dmit at 120 – 140 °C to form 3-thioxo-1,2-dithiole-4,5-bis(thiolate) stabilized by electron delocalization.[266]

Returning to the observed colors in Figure 5.18, the light-yellow color is attributed to the dithiolate. The dithiolate has been observed in light-yellow solutions by ^{13}C NMR spectroscopy on yellow crystals isolated by Tkachov et al.[281] The color change from yellow to black is hypothesized to be the unintended oxidation of the dithiolate to a bis(disulfide-linked) dimer[316] or an oligosulfide of 4,5-dithioxo-1,3-dithiolan-2-one, similar to the oxidation behavior of dmit.[290] The extent of premature oxidation is assumed to be minimal due to the rigorous exclusion of air and moisture. The color may result from a minimal fraction of the reaction undergoing oxidation, the color may result from an unidentified intermediate that also undergoes polymerization with nickel(II), or the color may result from an unidentified side reaction that is negatively impacting the performance of the final

NiETT. Understanding the reaction intermediates remains an important aspect to improving future NiETT synthesis.

5.3.4.3 Addition of Nickel

The next step in the reaction is the addition of a nickel(II) salt. This has previously been performed as a solid, as the premade hexahydrate, or in an unspecified addition manner. Drawing from the potential reaction sequences presented in Figure 5.19 to Figure 5.22, the rate and timing of nickel addition was investigated. The original hypothesis was that if the reaction followed Figure 5.20, it would be beneficial to have an early addition of nickel that was slowly added. The early addition prevents unintended oxidation of the dithiolate from occurring by capturing it as the nickel complex, and the slow addition prevents the flood of nickel(II) ions from undergoing counterion exchange with sodium and diminishing solubility of the growing chain.

These data were concurrently collected from the reactions utilizing five or ten equivalents of methoxide (Table 5.6). In trials 5.034A and 5.034B, a solution of nickel(II) was added dropwise over one hour after 23 hours of reaction time between thiapendione and methoxide. In trials 5.033A and 5.033B, the nickel(II) solution was added dropwise over 20 hours after one hour of reaction time between thiapendione and methoxide. All reactions were run 48 hours before quenching and oxidation. A moderate improvement in thermoelectric performance was observed in 5.034A over 5.033A and in 5.034B over 5.033B. Despite the color change and extended time for side reactions to occur, the 24-hour heating period before addition of nickel(II) provides a higher performance material. Reactions which had nickel(II) present from the start (See 5.3.6) gave unsatisfactory

materials. The optimum heating time may be between one hour and 24 hours or beyond 24 hours, again emphasizing the importance of understanding reaction intermediates.

During or after the addition of nickel, reactions became a semisolid "sol-gel"-like mass – shown in Figure 5.23 and Figure 5.24 – which impedes magnetic stirring. A significant increase in viscosity is noticeable during the nickel(II) addition in all reactions. All reactions were heated for 24 hours after nickel(II) addition. The importance of this time was not investigated and provides another handle for future optimizations. Precipitate has been noted in literature reports when using an excess of nickel(II).[312] Others deemed precipitate formed during the reaction as impurities which should be removed by filtration.[276] Our observations differ from a typical precipitate and instead form a coagulated mass. Only one other report in the literature describes this "sol-gel" or "organo-gel" formation in NiETT before oxidation.[317] A similar gelatinous reaction was reported in nickel(II) coordination polymers with 1,2,4,5-benzenetetrathiolate, but was not explained or investigated further.[318]

Because of the precautions taken to work under anhydrous, air-free conditions, we believe the sol-gel formation is not due to oxidation of the formed NiETT. Our work on oxidation equivalents (5.4.3) supports this hypothesis – despite all reactions solidifying during nickel(II) addition (*i.e.* oxidizing), the conductivity and oxidation level can be effectively set by adjusting the equivalents of iodine. Therefore, either minimal incidental oxidation can cause the reaction to solidify, or the solidification is due to another phenomenon.

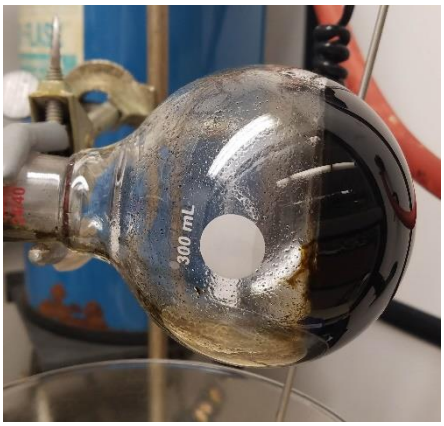

Figure 5.23 – A representative Na[NiETT] reaction held horizontally after nickel(II) addition and before chemical oxidation. A gelatinous mass of Na[NiETT] has formed in the flask that impedes stirring

5.3.4.4 Oxidation of NiETT

Because chemical oxidation agents act as Lewis acids and are incompatible with Lewis bases (*i.e.* methoxides), dilute acetic acid is used to quench any remaining methoxide in solution before the addition of the oxidant. Acetic acid was chosen to avoid addition of other counter ions to the reaction. Chemical oxidation is rapid and complete when using iodine. Figure 5.24a,b shows a reaction as a gelatinous mass before oxidation. Figure 5.24c,d show the same reaction after addition of iodine. The gelatinous mass has condensed to a fine black precipitate that settles out of solution. The minimal remaining counterion by elemental analyses and the disappearance of iodine color in solution when using stoichiometric equivalents of iodine (Na_0[NiETT]) indicate the oxidation is rapid and complete. All reactions are given several hours to complete the reaction between iodine and NiETT.

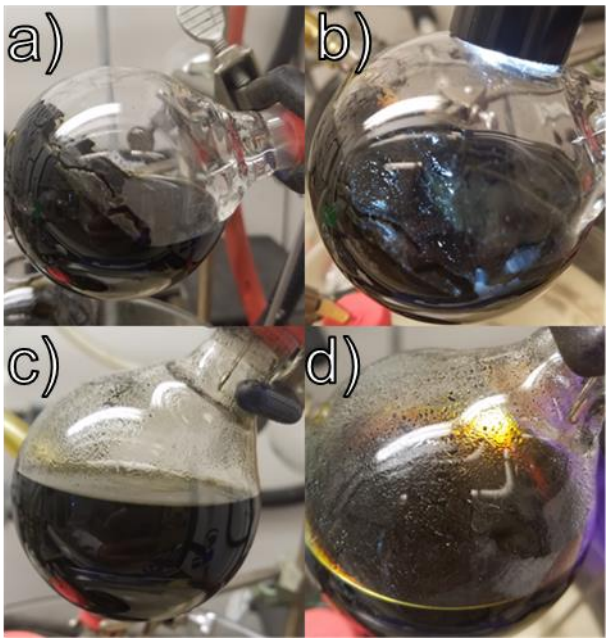

Figure 5.24 – a) Na[NiETT] "sol-gel" formed in a reaction flask. b) Na[NiETT] "sol-gel" under flashlight illumination. c) The same reaction after chemical oxidation by iodine with a fine precipitate visible on the walls of the flask. d) The same reaction with flashlight illumination from behind the flask showing residual iodine color and black precipitate

A few early reports of NiETT added oxidant *before* the addition of nickel(II), resulting in a green to brown color transition and precipitate formation. The addition of nickel(II) was assumed to stop quench the oxidation process. Despite the numerous side reactions possible, a conductive material was still obtained.[275,312] This highlights an important problem in the optimization of NiETT – many reaction conditions will yield n-type materials with some conductivity. A more thorough investigation is required to understand how and why certain conditions affect the final material.

5.3.5 *Workup, Purification, and Processing*

Beyond modifications to the synthetic method, workup and handling of the resultant material can also affect the final thermoelectric properties. Because NiETTs are insoluble, purification is limited to washing during material collection. Here, we outline

and recommend a procedure to standardize the handling of materials synthesized under different conditions. Reactions using less than two grams of thiapendione are most easily collected and washed on PTFE or nylon filters (47 mm diameter, 0.45 micron porosity) over coarse fritted break-apart filters. The filtrate and washes were collected and concentrated to determine if significant NiETT was passing through the filter. Only incidental amounts of black material were observed in the concentrated filtrates, indicating the effectiveness of this collection procedure. Centrifugation (3000 rpm, 5 to 30 minutes) was also investigated as a potential collection technique. Collection of the bulk material was easily accomplished; however, NiETT fines escaped this collection process. Filtering the supernatant using the above procedure proved to be a convenient method to collect these fines. NiETT that was collected only by centrifugation has a lower thermoelectric performance than NiETT collected by filtration or centrifugation with filtration. Reactions using greater than two grams of thiapendione, centrifugation was employed with success for multiple washing steps with filtration used for the final collection of fines and bulk material.

Common NiETT washing solvents include methanol, water, and ether. While diethyl ether is often used as a final solvent to speed drying of the filter cake, we observe ether removing a yellow color with a pungent, sulfurous odor from the material after methanol and water washes. Toluene also removed a yellow color from the NiETT. Attempts at GC-MS analysis failed to identify the removed impurity, indicating the impurity is not amenable to gas chromatography. Note, after washing with water, NiETT should be rewashed with methanol before transitioning to ether to transition between immiscible solvents. For reactions using less than two grams of thiapendione, we allow the

NiETT:solvent slurry to filter down to a viscous paste before changing wash solvents. For reactions using greater than two grams of thiapendione, we perform sequential washes in 50 mL centrifuge vials and collect all supernatant onto a 0.45 micron filter. Wash solvents are repeated three times to enhance the removal of impurities. The final, washed NiETT is collected onto the same filter as its supernatant with the aid of diethyl ether.

The air stability of NiETTs allows for the initial drying phase to be performed on the filter in atmosphere. Once dry enough to transfer to vial or glass bottle, a secondary drying is performed under high vacuum to remove residual solvent and volatile impurities. At this stage, the material appears homogeneous in composition but is inhomogeneous in size and not fit for processing into films, Figure 5.25a. Crushing by hand in an agate mortar gives a material suitable to further processing, Figure 5.25b. A noticeable odor of solvent and/or sulfurous off-gassing was sometimes emitted during crushing. Therefore, a tertiary drying of the crushed NiETT under high vacuum was implemented to fully remove any volatile impurities. The mortar and pestle were thoroughly cleaned with acetone and toluene between samples. Porcelain mortars and pestles are not recommended as NiETT fills in the rough surface, resulting in loss of material and difficult to clean equipment. Nitric acid is recommended when thorough cleaning of NiETT contaminated labware is required.

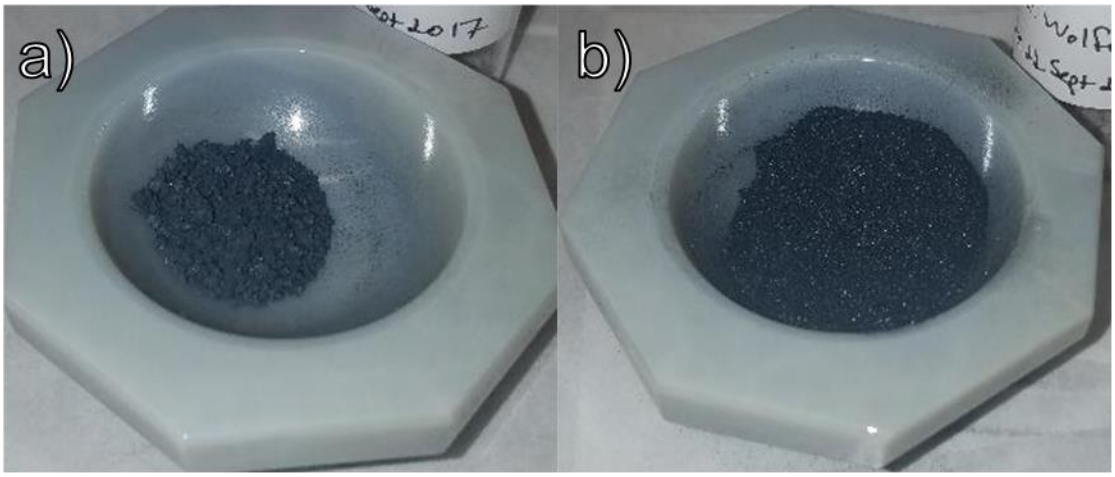

Figure 5.25 – a) An uncrushed sample of Na[NiETT] before hand-grinding with a 51mm I.D. agate mortar and pestle. b) The same sample after hand-grinding

The ability to purify NiETT after collection was a desirable feature. DMSO and acetone were tested as potential purification solvents. 50 mg of a NiETT sample was suspended in 20 mL of each solvent with 30 minutes of sonication. DMSO formed a dark brown-black solution that did not settle significantly upon standing, Figure 5.26a. Acetone formed a brown solution with a majority of the NiETT settled out, Figure 5.26b. Both samples were centrifuged at 4400 rpm for one hour. The acetone supernatant retained some brown color, not pictured. The DMSO supernatant remained a deep brown color, Figure 5.26c. After filtration through a 0.2 micron PTFE syringe filter, the DMSO kept a brown color, Figure 5.26d, and the acetone was a light yellow, Figure 5.26e. The light-yellow color of acetone is consistent with the color of washings during workup. The faint color intensity in the acetone filtrate is due to this material undergoing a thorough workup purification or due to acetone being a poor purification solvent. The higher color intensity in the DMSO filtrate is thought to be from ultrafine (< 200 nm) NiETT particles formed during sonication and not necessarily undesired impurities. Addition of a nonsolvent precipitated additional NiETT from the filtered DMSO supernatant.

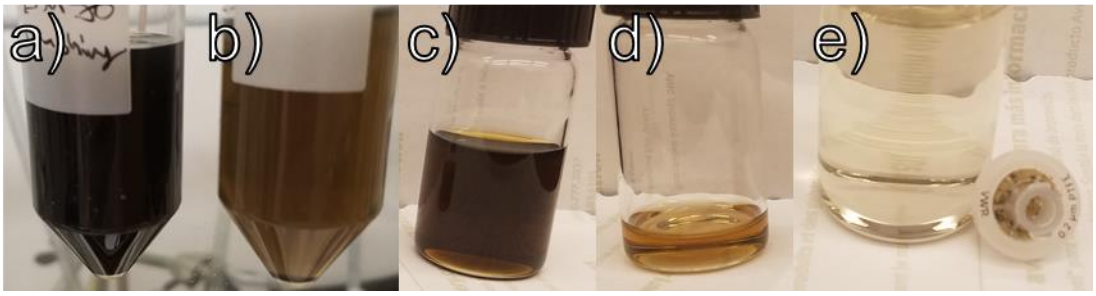

Figure 5.26 – Attempts at purification of NiETT through sonication in DMSO and acetone. a) NiETT suspended in DMSO after 30 min of sonication. b) NiETT suspended in acetone after 30 min of sonication. c) DMSO supernatant after centrifugation at 4400 rpm for 1 h. d) Acetone supernatant after centrifugation at 4400 rpm for 1 h. e) Acetone supernatant after filtration through a 0.2 µm PTFE filter

Two qualitatively distinct forms of NiETT are observed across all syntheses and detailed in Table 5.8: amorphous black powders and/or blue-gray particles that have reflective facets, indicating the formation of a poly-crystalline or heterogeneous material in contrast to the completely amorphous polymer reported in literature.[297] One reaction (5.047) gave us both forms, which were collected separately and analyzed. The elemental composition of both forms is identical, yet the blue-gray form provides improved thermoelectric properties.

Table 5.8 – Comparison of two distinct forms of NiETT. [a]Annealed at 160 °C

		5.047	5.047.B
Powder Appearance		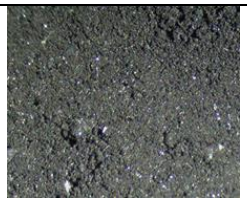	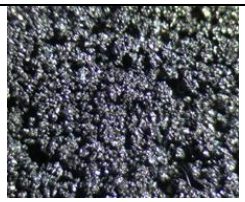
		Amorphous, black powder	Lustrous blue with shiny facets
σ (S/cm)[a]		14 ± 4	49 ± 1
S (μV/K)[a]		-69 ± 2	-67 ± 2
Elemental (%)	C	13.1	12.8
	H	0.9	0.9
	S	56.7	56.7
	Ni	21.07	21.82
	Na	1.26	1.35

5.3.6 *Reaction Failures and Observations*

Many of the aforementioned synthetic choices were devised after failed reactions. A NiETT reaction will undoubtedly yield some amount of insoluble material. A failed reaction is defined here as a material that does not give a conducting composite with PVDF (< 10 S/cm), that has a low thermopower (|< 20| μV/K), or that does not form continuous composite films with PVDF. The minimum metrics to warrant further study have increased during optimization trials and will certainly increase with further experiments. Below are brief descriptions of "failed" reactions, their main deviations from the optimized route, and speculations on their failures.

5.010 – Reaction run in HMPA at 60 °C. HMPA was not distilled and contained amine impurities which reacted with thiapendione. Unknown product formed which could not be isolated, because it did not precipitate after oxidation or upon addition of methanol. Only attempt with freshly distilled HMPA.

5.013 – A series of aliquots were taken at specific reaction times from a reaction between thiapendione and sodium methoxide and added to solutions of nickel(II) salt. The NiETTs were collected by centrifugation and decanting the supernatant after oxidation. The addition of the reactive ligand to nickel(II) and/or the collection of material by centrifugation does not give conductive NiETTs. This may be due to the reactive ligand encountering an excess of nickel(II) or because centrifugation does not adequately collect the fines of NiETT which are required to make continuous conductive networks in PVDF composites.

5.019 – This was a set of reactions to study the effect of nickel(II) stoichiometry. All reactions gave poorly conducting NiETTs. At this stage, the sodium methoxide being used was stored in a desiccator. It is believed that repeated exposure to atmosphere affected the efficacy of the sodium methoxide. This is contrary to evidence provided in Table 5.4, where sodium hydroxide gives conductive NiETT. A reaction (5.019.E) run with the same synthetic batch of sodium methoxide, but from a fresh portion that had been stored in a glovebox, yielded conductive NiETT.

5.022 – This NiETT was collected by centrifugation instead of filtration. It yielded conductivity ~ 5 S/cm.

5.026 – In this reaction, the nickel(II) salt was added as a solid in one portion. While the films with continuous NiETT networks were conductive (~ 30 S/cm) with adequate thermopower (-40 μV/K), the cast composite films were very rough and of poor quality. The rate of formation or entrapment of unreacted nickel(II) may cause poor film quality.

5.027 – In this reaction, nickel(II) was present from the start of the reaction with thiapendione and sodium methoxide. This NiETT was poorly conducting (< 5 S/cm).

5.3.7 *Optimized Synthesis Summary*

With the combined knowledge of success, failures, reports from literature, thermoelectric performance, and elemental composition, a standard optimized synthesis is presented here that provides consistent batch-to-batch performance. An example of batch-to-batch consistency is presented in Figure 5.27.

In a cool, dry round bottom flask with magnetic stir bar, was added thiapendione (500 mg, 2.4 mmol, 1.0 equiv.) against a positive flow of argon. The atmosphere was thoroughly purged with argon. Anhydrous, degassed methanol (15 mL) was added by syringe, and the reaction was heated to 60 °C. Separately, sodium methoxide (648 mg, 12 mmol, 5.0 equiv.) was dissolved in methanol (15 mL). The methoxide solution was added to the reaction. The reaction immediately turns a light-yellow color that becomes more pronounced over time. The reaction was stirred for 24 hours at 60 °C, resulting in a black solution. Separately, anhydrous nickel(II) acetate (424 mg, 2.4 mmol, 1.0 equiv.) was dissolved in anhydrous methanol (20 mL). At the 24 hour reaction mark, the addition of the nickel(II) solution was started at a rate of 20 mL/hour, such that the solution is added over 1 hour. The reaction becomes a “sol-gel” during the addition, such that stirring was significantly impeded. The reaction was stirred at 60 °C for an additional 23 hours, to give a total active reaction time of 48 hours. Glacial acetic acid (1 mL in 10 mL methanol) was added rapidly by syringe. The reaction vessel was shaken to homogenize the contents. Iodine (609 mg, 2.4 mmol, 2.0 equiv. of oxidant) in methanol (10 mL) was added in one

portion. The reaction was allowed to stir for several hours at 60 °C, at which point the iodine color had faded from the solution, the "sol-gel" had become a fine suspension, and the reaction suspension settles upon removal of stirring. The solids were collected on a 0.45 µm nylon filter. Without allowing the slurry to filter completely between washes, the product was washed three times each with methanol, distilled water, methanol again, and finally ether. The resulting lustrous grey-blue material was allowed to dry on the filter before being dried under high vacuum overnight. After crushing in an agate mortar and pestle, the powder was dried again under high vacuum to remove any trapped solvent.

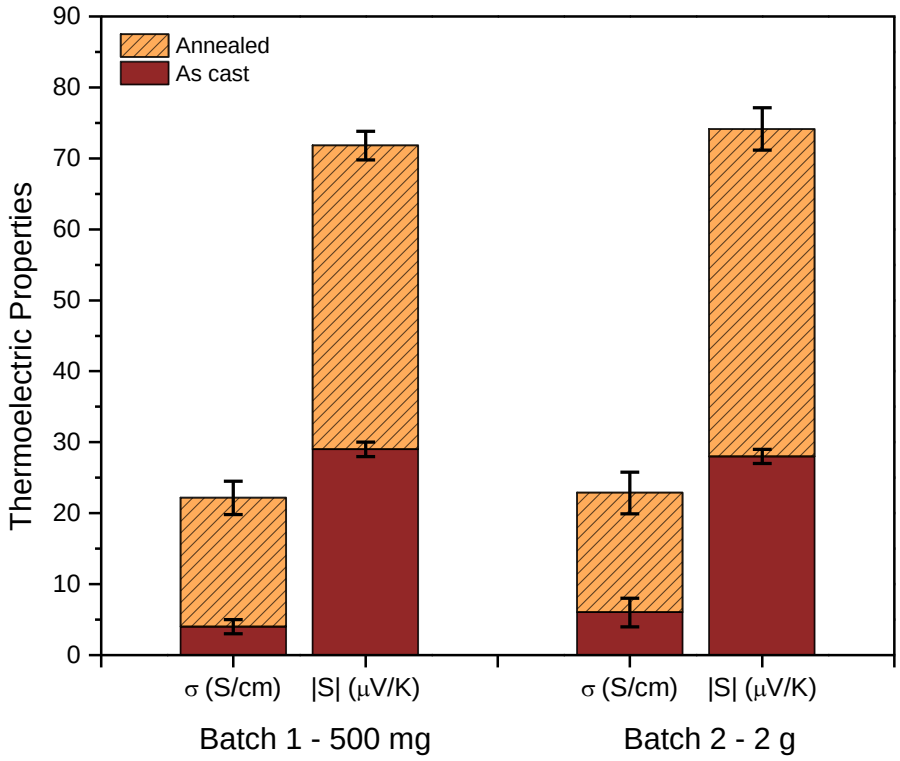

Figure 5.27 – Thermoelectric performance of two independent syntheses of Na_0[NiETT] on a 500 mg and 2 g scale. Consistent conductivity and Seebeck are measured in the PVDF composite films before and after annealing at 160 °C

5.4 Exploring NiETT through Controlled Synthesis Families

To explore the reaction and final materials more thoroughly, the reaction was systematically modified from the standard procedure at one of three steps in Figure 5.28:

Step 1: Methoxide Counter Ion; Step 2: Equivalents of Nickel; Step 3: Extent of oxidation. This allowed us to create families of material in which all other variables of influence and changes to the reaction were minimized.

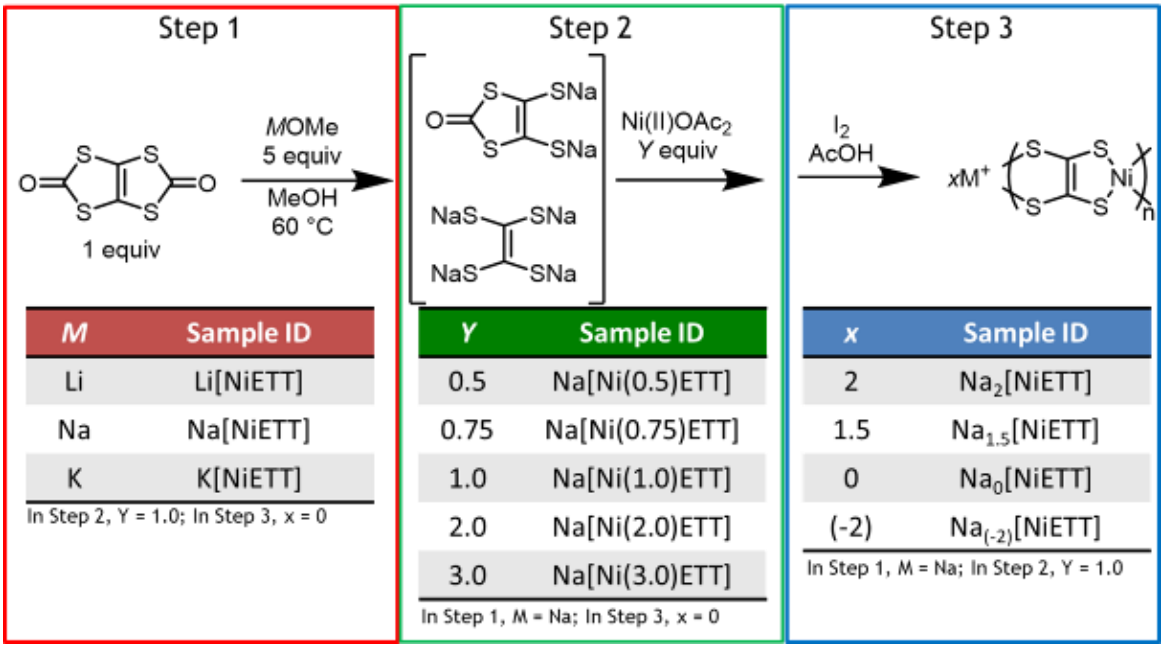

Figure 5.28 – The synthesis of NiETT is sub-divided into three modifiable steps for systematic thermoelectric property optimization

In Step 1, to isolate the effect of the counter ion on the reaction and final material, three methoxide species were used: lithium methoxide, sodium methoxide, and potassium methoxide. The three otherwise identical reactions yield Li[NiETT], Na[NiETT], and K[NiETT]. In Step 2, to isolate the effect of nickel deficiency or excess, five NiETTs with different equivalents of nickel(II) acetate were synthesized while keeping the counter ion fixed using sodium methoxide: Na[Ni(0.5)ETT], Na[Ni(0.75)ETT], Na[Ni(1.0)ETT], Na[Ni(2.0)ETT], and Na[Ni(3.0)ETT]. In Step 3, to isolate the effect of oxidation extent, four reactions using one equivalent of nickel(II) acetate and sodium methoxide were synthesized: no chemical oxidation, Na_2[NiETT]; partial chemical oxidation, $Na_{1.5}$[NiETT]; full oxidation to the neutral polymer, Na_0[NiETT]; and theoretical over-

oxidation, $Na_{(-2)}$[NiETT]. Here, the sodium subscript indicates the expected number of counter ions per repeat unit, and therefore the expected negative charge on the backbone per repeat unit of the polymer. The subscripts on sodium are used exclusively as a naming convention to indicate how the sample was prepared and do not indicate the actual number of counter ions per repeat unit. The negative subscript indicates a stoichiometric excess of oxidant was used resulting in a hypothetical charge of positive two on the backbone repeat unit; however, in practice with iodine, the oxidation stops at a neutrally charged backbone.

5.4.1 *Step 1: Exchanging the Counterion*

It is well-known that bulky counter ions such as tetraethylammonium can reside between polymer chains and impede charge transport. Alkali counter ions are preferred as their small size allows for close-packing of the polymer chains, thereby facilitating interchain interactions.[276,297] The origin of the counterion in NiETT is from the source of methoxide used in Step 1. We varied the counterion by using lithium methoxide (Li[NiETT]), sodium methoxide (Na[NiETT]), or potassium methoxide (K[NiETT]).

The thermoelectric properties of NiETT are found to be dependent on the counterion, Figure 5.29. The thermopower of all three variants is negative, confirming that n-type electrical transport is dominant. Interestingly, the electrical conductivity increases and the thermopower decreases when reducing the size of the counter ion; Li[NiETT], with the smallest counter, ion has the highest conductivity of 37 ± 1 S/cm, while K[NiETT] has the highest thermopower of -99 ± 8 μV/K. The power factor is highest for Na[NiETT] films at a value of 13 ± 2 μW/m-K^2 due to the combination of a moderate conductivity and Seebeck coefficient (23 ± 1 S/cm and -74 ± 3 μV/K). This is in contrast to what has been reported

for ETT pellets where K[NiETT] showed superior thermoelectric properties.[297] These differences can be attributed to the fact that the reactions conditions as well as reactant purity in each step dictate the final material performance. The alkali ion composition is consistent across all syntheses at 0.6-0.8 atomic percent or one counter ion per 10-15 nickel centers.

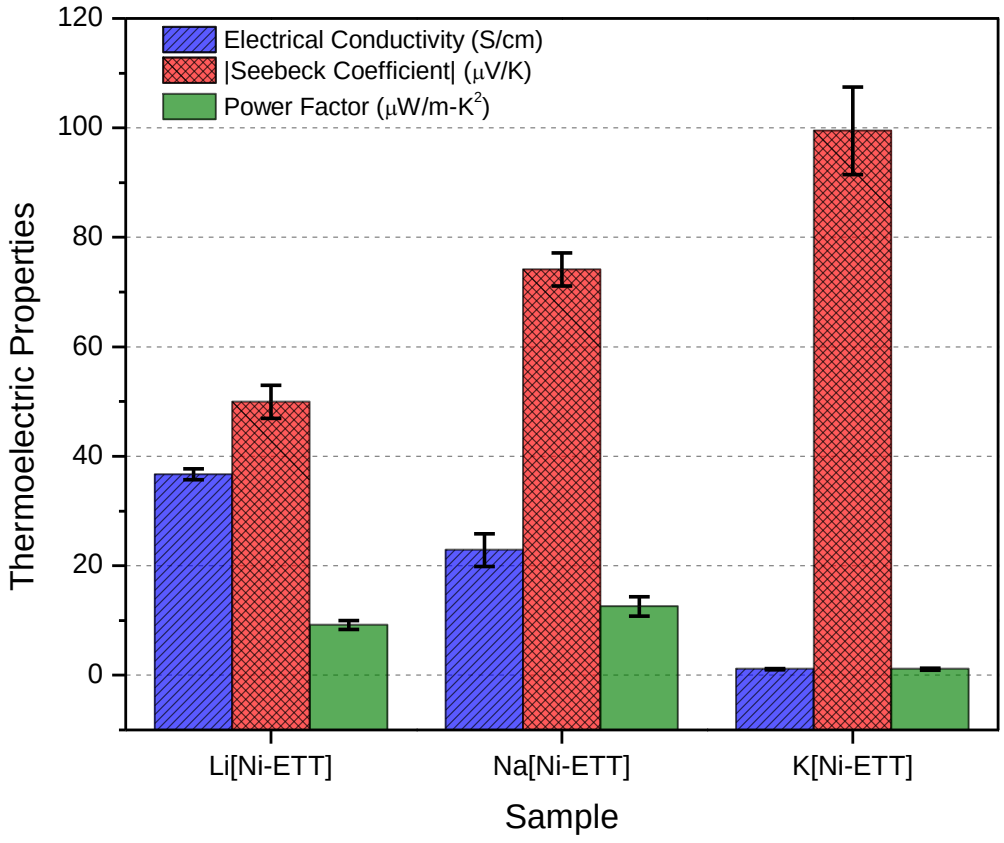

Figure 5.29 – Thermoelectric performance of NiETT with different alkali metal counter ions

The marked difference in thermoelectric performance, despite similar composition and oxidation extent, supports two hypotheses: (i) the counter ion affects the reaction pathway and produces a different final material beyond simply exchanging the counter ion;

and/or, (ii) a property of the counter ion, even at one counter ion per 10-15 nickel centers, directly affects NiETT's intra- and interchain interactions.

5.4.2 *Equivalents of Nickel(II)*

In Step 2, the stoichiometric equivalents of the nickel(II) salt were varied using Na_0[Ni(1.0)ETT] as the control material to identify the optimum equivalence under these reaction conditions, Figure 5.30. It has been claimed that excess nickel can produce Ni[NiETT] where it acts as a counterion with alkali metals;[297] an alternative hypothesis is that excess nickel acts as a detrimental impurity in the final material. Using anhydrous nickel(II) acetate, which was chosen due to the ease of obtaining the anhydrous salt and its solubility in methanol, removes any uncertainty around the molar mass of the hydrate and the effect on the reaction from hydrated nickel(II) species. The resulting thermoelectric properties indicate that a power factor enhancement up to 23 μW/m-K^2 is achieved by lowering the amount of nickel(II) to 0.75 equivalents.

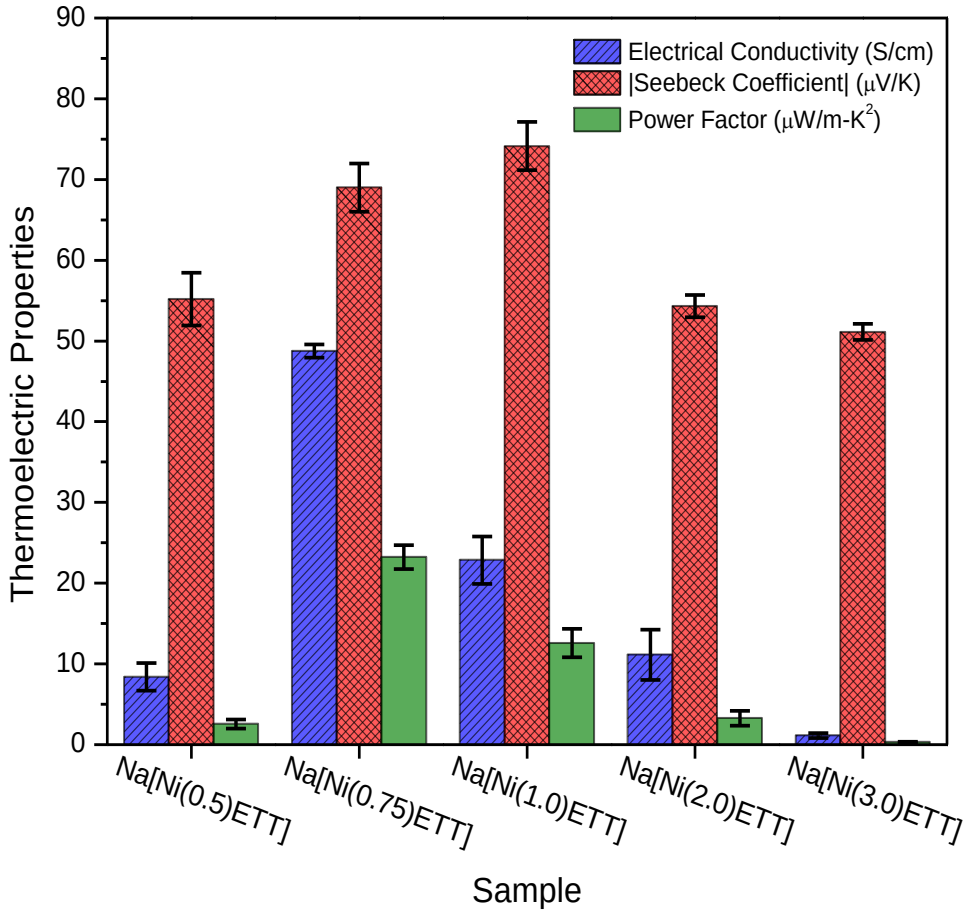

Figure 5.30 – Thermoelectric performance of annealed NiETT:PVDF composites from reactions with varied stoichiometry of nickel(II)

To understand the effect of changing the amount of nickel(II), the % Ni incorporation is calculated in these polymers to quantify how much of the nickel(II) from nickel(II) acetate is present in the NiETT backbone, Table 5.9. The higher percent incorporation is found in the sub-stoichiometric nickel equivalents with 80% incorporation for Ni(0.75) compared with 40% incorporation for Ni(2.0). Impurities in the thiapendione monomer or degradation during reaction Step 1 is hypothesized to result in less than 100% nickel incorporation, with the optimum level of nickel therefore being sub-stoichiometric. Furthermore, XPS analysis of the Na[NiETT] powders reveals that excess nickel(II), as in the case of Na[Ni(2.0)ETT], forms secondary products that are observed in the nickel and

sulfur elemental scans. These impurities are present in lower amounts in the stoichiometric and sub-stoichiometric equivalents. No evidence of excess nickel acting as a counterion was observed. For full reports and discussion of XPS, see Dr. Akanksha Menon's PhD Thesis.[300]

Table 5.9 – Elemental composition of nickel equivalents NiETT family with calculated nickel incorporation

	Ni(0.5)	Ni(0.75)	Ni(1.0)	Ni(2.0)	Ni(3.0)
C	15.7	12.8	16.4	14.1	15.6
H	1.1	0.9	0.9	1.5	1.2
S	59.5	56.7	56.6	47.1	54.5
Na	1.05	1.35	0.83	0.34	0.08
Ni	18.35	21.82	21.71	25.06	19.54
Percent Ni Incorporation	80%	81%	62%	43%	18%

5.4.3 *Extent of Oxidation*

As a final step, the effect of oxidation with iodine was investigated to understand the extent to which thermoelectric properties could be tuned by controlling the oxidation state and thus doping level of the polymer. For this, every attempt was made to prevent the ligand, prepared in situ, from being oxidized until the iodine addition step by handling under an inert atmosphere (argon) using standard Schlenk techniques (see Experimental Section). Most previous literature reports[276,297] claim the polymer does not precipitate until air is introduced as an oxidant. However, one previous report[275] shows that the polymer precipitates upon addition of the metal salt without any external oxidant. It has also been claimed that even by working under careful anaerobic conditions, there is some unintended oxidation that causes the polymer to precipitate.[311] The observations in this thesis are

contrary to these previous reports, as the reaction intermediately forms a sol-gel, Figure 5.23 and Figure 5.24, during Step 2 of the reaction. Furthermore, from the rigorous air-free reaction conditions employed in our work and observable consumption of iodine during reaction Step 3, unintended oxidation is not the cause of the precipitate or sol-gel formation prior to oxidation. Rather, higher molecular weight species (either branched or linear) are forming in reaction Step 2 and increasing the reaction viscosity. Even without the addition of any iodine, an "unoxidized" polymer is unobtainable as it oxidizes on exposure to air during work-up (filtering and drying) and film fabrication. These workup conditions make Na_2[NiETT] (which has no iodine added) an analog to an air-oxidized species moreso than a truly unoxidized polymer.

The family of Na[NiETT]s synthesized to study extent of oxidation is shown in Figure 5.31. Under these conditions, the electrical conductivity for Na_2[NiETT] is 37 ± 3 S/cm while the thermopower shows the lowest value for this family at –36 ± 2 μV/K. The elemental composition shows approximately two sodium atoms per five nickel atoms, indicating a more negative charge on the backbone compared to one sodium atom per ten nickel atoms in the fully oxidized Na_0[NiETT]. Upon addition of iodine in Step 3 of the reaction, electrons are extracted from the polymer backbone, which leads to a reduction in electrical conductivity and a simultaneous improvement in the thermopower. This *S*-σ tradeoff is analogous to extrinsically doping a polymer and shows that NiETTs can have their oxidation level tuned during synthesis to give desired values for S and σ.

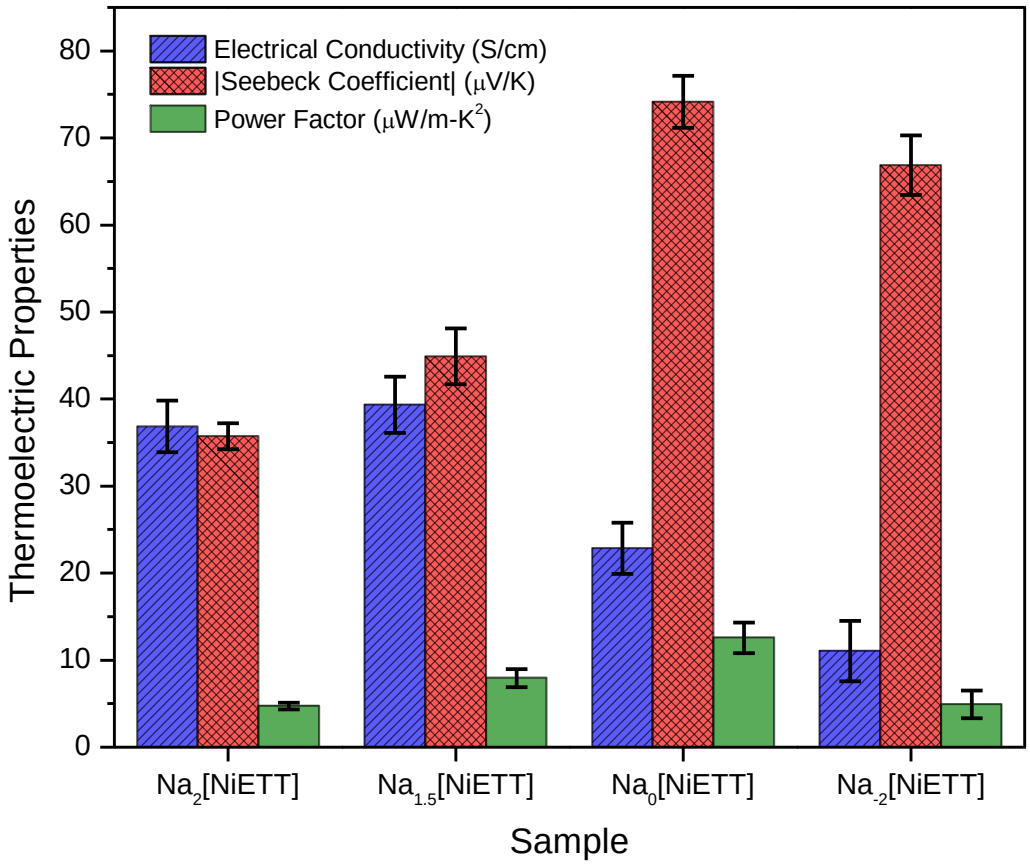

Figure 5.31 – Thermoelectric performance of NiETTs as a function of chemical oxidation equivalents using iodine

XPS analysis of Na_2[NiETT] shows an increase in sulfur oxide species due to air exposure of the unoxidized polymer. The use of air as an oxidant results in thermoelectric properties of NiETT that vary significantly, and this may explain challenges with material reproducibility in literature. The use of iodine provides greater control of the oxidation step and allows for some level of tunability in the thermoelectric properties; other oxidizing agents in future studies may enable greater tunability to provide insight into the charge transport in these materials.

5.5 Conclusions and Outlook

Starting from unreliable and under-detailed literature reports on the synthesis of NiETT, this chapter has developed a standardized, well-documented synthetic protocol for the production of NiETT from 100 mg to 15 g scales. This procedure is valuable within our own research group, for minimizing batch-to-batch variations and producing a reproducible material for device experimentation, and to the organic thermoelectric community at large. It urges fellow contributors to follow this procedure or rigorously document the procedure used. In this way, the many different materials all with the name "NiETT" can be compared more accurately across studies.

There is no doubt that this synthetic procedure is not the most optimized procedure that will give the highest performing NiETT possible. It does, however, provide a baseline from which to make synthetic modifications and study their impact. We have taken on three of these modifications and reported their effect: counterion exchange, nickel equivalents, and oxidation extent. There exist many synthetic modifications to make that may increase performance further.

From a synthetic standpoint, most of the empirically-derived improvements to the literature procedures have been explored in this work. Understanding the reaction mechanism across each synthetic step, individually, and across the entire reaction will be vital to discovering further improvements in reaction conditions. It is my belief that ^{13}C NMR spectroscopy will be an invaluable tool in this process. This work thoroughly explored the synthesis of NiETT in methanol at or near its boiling point using iodine as an

oxidant. Future studies on reaction solvent, base/nucleophile choice, reaction temperature, timing of addition of reagents, and reagent equivalence are “low-hanging fruit.”

5.6 Synthetic and Experimental Methods

5.6.1 *Nomenclature*

With the generation of a large number of samples with technically identical names, notebook page numbers were used as compound codes to avoid confusion and unnecessarily long names. Therefore material 5.072 corresponds to the synthesis described in Rylan Wolfe Notebook 5, Page 72. For the specific set of NiETTs created as Step 1, Step 2, and Step 3 investigative families, the nomenclature follows M_X[Ni(Y)ETT], where M is the alkali counterion, X is the hypothetical number of counterions per repeat unit based on iodine oxidation, and Y is the equivalents of nickel(II) used. Thus, Na_1[Ni(1.5)ETT] would be a NiETT with 1.5 equivalents of nickel(II) and one sodium ion per repeat unit. When X or Y are not given, X = 0 and Y = 1.0.

5.6.2 *Material Characterization*

Elemental analyses were carried out by Atlantic Microlabs on a PerkinElmer 2400 II analyzer (CH) and a Carlo Erba 1108 analyzer (S). The analysis of Ni and counterions (Li, Na and K) was carried out on an inductively coupled plasma optical emission spectrometer, ICP-OES (OPTIMA 7300 DV, PerkinElmer). Each sample was dissolved in concentrated nitric acid and diluted with deionized water prior to analysis. X-ray photoelectron spectroscopy (XPS) was performed on the powder samples using a Thermo K-Alpha XPS (Thermo Fisher Scientific Inc.). Thermogravimetric analysis (TGA) was

performed using Pyris 1 Thermogravimetric Analyzer (PerkinElmer) under nitrogen. IR spectra were collected on a Prestige 21 FT-IR spectrometer (Shimadzu) equipped with a PIKE Technologies MIRacle ATR accessory. Raman spectra were recorded on a Bruker Senterra Raman Microscope equipped with an Olympus BX51M w/ Inifinity 1 capture system using a crystalline silicon wafer as a support (Laser Wavelength: 532 nm). Solid state NMR spectra were record by Dr. Johannes Leisen of the Georgia Tech NMR Center on a Bruker Avance IIIHD 300 NMR spectrometer. Solution NMR spectra were recorded on a Bruker Avance IIIHD 700 NMR (700 MHz ^{1}H, 176 MHz ^{13}C) spectrometer and referenced to the residual solvent signal (Methanol-d4: 4.8 ppm (^{1}H), 49.00 ppm (^{13}C); DMSO-d6: 2.5 ppm (^{1}H), 39.52 ppm (^{13}C); Benzene-d6: 7.16 ppm (^{1}H), 128.06 ppm (^{13}C).

5.6.3 *Film Fabrication*

A composite film was obtained by blending the ETT powder with a polymer matrix to form a dispersion. First, PVDF (Sigma Aldrich, MW ~180,000) was dissolved in DMSO (Amresco) at 80 °C for 4 hours under continuous stirring in an Erlenmeyer flask to form a 10 mg/mL solution. Next, 40 mg of ETT powder was added to 1 mL of the PVDF/DMSO solution with 10 zirconia beads (diameter = 1 mm) in a micro-vibration mill for 30 minutes (MSK-SFM-12M, MTI Corporation). This matrix was chosen as it has the highest film performance as reported previously, and the ETT:PVDF mass ratio was fixed at 4:1.[299,301] The dispersion was pippetted out and films were prepared by drop-casting 35 µL on 1 cm × 1 cm pre-treated glass substrates and drying in a vacuum oven at 50 °C for 30 minutes (pre-treatment of glass substrates involves sequential cleaning with deionized water, acetone and isopropyl alcohol for 3 minutes each and placement in oxygen-plasma for 5 minutes). Four gold contact pads (1 mm × 1 mm, ~ 100 nm thick) were then deposited on

the prepared films using a shadow mask in an e-beam evaporator. All films were 5-10 μm thick as measured with a profilometer (Dektak XT, Bruker). Several samples (films) were prepared to capture sample-to-sample variations in thermoelectric properties generating representative error bars that are reported as the standard deviation.

5.6.4 *Thermoelectric Measurements*

All reports of thermoelectric performance are of NiETT:PVDF composite films. Annealing was performed on a hotplate set at 160 °C for one hour in atmospheric conditions. Micromanipulators with tungsten tips were used to make electrical contact to the gold contact pads and in-plane electrical conductivity was acquired using the four-probe Van der Pauw technique. Samples were placed on a temperature-controlled Peltier stage using thermal grease on the backside of the substrate to ensure good thermal contact. The Seebeck coefficient was measured by suspending the sample between two temperature-controlled Peltier units (separated ~3 mm) and applying a series of temperature differences upto ΔT = 10 °C between the stages. The thermoelectric voltage was measured between two contact pads on separate stages using the probe tips, while the temperature of each pad was measured with a K-type thermocouple in close proximity to the probe tips. Voltage and temperature data were acquired using a Keithley 2700 DMM with a 7708 Mux card via a LabVIEW interface. The Seebeck coefficient was extracted as the slope of the V - ΔT plot.

5.6.5 *Typical Reaction Procedure for NaNiETT*

In a cool, dry round bottom flask with magnetic stir bar, was added thiapendione (500 mg, 2.4 mmol, 1.0 equiv.) against a positive flow of argon. The atmosphere was

thoroughly purged with argon. Anhydrous, degassed methanol (15 mL) was added by syringe, and the reaction was heated to 60 °C. Separately, sodium methoxide (648 mg, 12 mmol, 5.0 equiv.) was dissolved in methanol (15 mL). The methoxide solution was added to the reaction. The reaction immediately turns a light-yellow color that becomes more pronounced over time. The reaction was stirred for 24 hours at 60 °C, resulting in a black solution. Separately, anhydrous nickel(II) acetate (424 mg, 2.4 mmol, 1.0 equiv.) was dissolved in anhydrous methanol (20 mL). At the 24 hour reaction mark, the addition of the nickel(II) solution was started at a rate of 20 mL/hour, such that the solution is added over 1 hour. The reaction becomes a "sol-gel" during the addition, such that stirring was significantly impeded. The reaction was stirred at 60 °C for an additional 23 hours, to give a total active reaction time of 48 hours. Glacial acetic acid (1 mL in 10 mL methanol) was added rapidly by syringe. The reaction vessel was shaken to homogenize the contents. Iodine (609 mg, 2.4 mmol, 2.0 equiv. of oxidant) in methanol (10 mL) was added in one portion. The reaction was allowed to stir for several hours at 60 °C, at which point the iodine color had faded from the solution, the "sol-gel" had become a fine suspension, and the reaction suspension settles upon removal of stirring. The solids were collected on a 0.45 μm nylon filter. Without allowing the slurry to filter completely between washes, the product was washed three times each with methanol, distilled water, methanol again, and finally ether. The resulting lustrous grey-blue material was allowed to dry on the filter before being dried under high vacuum overnight. After crushing in an agate mortar and pestle, the powder was dried again under high vacuum to remove any trapped solvent.

5.6.6 *Anhydrous, Degassed Methanol*[106]

ACS Grade methanol was dried by standing over freshly activated 3Å molecular sieves (20% m/v) for at least 48 hours prior to use. Molecular sieves were activated in a vacuum oven (200 °C, ~10 mbar) overnight. Dried methanol was sparged with argon for a minimum of 30 minutes before use in reactions.

5.6.7 *Sodium Methoxide*

Prepared by adapting a literature procedure.[319] Sodium (37 g) cut was cleaned of oil and surface oxides in anhydrous toluene. The sodium was cut into 1-3 g pieces under a protective solution of anhydrous toluene and added in small portions to stirred anhydrous, degassed methanol (800mL) in a 2L flask equipped with a stirrer and a condenser under argon. After all the sodium had dissolved, the methanol was removed by distillation under vacuum (~10 mbar) and the residual NaOMe is dried by heating at 150 °C under high vacuum overnight. The NaOMe was allowed to cool under argon and was directly transferred to an argon-filled glovebox for storage, handling, and weighing.

5.6.8 *Anhydrous Nickel(II) Acetate*[308]

A known quantity of $Ni(II)OAc_2 \cdot xH_2O$ (7.231 g, 29.06 mmol, assumed to be the tetrahydrate) from a commercial supplier was added to a tared vial. The vial was placed under high vacuum overnight. The measured mass difference was less than the accuracy of the balance (~ 1 mg), indicating that high vacuum is not sufficient for dehydration. The vial was capped with 3 layers of kimwipes to prevent powder from aerosolizing. The vial was placed into a vacuum oven (~10 mbar) and heated to 110 °C overnight. The powder

changed from bright green to a muted yellow-green powder. The oven was backfilled with argon to prevent reabsorption of water by the nickel salt. The salt was transferred to an argon-filled glovebox for storage. Final measured mass was 4.931 g corresponding to 27.89 mmol of anhydrous nickel(II) acetate, indicating the commercially available salt was the tetrahydrate and was completely dehydrated.

5.6.9 *Bis(tetraethylammonium)bis(1,3-dithiole-2-thione-4,5-dithiol)zincate (5.1)*

Compound **5.1** was prepared according to a literature procedure.[266] An optimized procedure has been reported and is recommended.[272] Yield: 64.2 g (63%)

HRMS (EI) *m/z* calculated for $C_6S_{10}Zn$ $[M]^-$ 455.6504; found 455.6512. EA: Anal. Calcd for $C_{22}H_{40}N_2S_{10}Zn$ (%): C, 36.77; H, 5.61; N, 3.90; S, 44.62. Found (%): C, 35.88; H, 5.55; N, 3.90; S, 45.25.

5.6.10 *S,S'-(2-thioxo-1,3-dithiole-4,5-diyl) dibenzothioate (5.2)*

Compound **5.2** was prepared according to a modified literature procedure.[320] To 1-L Erlenmeyer flask with stir bar was added $[TEA]_2[Zn(dmit)_2]$ (21.5 g, 30.0 mmol, 1.0 equiv.) and acetone (500 mL). The reaction was stirred while the benzoyl chloride was prepared. Note: full dissolution was not achieved, and $[TEA]_2[Ni(dmit)_2]$ will slowly oxidize in the presence of atmosphere. Benzoyl chloride (14.6 mL, 126 mmol, 4.2 equiv.) was added over three minutes. The undissolved $[TEA]_2[Ni(dmit)_2]$ was rapidly brought into solution and the red color of $[TEA]_2[Ni(dmit)_2]$ disappeared within 5 minutes of addition. $ZnCl_2$ is visible as a precipitate. The reaction was stirred for 4 additional hours at room temperature. The $ZnCl_2$ was allowed to settle before being filtered off. The yellow

reaction solution was concentrated under reduced pressure to a yellow-white solid which contained a significant amount of $ZnCl_2$ and TEACl. The solids were dissolved in DCM with the aid of sonication, washed with distilled H_2O (2x) to remove $ZnCl_2$ and benzoic acid, and washed with brine (1x). The organics were collected. Silica gel was added to the DCM, and the mixture concentrated to a free flowing solid. The silica gel was dry loaded onto a prepared plug (silica: 100% DCM) and eluted with DCM. The eluent was concentrated to a yellow-orange crystalline powder. Yield: 26.6 g (109 %) (Likely contaminated with byproducts or benzoic acid).

^{1}H NMR (300 MHz, $CDCl_3$) δ 7.98 – 7.91 (m, 4H), 7.71 – 7.63 (m, 2H), 7.54 – 7.47 (m, 4H).

5.6.11 *Bis(tetraethylammonium)bis(1,3-dithiole-2-thione-4,5-dithiol)nickelate (5.3)*

Compound **5.3** was prepared according to a modified literature procedure.[266] To a dry 250-mL 3-neck round bottom flask was added Compound 5.2 (813 mg, 2.0 mmol, 1.0 equiv.) and dry MeOH (10 mL). Separately, fresh NaOMe was made by adding sodium metal (138 mg, 6 mmol, 3.0 equiv.) to MeOH (10 mL). The NaOMe solution was added dropwise to the 5.2 to generate the sodium dmit ligand. After stirring for 1 hour, MeOH:H_2O (20 mL:20 mL) was added to quench excess NaOMe. Separately, Ni(II)Cl_2 (129.6 mg, 1.0 mmol, 0.5 equiv.) was dissolved in conc. aqueous NH_3:MeOH (5 mL:5 mL); Tetraethylammonium bromide (420.3 mg, 2.0 mmol, 1.0 equiv.) was dissolved in H_2O (5 mL).

The Ni(II) solution was added slowly by syringe to the dmit anion and allowed to stir for ~10 minutes. To the dark purple-black solution was added the tetraethylammonium

bromide solution. The reaction was allowed to stir for 2 hours. The reaction was collected on a 0.45 micron nylon filter and washed with IPA until the filtrate was colorless, then ether until the filtrate was colorless. The purple-black semicrystalline solid was dried under high vacuum. Yield: 623 mg (87.5%)

EA: Anal. Calcd for $C_{22}H_{40}N_2S_{10}Ni$ (%): C, 37.12; H, 5.66; N, 3.94; S, 45.05. Found (%): C, 36.60; H, 5.49; N, 3.88; S, 44.73.

5.6.12 *Bis(sodium)bis(1,3-dithiole-2-thione-4,5-dithiol)nickelate (5.4)*

To a 100-mL round bottom flask with stir bar was added $(TEA)_2Ni(dmit)_2$ (1424 mg, 2.0 mmol, 1.0 equiv.) and degassed, dry MeOH (40 mL, 0.05 M). The mixture was allowed to stir for several minutes to dissolve and disperse the material as a purple slurry. Sodium tetraphenylborate ($NaBPh_4$, 1369 mg, 4.0 mmol, 2.0 equiv.) was added in one portion. The reaction was allowed to stir for two days to complete the ion exchange. The reaction was filtered through a 0.45 micron nylon filter to remove the precipitated $(TEA)BPh_4$ as a white powder. The filtration was aided with additional methanol until the filtrate was colorless. The methanol filtrate was concentrated to a purple solid and further dried under high vacuum. Yield: 1240 mg (125 %) ^{13}C NMR spectroscopy indicates an excess of tetraphenyl borate remaining in the product.

$^{13}C\{^1H\}$ NMR (176 MHz, MeOD) δ 210.50, 142.43.

5.6.13 *Potassium isopropyl xanthate (5.5)*

Compound **5.5** was prepared according to a modified literature procedure.[303] To a 2-L round bottom flask under argon with mechanical stirring was added isopropanol (230

mL, 3.0 mol, 1.0 equiv.) and a saturated solution of potassium hydroxide (185 g, 3.3 mol, 1.1 equiv.) in H_2O (~165 mL). The reaction was cooled to 0 °C. Carbon disulfide (235 mL, 3.9 mol, 1.3 equiv.) was added dropwise such that the reaction was kept below 8 °C. A yellow precipitate forms immediately. An orange color begins to develop after ~100 mL of carbon disulfide has been added. The literature procedure notes a formation of a red impurity of poly alkali sulfides, which could be the origin of the orange color. No vibrant red color developed in this reaction. Running the reaction under argon, keeping the temperature below 10 °C instead of 20 °C as reported, or a higher purity carbon disulfide may have minimized by-product formation. The reaction was stirred for 30 minutes after complete addition of the carbon disulfide. The yellow precipitate was collected by filtration and compressed with a spatula to aid filtration. At this stage, the xanthate can be rinsed with diethyl ether to remove nonpolar impurities and dried under high vacuum. It is sufficiently pure for conversion to Compound **5.6**.

The reported purification method was attempted in this reaction. The pressed-dry yellow solid was dissolved in acetone, decanted from the red polysulfides (not observed), and precipitated with diethyl ether. At this scale (theoretical yield of 520 g), it was estimated that more than 10 L of acetone and a greater volume of ether would be required to fully dissolve and precipitate the xanthate. The extended workup time to realize this resulted in significant oxidation to the dixanthogen and decomposition to other odorous by-products. The final product was collected by filtration as a light-yellow, fluffy solid. Yield: 122 g (23 %)

Note: This reaction requires mechanical stirring as the only solvent is a slight excess of carbon disulfide. Warning: Stench! This reaction and its by-products have a powerful

stench. Work inside a well-ventilated fume hood. Waste Notice: In the United States, carbon disulfide is a P-listed chemical. Special precautions must be taken to separate it and contaminated waste from the typical hazardous waste stream.

5.6.14 *Methyl 2,2-bis((isopropoxycarbonothioyl)thio)acetate (5.6)*

Compound **5.6** was prepared according to a literature procedure with a modification in the purification step.[302] Without any measure to exclude atmosphere, Compound **5.5** (10.0 g, 57.4 mmol, 2.2 equiv.) was suspended in acetone (200 mL) in a 500-mL Erlenmeyer flask with a magnetic stir bar. Methyl 2,2-dichloroacetate (2.7 mL, 26.1 mmol, 1.0 equiv.) was added dropwise. A precipitate of KCl formed immediately. The reaction was warmed (~ 35 °C) to complete the reaction. The reaction was cooled to r.t. after 4 hours and filtered to remove KCl. The filtrate was concentrated to an oil. Hexanes were added to dissolve the desired product and precipitate remaining polar impurities. The solution was filtered again before concentration to a clear yellow-orange oil. Treating 5.6 with silica gel and passing over a short plug aids in the removal of salt impurities. Yield: 7.17 g (80.2 %).

^{1}H NMR (300 MHz, $CDCl_3$) δ 6.01 (s, 1H), 5.71 (hept, J = 6.2 Hz, 2H), 3.80 (s, 3H), 1.39 (dd, J = 6.2, 4.5 Hz, 12H). $^{13}C\{^{1}H\}$ NMR (75 MHz, $CDCl_3$) δ 209.10, 167.04, 79.65, 56.71, 53.93, 21.33.

5.6.15 *1,2,4,6-Tetrathiapentalene-2,5-dione (thiapendione) (5.7)*

Compound **5.7** was prepared according to the literature.[273] In a 1-L Erlenmeyer flask with stir bar, concentrated sulfuric acid (320 mL) was cooled to 0 °C. Diethyl ether

(30 mL) was added slowly. Compound **5.6** (32.9 g, 96.1 mmol) was added slowly, such that the temperature of the reaction was never above 5 °C. After the complete addition of **5.6**, the reaction was allowed to stir as it came to 20 °C. The reaction was poured over crushed ice (~1 L) (Caution: Extremely exothermic). A tacky, white, odorous solid precipitated from solution and was collected by filtration. The solid was washed thoroughly with water, then triturated in cold water to remove traces of acid. Crude Yield: 12.9 g (65 %).

$^{13}C\{^{1}H\}$ NMR (75 MHz, DMSO-d6) δ 191.82, 112.52. EA: Anal. Calcd for $C_4S_4O_2$ (%): C, 23.07; S, 61.57. Found (%): C, 23.04; S, 61.78.

Compound **5.7** was recrystallized twice prior to use sequentially from chloroform then acetonitrile. A tacky, yellow, insoluble impurity remained in both recrystallization that was removed by decanting. This significantly decreases the final pure yield.

Note: This reaction was repeated using 116 g of **5.6** in 1 L of sulfuric acid. The major product was the tacky, yellow, insoluble impurity. Less than 5 grams of chloroform soluble material were recovered. The impurity firmly attached itself to glassware, stainless steel utensils, frits, and porcelain funnels. Warm sulfuric acid was the only suitable cleaning agent, with laboratory-grade soaps, common solvents, and ethanolic KOH failing to remove it. Warning: Stench! Reaction and by-products have strong sulfurous odors. Work exclusively in a fume hood.

5.6.16 *NiETT Synthetic Procedures*

5.6.16.1 Na_0[Ni(1.0)ETT] – Batch 1 – (5.034A)

Synthesized following the general reaction procedure above with the amounts:

Thiapendione (500 mg, 2.4 mmol, 1.0 equiv.) in MeOH (15 mL);

NaOMe (648 mg, 12 mmol, 5.0 equiv.) in MeOH (15 mL);

Anhydrous Ni(II)OAc_2 (424 mg, 2.4 mmol, 1.0 equiv.) in MeOH (20 mL);

Glacial acetic acid (1 mL in 10 mL MeOH);

Iodine (609 mg, 2.4 mmol, 2.0 equiv. of oxidant) in MeOH (10 mL).

Yield: 420 mg

5.6.16.2 Na_0[Ni(1.0)ETT] – Batch 2 (5.039)

Synthesized following the general reaction procedure above with the amounts:

Thiapendione (2000 mg, 9.6 mmol, 1.0 equiv.) in MeOH (60 mL);

NaOMe (2592 mg, 48 mmol, 5.0 equiv.) in MeOH (60 mL);

Anhydrous Ni(II)OAc_2 (1696 mg, 9.6 mmol, 1.0 equiv.) in MeOH (40 mL);

Glacial acetic acid (4 mL in 40 mL MeOH);

Iodine (2436 mg, 9.6 mmol, 2.0 equiv. of oxidant) in MeOH (40 mL).

Yield: 1617 mg

5.6.16.3 K_0[Ni(1.0)ETT] (5.049)

Synthesized following the general reaction procedure above with the amounts:

Thiapendione (1000 mg, 4.8 mmol, 1.0 equiv.) in MeOH (30 mL);

KOMe (1682 mg, 24 mmol, 5.0 equiv.) in MeOH (30 mL);

Anhydrous Ni(II)OAc_2 (848 mg, 4.8 mmol, 1.0 equiv.) in MeOH (20 mL);

Glacial acetic acid (2 mL in 20 mL MeOH);

Iodine (1218 mg, 4.8 mmol, 2.0 equiv. of oxidant) in MeOH (20 mL).

Yield: 999 mg

5.6.16.4 Li_0[Ni(1.0)ETT] (5.048)

Synthesized following the general reaction procedure above with the amounts:

Thiapendione (1000 mg, 4.8 mmol, 1.0 equiv.) in MeOH (30 mL);

LiOMe (24 mL of 1.0M in MeOH solution, 24 mmol, 5.0 equiv.);

Anhydrous Ni(II)OAc_2 (848 mg, 4.8 mmol, 1.0 equiv.) in MeOH (20 mL);

Glacial acetic acid (2 mL in 20 mL MeOH);

Iodine (1218 mg, 4.8 mmol, 2.0 equiv. of oxidant) in MeOH (20 mL).

Yield: 946 mg

5.6.16.5 Na_0[Ni(0.5)ETT] (5.059)

Synthesized following the general reaction procedure above with the amounts:

Thiapendione (500 mg, 2.4 mmol, 1.0 equiv.) in MeOH (15 mL);

NaOMe (648 mg, 12 mmol, 5.0 equiv.) in MeOH (15 mL);

Anhydrous Ni(II)OAc_2 (212 mg, 1.2 mmol, 0.5 equiv.) in MeOH (10 mL);

Glacial acetic acid (1 mL in 10 mL MeOH);

Iodine (609 mg, 2.4 mmol, 2.0 equiv. of oxidant) in MeOH (10 mL).

Yield: 307 mg

5.6.16.6 Na_0[Ni(0.75)ETT] (5.047, 5.047.B)

Synthesized following the general reaction procedure above with the amounts:

Thiapendione (2000 mg, 9.6 mmol, 1.0 equiv.) in MeOH (60 mL);

NaOMe (2592 mg, 48 mmol, 5.0 equiv.) in MeOH (60 mL);

Anhydrous Ni(II)OAc_2 (1272 mg, 7.2 mmol, 0.75 equiv.) in MeOH (20 mL);

Glacial acetic acid (4 mL in 40 mL MeOH);

Iodine (2436 mg, 9.6 mmol, 2.0 equiv. of oxidant) in MeOH (40 mL).

Yield: 1628 mg (total); 1478 mg (black powder); 150 mg (blue-grey lustrous material)

Blue-grey lustrous material used for thermoelectric measurements

5.6.16.7 Na_0[Ni(2.0)ETT] (5.046)

Synthesized following the general reaction procedure above with the amounts:

Thiapendione (2000 mg, 9.6 mmol, 1.0 equiv.) in MeOH (60 mL);

NaOMe (2592 mg, 48 mmol, 5.0 equiv.) in MeOH (60 mL);

Anhydrous Ni(II)OAc_2 (3392 mg, 19.2 mmol, 2.0 equiv.) in MeOH (20 mL);

Glacial acetic acid (4 mL in 40 mL MeOH);

Iodine (2436 mg, 9.6 mmol, 2.0 equiv. of oxidant) in MeOH (40 mL).

Yield: 1946 mg

5.6.16.8 Na_0[Ni(3.0)ETT] (5.060)

Synthesized following the general reaction procedure above with the amounts:

Thiapendione (500 mg, 2.4 mmol, 1.0 equiv.) in MeOH (15 mL);

NaOMe (648 mg, 12 mmol, 5.0 equiv.) in MeOH (15 mL);

Anhydrous Ni(II)OAc_2 (1273 mg, 7.2 mmol, 3.0 equiv.) in MeOH (20 mL);

Glacial acetic acid (1 mL in 10 mL MeOH);

Iodine (609 mg, 2.4 mmol, 2.0 equiv. of oxidant) in MeOH (10 mL).

Yield: 381 mg

5.6.16.9 Na_2[Ni(1.0)ETT] (5.056)

Synthesized following the general reaction procedure above with the amounts:

Thiapendione (500 mg, 2.4 mmol, 1.0 equiv.) in MeOH (15 mL);

NaOMe (648 mg, 12 mmol, 5.0 equiv.) in MeOH (15 mL);

Anhydrous Ni(II)OAc_2 (424 mg, 2.4 mmol, 1.0 equiv.) in MeOH (10 mL);

Glacial acetic acid (1 mL in 10 mL MeOH);

Iodine (0 mg, 0 mmol, 0 equiv.).

Yield: 539 mg

5.6.16.10 $Na_{1.5}$[Ni(1.0)ETT] (5.057)

Synthesized following the general reaction procedure above with the amounts:

Thiapendione (500 mg, 2.4 mmol, 1.0 equiv.) in MeOH (15 mL);

NaOMe (648 mg, 12 mmol, 5.0 equiv.) in MeOH (15 mL);

Anhydrous Ni(II)OAc_2 (424 mg, 2.4 mmol, 1.0 equiv.) in MeOH (10 mL);

Glacial acetic acid (1 mL in 10 mL MeOH);

Iodine (153 mg, 0.6 mmol, 0.5 equiv. of oxidant) in MeOH (5 mL).

Yield: 493 mg

5.6.16.11 $Na_{(-2)}$[Ni(1.0)ETT] (5.058)

Synthesized following the general reaction procedure above with the amounts:

Thiapendione (500 mg, 2.4 mmol, 1.0 equiv.) in MeOH (15 mL);

NaOMe (648 mg, 12 mmol, 5.0 equiv.) in MeOH (15 mL);

Anhydrous Ni(II)OAc_2 (424 mg, 2.4 mmol, 1.0 equiv.) in MeOH (10 mL);

Glacial acetic acid (1 mL in 10 mL MeOH);

Iodine (1218 mg, 4.8 mmol, 4.0 equiv. of oxidant) in MeOH (20 mL).

Yield: 385 mg

5.6.16.12 5.037-A, B, C

Synthesized following the general reaction procedure above, with the exception that no attempt at drying or degassing ACS grade methanol was made, with the amounts:

Thiapendione (208 mg, 1.0 mmol, 1.0 equiv.) in MeOH (10 mL);

A: NaOH (200 mg, 5.0 mmol, 5.0 equiv.) in MeOH (10 mL); or

B: Na_2CO_3 (530 mg, 5.0 mmol, 5.0 equiv.) in MeOH (10 mL); or

C: NaOMe (270 mg, 5.0 mmol, 5.0 equiv.) in MeOH (10 mL);

Anhydrous Ni(II)OAc_2 (mg, 1.0 mmol, 1.0 equiv.) in MeOH (10 mL);

Glacial acetic acid (0.5 mL in 5 mL MeOH);

Iodine (254 mg, 1.0 mmol, 2.0 equiv. of oxidant) in MeOH (5 mL).

Yield: A: 177 mg; B: 115 mg; C: 187 mg

5.6.16.13 5.033.A,B

Synthesized following the general reaction procedure above, with the exception that the Ni(II) solution was added at the 1 hour reaction mark at a rate such that it was added over 20 hours, with the amounts:

Thiapendione (500 mg, 2.4 mmol, 1.0 equiv.) in MeOH (15 mL);

A: NaOMe (648 mg, 12 mmol, 5.0 equiv.) in MeOH (15 mL); or

B: NaOMe (1296 mg, 24 mmol, 10 equiv.) in MeOH (15 mL)

Anhydrous Ni(II)OAc_2 (424 mg, 2.4 mmol, 1.0 equiv.) in MeOH (20 mL);

Glacial acetic acid (1 mL in 10 mL MeOH);

Iodine (609 mg, 2.4 mmol, 2.0 equiv. of oxidant) in MeOH (10 mL).

Yield: A: 432 mg; B: 512 mg

5.6.16.14 5.034B

Synthesized following the general reaction procedure above with the amounts:

Thiapendione (500 mg, 2.4 mmol, 1.0 equiv.) in MeOH (15 mL);

NaOMe (1296 mg, 24 mmol, 10 equiv.) in MeOH (15 mL);

Anhydrous Ni(II)OAc_2 (424 mg, 2.4 mmol, 1.0 equiv.) in MeOH (20 mL);

Glacial acetic acid (1 mL in 10 mL MeOH);

Iodine (609 mg, 2.4 mmol, 2.0 equiv. of oxidant) in MeOH (10 mL).

Yield: 443 mg

5.6.16.15 5.008

Synthesized following the general reaction procedure above, with the exception of the oil bath at 70 °C instead of 60 °C, with the amounts:

Thiapendione (1000 mg, 4.8 mmol, 1.0 equiv.) in MeOH (30 mL);

NaOMe (1296 mg, 24 mmol, 5.0 equiv.) in MeOH (30 mL);

Anhydrous Ni(II)$OAc_2 \cdot 4H_2O$ (1190 mg, 4.8 mmol, 1.0 equiv.) in MeOH (20 mL);

Glacial acetic acid (2 mL in 20 mL MeOH);

Iodine (1218 mg, 4.8 mmol, 2.0 equiv. of oxidant) in MeOH (20 mL).

Yield: ~1000 mg

5.6.16.16 5.069

Synthesized following the general reaction procedure above, with the exception of the oil bath at 70 °C instead of 60 °C, with the amounts:

Thiapendione (500 mg, 2.4 mmol, 1.0 equiv.) in MeOH (15 mL);

NaOMe (648 mg, 12 mmol, 5.0 equiv.) in MeOH (15 mL);

Anhydrous Ni(II)OAc_2 (424 mg, 2.4 mmol, 1.0 equiv.) in MeOH (20 mL);

Glacial acetic acid (1 mL in 10 mL MeOH);

Iodine (609 mg, 2.4 mmol, 2.0 equiv. of oxidant) in MeOH (10 mL).

Yield: 364 mg

5.6.16.17 5.073

Synthesized following the general reaction procedure above, with the exception of the oil bath at 70 °C instead of 60 °C, with the amounts:

Thiapendione (250 mg, 1.2 mmol, 1.0 equiv.) in MeOH (10 mL);

NaOMe (324 mg, 6.0 mmol, 5.0 equiv.) in MeOH (10 mL);

Anhydrous Ni(II)Cl_2 (155.5 mg, 1.2 mmol, 1.0 equiv.) as a slurry in MeOH (10 mL);

Glacial acetic acid (0.5 mL in 5 mL MeOH);

Iodine (305 mg, 1.2 mmol, 2.0 equiv. of oxidant) in MeOH (5 mL).

Yield: 174 mg

5.6.16.18 5.072 – 2 gram synthesis

Na_0[Ni(1.0)(ETT)]

Synthesized following the general reaction procedure above, with the exception of the oil bath at 80 °C instead of 60 °C, with the amounts:

Thiapendione (2500 mg, 12.0 mmol, 1.0 equiv.) in MeOH (90 mL);

NaOMe (3240 mg, 60 mmol, 5.0 equiv.) in MeOH (60 mL);

Anhydrous Ni(II)OAc_2 (2120 mg, 12.0 mmol, 1.0 equiv.) in MeOH (50 mL);

Glacial acetic acid (5 mL in 50 mL MeOH);

Iodine (3045 mg, 12.0 mmol, 2.0 equiv. of oxidant) in MeOH (50 mL).

Yield: 1.807 g of a steel blue solid

5.6.16.19 5.077 – 5 gram synthesis

Na_0[Ni(1.0)(ETT)]

Synthesized following the general reaction procedure above, with the exception of the oil bath at 80 °C instead of 60 °C, with the amounts:

Thiapendione (5000 mg, 24.0 mmol, 1.0 equiv.) in MeOH (200 mL);

NaOMe (6480 mg, 120 mmol, 5.0 equiv.) in MeOH (150 mL);

Anhydrous Ni(II)OAc_2 (4240 mg, 24.0 mmol, 1.0 equiv.) in MeOH (100 mL);

Glacial acetic acid (10 mL in 100 mL MeOH);

Iodine (6090 mg, 24.0 mmol, 2.0 equiv. of oxidant) in MeOH (100 mL).

Yield: Not Taken (Two portions of the slurry were removed from the filtration setup. One was kept suspended in acetone. One was kept suspended in a minimal amount of DMSO.)

5.6.16.20 5.079 – 15 gram synthesis

Na_0[Ni(1.0)(ETT)]

In a cool, dry 3000 mL round bottom flask with mechanical stirrer and condenser was added thiapendione (15000 mg, 72.0 mmol, 1.0 equiv.) and anhydrous MeOH (~600 mL, stored over activated 3Å molecular sieves, degassed by sparging) was added by canula. The reaction was heated to reflux; the thiapendione did not fully dissolve. In a separate flask, NaOMe (19.44 g, 360 mmol, 5.0 equiv.) was dissolved in MeOH (600 mL). The fully dissolved NaOMe solution was added to the TPD by canula. The reaction immediately turns a light-yellow color that becomes more pronounced over time. The reaction vessel heated using a heating mantle to maintain an active reflux ring and stirred for 24 hours. Separately, anhydrous Ni(II)OAc_2 (12.72 g, 72.0 mmol, 1.0 equiv.) was dissolved in anhydrous MeOH (300 mL). At the 24 hour reaction mark, the addition of the nickel(II) solution was commenced by cannula such that the solution is added over 15 minutes. The reaction viscosity increases significantly with some gelling along the sides of the flask. The reaction was stirred for an additional 24 hours, to give a total active reaction time of 48 hours. Acetic acid (30 mL in 300 mL MeOH) was added rapidly by syringe. The reaction vessel was stirred aggressively to homogenize the contents. Iodine (18.27 g, 72 mmol, 2.0 equiv. of oxidant) in MeOH (300 mL) was added by cannula. The reaction was allowed to stir for 12 hours at 60 °C, at which point the iodine color had faded from the solution and the reaction mixture settled without stirring.

The solids were collected and washed in ~20 50mL-centrifuge tubes. All supernatants were collected on a 0.45 μm nylon filter. The product was washed with methanol, 1:1 MeOH:H_2O, methanol, and ether. The contents of each centrifuge tube were transferred to the nylon filter using a minimal amount of ether. The material was allowed to dry on the filter before being dried under high vacuum, crush in a mortar and pestle, and dried again under high vacuum

Yield: 11.410 g of a steel blue solid

5.6.16.21 4.096

Na_0[Ni(0.5)ETT]

A 100 mL 2-neck round bottom flask fitted with a condenser was charged with thiapendione (1.0 g, 4.8 mmol, 1.0 equiv.) and NaOMe (1.296g, 24 mmol , 5.0 equiv.). Anhydrous MeOH (50 mL, ~0.1M) was added via syringe. The reaction was heated at reflux for 24 hours. Ni(II)OAc_2•$4H_2O$ (0.597 g, 2.4 mmol, 0.5 equiv.) was dissolved in anhydrous MeOH (20 mL) before rapid addition to the reaction via syringe. The reaction was heated at reflux for an additional 24 hours. I_2 (0.609 g, 2.4 mmol, 2.0 equiv. oxidant) was dissolved in anhydrous MeOH (20 mL) before rapid addition to the reaction via syringe. Precipitation was observed immediately. The reaction was heated at reflux for an additional 24 hours, then poured into 100 mL of ACS grade methanol. The precipitate was collected on a 0.45 µm nylon filter. The precipitate was washed sequentially with ~75 mL portions of methanol, water, methanol, and diethyl ether before drying completely. The resultant reflective blue solid was dried under high vacuum overnight.

Yield: 590 mg

5.6.16.22 4.097

$Na_{(-1)}$[Ni(0.5)ETT]

A 100 mL 2-neck round bottom flask fitted with a condenser was charged with thiapendione (1.0 g, 4.8 mmol, 1.0 equiv.) and NaOMe (1.296g, 24 mmol , 5.0 equiv.). Anhydrous MeOH (50 mL, ~0.1M) was added via syringe. The reaction was heated at reflux for 24 hours. Ni(II)OAc_2•$4H_2O$ (0.597 g, 2.4 mmol, 0.5 equiv.) was dissolved in

anhydrous MeOH (20 mL) before rapid addition to the reaction via syringe. The reaction was heated at reflux for an additional 24 hours. I_2 (1.218 g, 4.8 mmol, 4.0 equiv. oxidant) was dissolved in anhydrous MeOH (20 mL) before rapid addition to the reaction via syringe. Precipitation was observed immediately. The reaction was heated at reflux for an additional 24 hours, then poured into 100 mL of ACS grade methanol. The precipitate was collected on a paper filter (VWR qualitative grade 415, 25 μm particle retention). Traces of precipitate passed through the filter initially, indicating that the effective particle retention was much smaller after exposure to the precipitate solution. The precipitate was washed sequentially with ~75 mL portions of methanol, water, methanol, and diethyl ether before drying completely. The resultant reflective blue solid was dried under high vacuum overnight.

Yield: 660 mg

5.6.16.23 4.098

Na_x[Ni(0.5)ETT]

A 100 mL 2-neck round bottom flask fitted with a condenser was charged with thiapendione (1.0 g, 4.8 mmol, 1.0 equiv.) and NaOMe (1.296g, 24 mmol , 5.0 equiv.). Anhydrous MeOH (50 mL, ~0.1M) was added via syringe. The reaction was heated at reflux for 24 hours. Ni(II)OAc_2•$4H_2O$ (0.597 g, 2.4 mmol, 0.5 equiv.) was dissolved in anhydrous MeOH (20 mL) before rapid addition to the reaction via syringe. The reaction was heated at reflux for an additional 24 hours. The reaction was removed from heat and exposed to atmosphere while stirring through two 14/20 openings for 30 minutes before being poured into 100 mL of ACS grade MeOH. No precipitate was collected when filtered

through a paper filter (VWR Grade 415, 25 µm particle retention) or a 0.45 µm nylon filter. Air, via exhaust of a clean PTFE diaphragm pump, was bubbled into the solution through a 21-gauge needle at an unmeasured rate (~ 5 bubbles/second) for 30 minutes. Thickening of the mixture and precipitation were observed. The precipitate was collected on a 0.45 um nylon filter. The precipitate was washed sequentially with ~75 mL portions of methanol, water, methanol, and diethyl ether before drying completely. The resultant reflective blue solid was dried under high vacuum overnight.

Yield: 410 mg

5.6.17 *Elemental Analyses for NiETTs*

Table 5.10 – Elemental analyses of NiETT materials

	4.096	**4.097**	**4.098**	**5.008**	**5.034.A**
C	13.0	10.8	11.0	12.1	14.3
H	1.0	0.8	0.7	1.4	1.0
S	51.3	60.9	55.4	48.5	55.3
Na	1.80	2.00	2.70	2.80	1.00
Ni	13.90	17.90	22.40	22.30	19.50
	5.039	**5.046**	**5.047 (B)**	**5.048**	**5.049**
C	16.4	14.1	13.1 (12.8)	14.5	13.9
H	0.9	1.5	0.9 (0.9)	1.2	1.3
S	56.6	47.1	56.7 (56.7)	49.4	47.5
Na	0.83	0.34	1.26 (1.35)	0.29 (Li)	0.94 (K)
Ni	21.71	25.06	21.07 (21.82)	22.11	24.80
	5.056	**5.057**	**5.058**	**5.059**	**5.060**
C	10.5	10.2	14.0	15.7	15.6
H	1.4	1.1	1.0	1.1	1.2
S	45.1	50.7	56.9	59.48	54.5
Na	3.56	1.53	0.59	1.05	0.08
Ni	23.36	24.08	23.05	18.35	19.54

5.6.18 *NiETT:PVDF Thermoelectric Data*

Table 5.11 – Thermoelectric performance data for select NiETT:PVDF composites not reported elsewhere. [a]Annealed

ETT Sample	σ (S/cm)	S (μV/K)	PF (μW/m-K^2)
4.096	114 ± 2	-39 ± 2	23.0
4.097	145 ± 3	-34.5 ± 0.5	20.7
4.098	122 ± 2	-39 ± 2	22.4
5.072[a]	9.1 ± 0.1	-112 ± 5	10.5

5.7 Vibrational Spectroscopy Techniques

5.7.1 *Infrared-Red Vibrational Spectroscopy*

Infrared spectroscopy was attempted on Na_0[Ni(1.0)ETT] using an attenuated total reflectance attachment. The absorption was broad across the entire spectrum, typical of absorptions free charge carriers in conductive materials. IR spectroscopy was not pursued further.

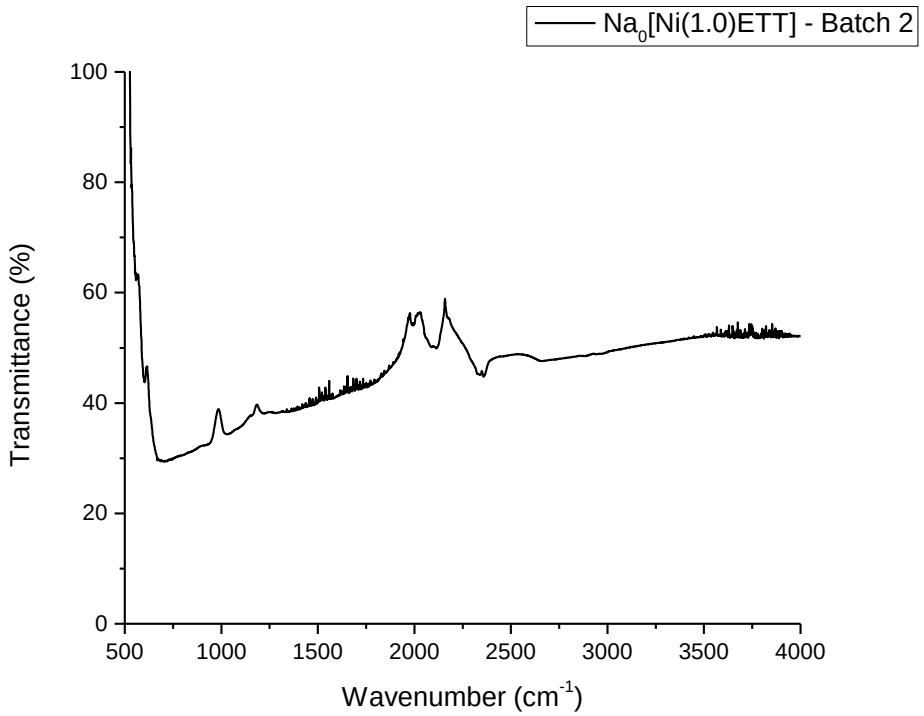

Figure 5.32 – IR Transmittance Spectrum of Na_0[Ni(1.0)ETT] - Batch 2 taken with an ATR equipped FT-IR

5.7.2 *Raman Vibrational Spectroscopy*

In contrast to IR spectroscopy as a transmission-absorption measurement, Raman spectroscopy is a scattering technique. One Na[NiETT] (5.039), Figure 5.33, and one Na[NiTTO] (5.004), Figure 5.34, sample were analysed to investigate potential differences detectable by Raman spectroscopy. Raman spectroscopy yields interesting information, but a full interpretation of these data has not been completed. The experiment requires additional optimization to avoid destruction of the sample due to overheating. The Raman spectrum of Na[NiETT] shows peaks at 840, 1216, 1250, and 1448 cm^{-1}, which could be attributable to C=C and C-S modes. The peaks at 361, 481, and 492 cm^{-1}, which are characteristic of Ni-S and C-S modes. These three signals also show up in Na[NiTTO] with

different intensities between 481 and 492 cm^{-1}. This may be a future method to determine the amount of ETT versus TTO character in nickel coordination polymers.

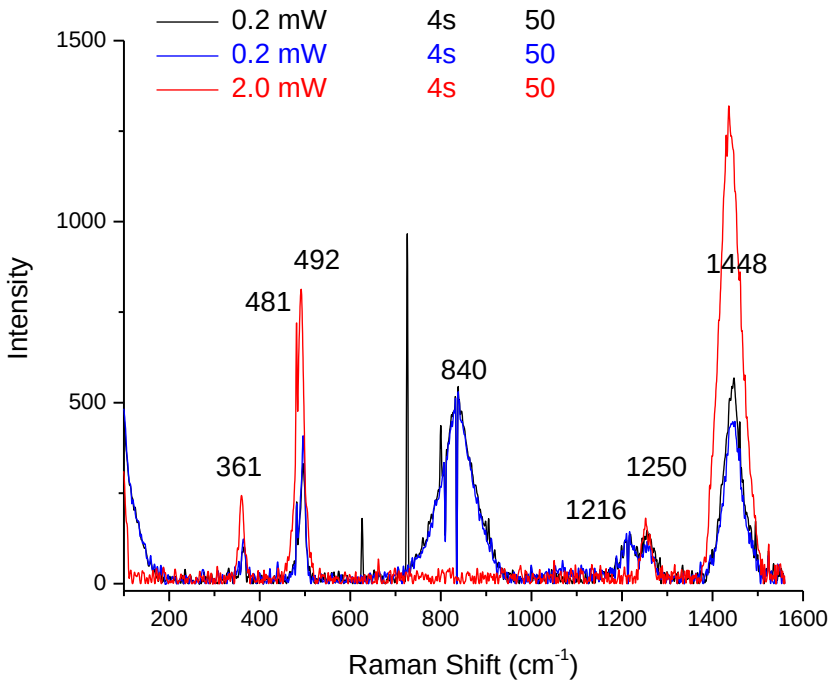

Figure 5.33 – Raman spectra of Na[NiETT] (5.039) at 0.2 mW and 2.0 mW laser power with four second integration times and 50 co-additions

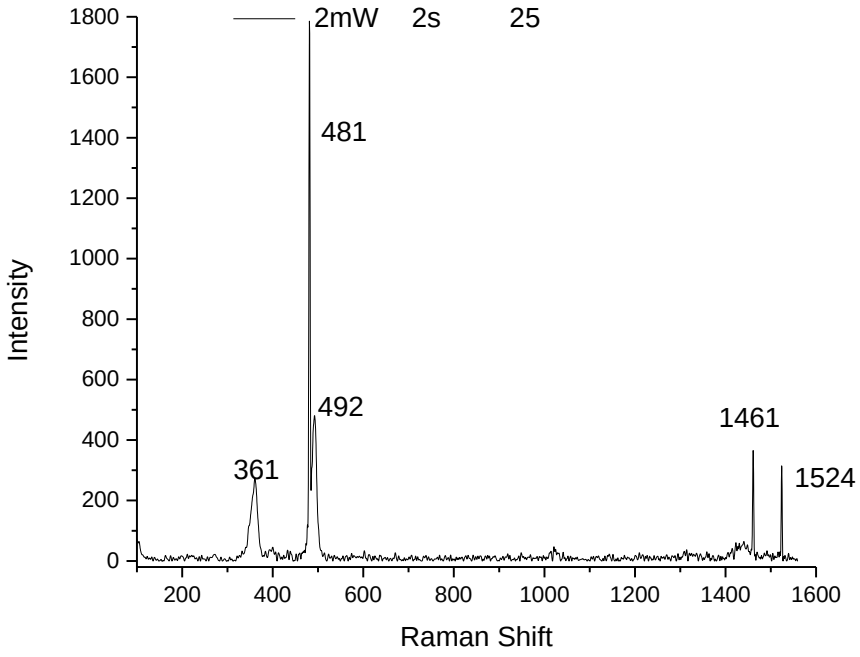

Figure 5.34 – Raman spectrum of Na[NiTTO] (5.004) at 2.0 mW laser power with two second integration time and 25 co-additions

CHAPTER 6. EFFECTS OF ANNEALING ON POWDERS AND FILMS OF SODIUM POLY(NICKEL ETHENETETRATHIOLATE)

6.1 Introduction

Annealing of NiETT films proved a reliable method of performance enhancement. chapter is the exploration of decomposition products of NiETT as an explanation into the performance enhancement after annealing. As a benefit, this study identifies safe maximum processing and operating temperatures for other applications, such as textiles, melt-processing, 3-D printing, etc.

The low solubility of NiETTs makes a thorough analysis through solution-based techniques difficult. Destructive techniques can still be applied, and thermogravimetric analysis (TGA) offers insights into the material through its decomposition rate, temperature, and residual mass. Previously with NiETTs, TGA was used to illustrate water loss from the material.[276] Coupling the off-gas stream to another analysis method increases the amount of information obtained from an experiment. Due to its sensitivity and specificity, combined thermogravimetric analysis with mass spectroscopy (TGA-MS) was utilized to analyze NiETT powders and films during and after the thermal annealing process.

Figure 6.1a depicts the idealized repeat structure of NiETT, and Figure 6.1b depicts a NiETT structure with many, but certainly not all, possible deviations from the ideal structure. Unknowns about the material include (1) presence and structure of end groups,

(2) the presence or extent of cross-linking, (3) the true amount and type of counter ion and, related, the true change on the backbone, (4) impurity presence, identity, and amount, (5) any modifications to the backbone that deviate from the ideal structure, and (6) water or oxygen coordination to nickel in the backbone.[264,321,322]

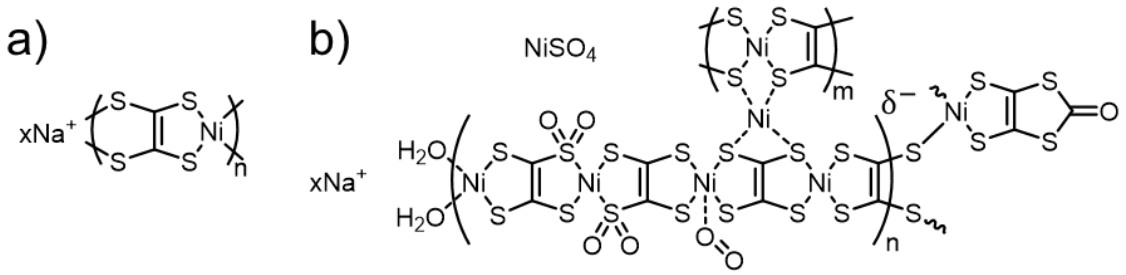

Figure 6.1 – a) Idealized repeat structure of Na[NiETT]. b) Repeat structure of Na[NiETT] with possible deviations from the ideal structure

We and others have attempted to use other characterization techniques, such as XPS and EA to make inferences about these materials. However, interpretation of XPS is often not agreed upon or done rigorously; and elemental analysis supplies limited information about the macroscopic composition of the material. With the enhancements in performance through film annealing, we employed TGA-MS to study Na[NiETT]s behavior at elevated temperatures.

6.2 Annealing Parameter Selection and Performance Enhancements

Optimizing the annealing parameters for the highest, yet still consistent, increase in thermoelectric performance was the priority. A stepwise annealing study was devised, Figure 6.2. To drive off the DMSO, NiETT:PVDF films are dried at 50 °C under vacuum. Therefore, the temperature of the annealing study was begun at 80 °C and increased in 20 °C increments. A consistent performance increase at each increment was observed up to 160 °C. The conductivity increases from 6 ± 2 S/cm for an as-cast film (control) to 23 ± 3

S/cm (160 ^{0}C); this is accompanied by an increase in the Seebeck coefficient from -28 ± 3 μV/K (control) to -74 ± 4 μV/K (160 °C), to yield a power factor over 10 μW/m-K^2 for this n-type composite film. At higher temperatures, the films developed cracks and often delaminated. The melt temperature of PVDF used in this study is 169 °C, which is coincident, and perhaps causal, to these problems. Near and above this temperature, phase separation between NiETT and PVDF is observed. 160 °C was instituted as the standard annealing temperature for all future films and TGA procedures.

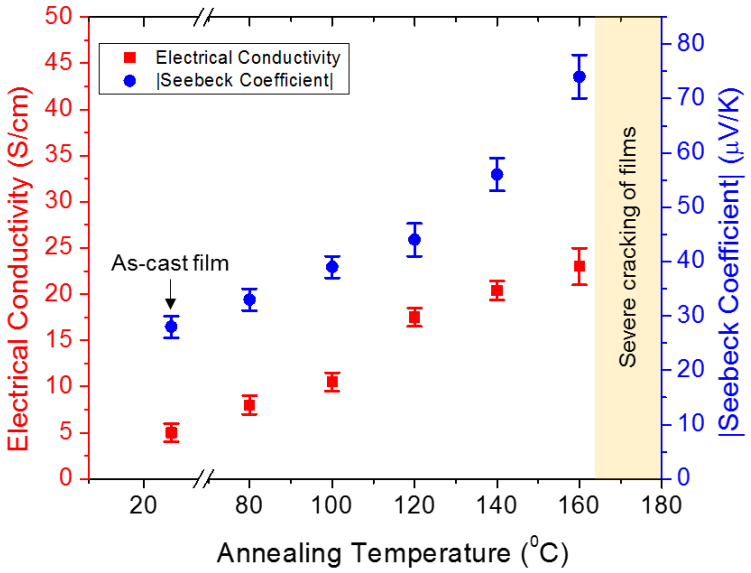

Figure 6.2 – Electrical conductivity (red, left) and Seebeck coefficient (magnitude) of NiETT/PVDF composite films when annealed in air for one hour at the indicated temperature

While previous experiments have indicated long-term atmospheric stability of these materials,[301,323] exposure to atmosphere at elevated temperatures had not been evaluated thoroughly. To ensure the exposure to atmosphere was not causing a detrimental effect, or even responsible for the performance increase, composite films were also annealed at 160 ^{0}C under vacuum and under nitrogen. The resulting thermoelectric properties are identical. No component of atmosphere is responsible for the performance increases, and no

malicious or beneficial degradation occurs. We infer that no chain degradation or oxidation is occurring, as that would manifest as a change in conductivity and Seebeck coefficient.

The conductivity improvement from 6 to 23 S/cm can be explained through a simple morphological change facilitated by increased domain connectivity and crack disappearance. Seebeck coefficient, being an inherent material property, would not change due to increased connectivity – an additional process must be occurring in the film or NiETT itself that leads to this increase.

To isolate changes in NiETT powders from morphological changes in NiETT:PVDF composite films upon annealing, the NiETT powder itself was annealed. The results are shown in Figure 6.3. Sample #1 is the as-cast film with NiETT that has not been annealed as control (-28 μV/K). Sample #2 is the as-cast film annealed at 160 °C for one hour. The expected increase in thermopower to -74 μV/K is observed. Sample #3 uses a NiETT powder that was annealed at 160 °C before film processing. In a thin film composite, the thermopower is -45 μV/K. This is a measurable increase from Sample #1, confirming that a chemical change is occurring in the NiETT powder. It does not obtain the full increase as in film-annealing, Sample #2. This could indicate degradation of the NiETT when annealed outside of a PVDF matrix. Sample #3 is then annealed to give Sample #4, the annealed powder cast into a film which is then annealed again. An increase in thermopower to -80 μV/K is observed. This is statistically equivalent to Sample #2, the annealed film, suggesting that no degradation of the NiETT occurs during annealing and both a chemical change in the NiETT and a morphological change in the film are responsible for the increase in thermopower.

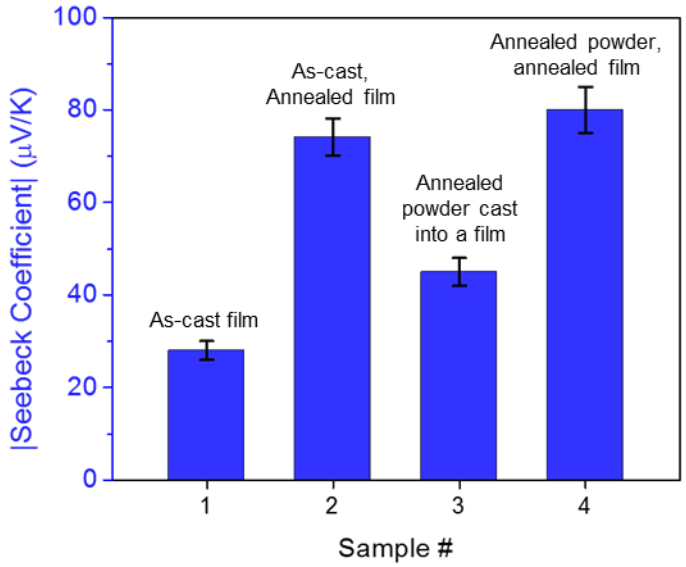

Figure 6.3 – Seebeck coefficient (magnitude) of NiETT/PVDF composite films can be tuned by annealing the pristine powder as well as the film. All samples are annealed in air for one hour on a hot-plate

Scanning electron microscopy, Figure 6.4, confirms that annealing just below the melting temperature of PVDF allows NiETT to reorganize into better connected domains. Similar observations have been made with carbon nanotubes in an inert matrix, where the filler reorganizes into more conducting pathways upon annealing.[324,325] This morphological effect is reflected in a higher conductivity for annealed NiETT:PVDF films compared to as-cast films. However, an increase in the thermopower is also observed which cannot be explained by reorganized conducting pathways alone; this suggests that another mechanism is present during the annealing process. We hypothesize that annealing results in the removal of volatile impurities in addition to the observed morphological effects.

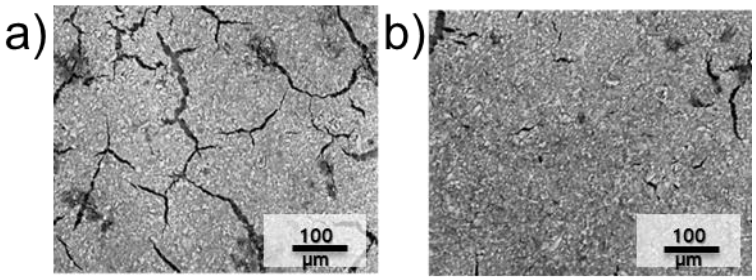

Figure 6.4 – SEM images of NiETT/PVDF composite films (a) before annealing and (b) after annealing for one hour in air at 160 ºC

Elemental analysis was used to confirm the NiETT were not undergoing degradation during the annealing process. Table 6.1 shows the elemental composition of the pristine powder and the annealed powder (after 160 °C in air for one hour). The reduced S:Ni and C:Ni ratios (higher loss of sulfur and carbon relative to nickel), the constant S:C ratio (equal loss of sulfur and carbon), and the increased H:O ratio (loss of oxygen without the loss of hydrogen – not water) in the annealed powder compared to the pristine powder support the removal of some material during the annealing process. The minor changes in overall composition suggest that annealing in air does not destroy NiETT.

Table 6.1 – Elemental composition of Pristine Powder and Annealed Powder. [a]Determined by CHNS analysis [b]Determined by ICP-OES analysis [c]Determined by assuming unaccounted mass was oxygen

		Pristine Powder (PP)	Annealed Powder (AP)
Mass Percent (%)	C[a]	14.33	13.98
	Na[b]	1.00	1.03
	Ni[b]	19.50	23.65
	S[a]	55.29	54.75
	H[a]	0.95	0.96
	O[c]	8.93	5.63
Atomic Ratios	S:C	1.45	1.47
	S:Ni	5.19	4.24
	C:Ni	3.59	2.89
	Na:Ni	0.13	0.11
	Ni:Na	7.64	8.99
	H:O	1.69	2.71

6.3 Thermogravimetric Analysis – Mass Spectroscopy Experiment

Initial work on annealing interested us as to how these materials may behave at elevated temperatures. TGA conditions identical to the annealing conditions, albeit in nitrogen, were run to identify potential material changes. The first TGA experiments were run on a Na[NiETT]:PVDF composite (4.097). Results show a 20% mass loss from the composite during the annealing process. As confirmation of an appropriate length of annealing, the mass loss stabilization occurred within the one-hour isothermal hold.

The identity of the off gasses could piece together the picture of the original structure of or impurities present in NiETT. As a stand in for a tandem TGA-MS, which was not available at the time, the same temperature ramp profile was set on the probe on a mass

spectrometry (MS). The ion signals were recorded over time and thus temperature. The MS is not designed for this experiment, and equipment malfunctions prevented this from becoming a truly useful technique. It did provide the basis for future studies and confirmation that some off-gas could be detected and identified

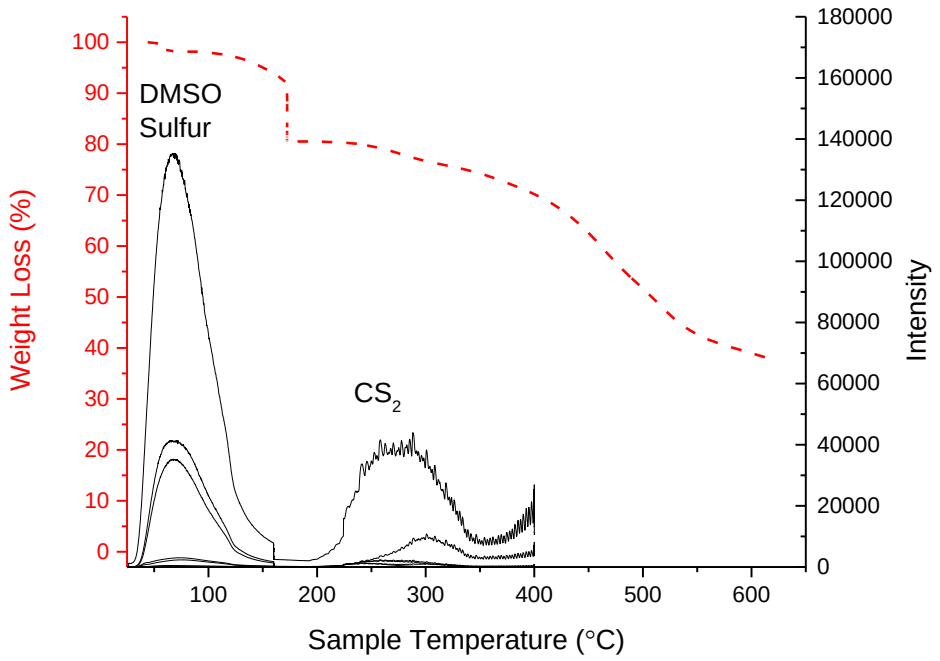

Figure 6.5 – Thermogravimetric analysis of Na[NiETT]:PVDF composite (4.097) including an isothermal hold at 160 °C for one hour (red line). Intensities of ions detected in a separate experiment on the same material. Characteristics ions of DMSO and sulfur were detected before and during annealing. Above the annealing temperature, carbon disulfide was detected

To investigate the thermal annealing and decomposition of NiETT further, we utilized a NETZSCH STA 449F1 Jupiter coupled with a NETZSCH QMS 403 Aeolos mass spectrometer operated by NETZSCH Applications Laboratory Thermoanalytical Section.

The ion currents are quantitative within their own trace, but difficult to understand when considering order of magnitude differences on various graphs. The data was normalized to its highest value to ease comparison. Now, a qualitative comparison could be made between traces, but weak signals were overemphasized. The data was normalized to the average noise (standard deviation) in a subsection of the annealing period during which there were no true signals. All samples were normalized to the same noise during the subsection of the annealing period, so that signal intensity comparisons are relative to each other and their baselines.

The furnace of the TGA-MS was run under argon and begins the experiment at 50 °C following the temperature curve in Figure 6.6. The temperature was increased to 160 °C at 10 °C/min to replicate a fast rise to annealing temperatures while still observing off-gasses during that stage. Due to the ramp rate, the furnace temperature peaks at ~170 °C before returning to 160 °C. The furnace was held at 160 °C for one hour, to replicate the annealing conditions and monitor the length of annealing necessary. The temperature was then ramped again at 10 °C/min to 600 °C to gain any information possible on decomposition products and when they occur.

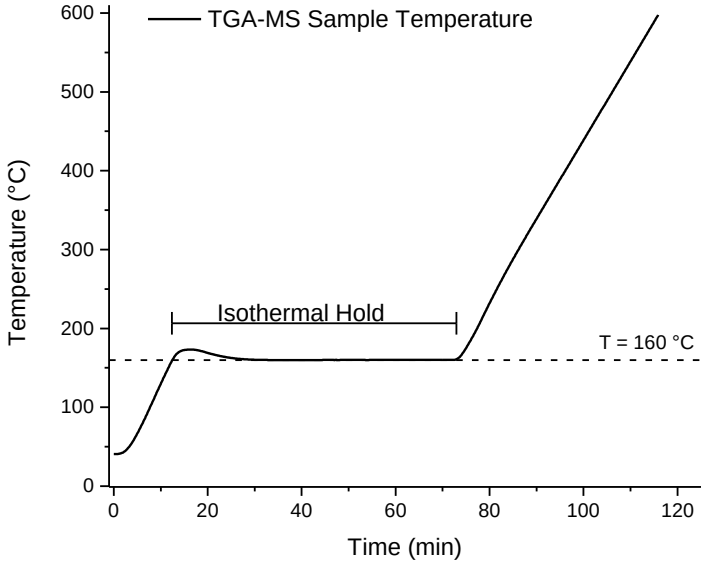

Figure 6.6 – Sample temperature profile in all TGA-MS sample runs. The isothermal hold of one hour begins as the sample reaches 160 °C

Thermogravimetric analysis indicates four mass loss events (Events A-D) occur in the NiETT powder and in the NiETT:PVDF composite films during heating to 600 °C. Event A, mimicking the annealing conditions, occurs upon heating to and holding at the annealing temperature of 160 °C for one hour. Event B begins at ~190 °C and shows a peak mass loss rate at ~235 °C, indicating significant decomposition of the polymer at these temperatures. Event C (peak loss rate at 385 °C) and Event D (peak loss rate at 595 °C in powders, 470 °C in films) are attributed to continued decomposition of NiETT and PVDF. Mass loss Event A is critical to understanding the effect of annealing on NiETT powders and NiETT/PVDF composites.

First, NiETT powder in its original state (Pristine Powder, PP) and NiETT powder after annealing at 160 °C for one hour in air (Annealed Powder, AP) are considered, Figure 6.7. In these samples, the onset of mass loss is as early as 50 °C (the full duration at half-maximum, FDHM, of the differential thermal gravimetry (DTG) curve is used to identify

the temperature range of each event). While this corresponds to the vacuum drying temperature of the films, water is the only signal active at 50 °C. In pristine powders (PP), Event A is a broad, shallow loss that begins at 70 °C and ends during the isothermal hold, and Figure 6.7a shows two species are evolved – water and carbonyl sulfide – contributing to a total mass loss of 5.3%. The presence of water is expected as mass losses up to 7% have been previously attributed to water in NiETTs.[276] However, this is the first reported observation of an impurity or decomposition product such as carbonyl sulfide being removed upon annealing a NiETT polymer. The water evolved is hypothesized to be contact moisture; the heating rate (10 °C/min) prevents differentiation between water removed at or below the boiling point (surface or contact moisture) and water removed above the boiling point (incorporated water). For example, $NiSO_4 \bullet 6H_2O$ shows incorporated water removed at 100 – 220 °C and >300 °C;[326] β-$Ni(OH)_2$ shows surface moisture removed at 80 – 90 °C, and incorporated water removed at 160 °C; and α-$Ni(OH)_2$ shows incorporated water removed at 240 – 300 °C.[327] The second component, carbonyl sulfide, is an unexpected decomposition product when considering the ideal atomic composition $Na_x[Ni(C_2S_4)]_n$ for these polymers, The source of this signal is potentially from unreacted carbonyl end groups or sulfonyl irregularities[322] in the polymer backbone. Previous elemental analyses and XPS data support the presence of such impurities.[323] Even in carefully controlled syntheses, impurities and deviations from the idealized structure are present and should be expected.

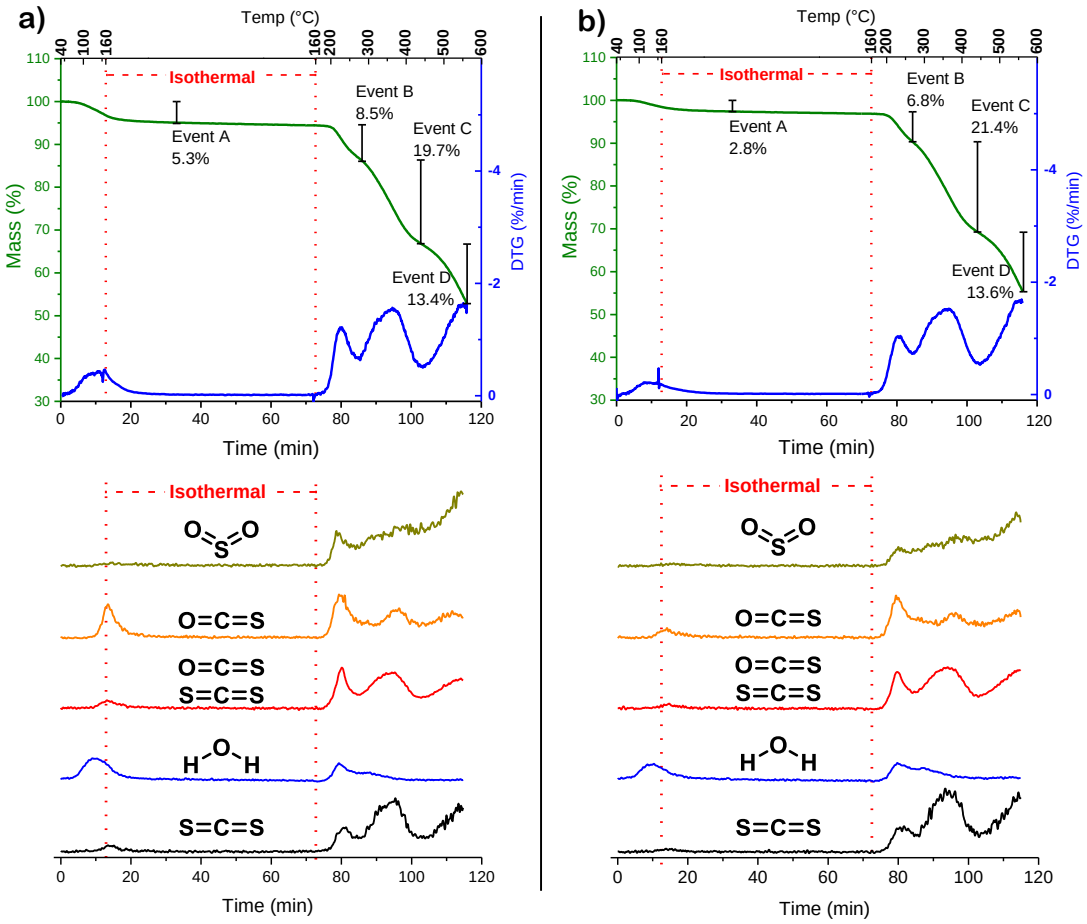

Figure 6.7 – Thermogravimetric analysis with tandem Mass Spectroscopy (TGA-MS) of Pristine Powder (PP) and Annealed Powder (AP) samples of NiETT. (a) TGA with plotted differential (DTG) of PP and normalized ion signals from QMID, (b) TGA with plotted DTG of AP and normalized ion signals from QMID

In annealed powders (AP), Event A consists of 2.8% mass loss during annealing, as shown in Figure 6.7b, and the signal from carbonyl sulfide is significantly reduced compared to PP. Water, specifically contact moisture, is the major contributor to the 2.8% mass loss, along with small amounts of carbonyl sulfide as evidenced from the MS ion traces for AP. Therefore, the mass loss in PP (5.3%) is approximated to be ~2.8% contact moisture and ~2.5% carbonyl sulfide. This highlights the importance of proper reaction and work-up conditions as well as material post-treatment as removing a small amount of

impurity (e.g., carbonyl sulfide) by annealing the NiETT powder increases the thermopower from –28 to –42 μV/K when cast into a film.

Event B (203 – 288 °C FDHM), in both PP and AP, begins the irreversible and destructive decomposition of the NiETT polymer. The onset temperature (180 °C) is recommended as the maximum temperature for any processing method (*e.g.* annealing, printing, extruding) for NiETT. Event B evolves additional water and carbonyl sulfide and begins the release of sulfur dioxide and carbon disulfide. As no combustion is taking place, the water released is expected to originate from incorporated water. The strong signal in Event B from carbonyl sulfide alongside the signals from sulfur dioxide and carbon disulfide indicate that carbonyl sulfide is released as both a beneficial removal of impurities (Event A) and as a destructive decomposition of the NiETT backbone (Event B). The presence of sulfur dioxide provides additional evidence of sulfonyl groups in the backbone, as it is evolved at a lower temperature (200 °C) than sulfur dioxide from $NiSO_4$ decomposition (>700 °C).[328] The start of evolution of carbon disulfide indicates that the main backbone of NiETT is decomposing at these elevated temperatures. Event C (288 – 444 °C) is a continuation of Event B, and releases additional carbon disulfide, hydrogen sulfide, and sulfur dioxide. The final decomposition, Event D (515 – 600 °C), continues to the end of the run releasing carbon disulfide, sulfur dioxide, hydrogen sulfide and water. Based on these observations from TGA-MS, we hypothesize some additional structures that likely represent these NiETT polymers, shown in Figure 6.8**.** Elemental analysis confirms the chemical compositional changes observed in the TGA-MS.

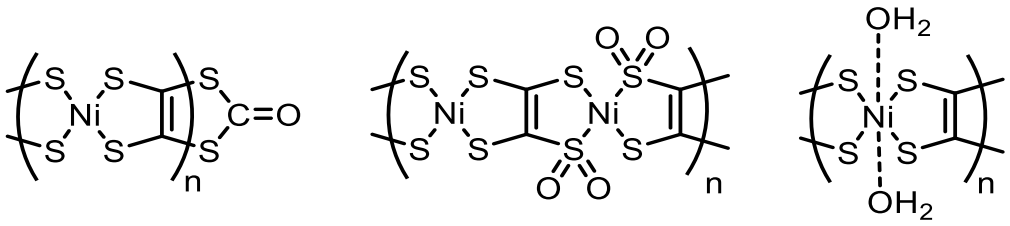

Figure 6.8 – Possible structures present in NiETT that give rise to carbonyl sulfide, water, or sulfur dioxide signals. These are in contrast to the idealized backbone represented by $Na_x[Ni(C_2S_4)]_n$ found in literature

Extending the analysis to composite films, Figure 6.9 shows the TGA-MS curves with associated ion signals for two film samples: a NiETT/PVDF film cast from DMSO (Pristine Film, PF) and a NiETT/PVDF film cast from DMSO that is annealed at 160 °C in air for one hour (Annealed Film, AF). As in the powder samples, the films show four mass loss events, denoted Events A-D. The signal-to-noise ratio is decreased in these samples due to the small mass of an individual film. We note that the NiETT powder used in both these films is not annealed (similar to PP discussed earlier). For both film samples, Event A (~80 – 160 °C) aligns with the annealing process and is crucial for obtaining high thermoelectric properties. Event B (206 – 266 °C) and Event C (346 – 438 °C) are the major NiETT decomposition events that occur after annealing. Both have similar FDHM and peak mass loss temperatures as the powders, confirming that this is a NiETT decomposition. Event D (440 – 487 °C) occurs at a lower temperature in the films that is consistent with the decomposition onset of PVDF (Figure S7). In pristine films (PF), the mass loss in Event A totals 7.0% and shows a very weak signal of water and almost no signal of carbonyl sulfide when compared to the powder samples. The most prominent mass loss signal during this step is from DMSO. Beyond Event A, during the isothermal hold, there is an additional 1.7% mass loss in PF that is believed to be the slow release of DMSO from the film. In contrast for the annealed films (AF), Event A consists of a smaller

mass loss of 4.3%, with no discernable water or carbonyl sulfide signals; the most prominent ion signal is also from DMSO. Less surface moisture is expected to return to the films compared to the powders upon exposure to atmosphere after annealing, as the hydrophobic PVDF surrounding the NiETT particles prevents reabsorption of water. Vacuum drying films at 50 °C for 30 minutes followed by annealing for one hour at 160 °C, does not fully remove DMSO from the composite films. However, complete removal of DMSO is not required to realize the full enhancement in thermoelectric performance.

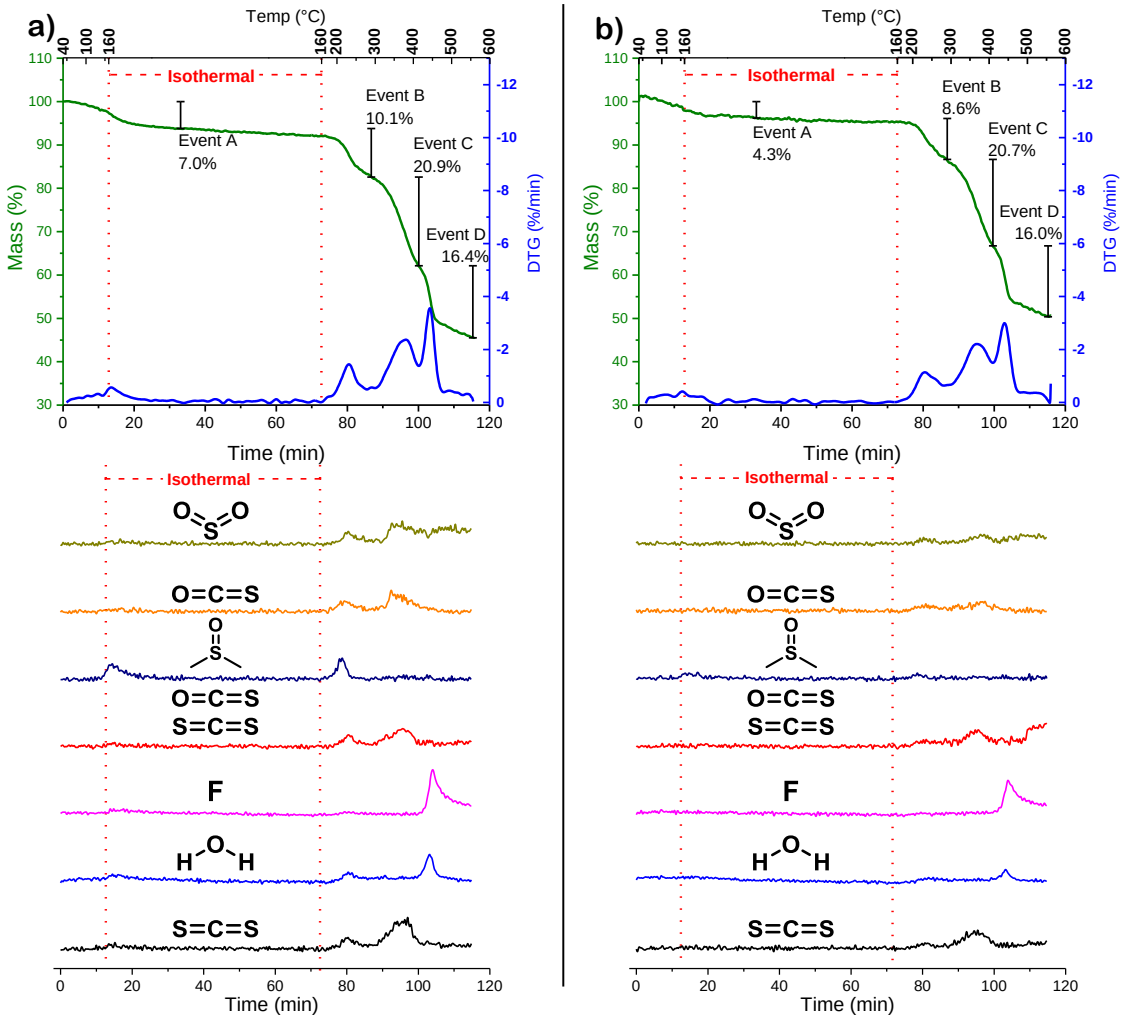

Figure 6.9 – Thermogravimetric analysis with tandem Mass Spectroscopy (TGA-MS) of Pristine Film (PF) and Annealed Film (AF) samples of NiETT/PVDF/DMSO. (a) TGA with plotted differential (DTG) of PF and normalized PF ion signals from QMID, (b) TGA with DTG of AF and normalized AF ion signals from QMID. See Figures S3 and S4 for additional data

As with the powder samples, Event B in both films (PF and AF) reveals the loss of sulfur dioxide and carbon disulfide from the decomposition of NiETT. The signal for water is minimal in PF and indiscernible in AF; and instead, a signal for DMSO is observed in both. The DMSO released in Event B originates from a separate source more strongly bound within the film (analogous to the incorporated water in PP and AP), as compared to the DMSO released in Event A (which is DMSO trapped within the PVDF). We

hypothesize that, in the NiETT powder form, water is bound to both the particle surface and to nickel centers, either in the backbone of the NiETT or as impurities in the film. Annealing the powder removes surface moisture (Event A signals) but does not remove the more strongly bound hydrates (Event B signals). In these powder samples, the surface moisture is rapidly replaced upon cooling in atmosphere causing a similar water signal in both PP and AP in Event A. During the film fabrication process, NiETT experiences a saturated DMSO environment, and contact moisture moves from the surface into the bulk solution. Water bound to nickel centers, both main chain and impurity hydrates, is also exchanged for DMSO. This results in the formation of a nickel-DMSO complex in the film forming process.[329]

When both film samples (PF and AF) are dried at 50 °C under vacuum, the contact moisture and previously bound water is removed along with the majority of DMSO. Some DMSO remains trapped in the PVDF film and is released in PF – Event A, or is bound to nickel centers and released in PF – Event B. For the annealed film, DMSO trapped within the PVDF matrix is readily removed, as evidenced by the rapid decline of DMSO ion signal in AF – Event A, and the significantly smaller DMSO signal in AF – Event B than PF – Event B. This suggests that the process of removing DMSO from the film helps drive the film reorganization, which manifests as a boost in electrical conductivity. Event C in AF and PF show the same evolution of carbon disulfide and sulfur dioxide as the powder samples, suggesting the NiETT polymer is unaffected by processing into a composite. Event D shows a spike in fluorine signal that matches well with the decomposition of neat PVDF.

6.4 Conclusions and Outlook

NiETT:PVDF is a promising air-stable n-type thermoelectric material. This work investigates the use of an annealing post-treatment process to enhance the performance of NiETT:PVDF thin films cast from DMSO. While we previously demonstrated the reproducibility between batches and batch sizes,[323] nonetheless a single batch of Na(NiETT) was selected for all annealing studies to remove any possible differences in particle size or composition. The thermoelectric properties were simultaneously enhanced upon annealing composite films and are attributed to *(i)* improved film morphology and *(ii)* compositional changes in the NiETT material. TGA-MS reveals the reversible removal of water (as contact moisture and incorporated in the polymer backbone) and the irreversible removal of carbonyl sulfide upon annealing NiETT powder. For the pristine powder, removal of ~3% mass, corresponding to carbonyl sulfide as an impurity, results in an increase in the thermopower from -28 μV/K to -42 μV/K. For the films, TGA-MS indicates DMSO is the major contributor to mass loss during the annealing process; the solvent replaces both contact moisture and incorporated water in NiETT during film fabrication. Annealing near the melting point of the binder (PVDF) allows for reorganization of domains to form highly interconnected pathways that increases the conductivity from 6 S/cm to 23 S/cm. The removal of moisture, residual solvent, and impurities through annealing works in tandem with the thermal- or solvent-driven morphological changes to yield a 25× increase in power factor from 0.5 μW/m-K^2 in pristine films to 12.5 μW/m-K^2 in annealed films.

This work demonstrates that there is a significant influence of material and device processing on the final thermoelectric performance. This influence may be negated or

increased through judicious selection of alternative binders, processing solvents, drying conditions, and annealing conditions. For the fabrication of thermoelectric devices using NiETT, alternative binders beyond PVDF may be required to address issues such as ink viscosity and solvent compatibility. A preliminary study suggests that the efficacy of annealing is highly dependent of the choice of binder. As such, a systematic study of binder and solvent systems is necessary to provide further understanding of this mechanism.

6.5 Methods

6.5.1 *Polymer Synthesis, Film Fabrication, and Thermoelectric Measurements*

The NiETT samples used in this chapter (4.097 and 5.034.A), film fabrication techniques, and thermoelectric measurements have been previously described in 5.6.

For the annealing post-treatment process, films were placed on an aluminium block and heated on a hot plate set to 160 ^{0}C in a fumehood. After one hour, samples were removed from the hot plate and allowed to cool to room temperature over a 30-minute period in air to give annealed film (AF), following which thermoelectric measurements were performed.

6.5.2 *Characterization*

The content of carbon, hydrogen and sulfur were obtained by Atlantic Microlabs (2400 II analyzer, PerkinElmer for CH, 1108 analyzer, Carlo Erba for S). The analysis of nickel and sodium was carried out on an inductively coupled plasma optical emission spectrometer, ICP-OES (OPTIMA 7300 DV, PerkinElmer) by the Renewable Bioproducts Institute at Georgia Tech. Each sample was dissolved in concentrated nitric acid and diluted

with deionized water prior to analysis. XPS was performed on the powder samples using a Thermo K-Alpha XPS (Thermo Fisher Scientific Inc.). Thermogravimetric analysis (TGA) on PVDF was performed using Pyris 1 Thermogravimetric Analyzer (PerkinElmer) under nitrogen. SEM images were obtained using the SU-8230 tool (Hitachi). The melting point of PVDF was obtained on a Q200 Differential Scanning Calorimeter (TA Instruments) and taken to be at the point of maximum heat flow. Thermogravimetric analysis coupled with mass spectrometry was performed by the NETZSCH Applications Laboratory Thermoanalytical Section on a NETZSCH STA 449F1 Jupiter coupled with a NETZSCH QMS 403 Aeolos mass spectrometer via a transfer line kept at 300 °C. Samples were run in a 25 μL Aluminum Crucible under a constant flow of Argon (70 mL/min). The heating profile was 40 to 160 °C at 10 K/min, isothermal at 160 °C for 60 min, and 160 to 600 °C at 10 K/min. Ion traces were normalized to the noise in the signal during the end of the isothermal hold (34 – 71 min).

6.5.3 *Additional Spectra*

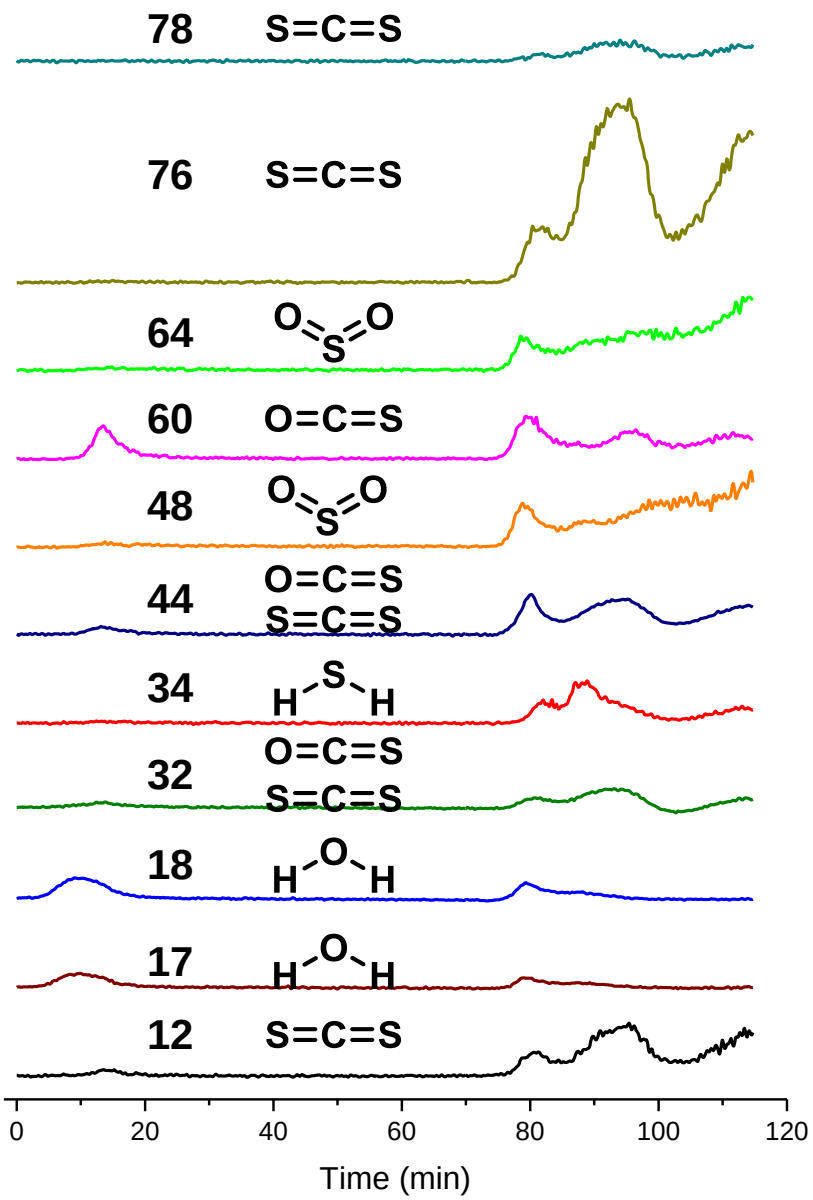

Figure 6.10 – Pristine Powder (PP): Complete set of mass ion signals and chemical assignments showing the evolution of carbonyl sulfide and water during a second annealing step in the TGA.

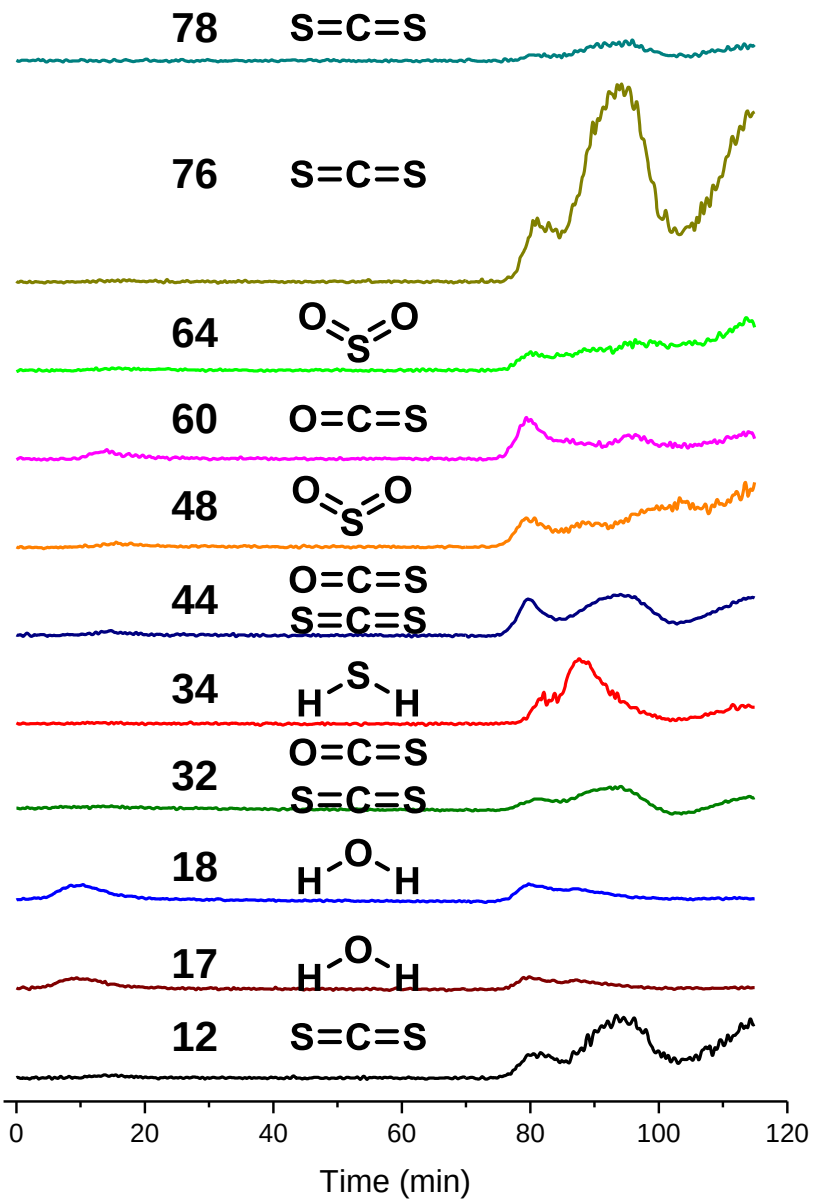

Figure 6.11 – Annealed Powder (AP): Complete set of mass ion signals and chemical assignments showing the evolution of carbonyl sulfide and water during a second annealing step in the TGA.

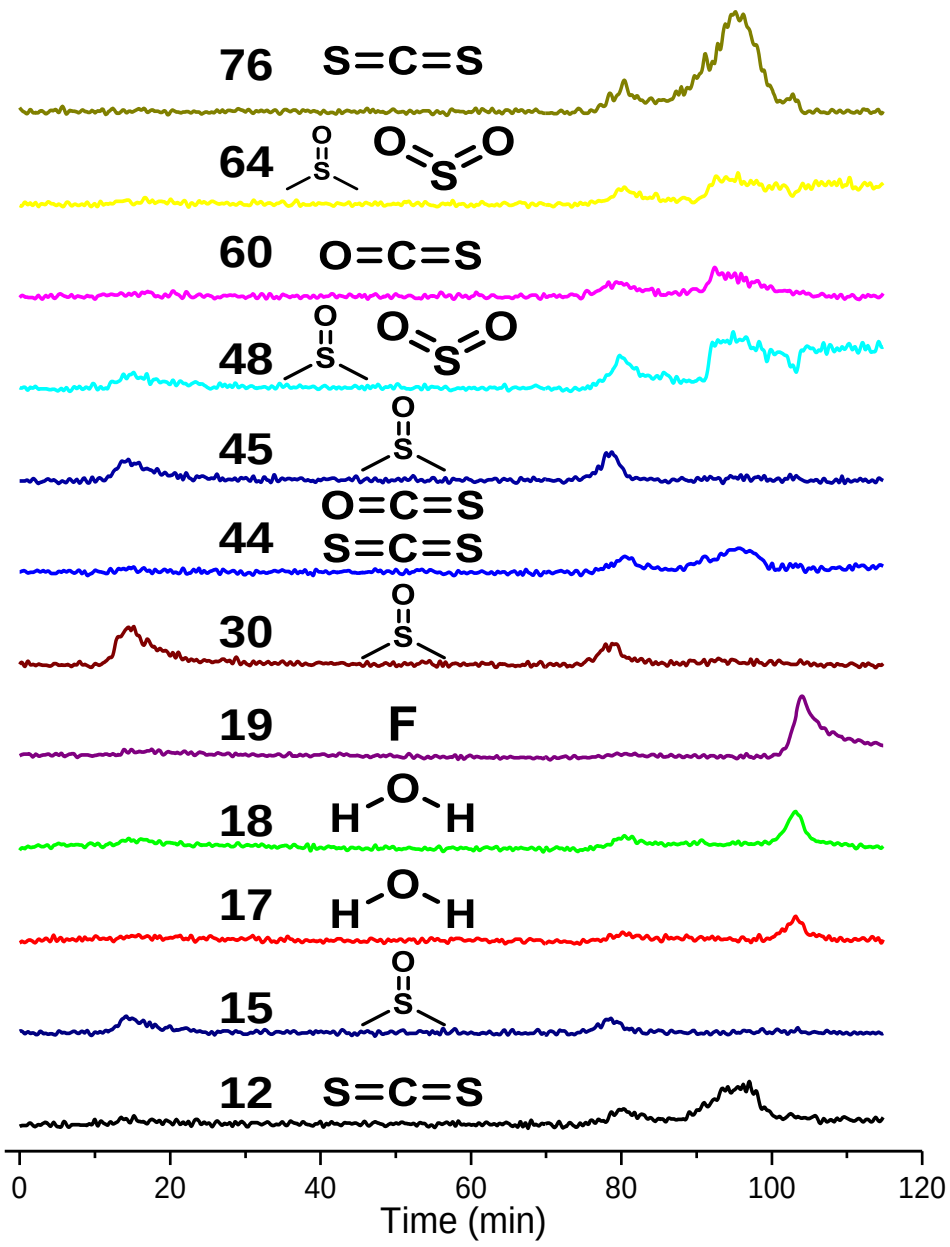

Figure 6.12 – Pristine Film (PF): Complete set of mass ion signals and chemical assignments showing the evolution of DMSO during the annealing process.

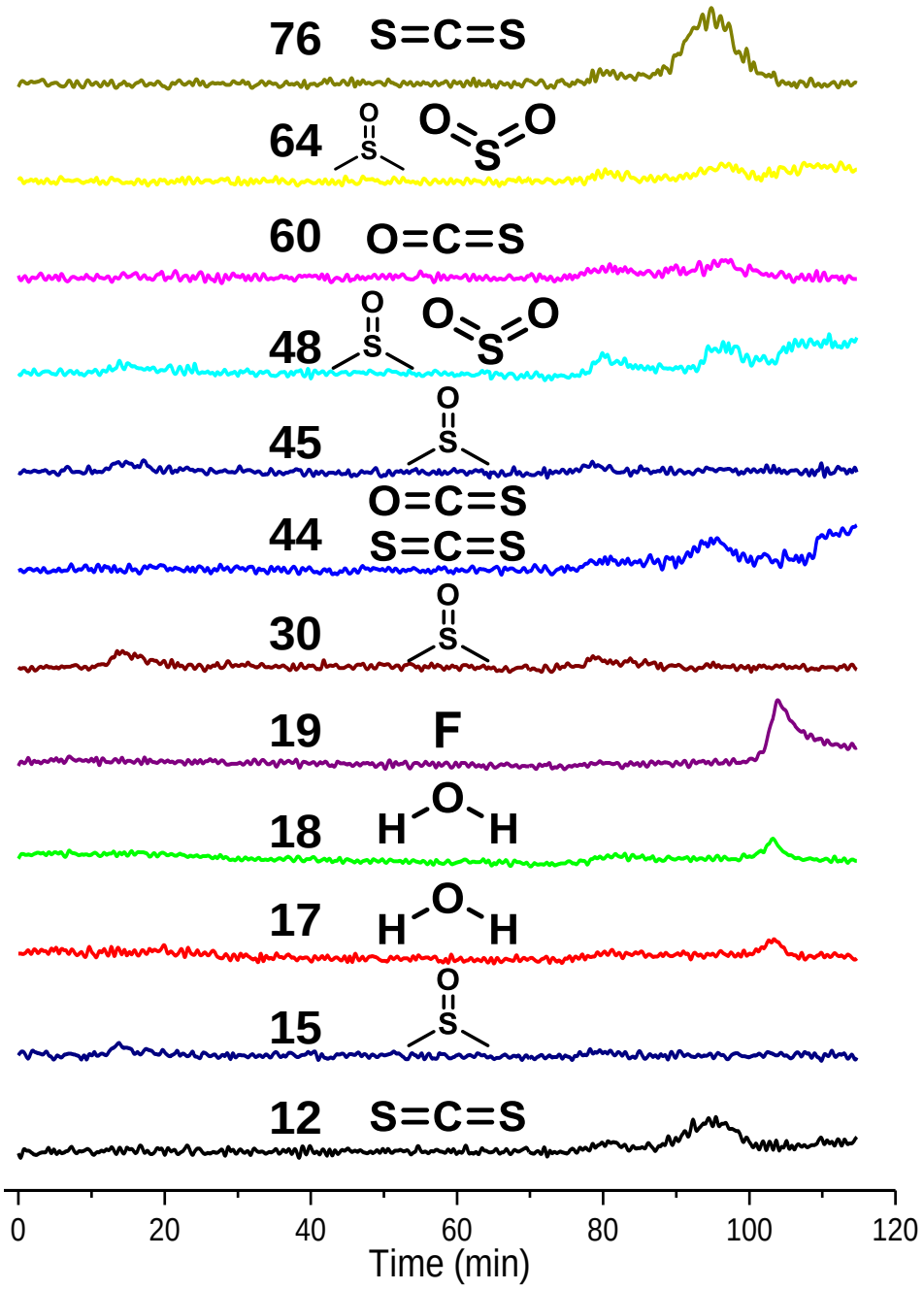

Figure 6.13 – Annealed Film (AF): Complete set of mass ion signals and chemical assignments showing the evolution of smaller amounts of DMSO in annealed films.

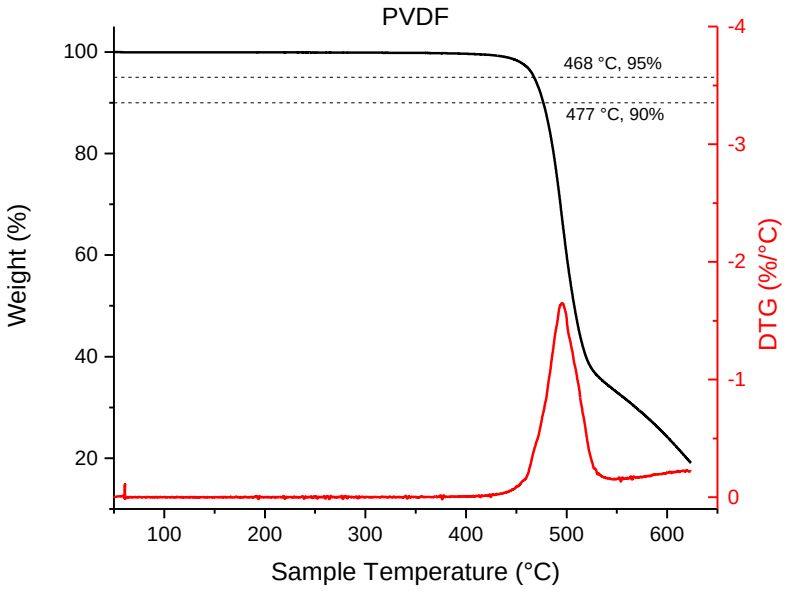

Figure 6.14 – TGA and DTG plots of PVDF showing a 5% mass loss at 468 °C

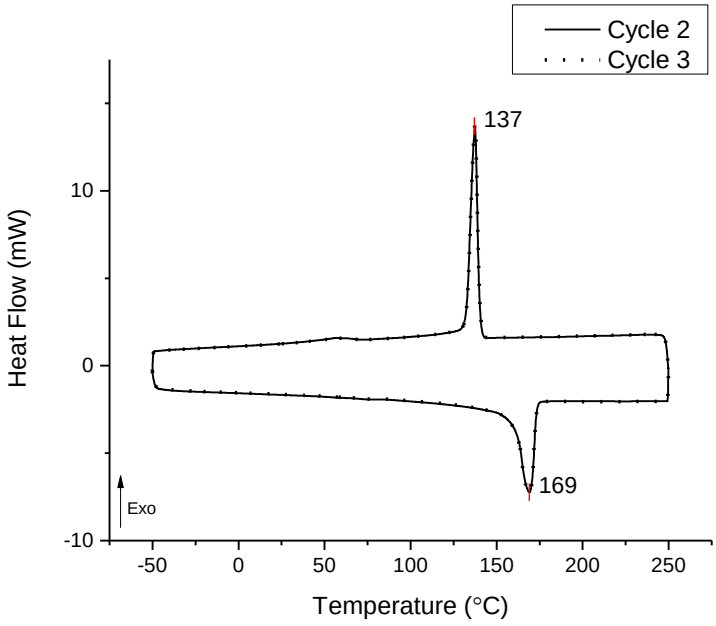

Figure 6.15 – DSC trace of PVDF showing a melting temperature of 169 °C

CHAPTER 7. NICKEL TETRATHIOOXALATES

7.1 Introduction

Nickel bis(dithiolene)s are one class of materials that are air-stable, n-type semiconductors. A subclass of bis(dithiolene)s are those of the $(C_2S_4)^{n-}$ structure – poly(nickel tetrathiooxalate)s (NiTTOs, n = 2) and poly(nickel ethenetetrathiolate)s (NiETTs, n = 4). NiETT, discussed thoroughly in Chapter 5, has recently seen significant improvements in conductivity and thermopower from synthetic modifications[298] or carefully controlled synthetic methods,[323] and processing techniques.[330] A better understanding of structure, corresponding property, and how to control that relationship is vital for future improvements. However, nickel bis(dithiolene)s are insoluble, intractable materials that are difficult to characterize. Furthermore, the difference in the final material called either NiETT or NiTTO may be negligible.

A note on nomenclature used in this chapter: R_2TTO is used for tetrathiooxalate salts used as monomers, and M[NiTTO] is used to denote the coordination polymer synthesized from nickel(II) and the tetrathiooxalate, M_2TTO, even if no counterion, M, is present or expected in the final material. M[NiETT] is used to denote materials synthesized from the ring opening of thiapendione with an alkali methoxide, MOMe. The naming is indicative of the synthetic route to the material, not necessarily the final structure, which is both difficult to determine and still a subject of research. If written as NiTTO or NiETT with no counterion indicated, it is broadly referencing the entire class of materials.

7.1.1 *Theory of NiTTO Versus NiETT*

NiTTO and NiETT polymers have ill-defined structures and are typically classified or named only by the monomer used. The relationship between TTO and ETT as monomers and as nickel coordinated polymers is shown in Figure 7.1. NiTTOs are polymerized by coordinating nickel(II) with tetrathiooxalate (TTO), while NiETTs are based on the ethenetetrathiolate (ETT) anion, generated from thiapendione, coordinated with nickel(II), and then oxidized to some degree. These two monomers are electronic isomers differentiated by 2-electrons. The strict differentiation between TTO and ETT, especially in coordination polymers with unknown oxidation states, is difficult. Hoffman and coworkers show through molecular orbital theory, and supported by experimental vibration spectra, that adding electrons to a neutral nickel dithiolene complex increases the C-C bond force constant while decreasing the C-S and Ni-S force constants.[264] That is, the ligands become more ETT-like with the addition of electrons and more TTO-like upon oxidation.

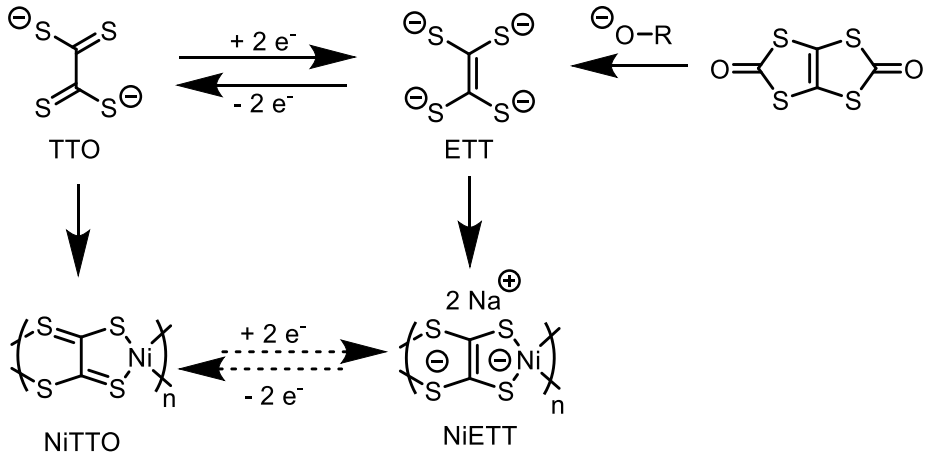

Figure 7.1 – Electronic relationship between TTO and ETT monomers, the idealized structures generated from coordination with nickel(II), and the potential interconversion between NiTTO and NiETT after polymerization

Recently, Tkachov et al. proposed that the true monomer for reported NiETT materials is not ETT but instead TTO.[281] 4,5-Bis(methylthio)-1,3-dithio1-2-one, generated by treating thiapendione with an alkali methoxide, undergoes disproportionation, releasing carbon monoxide and yielding TTO. Similar transformations of 4,5-bis(methylthio)-1,3-dithio1-2-one[270,315] to dimethyl tetrathiooxalate and thiapendione to bis([1,3]dithiolo)[4,5-*c*:4',5'-*g*][1,2,5,6]tetrathiocine-2,7-dione[316] under UV-irradiation are well known. The thermally driven transformation of 4,5-bis(methylthio)-1,3-dithio1-2-one to dimethyl tetrathiooxalate has been reported under pyrolysis conditions at 450 °C and 0.05 torr.[315] Tkachov's study is the first report of 1,3-dithiole-2-one-4,5-dithiolate undergoing such a transformation. The required experimental conditions were not thoroughly delineated. Further investigation whether this reaction was facilitated by UV-irradiation, thermal energy, presence of methoxide, or some combination of these factors is warranted.

Despite yielding final materials that in theory are identical, the reactions to form NiTTO and NiETT are quite different. TTO is a reactive monomer that will directly form a coordination polymer with nickel(II). The ideal NiTTO repeat unit is neutral, and the

only expected counterions during the polymerization and in the final material will be at the chain end. This may reduce the solubility of the growing chain, resulting in lower degrees of polymerization. It may also reduce unwanted oxidation and the formation of side-products, as the chain is not susceptible to oxidation during or after polymerization. In contrast, ETT is generated through the reaction of thiapendione and a nucleophile, often methoxide. This does not directly give the tetraanion, instead the coordination polymer forms through a stepwise reaction or other another route.[281] The idealized repeat structure of NiETT during polymerization bears a -2 charge with alkali or nickel(II) counterions. The polymer is susceptible to unintended oxidation processes and by-product formation during the polymerization and before it is purposefully oxidized. Oxidation is done through exposure to atmosphere or in a controlled fashion with a chemical oxidant, such as iodine.

7.1.2 *Literature Reports of Nickel Tetrathiooxalate Polymers*

There exist few reports of coordination polymers of nickel(II) and tetrathiooxalate and most originate from this thesis' advisor, Prof. John Reynolds. The required electrochemical monomer synthesis over a mercury electrode likely dissuades potential researchers.

Pressed pellets of NiTTO have shown conductivities of 4 – 20 S/cm and thermopowers of -20 uV/K.[127,265] Incorporation of TTO into films of nickel(II) acetate saturated poly(vinyl alcohol) films increased conductivity of the films five orders of magnitude, from 10^{-8} to 10^{-3} S/cm.[331] Others have grown coordination polymers from a surface through an alternating dip-coating process. However, these films exhibit a much lower conductivity of 10^{-3} S/cm compared to bulk samples.[332]

An alternative method to incorporate TTO into coordination molecules was reacting TTO, a metal salt, and an end-capping ligand source, such as $Zn(dmit)_2$.[283,284] This method yields isolatable bimetallic complexes of nickel and copper. Single crystal structures of the bimetallic nickel complex, $(Bu_4N)_2\{tto[Ni(dmit)]_2\}$, provides a view of the final molecule geometry when TTO is directly used as a ligand source. Within the TTO moiety, C-C bond length is 1.42 Å and the C-S bond length is 1.70 Å. When compared to the C-C bond (1.35 Å) and C-S (1.75 Å) bond in the dmit moiety, greater single bond character is observed in the TTO C-C bond and in the dmit C-S bond. In the uncoordinated crystal structure of K_2TTO, the C-C bond length is 1.50 Å and the C-S bond length is 1.68-1.69 Å, showing true single bond character in the C-C bond and thorough delocalization through S-C-S thiocarbonyl.[281]

Others have synthesized $(Bu_4N)_2\{tto[Ni(dmit)]_2\}$ from $(Bu_4N)_2Ni(dmit)_2$ without using TTO as a direct reagent. They propose to reverse the typical TTO-to-dmit transformation, seen in the synthesis of TTO and dmit, with sodium dithionite to extended $Ni(dmit)_2$ with a central TTO ligand.[286] The reported crystal structure gives the same bond lengths reported previously. The difference between the central ligand having more TTO character or ETT character may depend on the oxidation state of the final material more so than the reagents used. This furthers confirms that the ligand source may serve as a useful naming tool but has fewer implications when looking at the actual structure.

7.2 Electrochemical Synthesis of TEA_2TTO

The reactive monomer, TEA_2TTO, was synthesized through an electrochemically driven dimerization of carbon disulfide, Figure 7.2.[126,333] Tetrathiooxalate will react with

additional carbon disulfide or sulfur in solution and undergo additional reduction reactions.[128,266,272,288,334] Running the reaction with a tetraethylammonium bromide supporting electrolyte at low temperatures (–5 °C) traps the desired intermediate as TEA_2TTO by exploiting its insolubility in cold acetonitrile. A red color, partly from 1,3-dithiole-2-thione-4,5-dithiolate, develops in solution as a concoction of sulfur-based impurities are formed. This same method is used to prepare tetraselenooxalate.[335]

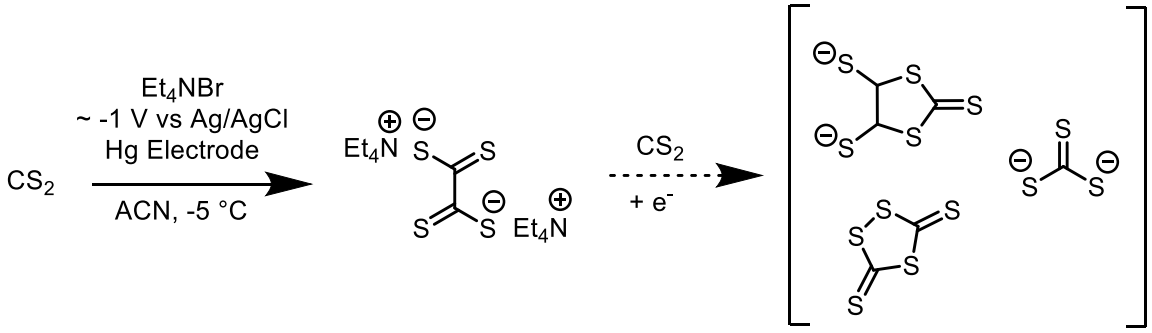

Figure 7.2 – Electrochemical dimerization of TEA_2TTO, which is susceptible to further reduction and reactions with carbon disulfide if not trapped as the insoluble bis(tetraethylammonium) salt

An equal charge must be passed at the counter electrode. The reaction is the formation of the tribromide ion.[336] In practice, a murky yellow solid is formed in the counter electrode compartment that is believed to be tetraethylammonium tribromide from the color. The counter electrode electrolyte is replaced continuously to prevent soiling and obstruction of the platinum basket counter electrode and to prevent diffusion of the tribromide into the working electrode compartment. Over time, a black solid forms at the frit between the two compartments (due to diffusion and reaction between the contents of the two compartments) which requires complete disassembly of the apparatus and cleaning with nitric acid.

Alternative counterions to bromide that undergo an oxidation to a benign substance are desirable. One such possibility is oxalic acid, which undergoes a two-electron process to form carbon dioxide. However this requires an acidic medium and may not be amenable to this setup.[337,338]

TEA_2TTO has been synthesized without access to a potentiostat or electrochemical H-cell. The same reduction of carbon disulfide over mercury with a platinum counter electrode was performed in a beaker with a Soxhlet thimble serving as the counter electrode compartment and electrolyte bridge. A 12 VDC power source was used in place of a potentiostat. The researchers report separating out an insoluble brown material during purification.[125] This may be the same by-product formed during the chemical synthesis with sodium naphthalide described below.

7.2.1 *Attempts at Chemical Synthesis of Tetrathiooxalate*

The reduction of carbon disulfide with sodium amalgam was first reported by M. Herrmann in 1860 and M. Guignet in 1861. The products formed were of the composition NaC_8S_3, NaC_2S_8, and $NaC_{10}S_5$. Attempts at isolating the reaction intermediates as stable methyl derivatives was attempted in 1927, with the product claimed to be dimethyl tetrathiooxalate.[339] However, it was later shown that the actual product formed was 4,5-bis(methylthio)-1,3-dithiole-2-thione (dimethyl dmit).[340] Many other attempts at the direct chemical synthesis of tetrathiooxalate have failed to give the desired product.[271,288]

A chemical route was reported by Hartzler in a 1973 patent using sodium naphthalide in tetrahydrofuran.[341] Na_2TTO was obtained as a brown solid and collected by filtration. In my hands, the addition of carbon disulfide to naphthalide also yielded a brown solid with

dissipation of the green color of the radical. Upon sitting, filtration, or any exposure to atmosphere, the brown solid rapidly became a soluble red material (presumably dmit). In practise, the brown solid, if indeed Na_2TTO, was too unstable to handle and, coupled with its rapid decomposition to odorous by-products, was not suitable for further polymerizations. The patent directly uses this monomer to create polymer sulfides, of which the purity of Na_2TTO or presence of dmit may not be an issue. Only one other report of this procedure was found in the open literature in the *Journal of New Materials for Electrochemical Systems*.[342]

An alternate chemical route, which does not rely on the reduction of carbon disulfide, was reported in 1992.[343] A related method was reported in 1998.[334] The authors use sodium persulfide (Na_2S_2) on tetrachloroethylene to generate Na_2TTO which is captured as TEA_2TTO. The route was not attempted due to the requirement of sodium persulfide or sodium sulfide as a starting material.

7.3 Optimization of NiTTO Synthesis

With the monomer in hand, the previously reported polymer of TEA[NiTTO] was resynthesized. Optimizations to increase the degree of polymerization have previously tested nickel(II) salts, extended polymerization times, fresh monomer infusions, and long-chain alkylammonium solubilizing counterions. Using elemental analysis, no dependence of degree of polymerization on these parameters was found.[127,333] Following the same procedure, a black material was obtained with 0.10 ± 0.04 S/cm and -20 ± 2 μV/K in PVDF composite thin films compared to 4 – 20 S/cm and -20 μV/K reported in a pressed pellet.[265]

The consistent, negative thermopower motivated further studies on NiTTOs, but the low conductivity discouraged further work on specifically TEA[NiTTO].

7.3.1 *Exchanging Tetraethylammonium for Sodium*

Most of our previous optimizations were performed on Na[NiETT], and we expected a higher performing material to result from an alkali metal counterion material. Na_2TTO was prepared according to a literature procedure using sodium tetraphenylborate in methanol.[333] This exploits both the increased solubility of Na_2TTO in methanol compared to TEA_2TTO and insolubility of tetraethylammonium tetraphenylborate ($TEABPh_4$) in methanol. Filtration under inert atmosphere directly into a methanolic solution of nickel(II) acetate yielded a black material, Na[NiTTO]-MeOH. When blended with PVDF to form a composite film, a conductivity of 3.9 ± 0.5 S/cm and a thermopower of -34 ± 2 μV/K was achieved. This was a promising improvement to the lower conductivity TEA[NiTTO], and further explorations into reaction optimization were planned.

7.3.2 *Solvent Testing*

Original reports of NiTTOs utilized a mixture of methanol and DMF for polymerizations. DMF, as a polar aprotic solvent, was expected to increase the solubility of the rigid backbone compared to methanol. A portion of the reaction solvent mixture remained as methanol to solubilize TEA_2TTO, which was not fully soluble in DMF. After completing the counterion exchange to Na_2TTO, the monomer was fully soluble in DMF, and methanol was removed completely from the polymerization procedure.

After completing the ion exchange and filtration, the methanol was removed under high vacuum with a liquid nitrogen trap to avoid atmospheric exposure. Na_2TTO dried to a red, brown solid with residual $TEABPh_4$ visible. Complete conversion and 100% retainment of material was assumed for calculating nickel(II) stoichiometry.

Two polymerizations in DMF at 80 °C were attempted – the first had Na_2TTO in DMF added to a warm solution of nickel(II) acetate in DMF (Na[NiTTO]-DMF_A), the second had a solution of nickel(II) acetate in DMF added to a solution of Na_2TTO in DMF (Na[NiTTO]-DMF_B). Elemental analysis and qualitative observations of color and behavior noted no difference between the two materials. Both materials were lustrous and steel-blue in color – very similar to our observations of NiETT[323] and apart from all prior reports of either NiTTO or NiETT as a black powder. Na[NiTTO]-DMF_A was transferred to a collaborator for thermoelectric testing and is the Na[NiTTO] used in this work. Na[NiTTO]-DMF:PVDF composite thin films gave a conductivity of 18.2 ± 1.5 S/cm and a thermopower of -36 ± 2 μV/K. The increase in conductivity without an adverse impact on thermopower is attributed to longer chains of Na[NiTTO] forming in warm DMF compared to room temperature methanol.

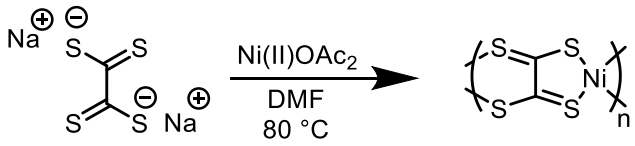

Figure 7.3 – Polymerization of Na_2TTO with nickel(II) acetate in DMF at 80 °C to give Na[NiTTO]-DMF.

7.4 Alkali NiTTO Family

The two-dimensional conduction that make nickel coordination materials interesting for superconductors relies on interchain interactions,[257,264] and the conductivity of single

crystals of nickel dithiolene salts depends on the counterion and extent of oxidation.[289] NiETT polymers also show a dependence of conductivity and thermopower on the counterion used;[297,323] therefore, the effect of the counterion in NiTTO was investigated. In the ideal NiTTO polymer, no counter ion should be present in the final material. Therefore, properties of the final NiTTO materials are expected to be independent of the alkali salt used as a monomer. To test this hypothesis, a series of NiTTOs were prepared with alkali metal counterions from lithium to cesium.

7.4.1 *Exchange Reactions*

The M_2TTO monomer is unstable, as demonstrated by its rare crystal structure,[281,344] low direct synthesis yields,[124] and troublesome chemical synthesis.[334,341,345] M_2TTO was prepared from TEA_2TTO by a counterion exchange in degassed methanol with the desired alkali salt of tetraphenylborate, Figure 7.4.[333] M_2TTO was concentrated to a solid under inert conditions to yield a monomer ready for polymerization in other solvents.

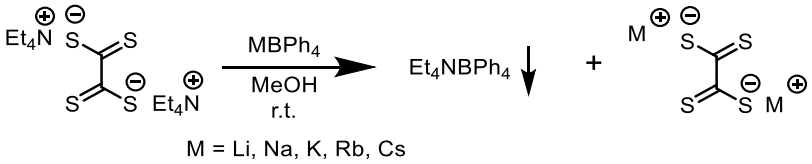

Figure 7.4 – Counterion exchange of tetraethylammonium for an alkali metal in methanol

The precipitate of tetraethylammonium tetraphenylborate ($TEABPh_4$) is an ultrafine powder that clogs or goes through many coarse filters. Coupled with the atmospheric instability, special care was necessary for filtrations. Schlenk techniques[346]

were first used to filter away the $TEABPh_4$. The filter paper clogged easily due to its low surface area for filtration.

An alternate technique was utilized for Li, K, Rb, and Cs counterion exchanges. Li and K were exchanged in a round bottom flask under argon with stirring at room temperature, similar to Na. Using degassed methanol and a blanket of argon, the slurry was transferred to a 50 mL centrifuge tube. Centrifuging for five minutes at 3000 rpm gave a clear supernatant with $TEABPh_4$ collected at the bottom of the tube. Decanting under an argon blanket to a new flask for concentration under inert atmosphere was aided with one additional portion of methanol, agitation, and centrifugation. Rb and Cs counterion exchanges were performed directly in a 50 mL centrifuge tube under argon and concentrated after the same decanting procedure.

7.4.2 *Polymerizations*

The polymerization procedures for each material are given in detail in Section 7.6. All polymers except Na[NiTTO]-DMF follow a procedure briefly described here. A freshly made and isolated batch of M_2TTO is dissolved in degassed, dry DMF and heated to 60 °C. A stoichiometric amount of nickel(II) acetate is dissolved in DMF and added to the M_2TTO over 5-10 minutes. The reaction is run for 24 hours with precipitation or gelation visible in some reactions, but not all. Quenching in 4× volume excess of methanol precipitates a solid that is collected on a 0.45 micron nylon filter, and washed successively with methanol, methanol:water mixture, methanol again, and ether. Na[NiTTO]-DMF follows the above with the following changes. The reaction was run at 80 °C, and the Na_2TTO solution was added to nickel(II) solution.

Li[NiTTO], Na[NiTTO]-DMF, and K[NiTTO] give lustrous, steel-blue materials reminiscent of our prior work on NiETT.[323] Rb[NiTTO] and Cs[NiTTO] are black powders with increased carbon, nitrogen, and hydrogen content by elemental analysis, similar to TEA[NiTTO]. This could be due to poor counterion exchange using $RbBPh_4$ and $CsBPh_4$, or batch-to-batch variations in the starting material, TEA_2TTO. Thermoelectric performance will focus on Li[NiTTO], Na[NiTTO]-DMF, and K[NiTTO]. Improved thermoelectric performance may be realized in future syntheses of Rb[NiTTO] or Cs[NiTTO], and their future investigations should not be discouraged.

7.4.3 *Elemental Analysis*

Comparing the polymerization reactions of NiTTO and NiETT, a material more closely representing the idealized repeat structure with fewer side products, fewer oxidation products, and less counterion is expected from NiTTO. Table 7.1 shows the elemental ratios for Li-, Na-, and K[NiTTO] as compared to the idealized repeat unit, $[Ni(C_2S_4)]$ (EA of all samples given in Section 7.6). All samples have the expected content of ratio of S:Ni, giving evidence that the backbone of the polymer is indeed NiTTO. However, an excess of carbon is present in all samples. The presence of nitrogen and hydrogen, along with excess carbon, could indicate that the counterion exchange did not go to completion (however, one would still expect a low amount of nitrogen from the counterion). These materials may also hold onto DMF from the reaction, such that washing and vacuum drying at room temperature is not sufficient to remove all DMF. Li, Na, and K show < 1% mass of counterion, indicating the NiTTO polymers are structures with low amounts of counterion present. Rb and Cs were not capable of being tested.

Table 7.1 – Atomic ratios of sulfur, carbon, nickel, and alkali counterion in Li-, Na-, and K[NiTTO]s compared to the idealized repeat structure $[Ni(C_2S_4)]_n$

	Li[NiTTO]	Na[NiTTO]	K[NiTTO]	Idealized
S:C	1.4	0.9	1.2	2.0
S:Ni	3.6	3.5	3.7	4.0
C:Ni	2.7	3.8	3.0	2.0
M:Ni	0.00	0.04	0.05	0.0

7.4.4 *Thermoelectric Evaluation Before Annealing*

A weak trend of increasing conductivity is observed in Figure 7.5 from Li[NiTTO], 4.5 ± 1.2 S/cm, to K[NiTTO], 28.3 ± 7.4 S/cm. The opposite trend is observed in thermopower, with the highest value, -43 ± 2 μV/K, observed in Li[NiTTO], and the lowest value, -35 ± 2 μV/K, observed in K[NiTTO]. For comparison, Na[NiETT] is 17 ± 1.5 S/cm and -36 ± 2 μV/K before annealing.[323] This improvement from Na[NiETT] to Na[NiTTO] should be taken with caution for these reasons: (i) it does not take into account thermal annealing, from which Na[NiETT] appears to benefit from to a greater extent, (ii) the measurements for Na[NiETT] were taken from the most reproducible synthesis available, with our additional NiETT experiments yielding materials with conductivities from less than 1 S/cm to greater than 100 S/cm, and (iii) the metrics obtained for Na[NiTTO] are the result of one batch of material with little synthetic optimization.

We postulate potential reasons for the improvement in thermoelectric performance of unannealed NiTTO films in comparison to unannealed NiETT films, but we emphasize this is a preliminary report of M[NiTTO]s. Despite having similar idealized final structures, variations can include, but are not limited to: by-products and impurities from the reaction

or workup process, unintended oxidation reactions during the reaction or afterwards, different polymer molecular weight and dispersity, cross-linking and other deviations from the ideal linear repeat structure. The increased conductivity in NiTTO could be macroscopic, that is, NiTTO forms a more interconnected network when cast with PVDF in DMSO. Or it could be microscopic, that is, the molecular structure of NiTTO allows for increased interchain charge transport. The slight increase in thermopower could be indicative of increased chain length (though unlikely due to the lack of solubilizing counterions in the synthesis of NiTTO), a cleaner material due to its synthetic route with fewer impurities that negatively affect thermopower, or a more neutral (more oxidized material) in NiTTO, exchanging a lower conductivity for greater thermopower.

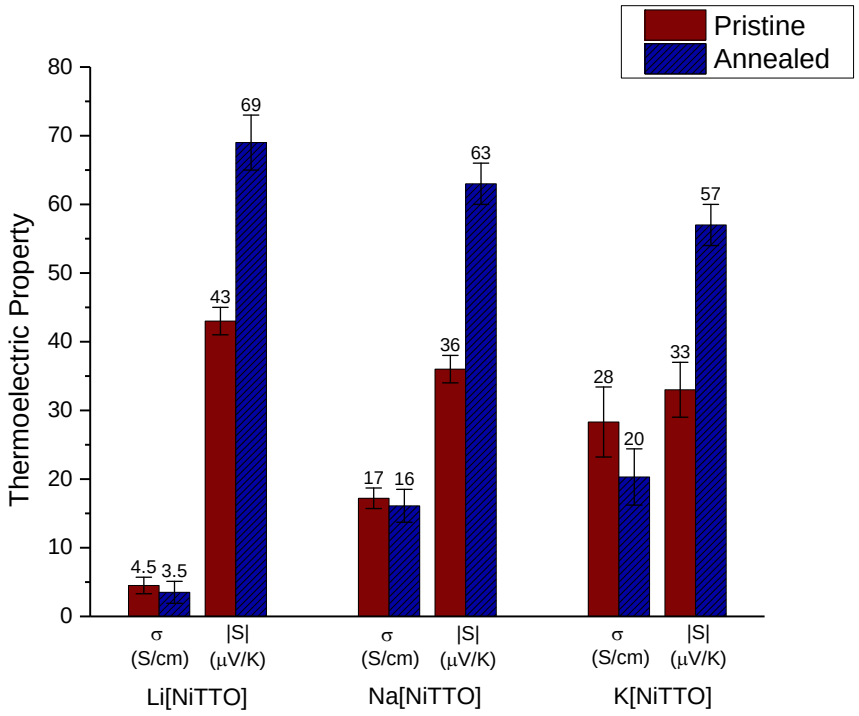

Figure 7.5 – Thermoelectric performance of Li-, Na-, and K[NiTTO]:PVDF composite thin films before annealing (red) and after annealing at 160 °C for one hour (blue)

7.4.5 *Thermal Annealing of NiTTO:PVDF Composites*

We have previously shown annealing to be beneficial to conductivity and thermopower in NiETT:PVDF composite films.[330] Contrary to NiETT, the conductivity is decreased slightly in all NiTTO samples, indicating that the NiTTO:PVDF composites do not undergo the same beneficial morphological or chemical changes upon annealing that generate the conductivity improvement in NiETT:PVDF. Annealing results in an improvement to thermopower in Li-, Na-, and K[NiTTO]. Li, Na, and K see an increase in thermopower magnitude to ~ -60 μV/K. A full study on optimum annealing conditions or the full effects of annealing has not been undertaken.

We hypothesis that a thermal rearrangement is leading to positive effects in interchain connectivity, such as S-S and Ni-S interchain alignment. Concurrently, on a macroscopic scale, overall connectivity between NiTTO domains in the film is decreased. Interestingly, no improvement in Seebeck is observed in TEA-, Rb-, or Cs[NiTTO], potentially suggesting that these materials do not – or cannot – undergo the same beneficial improvement during annealing.

7.5 Conclusions and Outlook

The concept that NiETTs and NiTTOs are difficult to synthesize reproducibly and characterize is well understood. This report is viewed as a first insight into NiTTO:PVDF composite films utilizing a TTO monomer that was electrochemically synthesized. Adaptations to the process and improvements to the material are both required and encouraged. We stress that these are single batches of materials: reproducibility tests, full condition optimizations, and annealing conditions studies have not yet been performed.

Regardless of the starting monomer (TTO or ETT), the formed coordination polymers have a similar backbone when oxidized to the same extent. Changes in thermoelectric performance may be attributable to the reaction pathway, formation and presence of impurities, degree of polymerization or dispersity of the oligomeric backbone, or the partial degree of oxidation resulting in mixed valence states.

The formation of a neutral backbone in NiTTO may result in lower degrees of polymerization compared to NiETT, which theoretically, has one or two solubilizing counterions per repeat unit before oxidation. The final oxidation state of NiTTO may also be more neutral when compared to NiETT. As iodine exposure has been shown to reduce conductivity in pressed pellets of NiTTO,[265] they may benefit from an injection of charge carriers through reduction.

The changes in material properties induced by different counterions are difficult to explain in both NiETT and NiTTO. While no difference is expected when considering the final structure of NiTTO, the counterion exchange from TEA, and potentially the solubility of the growing chain, is affected by the counterion. In our NiETT studies, only sodium methoxide was rigorously prepared in-house. The observed changes in NiETT samples may result from using impure lithium and potassium methoxide sources. A different counterion may also modify the reaction pathway, resulting in a distinct material, or change the final material composite behavior through the minute quantities of counterion remaining.

While Tkachov et al. directly proved conditions that can give K_2TTO from the standard NiETT synthesis,[281] and hence NiTTO can be generated from NiETT conditions,

we do not believe this to be the case in all NiETT conditions or materials. We summarize NiETT as a material with many more variables that must be cared for and controlled in order to yield a high-performing, reproducible material. While this makes the overall process more involved and difficult, it also gives more knobs to turn during optimization proceedings. NiTTO, on the other hand, is more likely to give a consistent material when following the same procedure, given that the monomer is pure. There is less control during the synthesis over aspects, especially less control over oxidation. NiTTO yields a neutral chain; NiETT yields the oxidation level set by iodine.

7.6 Synthetic Methods

7.6.1 *General Instrumentation*

Elemental analyses were carried out by Atlantic Microlabs on a PerkinElmer 2400 II analyzer (CHN) and a Carlo Erba 1108 analyzer (S). The analysis of nickel, lithium, sodium, and potassium was carried out on an inductively coupled plasma optical emission spectrometer, ICP-OES (OPTIMA 7300 DV, PerkinElmer) by the Renewable Bioproducts Institute at Georgia Tech. Each sample was dissolved in concentrated nitric acid and diluted with deionized water prior to analysis.

Film fabrication, annealing, and thermoelectric measurements were performed by Dr. Akanksha K. Menon, and a more thorough description may be found in her thesis (2018 Georgia Tech). A composite film was obtained by blending the TTO powder with a polymer matrix to form a dispersion. First, PVDF (Sigma Aldrich, MW ~180,000) was dissolved in DMSO (Amresco) at 80 °C for 4 hours under continuous stirring in an Erlenmeyer flask to form a 10 mg/mL solution. Next, 40 mg of TTO powder was added to

1 mL of the PVDF/DMSO solution with 10 zirconia beads (diameter = 1 mm) in a micro-vibration mill for 30 minutes (MSK-SFM-12M, MTI Corporation). This matrix was chosen as it has the highest film performance as reported previously for NiETTs, and the NiTTO:PVDF mass ratio was fixed at 4:1.[301] Films were prepared by drop-casting 35 µL of the composite on 1 cm × 1cm pre-treated glass substrates and drying in a vacuum oven at 50 °C for 30 minutes (pre-treatment of glass substrates involves sequential cleaning with deionized water, acetone and isopropyl alcohol for 3 minutes each and placement in oxygen-plasma for 5 minutes). Four gold contact pads (1mm × 1mm, ~ 100 nm thick) were then deposited on the prepared films using a shadow mask in an e-beam evaporator. All films were 5-10 µm thick as measured with a profilometer (Dektak XT, Bruker). Several samples (films) were prepared to capture sample-to-sample variations in thermoelectric properties generating representative error bars that are reported as the standard deviation. Annealed films were placed on a hotplate held at 160 °C in a fumehood for one hour before cooling to room temperature.

Micromanipulators with tungsten tips were used to make electrical contact to the gold contact pads and in-plane electrical conductivity was acquired using the four-probe Van der Pauw technique. Samples were placed on a temperature-controlled Peltier stage using thermal grease on the backside of the substrate to ensure good thermal contact. The Seebeck coefficient was measured by suspending the sample between two temperature-controlled Peltier units (separated ~3 mm) and applying a series of temperature differences upto ΔT = 10 °C between the stages. The thermoelectric voltage was measured between two contact pads on separate stages using the probe tips, while the temperature of each pad was measured with a K-type thermocouple in close proximity to the probe tips. Voltage

and temperature data were acquired using a Keithley 2700 DMM with a 7708 Mux card via a LabVIEW interface. The Seebeck coefficient was extracted as the slope of the V - ΔT plot.

7.6.2 *General Synthetic Methods*

All reaction solvents were made anhydrous and oxygen-free to the greatest extent possible before use. All solvents used for washing NiTTO polymers were reagent grade and used without further purification. Anhydrous acetonitrile was prepared by drying HPLC grade acetonitrile over activated 3Å molecular sieves (10% w/w). Anhydrous methanol was prepared by drying ACS grade methanol over activated 3Å molecular sieves (10% w/w) for 72 hours. Anhydrous DMF (EMD DriSolv^{TM}) was used as is and considered anhydrous. All solvents were sparged with argon for 30 minutes prior to use.

Mercury was cleaned of surface and oxide contaminants by filtering through a conical paper filter with a small hole punched in the bottom. Mercury will pass through the hole while the surface contaminants stick to the filter paper. Surface tension prevents the last drops of mercury from passing through the filter, keeping all surface contaminants in the filter. Excess water was removed from mercury by drawing water up strips of coarse filter paper by capillary action.

The Ag/AgCl reference electrode was prepared by submersing a silver wire into a ferric chloride solution in acetonitrile.[129] All other reagents were obtained from commercial suppliers and used without further purification. All glassware was oven dried and cooled under an inert atmosphere. All reactions (apart from the electrochemical synthesis) were run in the absence of moisture and ambient atmosphere using standard Schlenk techniques.

The electrochemical synthesis was run under an argon blanket to the greatest extent possible.

7.6.3 *Electrochemical Synthesis of Bis(tetraethylammonium) Tetrathiooxalate (TEA_2TTO)*

TEA_2TTO was synthesized by adapting literature procedures.[124,126] An electrochemical H-cell separated by a fine porosity glass frit was placed in an isopropanol bath kept at –10 °C via a mechanical chiller. The H-cell dimensions are as follows: working compartment – 9.5 cm diameter x 13 cm height; counter compartment – 6 cm diameter x 13 cm height; salt bridge frit – 2.5 cm diameter. The working electrode was a mercury pool (~70 cm^2, 1-2 cm deep), the counter electrode was a mesh platinum basket (3.5 cm diameter, 4.5 cm height), and the reference electrode was a silver wire (Ag/AgCl). A typical Ag/Ag^+ reference electrode was not successful, as the Vycor-frit quickly clogged with contaminants. Both compartments were outfitted with rubber stoppers to minimize the ingress of water and moisture. In the counter electrode stopper, two holes were drilled for an electrical wire and an argon hose. In the working electrode stopper, six holes were drilled for an electrical wire, an argon hose, a mechanical stirrer, a reference electrode, a collection port, and a return port. Mercury was added to the working electrode side to form a pool of mercury ~1 cm deep. The supporting electrolyte was 0.25 M Et_4NBr in acetonitrile. Carbon disulfide was added to the working side to make a 0.5 M solution of carbon disulfide in acetonitrile. An insulated copper wire was used to make connection to the mercury pool. The DC current source was a Princeton Applied Research Model 273 potentiostat. The potential was progressively stepped negative from 0.0 V (vs. Ag/AgCl reference) until a yellow color formed at the Pt basket and an orange color developed at

the surface of the mercury. Typical potentials were between -1 V and -2 V (depending on the drift of the Ag/AgCl reference) with typical currents from 100 mA to 400 mA. As product formed and crystallized as orange crystals, the mercury surface is obscured. Very slow stirring was used to gently suspend the formed crystals and renew the mercury surface while keeping the highest radical concentration at the surface of the electrode. The reference electrode drifts throughout the experiment and the carbon disulfide and supporting electrolyte are consumed during the reaction, and so the current must be carefully monitored. When necessary, the counter electrode chamber was exchanged with fresh electrolyte, additional carbon disulfide was added to the working electrode chamber, or the entire setup was cleaned and remade.

Product was harvested through continuous collection from the surface or solution by pipetting aliquots into a syringe fitted with a cotton filter plug, which returned the electrolyte filtrate to the reaction or a collection flask, which was occasionally decanted to return electrolyte to the reaction. Crude product was suspended in cold acetonitrile to remove excess electrolyte or byproducts, decanted from any mercury, and collected by centrifugation or filtration under an inert atmosphere. Immediate removal (by placing under high vacuum) from excess carbon disulfide and solvent was required to prevent decomposition of the material Further purification can be done by recrystallization from degassed methanol or by dissolving in degassed water and precipitating by addition of degassed acetone.

7.6.4 *Polymerization of Poly(nickel tetrathiooxalate) Tetraethylammonium Salt (TEA[NiTTO])*

To a 50-mL round bottom flask was added TEA_2TTO (1.032 g, 2.5 mmol, 1.0 equiv.) and a stir bar. DMF (20 mL) and MeOH (5 mL) were added via syringe. Separately, nickel(II) acetate tetrahydrate (622 mg, 2.5 mmol, 1.0 equiv.) was dissolved in MeOH (5 mL) The nickel solution was added slowly to the TTO monomer with vigorous stirring at room temperature. A black precipitate immediately forms upon addition. The reaction was stirred overnight. The black powder was collected on a 0.45 micron nylon filter, washed with MeOH, water, MeOH, and ether. The product was dried under high vacuum overnight.

Yield: 642 mg

7.6.5 *Alkali Metal NiTTOs*

The counterion exchange was performed directly before the polymerization procedure due to the instability of the alkali TTO salts. The procedure for counterion exchange is given with each M[NiTTO] synthesis.

7.6.5.1 Polymerization of poly(nickel tetrathiooxalate) lithium salt (Li[NiTTO])

In a dry 50-mL single neck round bottom flask, $LiBPh_4 \cdot 3$(MeOEtEtOMe) (2.625 g, 4.4 mmol, 2.2 equiv.) was dissolved in MeOH (~20 mL). TEA_2TTO (825.5 mg, 2.0 mmol, 1.0 equiv.) was added in one portion. The reaction was stirred at room temperature for one hour. Immediately, white precipitate formed from the solution, and the solvent became a dark red color. Filtering ultrafine solids via cannula filtration is exceedingly difficult. Under an argon blanket, the contents of the flask were added to a 50 mL centrifuge

tube. The transfer was aided with MeOH (~20 mL). The reaction was centrifuged (5 min @ 3000 rpm), during which the fine white precipitate – $TEABPh_4$ – settled out. Under an argon blanket, the supernatant was transferred to clean, dry 100 mL round bottom flask with stir bar. The MeOH was removed under high vacuum, yielding a dark red solid with some white precipitate remaining.

The newly synthesized Li_2TTO was dissolved in DMF (20 mL) and heated to 60 °C. Separately, $Ni(II)OAc_2$ (353.56 mg, 2.0 mmol, 1.0 equiv.) was suspended in DMF (20 mL). The slurry of Ni(II) was transferred by syringe to the Li_2TTO reaction, aided by DMF (10 mL). The reaction was heated for 24 hours at 60 C. The color of the reaction darkened to brown/black. The viscosity increased, but not precipitate or sol-gel formation was observed.

The reaction was cooled to r.t. and poured into a 4x volume of MeOH (200 mL). A fine suspension of Li[NiTTO] was observed. The precipitate was collected on a 0.45 um nylon filter, washed with ~100 mL portions of MeOH, 1:1 MeOH:H_2O, MeOH, and diethyl ether, and partially dried via filtration. The steel blue solid was dried under high vacuum overnight.

Yield: 276 mg

7.6.5.2 Polymerization of poly(nickel tetrathiooxalate) sodium salt in methanol (Na[NiTTO]-MeOH)

In a 250 ml RBF with stir bar, $NaBPh_4$(4.145 g, 12.11 mmol, 2.5 equiv.) was dissolved in MeOH (100 mL). TEA_2TTO (2000 mg, 4.845 mmol, 1.0 equiv.) was added in

one portion. Rapid precipitation of $TEABPh_4$ as a white powder was observed. Using Schlenk filtering techniques, the Na_2TTO was filtered through a paper filter and cotton ball directly into a solution of $Ni(II)OAc_2 \cdot 4H_2O$ (1.206 g, 4.84 mmol, 1.0 equiv.) in MeOH (100 mL). The transfer was aided with two additional portions of MeOH (2x10 mL). Immediate formation and precipitation of black P[Na(NiTTO)] was observed. Stirring was continued for 24 hours to ensure the reaction was complete. The precipitate was collected directly onto a 0.45 um nylon filter, washed with ~50 mL sequential portions of MeOH, H_2O, MeOH, and diethyl ether. The black solid was dried under high vacuum overnight.

Yield: 815 mg

7.6.5.3 Polymerization of poly(nickel tetrathiooxalate) sodium salt in DMF ($Na[NiTTO]\text{-}DMF_{A/B}$)

In a 100mL 2-neck round bottom flask, $NaBPh_4$ (1.459 g, 4.263 mmol, 2.2 equiv.) was dissolved in anhydrous MeOH (40 mL, ~0.1 M). TEATTO (800 mg, 1.938 mmol, 1.0 equiv.) was added in one portion. $TEABPh_4$ precipitates immediately upon formation, and the low solubility TEA_2TTO is continually brought into solution as Na_2TTO. The reaction was stirred for 2 hours, at which point no undissolved TEA_2TTO was observed. An inert filtering device was constructed from a 20-mL Luer-lock plastic syringe barrel using cotton as the filtering medium. The barrel was capped with a septum, attached to a separate dry 100 mL 2neck flask via an 18-gauge needle through the flask's top septum, and purged by subjecting the flask to 3 evacuation-backfill cycles. The solution was cannulated into the syringe and through the cotton filter by applying vacuum to the empty

flask. The transfer was aided with 2x5mL washes of anhydrous MeOH. The clear, red solution was concentrated by heating at 40 °C under high vacuum to afford a dark red solid.

Separately, two portions of $Ni(II)OAc_2 \cdot 4H_2O$ (241 mg, 0.969 mmol, 0.5 equiv.) were prepared. One was dissolved in DMF (25 mL) in a dry vial (Solution A). The other was dissolved in DMF (50 mL) in a dry 100 mL flask (Solution B) at 80 °C. The Na_2TTO solid was fully dissolved in DMF (50 mL). 25 mL of this solution was removed by syringe and added slowly to Solution B. Another portion of DMF (25 mL) was added to the remaining Na_2TTO and heated to 80 °C to return the overall volume to 50 mL. Solution A of Ni(II) was added slowly to the TTO monomer.

Both reactions were heated for 24 hours at 80 °C, then poured into 300 mL MeOH. A fine suspension of P[Na(NiTTO)] was observed for both A and B. The precipitate was collected directly onto a 0.45 micron nylon filter, washed with ~50 mL sequential portions of MeOH, H_2O, MeOH, and diethyl ether. The steel blue solid was dried under high vacuum overnight.

Yield: A: 233 mg B: 229 mg

A and B did not yield significantly different materials by elemental analysis, and reaction A was used as Na[NiTTO]-DMF in this study.

7.6.5.4 Polymerization of poly(nickel tetrathiooxalate) potassium salt (K[NiTTO])

In a dry 50-mL single neck RBF, $KBPh_4$ (1.58 g, 4.4 mmol, 2.2 equiv.) was dissolved in MeOH (~20 mL). TEA_2TTO (825.5 mg, 2.0 mmol, 1.0 equiv.) was added in one portion. The reaction was stirred at room temperature for one hour. Immediately, white

precipitate formed from the solution, and the solvent became a dark red color. Filtering ultrafine solids via cannula filtration is exceedingly difficult. Under an argon blanket, the contents of the flask were added to a 50 mL centrifuge tube. The transfer was aided with MeOH (~20 mL). The reaction was centrifuged (5 min @ 3000 rpm), during which the fine white precipitate – $TEABPh_4$ – settled out. Under an argon blanket, the supernatant was transferred to clean, dry 100 mL RBF with stir bar. The MeOH was removed under high vacuum, yielding a dark red solid with some white precipitate remaining.

The newly synthesized K_2TTO was dissolved in DMF (20 mL) and heated to 60 °C. Separately, $Ni(II)OAc_2$ (353.56 mg, 2.0 mmol, 1.0 equiv.) was suspended in DMF (20 mL). The slurry of Ni(II) was transferred by syringe to the K_2TTO reaction, aided by DMF (10 mL). The reaction was heated for 24 hours at 60 °C. The color of the reaction darkened to brown/black. The viscosity increased, but not precipitate or sol-gel formation was observed.

The reaction was cooled to r.t. and poured into a 4x volume of MeOH (200 mL). A fine suspension of K[NiTTO] was observed. The precipitate was collected on a 0.45 um nylon filter, washed with ~100 mL portions of MeOH, 1:1 MeOH:H_2O, MeOH, and diethyl ether, and partially dried via filtration. The steel blue solid was dried under high vacuum overnight.

Yield: 386 mg

7.6.5.5 Polymerization of poly(nickel tetrathiooxalate) rubidium salt (Rb[NiTTO])

To an argon-purged 50-mL HDPE centrifuge tube was added $RbBPh_4$ (1185 mg, 2.93 mmol, 2.2 equiv.) and TEA_2TTO (549.5 mg, 1.33 mmol, 1.0 equiv.). MeOH (20 mL) was added under an argon blanket. The reaction was sealed and briefly sonicated to complete the ion exchange. The reaction was centrifuged (5 min @ 2500 rpm). The clear, red supernatant was decanted into a dry 100 mL RBF w/ stir bar under an argon blanket. An additional portion of MeOH (7 mL) was added to the centrifuge tube, sonicated, centrifuged, and decanted in order to complete the transfer of Rb_2TTO. The MeOH was removed under high vacuum at 30 °C.

The newly synthesized Rb_2TTO was dissolved in DMF (40 mL) and heated to 60 °C. $Ni(II)OAc_2$ (235 mg, 1.33 mmol, 1.0 equiv.) was added in one portion against a positive argon flow. The reaction was heated for 24 hours at 60 °C. The color of the reaction darkened to brown/black. The viscosity increased, but not precipitate or sol-gel formation was observed. At 24 hours, some precipitate could be found along the sides of the flask.

The reaction was cooled to r.t. and poured into a 4x volume of MeOH (200 mL). A fine suspension of Rb[NiTTO] was observed. The precipitate was collected on a 0.45 um nylon filter, washed with ~100 mL portions of MeOH, 1:1 MeOH:H_2O, MeOH, and diethyl ether, and partially dried via filtration. The first portion of DMF:MeOH and MeOH washes were light green in color, possibly due to excess $Ni(II)OAc_2$ being removed. The solid was dried under high vacuum overnight.

Yield: 263 mg

7.6.5.6 Polymerization of poly(nickel tetrathiooxalate) cesium salt (Cs[NiTTO])

To an argon-purged 50-mL HDPE centrifuge tube was added $CsBPh_4$ (1184 mg, 2.38 mmol, 2.2 equiv.) and TEA_2TTO (490 mg, 1.19 mmol, 1.0 equiv.). MeOH (20 mL) was added under an argon blanket. The reaction was sealed and briefly sonicated to complete the ion exchange. The reaction was centrifuged (5 min @ 2500 rpm). The clear, red supernatant was decanted into a dry 100 mL RBF w/ stir bar under an argon blanket. An additional portion of MeOH (7 mL) was added to the centrifuge tube, sonicated, centrifuged, and decanted in order to complete the transfer of Cs_2TTO. The MeOH was removed under high vacuum at 30 °C.

The newly synthesized Cs_2TTO was dissolved in DMF (40 mL) and heated to 60 °C. $Ni(II)OAc_2$ (210 mg, 1.19 mmol, 1.0 equiv.) was added in one portion against a positive argon flow. The reaction was heated for 24 hours at 60 °C. The color of the reaction darkened to brown/black. The viscosity increased, but not precipitate or sol-gel formation was observed. At 24 hours, some precipitate could be found along the sides of the flask.

The reaction was cooled to r.t. and poured into a 4x volume of MeOH (200 mL). A fine suspension of Cs[NiTTO] was observed. The precipitate was collected on a 0.45 um nylon filter, washed with ~100 mL portions of MeOH, 1:1 MeOH:H_2O, MeOH, and diethyl ether, and partially dried via filtration. The first portion of DMF:MeOH and MeOH washes were light green in color, possibly due to excess $Ni(II)OAc_2$ being removed. The solid was dried under high vacuum overnight.

Yield: 211 mg

7.6.5.7 Combined Elemental Analysis

Table 7.2 – Combined elemental analysis of NiTTO polymers. [a]Obtained from combustion analysis. [b]Obtained from ICP-OES. [c]M = Li, Na, or K. [d]Rb and Cs were not able to be measured on ICP-OES. [e]ICP-OES was not performed on TEA[NiTTO]

	LiNiTTO	NaNiTTO -DMF$_A$	KNiTTO	RbNiTTO	CsNiTTO	TEANiTTO
C[a]	13.4	16.7	14.9	25.3	24.6	28.2
H[a]	1.2	2.3	1.3	4.2	4.2	4.3
N[a]	0.4	3.2	1.2	2.7	2.6	3.5
S[a]	48.7	40.7	49.1	38.2	38.5	43.8
Ni[b]	24.63	21.45	24.15	16.92	17.39	-[e]
M[b,c]	0.00[d]	0.37	0.78	-[d]	-[d]	-[e]
S:C	1.36	0.92	1.24	0.57	0.59	0.58
S:Ni	3.62	3.47	3.72	4.13	4.05	-
C:Ni	2.66	3.79	3.01	7.32	6.91	-
M[c]:Ni	0.00	0.04	0.05	-	-	-
Ni:M[c]	-	22.71	20.62	-	-	-

7.6.6 *^{13}C Solid State-NMR spectroscopy*

To test whether ^{13}C SS-NMR spectroscopy could identify the carbon environment in a polymeric species with hydrogen containing counterions, TEA[NiTTO] was analyzed, Figure 7.6. The only detectable carbon signals were from tetraethylammonium. These peaks were broadened in comparison with $[TEA]_2[Ni(dmit)_2]$, likely due to the increased conductivity of the TEA[NiTTO] sample (0.28 S/cm). This confirms materials with higher conductivities and no hydrogen nuclei will not yield ^{13}C SS-NMR signals.

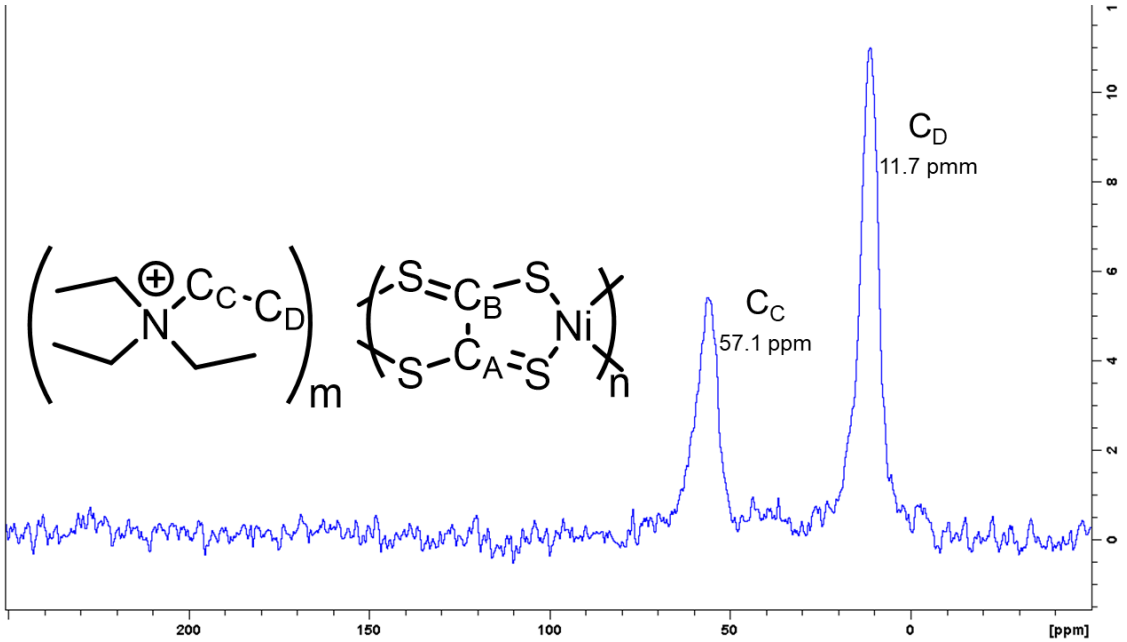

Figure 7.6 – ^{13}C SS-NMR (Variable-Amplitude Cross Polarization technique) spectrum of TEA[NiTTO] with only broad signals for tetraethylammonium

REFERENCES

(1) Shirakawa, H. The Discovery of Polyacetylene Film – the Dawning of an Era of Conducting Polymers. *Curr. Appl. Phys.* **2001**, *1* (4–5), 281–286 DOI: 10.1016/S1567-1739(01)00052-9.

(2) McNeill, R.; Siudak, R.; Wardlaw, J.; Weiss, D. Electronic Conduction in Polymers. I. The Chemical Structure of Polypyrrole. *Aust. J. Chem.* **1963**, *16* (6), 1056 DOI: 10.1071/CH9631056.

(3) Muspratt, J. S.; Hofmann, A. W. CXXVI. On Certain Processes in Which Anilene Is Formed. *Mem. Proc. Chem. Soc.* **1843**, *2*, 249 DOI: 10.1039/mp8430200249.

(4) Letheby, H. XXIX.—On the Production of a Blue Substance by the Electrolysis of Sulphate of Aniline. *J. Chem. Soc.* **1862**, *15* (161), 161–163 DOI: 10.1039/JS8621500161.

(5) Arroyave, F. A. Methodologies for the Synthesis of 3,4-Dioxypyrrole-Based π-Conjugated Materials, University of Florida, 2011.

(6) Grand, C. Controlling Electronic Properties and Morphology of Isoindigo-Based Polymers for Photovoltaic Applications, Georgia Institute of Technology, 2015.

(7) Teran, N. B. Customized Conjugation: Tailored π-Systems for Organic Electronic Applications, Georgia Institute of Technology, 2015.

(8) Tremblay, J.-F. The Rise of OLED Displays. *Chem. Eng. News* **2016**, *94* (28), 30–34 DOI: 10.1021/cen-09428-cover.

(9) Wong, W. W. H.; Banal, J. L.; Geraghty, P. B.; Hong, Q.; Zhang, B.; Holmes, A. B.; Jones, D. J. Organic Photovoltaic Materials-Design, Synthesis and Scale-Up. *Chem. Rec.* **2015**, *15* (6), 1006–1020 DOI: 10.1002/tcr.201500019.

(10) Zhang, G.; Zhao, J.; Chow, P. C. Y.; Jiang, K.; Zhang, J.; Zhu, Z.; Zhang, J.; Huang, F.; Yan, H. Nonfullerene Acceptor Molecules for Bulk Heterojunction Organic Solar Cells. *Chem. Rev.* **2018**, *118* (7), 3447–3507 DOI: 10.1021/acs.chemrev.7b00535.

(11) Luber, E. J.; Buriak, J. M. Reporting Performance in Organic Photovoltaic Devices. *ACS Nano* **2013**, *7* (6), 4708–4714 DOI: 10.1021/nn402883g.

(12) Roncali, J.; Leriche, P.; Blanchard, P. Molecular Materials for Organic Photovoltaics: Small Is Beautiful. *Adv. Mater.* **2014**, *26* (23), 3821–3838 DOI: 10.1002/adma.201305999.

(13) Lin, Y.; Zhan, X. Non-Fullerene Acceptors for Organic Photovoltaics: An Emerging

Horizon. *Mater. Horizons* **2014**, *1* (5), 470 DOI: 10.1039/C4MH00042K.

(14) Bharti, M.; Singh, A.; Samanta, S.; Aswal, D. K. Conductive Polymers for Thermoelectric Power Generation. *Prog. Mater. Sci.* **2018**, *93*, 270–310 DOI: 10.1016/j.pmatsci.2017.09.004.

(15) Russ, B.; Glaudell, A.; Urban, J. J.; Chabinyc, M. L.; Segalman, R. A. Organic Thermoelectric Materials for Energy Harvesting and Temperature Control. *Nat. Rev. Mater.* **2016**, *1* (10) DOI: 10.1038/natrevmats.2016.50.

(16) He, J.; Tritt, T. M. Advances in Thermoelectric Materials Research: Looking Back and Moving Forward. *Science* **2017**, *357* (6358), eaak9997 DOI: 10.1126/science.aak9997.

(17) Yang, L.; Chen, Z. G.; Dargusch, M. S.; Zou, J. High Performance Thermoelectric Materials: Progress and Their Applications. *Adv. Energy Mater.* **2017**, *1701797*, 1–28 DOI: 10.1002/aenm.201701797.

(18) Yao, H.; Fan, Z.; Cheng, H.; Guan, X.; Wang, C.; Sun, K.; Ouyang, J. Recent Development of Thermoelectric Polymers and Composites. *Macromol. Rapid Commun.* **2018**, *39* (6), 1700727 DOI: 10.1002/marc.201700727.

(19) Blackburn, J. L.; Ferguson, A. J.; Cho, C.; Grunlan, J. C. Carbon-Nanotube-Based Thermoelectric Materials and Devices. *Adv. Mater.* **2018**, *30* (11), 1704386 DOI: 10.1002/adma.201704386.

(20) Kerszulis, J. A. Reading the Rainbow : Tailoring the Properties of Electrochromic Polymers, Georgia Institute of Technology, 2014.

(21) Facchetti, A. Made to Order. *Nat. Mater.* **2013**, *12* (7), 598–600 DOI: 10.1038/nmat3686.

(22) Torsi, L.; Magliulo, M.; Manoli, K.; Palazzo, G. Organic Field-Effect Transistor Sensors: A Tutorial Review. *Chem. Soc. Rev.* **2013**, *42* (22), 8612 DOI: 10.1039/c3cs60127g.

(23) Sirringhaus, H. 25th Anniversary Article: Organic Field-Effect Transistors: The Path Beyond Amorphous Silicon. *Adv. Mater.* **2014**, *26* (9), 1319–1335 DOI: 10.1002/adma.201304346.

(24) Choi, D.; Chu, P.-H.; McBride, M.; Reichmanis, E. Best Practices for Reporting Organic Field Effect Transistor Device Performance. *Chem. Mater.* **2015**, *27* (12), 4167–4168 DOI: 10.1021/acs.chemmater.5b01982.

(25) Wu, X.; Mao, S.; Chen, J.; Huang, J. Strategies for Improving the Performance of Sensors Based on Organic Field-Effect Transistors. *Adv. Mater.* **2018**, *30* (17), 1705642 DOI: 10.1002/adma.201705642.

(26) Inal, S.; Rivnay, J.; Suiu, A.-O.; Malliaras, G. G.; McCulloch, I. Conjugated Polymers in Bioelectronics. *Acc. Chem. Res.* **2018**, *51* (6), 1368–1376 DOI: 10.1021/acs.accounts.7b00624.

(27) Rivnay, J.; Inal, S.; Salleo, A.; Owens, R. M.; Berggren, M.; Malliaras, G. G. Organic Electrochemical Transistors. *Nat. Rev. Mater.* **2018**, *3* (2), 17086 DOI: 10.1038/natrevmats.2017.86.

(28) Zhang, X.; Bäuerle, P.; Aida, T.; Skabara, P.; Kagan, C. *Organic Electronics for a Better Tomorrow: Innovation, Accessibility, Sustainability*; San Fransisco, California, 2012.

(29) Yee, S. K.; LeBlanc, S.; Goodson, K. E.; Dames, C. $ per W Metrics for Thermoelectric Power Generation: Beyond ZT. *Energy Environ. Sci.* **2013**, *6* (9), 2561–2571 DOI: 10.1039/C3EE41504J.

(30) Moliton, A.; Hiorns, R. C. The Origin and Development of (Plastic) Organic Electronics. *Polym. Int.* **2012**, *61* (3), 337–341 DOI: 10.1002/pi.4173.

(31) Darling, S. B.; You, F. The Case for Organic Photovoltaics. *RSC Adv.* **2013**, *3* (39), 17633–17648 DOI: 10.1039/c3ra42989j.

(32) Bell, L. E. Cooling, Heating, Generating Power, and Recovering Waste Heat with Thermoelectric Systems. *Science* **2008**, *321* (5895), 1457–1461 DOI: 10.1126/science.1158899.

(33) Carlson, R.; Hudlicky, T. On Hype, Malpractice, and Scientific Misconduct in Organic Synthesis. *Helv. Chim. Acta* **2012**, *95* (10), 2052–2062 DOI: 10.1002/hlca.201200431.

(34) Smith, A. B. Data Integrity. *Org. Lett.* **2013**, *15* (12), 2893–2894 DOI: 10.1021/ol401445g.

(35) Lowe, D. (Don't) Trust And (Don't) Verify http://blogs.sciencemag.org/pipeline/archives/2009/03/23/dont_trust_and_dont_verify (accessed May 13, 2018).

(36) Jogalekar, A. What is chemical intuition? https://blogs.scientificamerican.com/the-curious-wavefunction/what-is-chemical-intuition.

(37) Frontier, A. May Require Mojo http://www2.chem.rochester.edu/~nvd/pages/collective_wisdom.php?page=mojo (accessed May 14, 2018).

(38) Singh, D.; Alberto, E. E.; Rodrigues, O. E. D.; Braga, A. L. Eco-Friendly Cross-Coupling of Diaryl Diselenides with Aryl and Alkyl Bromides Catalyzed by CuO Nanopowder in Ionic Liquid. *Green Chem.* **2009**, *11* (10), 1521 DOI: 10.1039/b916266f.

(39) Sueki, S.; Kuninobu, Y. Copper-Catalyzed *N*- and *O*-Alkylation of Amines and Phenols Using Alkylborane Reagents. *Org. Lett.* **2013**, *15* (7), 1544–1547 DOI: 10.1021/ol400323z.

(40) Nicolaou, K. C.; Montagnon, T.; Baran, P. S.; Zhong, Y.-L. Iodine(V) Reagents in Organic Synthesis. Part 4. *o*-Iodoxybenzoic Acid as a Chemospecific Tool for Single Electron Transfer-Based Oxidation Processes. *J. Am. Chem. Soc.* **2002**, *124* (10), 2245–2258 DOI: 10.1021/ja012127+.

(41) Sun, C.-L.; Li, H.; Yu, D.-G.; Yu, M.; Zhou, X.; Lu, X.-Y.; Huang, K.; Zheng, S.-F.; Li, B.-J.; Shi, Z.-J. An Efficient Organocatalytic Method for Constructing Biaryls through Aromatic C–H Activation. *Nat. Chem.* **2010**, *2* (12), 1044–1049 DOI: 10.1038/nchem.862.

(42) Baker, M. Over Half of Psychology Studies Fail Reproducibility Test. *Nature* **2015**, 3–5 DOI: 10.1038/nature.2015.18248.

(43) Niven, D. J.; McCormick, T. J.; Straus, S. E.; Hemmelgarn, B. R.; Jeffs, L.; Barnes, T. R. M.; Stelfox, H. T. Reproducibility of Clinical Research in Critical Care: A Scoping Review. *BMC Med.* **2018**, *16* (1), 26 DOI: 10.1186/s12916-018-1018-6.

(44) Baker, M. 1,500 Scientists Lift the Lid on Reproducibility. *Nature* **2016**, *533* (7604), 452–454 DOI: 10.1038/533452a.

(45) Danheiser, R. L. Organic Syntheses: The "Gold Standard" in Experimental Synthetic Organic Chemistry. *Org. Synth.* **2011**, *88* (September), 1 DOI: 10.15227/orgsyn.088.0001.

(46) Blog Syn http://blog-syn.blogspot.com.

(47) *The Merriam-Webster Dictionary*; Merriam Webster Inc: Springfield, MA, 2016.

(48) History | The Perth Mint https://www.perthmint.com/visit_the_mint_the_perth_mint_history.aspx (accessed May 2, 2018).

(49) Organic Letters 2018 Guidelines for Authors https://pubs.acs.org/paragonplus/submission/orlef7/orlef7_authguide.pdf (accessed May 26, 2018).

(50) The Journal of Organic Chemistry Guidelines for Authors https://pubs.acs.org/paragonplus/submission/joceah/joceah_authguide.pdf.

(51) Kosugi, M.; Sasazawa, K.; Shimizu, Y.; Migita, T. Reactions of Allyltin Compounds III. Allylation of Aromatic Halides with Allyltributyltin in the Presence of Tetrakis(Triphenylphosphine)Palladium(0). *Chem. Lett.* **1977**, *6* (3), 301–302 DOI: 10.1246/cl.1977.301.

(52) Stille, J. K. The Palladium-Catalyzed Cross-Coupling Reactions of Organotin Reagents with Organic Electrophiles. *Angew. Chemie Int. Ed. English* **1986**, *25* (6), 508–524 DOI: 10.1002/anie.198605081.

(53) Espinet, P.; Echavarren, A. M. The Mechanisms of the Stille Reaction. *Angew. Chemie Int. Ed.* **2004**, 4704–4734 DOI: 10.1002/anie.200300638.

(54) Carsten, B.; He, F.; Son, H. J.; Xu, T.; Yu, L. Stille Polycondensation for Synthesis of Functional Materials. *Chem. Rev.* **2011**, *111* (3), 1493–1528 DOI: 10.1021/cr100320w.

(55) Bao, Z.; Chan, W. K.; Yu, L. Exploration of the Stille Coupling Reaction for the Synthesis of Functional Polymers. *J. Am. Chem. Soc.* **1995**, *117* (50), 12426–12435 DOI: 10.1021/ja00155a007.

(56) Kimbrough, R. D. Toxicity and Health Effects of Selected Organotin Compounds: A Review. *Environ. Health Perspect.* **1976**, *vol.14* (April), 51–56 DOI: 10.1289/ehp.761451.

(57) Boyer, I. J. Toxicity of Dibutyltin, Tributyltin and Other Organotin Compounds to Humans and to Experimental Animals. *Toxicology* **1989**, *55* (3), 253–298 DOI: 10.1016/0300-483X(89)90018-8.

(58) Penninks, A. H.; Seinen, W. Toxicity of Organotin Compounds IV. Impairment of Energy Metabolism of Rat Thymocytes by Various Dialkyltin Compounds. *Toxicol. Appl. Pharmacol.* **1980**, *56* (2), 221–231 DOI: 10.1016/0041-008X(80)90293-8.

(59) Snoeij, N. J.; Penninks, A. H.; Seinen, W. Biological Activity of Organotin Compounds—An Overview. *Environ. Res.* **1987**, *44* (2), 335–353 DOI: 10.1016/S0013-9351(87)80242-6.

(60) Graf, G. G. Tin, Tin Alloys, and Tin Compounds. In *Ullmann's Encyclopedia of Industrial Chemistry*; Wiley-VCH Verlag GmbH & Co. KGaA: Weinheim, Germany, 2000.

(61) Nath, M. Toxicity and the Cardiovascular Activity of Organotin Compounds: A Review. *Appl. Organomet. Chem.* **2008**, *22* (10), 598–612 DOI: 10.1002/aoc.1436.

(62) Coffin, R. C.; Peet, J.; Rogers, J. T.; Bazan, G. C. Streamlined Microwave-Assisted Preparation of Narrow-Bandgap Conjugated Polymers for High-Performance Bulk Heterojunction Solar Cells. *Nat. Chem.* **2009**, *1* (8), 657–661 DOI: 10.1038/nchem.403.

(63) Farina, V.; Kapadia, S.; Krishnan, B.; Wang, C.; Liebeskind, L. S. On the Nature of the "Copper Effect" in the Stille Cross-Coupling. *J. Org. Chem.* **1994**, *59* (20), 5905–5911 DOI: 10.1021/jo00099a018.

(64) Mee, S. P. H.; Lee, V.; Baldwin, J. E. Stille Coupling Made Easier—The Synergic

Effect of Copper(I) Salts and the Fluoride Ion. *Angew. Chemie Int. Ed.* **2004**, *43* (9), 1132–1136 DOI: 10.1002/anie.200352979.

(65) Farina, V.; Krishnan, B. Large Rate Accelerations in the Stille Reaction with Tri-2-Furylphosphine and Triphenylarsine as Palladium Ligands: Mechanistic and Synthetic Implications. *J. Am. Chem. Soc.* **1991**, *113* (25), 9585–9595 DOI: 10.1021/ja00025a025.

(66) Hoshino, S.; Yoshida, M.; Uemura, S.; Kodzasa, T.; Takada, N.; Kamata, T.; Yase, K. Influence of Moisture on Device Characteristics of Polythiophene-Based Field-Effect Transistors. *J. Appl. Phys.* **2004**, *95* (9), 5088–5093 DOI: 10.1063/1.1691190.

(67) Graham, K. R.; Mei, J.; Stalder, R.; Shim, J. W.; Cheun, H.; Steffy, F.; So, F.; Kippelen, B.; Reynolds, J. R. Polydimethylsiloxane as a Macromolecular Additive for Enhanced Performance of Molecular Bulk Heterojunction Organic Solar Cells. *ACS Appl. Mater. Interfaces* **2011**, *3* (4), 1210–1215 DOI: 10.1021/am2000328.

(68) Odian, G. *Principles of Polymerization*, 4th ed.; John Wiley & Sons, Inc.: Hoboken, NJ, 2004.

(69) Kline, R. J.; McGehee, M. D.; Kadnikova, E. N.; Liu, J.; Fréchet, J. M. J. Controlling the Field-Effect Mobility of Regioregular Polythiophene by Changing the Molecular Weight. *Adv. Mater.* **2003**, *15* (18), 1519–1522 DOI: 10.1002/adma.200305275.

(70) Chang, J.-F.; Clark, J.; Zhao, N.; Sirringhaus, H.; Breiby, D. W.; Andreasen, J. W.; Nielsen, M. M.; Giles, M.; Heeney, M.; McCulloch, I. Molecular-Weight Dependence of Interchain Polaron Delocalization and Exciton Bandwidth in High-Mobility Conjugated Polymers. *Phys. Rev. B* **2006**, *74* (11), 115318 DOI: 10.1103/PhysRevB.74.115318.

(71) Ballantyne, A. M.; Chen, L.; Dane, J.; Hammant, T.; Braun, F. M.; Heeney, M.; Duffy, W.; McCulloch, I.; Bradley, D. D. C.; Nelson, J. The Effect of Poly(3-Hexylthiophene) Molecular Weight on Charge Transport and the Performance of Polymer:Fullerene Solar Cells. *Adv. Funct. Mater.* **2008**, *18* (16), 2373–2380 DOI: 10.1002/adfm.200800145.

(72) Hayashi, S.; Yamamoto, S.; Koizumi, T. Effects of Molecular Weight on the Optical and Electrochemical Properties of EDOT-Based π-Conjugated Polymers. *Sci. Rep.* **2017**, *7* (1), 1078 DOI: 10.1038/s41598-017-01132-5.

(73) Noriega, R.; Rivnay, J.; Vandewal, K.; Koch, F. P. V; Stingelin, N.; Smith, P.; Toney, M. F.; Salleo, A. A General Relationship between Disorder, Aggregation and Charge Transport in Conjugated Polymers. *Nat. Mater.* **2013**, *12* (11), 1038–1044 DOI: 10.1038/nmat3722.

(74) Li, W.; Yang, L.; Tumbleston, J. R.; Yan, L.; Ade, H.; You, W. Controlling Molecular Weight of a High Efficiency Donor-Acceptor Conjugated Polymer and Understanding Its Significant Impact on Photovoltaic Properties. *Adv. Mater.* **2014**,

26 (26), 4456–4462 DOI: 10.1002/adma.201305251.

(75) Tong, M.; Cho, S.; Rogers, J. T.; Schmidt, K.; Hsu, B. B. Y.; Moses, D.; Coffin, R. C.; Kramer, E. J.; Bazan, G. C.; Heeger, A. J. Higher Molecular Weight Leads to Improved Photoresponsivity, Charge Transport and Interfacial Ordering in a Narrow Bandgap Semiconducting Polymer. *Adv. Funct. Mater.* **2010**, *20* (22), 3959–3965 DOI: 10.1002/adfm.201001271.

(76) Farina, V.; Krishnan, B.; Marshall, D. R.; Roth, G. P. Palladium-Catalyzed Coupling of Arylstannanes with Organic Sulfonates: A Comprehensive Study. *J. Org. Chem.* **1993**, *58* (20), 5434–5444 DOI: 10.1021/jo00072a028.

(77) Ritter, S. K. Chemists Introduce a User's Guide for Palladium Acetate. *Chemical & Engineering News*. 2016, pp 20–21.

(78) Hassan, J.; Sévignon, M.; Gozzi, C.; Schulz, E.; Lemaire, M. Aryl−Aryl Bond Formation One Century after the Discovery of the Ullmann Reaction. *Chem. Rev.* **2002**, *102* (5), 1359–1470 DOI: 10.1021/cr000664r.

(79) Amatore, C.; Jutand, A.; Thuilliez, A. Formation of Palladium(0) Complexes from $Pd(OAc)_2$ and a Bidentate Phosphine Ligand (dppp) and Their Reactivity in Oxidative Addition. *Organometallics* **2001**, *20* (15), 3241–3249 DOI: 10.1021/om0101137.

(80) Carole, W. A.; Colacot, T. J. Understanding Palladium Acetate from a User Perspective. *Chem. - A Eur. J.* **2016**, *22* (23), 7686–7695 DOI: 10.1002/chem.201601450.

(81) Carole, W. A.; Bradley, J.; Sarwar, M.; Colacot, T. J. Can Palladium Acetate Lose Its "Saltiness"? Catalytic Activities of the Impurities in Palladium Acetate. *Org. Lett.* **2015**, *17* (21), 5472–5475 DOI: 10.1021/acs.orglett.5b02835.

(82) Nyman, C. J.; Wymore, C. E.; Wilkinson, G. Reactions of Tris(Triphenylphosphine)Platinum(0) and Tetrakis(Triphenylphosphine)Palladium(0) with Oxygen and Carbon Dioxide. *J. Chem. Soc. A Inorganic, Phys. Theor.* **1968**, 561 DOI: 10.1039/j19680000561.

(83) Zalesskiy, S. S.; Ananikov, V. P. $Pd_2(dba)_3$ as a Precursor of Soluble Metal Complexes and Nanoparticles: Determination of Palladium Active Species for Catalysis and Synthesis. *Organometallics* **2012**, *31* (6), 2302–2309 DOI: 10.1021/om201217r.

(84) Fleckenstein, C. A.; Plenio, H. Sterically Demanding Trialkylphosphines for Palladium-Catalyzed Cross Coupling Reactions—alternatives to $PtBu_3$. *Chem. Soc. Rev.* **2010**, *39* (2), 694–711 DOI: 10.1039/B903646F.

(85) Beletskaya, I. P. The Cross-Coupling Reactions of Organic Halides with Organic Derivatives of Tin, Mercury and Copper Catalyzed by Palladium. *J. Organomet.*

Chem. **1983**, *250* (1), 551–564 DOI: 10.1016/0022-328X(83)85077-3.

(86) Segelstein, B. E.; Butler, T. W.; Chenard, B. L. Equilibration of the Oxidative Addition Product of Tetrakis(Triphenylphosphine)Palladium and Electron-Rich Aryl Halides Leads to Product Scrambling in the Stille Reaction. *J. Org. Chem.* **1995**, *60* (1), 12–13 DOI: 10.1021/jo00106a006.

(87) Kong, K. C.; Cheng, C. H. Facile Aryl-Aryl Exchange between the Palladium Center and Phosphine Ligands in Palladium(II) Complexes. *J. Am. Chem. Soc.* **1991**, *113* (16), 6313–6315 DOI: 10.1021/ja00016a082.

(88) Morita, D. K.; Stille, J. K.; Norton, J. R. Methyl/Phenyl Exchange between Palladium and a Phosphine Ligand. Consequences for Catalytic Coupling Reactions. *J. Am. Chem. Soc.* **1995**, *117* (33), 8576–8581 DOI: 10.1021/ja00138a012.

(89) Grushin, V. V. Thermal Stability, Decomposition Paths, and Ph/Ph Exchange Reactions of $[(Ph_3P)_2Pd(Ph)X]$ (X = I, Br, Cl, F, and HF_2). *Organometallics* **2000**, *19* (10), 1888–1900 DOI: 10.1021/om0001265.

(90) Kaake, L. G.; Barbara, P. F.; Zhu, X.-Y. Intrinsic Charge Trapping in Organic and Polymeric Semiconductors: A Physical Chemistry Perspective. *J. Phys. Chem. Lett.* **2010**, *1* (3), 628–635 DOI: 10.1021/jz9002857.

(91) Vangerven, T.; Verstappen, P.; Drijkoningen, J.; Dierckx, W.; Himmelberger, S.; Salleo, A.; Vanderzande, D.; Maes, W.; Manca, J. V. Molar Mass versus Polymer Solar Cell Performance: Highlighting the Role of Homocouplings. *Chem. Mater.* **2015**, *27* (10), 3726–3732 DOI: 10.1021/acs.chemmater.5b00939.

(92) Vangerven, T.; Verstappen, P.; Patil, N.; D'Haen, J.; Cardinaletti, I.; Benduhn, J.; Van den Brande, N.; Defour, M.; Lemaur, V.; Beljonne, D.; Lazzaroni, R.; Champagne, B.; Vandewal, K.; Andreasen, J. W.; Adriaensens, P.; Breiby, D. W.; Van Mele, B.; Vanderzande, D.; Maes, W.; Manca, J. Elucidating Batch-to-Batch Variation Caused by Homocoupled Side Products in Solution-Processable Organic Solar Cells. *Chem. Mater.* **2016**, *28* (24), 9088–9098 DOI: 10.1021/acs.chemmater.6b04143.

(93) Hendriks, K. H.; Li, W.; Heintges, G. H. L.; van Pruissen, G. W. P.; Wienk, M. M.; Janssen, R. a J. Homo-Coupling Defects in Diketopyrrolopyrrole Based Co-Polymers and Their Effect on Photovoltaic Performance. *J. Am. Chem. Soc.* **2014**, *136* (31), 11128–11133 DOI: 10.1021/ja505574a.

(94) Krebs, F. C.; Nyberg, R. B.; Jørgensen, M. Influence of Residual Catalyst on the Properties of Conjugated Polyphenylenevinylene Materials: Palladium Nanoparticles and Poor Electrical Performance. *Chem. Mater.* **2004**, *16* (7), 1313–1318 DOI: 10.1021/cm035205w.

(95) Estrada, L. A.; Deininger, J. J.; Kamenov, G. D.; Reynolds, J. R. Direct (Hetero)Arylation Polymerization: An Effective Route to 3,4-

Propylenedioxythiophene-Based Polymers with Low Residual Metal Content. *ACS Macro Lett.* **2013**, *2* (10), 869–873 DOI: 10.1021/mz4003886.

(96) Erwin, M. M.; McBride, J.; Kadavanich, A. V.; Rosenthal, S. J. Effects of Impurities on the Optical Properties of Poly-3-Hexylthiophene Thin Films. *Thin Solid Films* **2002**, *409* (2), 198–205 DOI: 10.1016/S0040-6090(02)00124-4.

(97) Kuwabara, J.; Yasuda, T.; Takase, N.; Kanbara, T. Effects of the Terminal Structure, Purity, and Molecular Weight of an Amorphous Conjugated Polymer on Its Photovoltaic Characteristics. *ACS Appl. Mater. Interfaces* **2016**, *8* (3), 1752–1758 DOI: 10.1021/acsami.5b09482.

(98) Park, J. K.; Jo, J.; Seo, J. H.; Moon, J. S.; Park, Y. D.; Lee, K.; Heeger, A. J.; Bazan, G. C. End-Capping Effect of a Narrow Bandgap Conjugated Polymer on Bulk Heterojunction Solar Cells. *Adv. Mater.* **2011**, *23* (21), 2430–2435 DOI: 10.1002/adma.201004629.

(99) Koldemir, U.; Puniredd, S. R.; Wagner, M.; Tongay, S.; McCarley, T. D.; Kamenov, G. D.; Müllen, K.; Pisula, W.; Reynolds, J. R. End Capping Does Matter: Enhanced Order and Charge Transport in Conjugated Donor–Acceptor Polymers. *Macromolecules* **2015**, *48* (18), 6369–6377 DOI: 10.1021/acs.macromol.5b01252.

(100) Leong, W. L.; Welch, G. C.; Kaake, L. G.; Takacs, C. J.; Sun, Y.; Bazan, G. C.; Heeger, A. J. Role of Trace Impurities in the Photovoltaic Performance of Solution Processed Small-Molecule Bulk Heterojunction Solar Cells. *Chem. Sci.* **2012**, *3* (6), 2103 DOI: 10.1039/c2sc20157g.

(101) Fulmer, G. R.; Miller, A. J. M.; Sherden, N. H.; Gottlieb, H. E.; Nudelman, A.; Stoltz, B. M.; Bercaw, J. E.; Goldberg, K. I. NMR Chemical Shifts of Trace Impurities: Common Laboratory Solvents, Organics, and Gases in Deuterated Solvents Relevant to the Organometallic Chemist. *Organometallics* **2010**, *29* (9), 2176–2179 DOI: 10.1021/om100106e.

(102) Yamazaki, K.; Kuwabara, J.; Kanbara, T. Detailed Optimization of Polycondensation Reaction via Direct C-H Arylation of Ethylenedioxythiophene. *Macromol. Rapid Commun.* **2013**, *34* (1), 69–73 DOI: 10.1002/marc.201200550.

(103) Lo, C. K.; Gautam, B. R.; Selter, P.; Zheng, Z.; Oosterhout, S. D.; Constantinou, I.; Knitsch, R.; Wolfe, R. M. W.; Yi, X.; Brédas, J.-L.; So, F.; Toney, M. F.; Coropceanu, V.; Hansen, M. R.; Gundogdu, K.; Reynolds, J. R. Every Atom Counts: Elucidating the Fundamental Impact of Structural Change in Conjugated Polymers for Organic Photovoltaics. *Chem. Mater.* **2018**, *30* (9), 2995–3009 DOI: 10.1021/acs.chemmater.8b00590.

(104) Nielsen, C. B.; Bjørnholm, T. New Regiosymmetrical Dioxopyrrolo- and Dihydropyrrolo-Functionalized Polythiophenes. *Org. Lett.* **2004**, *6* (19), 3381–3384 DOI: 10.1021/ol048659n.

(105) Armarego, W. L. F.; Chai, C. L. L. *Purification of Laboratory Chemicals*, 5th ed.

(106) Williams, D. B. G.; Lawton, M. Drying of Organic Solvents: Quantitative Evaluation of the Efficiency of Several Desiccants. *J. Org. Chem.* **2010**, *75* (24), 8351–8354 DOI: 10.1021/jo101589h.

(107) Burfield, D. R.; Smithers, R. H. Desiccant Efficiency in Solvent Drying. 3. Dipolar Aprotic Solvents. *J. Org. Chem.* **1978**, *43* (20), 3966–3968 DOI: 10.1021/jo00414a038.

(108) Lu, G.; Cai, C.; Lipshutz, B. H. Stille Couplings in Water at Room Temperature. *Green Chem.* **2013**, *15* (1), 105–109 DOI: 10.1039/C2GC36042J.

(109) Brown, J. N.; Hewins, M.; Van Der Linden, J. H. M.; Lynch, R. J. Solvent Degassing and Other Factors Affecting Liquid Chromatographic Detector Stability. *J. Chromatogr. A* **1981**, *204* (C), 115–122 DOI: 10.1016/S0021-9673(00)81646-5.

(110) Amb, C. M.; Chen, S.; Graham, K. R.; Subbiah, J.; Small, C. E.; So, F.; Reynolds, J. R. Dithienogermole as a Fused Electron Donor in Bulk Heterojunction Solar Cells. *J. Am. Chem. Soc.* **2011**, *133* (26), 10062–10065 DOI: 10.1021/ja204056m.

(111) Pirotte, G.; Agarkar, S.; Xu, B.; Zhang, J.; Lutsen, L.; Vanderzande, D.; Yan, H.; Pollet, P.; Reynolds, J. R.; Maes, W.; Marder, S. R. Molecular Weight Tuning of Low Bandgap Polymers by Continuous Flow Chemistry: Increasing the Applicability of PffBT4T for Organic Photovoltaics. *J. Mater. Chem. A* **2017**, *5* (34), 18166–18175 DOI: 10.1039/C7TA05627C.

(112) Gibson, G. L.; Gao, D.; Jahnke, A. A.; Sun, J.; Tilley, A. J.; Seferos, D. S. Molecular Weight and End Capping Effects on the Optoelectronic Properties of Structurally Related 'Heavy Atom' Donor–acceptor Polymers. *J. Mater. Chem. A* **2014**, *2* (35), 14468–14480 DOI: 10.1039/C4TA02820A.

(113) Cheng, K. L.; Ueno, K.; Imamura, T. CRC Handbook of Organic Analytical Reagents, Second Edition. In *CRC Handbook of Organic Analytical Reagents, Second Edition*; CRC PRess, 1995; pp 462–465.

(114) Gao, J.; Wang, W.; Zhang, S.; Xiao, S.; Zhan, C.; Yang, M.; Lu, X.; You, W. Distinction between PTB7-Th Samples Prepared from $Pd(PPh_3)_4$ and $Pd_2(dba)_3$/P(*o*-Tol)$_3$ Catalysed Stille Coupling Polymerization and the Resultant Photovoltaic Performance. *J. Mater. Chem. A* **2018**, *6* (1), 179–188 DOI: 10.1039/C7TA09464G.

(115) Dean, J. A. *Lange's Handbook of Chemistry*, 15th ed.; McGraw-Hill, 1998.

(116) Walsh, R. Bond Dissociation Energy Values in Silicon-Containing Compounds and Some of Their Implications. *Acc. Chem. Res.* **1981**, *14* (8), 246–252 DOI: 10.1021/ar00068a004.

(117) Weast, R.; Astle, M.; Beyer, W. *CRC Handbook of Chemistry and Physics*; 2005.

(118) Rosen, B. R.; Werner, E. W.; O'Brien, A. G.; Baran, P. S. Total Synthesis of Dixiamycin B by Electrochemical Oxidation. *J. Am. Chem. Soc.* **2014**, *136* (15), 5571–5574 DOI: 10.1021/ja5013323.

(119) Gütz, C.; Stenglein, A.; Waldvogel, S. R. Highly Modular Flow Cell for Electroorganic Synthesis. *Org. Process Res. Dev.* **2017**, *21* (5), 771–778 DOI: 10.1021/acs.oprd.7b00123.

(120) Atobe, M.; Tateno, H.; Matsumura, Y. Applications of Flow Microreactors in Electrosynthetic Processes. *Chem. Rev.* **2018**, *118* (9), 4541–4572 DOI: 10.1021/acs.chemrev.7b00353.

(121) Pletcher, D.; Green, R. A.; Brown, R. C. D. Flow Electrolysis Cells for the Synthetic Organic Chemistry Laboratory. *Chem. Rev.* **2018**, *118* (9), 4573–4591 DOI: 10.1021/acs.chemrev.7b00360.

(122) Frontana-Uribe, B. A.; Little, R. D.; Ibanez, J. G.; Palma, A.; Vasquez-Medrano, R. Organic Electrosynthesis: A Promising Green Methodology in Organic Chemistry. *Green Chem.* **2010**, *12* (12), 2099 DOI: 10.1039/c0gc00382d.

(123) Matthews, M. A. Green Electrochemistry. Examples and Challenges. *Pure Appl. Chem.* **2001**, *73* (8), 1305–1308 DOI: 10.1351/pac200173081305.

(124) Reynolds, J. R. Electrically Conducting Polymers, University of Massachusetts - Amherst, 1985.

(125) Breitzer, J. G.; Holloway, G. A.; Rauchfuss, T. B.; Salata, M. R.; Kee, C. L.; Yan, Y. K. Electrochemical Synthesis of Tetraethylammonium Tetrathiooxalate. *Inorg. Synth.* **2014**, *36*, 201–203 DOI: 10.1002/9781118744994.ch36.

(126) Jeroschewski, P. Elektrochemische Darstellung von Tetraalkylammoniumsalzen Der Tetrathiooxaisäure. *Zeitschrift für Chemie* **1981**, *21* (11), 412–412 DOI: 10.1002/zfch.19810211115.

(127) Reynolds, J. R.; Karasz, F. E.; Lillya, C. P.; Chien, J. C. W. Electrically Conducting Transition Metal Complexes of Tetrathio-Oxalate. *J. Chem. Soc. Chem. Commun.* **1985**, No. 5, 268 DOI: 10.1039/c39850000268.

(128) Wawzonek, S. Intermediates in the Electrochemical Reduction of Carbon Disulfide at a Mercury Cathode in Aprotic Solvents. *J. Electrochem. Soc.* **1983**, *130* (4), 803 DOI: 10.1149/1.2119808.

(129) Manjakkal, L.; Cvejin, K.; Kulawik, J.; Zaraska, K.; Szwagierczak, D.; Socha, R. P. Fabrication of Thick Film Sensitive RuO_2-TiO_2 and Ag/AgCl/KCl Reference Electrodes and Their Application for PH Measurements. *Sensors Actuators B Chem.* **2014**, *204*, 57–67 DOI: 10.1016/j.snb.2014.07.067.

(130) Oelßner, W.; Berthold, F.; Guth, U. The IR Drop – Well-Known but Often

Underestimated in Electrochemical Polarization Measurements and Corrosion Testing. *Mater. Corros.* **2006**, *57* (6), 455–466 DOI: 10.1002/maco.200603982.

(131) Elgrishi, N.; Rountree, K. J.; McCarthy, B. D.; Rountree, E. S.; Eisenhart, T. T.; Dempsey, J. L. A Practical Beginner's Guide to Cyclic Voltammetry. *J. Chem. Educ.* **2018**, *95* (2), 197–206 DOI: 10.1021/acs.jchemed.7b00361.

(132) Brownson, D. A. C.; Banks, C. E. Interpreting Electrochemistry. In *The Handbook of Graphene Electrochemistry*; Springer London: London, 2014; pp 23–77.

(133) Strong, F. C. Faraday's Laws in One Equation. *J. Chem. Educ.* **1961**, *38* (2), 98 DOI: 10.1021/ed038p98.

(134) Jensen, W. B. Faraday's Laws or Faraday's Law? *J. Chem. Educ.* **2012**, *89* (9), 1208–1209 DOI: 10.1021/ed101193q.

(135) Baur, J. E. Diffusion Coefficients. In *Handbook of Electrochemistry*; Elsevier, 2007; pp 829–848.

(136) Bond, A. M.; Oldham, K. B.; Snook, G. A. Use of the Ferrocene Oxidation Process to Provide Both Reference Electrode Potential Calibration and a Simple Measurement (via Semiintegration) of the Uncompensated Resistance in Cyclic Voltammetric Studies in High-Resistence Organic Solvents. *Anal. Chem.* **2000**, *72* (15), 3492–3496 DOI: 10.1021/ac000020j.

(137) Londenberg, J.; Saragi, T. P. I.; Suske, I.; Salbeck, J. 4,4′-Spirobi[Cyclopenta[2,1-b;3,4-b′]Dithiophene: A New Generation of Heterocyclic Spiro-Type Molecules. *Adv. Mater.* **2007**, *19* (22), 4049–4053 DOI: 10.1002/adma.200700401.

(138) Moudgil, K. Design and Development of Dimeric Sandwich Compounds as N-Dopants for Organic Electronics, Georgia Institute of Technology, 2016.

(139) DeAngelis, T. P.; Heineman, W. R. An Electrochemical Experiment Using an Optically Transparent Thin Layer Electrode. *J. Chem. Educ.* **1976**, *53* (9), 594 DOI: 10.1021/ed053p594.

(140) Dou, L.; You, J.; Hong, Z.; Xu, Z.; Li, G.; Street, R. A.; Yang, Y. 25th Anniversary Article: A Decade of Organic/Polymeric Photovoltaic Research. *Adv. Mater.* **2013**, *25* (46), 6642–6671 DOI: 10.1002/adma.201302563.

(141) Lu, L.; Zheng, T.; Wu, Q.; Schneider, A. M.; Zhao, D.; Yu, L. Recent Advances in Bulk Heterojunction Polymer Solar Cells. *Chem. Rev.* **2015**, *115* (23), 12666–12731 DOI: 10.1021/acs.chemrev.5b00098.

(142) Huang, H.; Yang, L.; Facchetti, A.; Marks, T. J. Organic and Polymeric Semiconductors Enhanced by Noncovalent Conformational Locks. *Chem. Rev.* **2017**, *117* (15), 10291–10318 DOI: 10.1021/acs.chemrev.7b00084.

(143) Hu, H.; Chow, P. C. Y.; Zhang, G.; Ma, T.; Liu, J.; Yang, G.; Yan, H. Design of Donor Polymers with Strong Temperature-Dependent Aggregation Property for Efficient Organic Photovoltaics. *Acc. Chem. Res.* **2017**, *50* (10), 2519–2528 DOI: 10.1021/acs.accounts.7b00293.

(144) Hou, J.; Inganäs, O.; Friend, R. H.; Gao, F. Organic Solar Cells Based on Non-Fullerene Acceptors. *Nat. Mater.* **2018**, *17* (2), 119–128 DOI: 10.1038/nmat5063.

(145) Yan, C.; Barlow, S.; Wang, Z.; Yan, H.; Jen, A. K. Y.; Marder, S. R.; Zhan, X. Non-Fullerene Acceptors for Organic Solar Cells. *Nat. Rev. Mater.* **2018**, *3* (3), 18003 DOI: 10.1038/natrevmats.2018.3.

(146) Root, S. E.; Savagatrup, S.; Printz, A. D.; Rodriquez, D.; Lipomi, D. J. Mechanical Properties of Organic Semiconductors for Stretchable, Highly Flexible, and Mechanically Robust Electronics. *Chem. Rev.* **2017**, *117* (9), 6467–6499 DOI: 10.1021/acs.chemrev.7b00003.

(147) Ibanez, J. G.; Rincón, M. E.; Gutierrez-Granados, S.; Chahma, M.; Jaramillo-Quintero, O. A.; Frontana-Uribe, B. A. Conducting Polymers in the Fields of Energy, Environmental Remediation, and Chemical–Chiral Sensors. *Chem. Rev.* **2018**, *118* (9), 4731–4816 DOI: 10.1021/acs.chemrev.7b00482.

(148) Chen, D.; Pei, Q. Electronic Muscles and Skins: A Review of Soft Sensors and Actuators. *Chem. Rev.* **2017**, *117* (17), 11239–11268 DOI: 10.1021/acs.chemrev.7b00019.

(149) Ambrosi, A.; Pumera, M. 3D-Printing Technologies for Electrochemical Applications. *Chem. Soc. Rev.* **2016**, *45* (10), 2740–2755 DOI: 10.1039/C5CS00714C.

(150) Gao, M.; Li, L.; Song, Y. Inkjet Printing Wearable Electronic Devices. *J. Mater. Chem. C* **2017**, *5* (12), 2971–2993 DOI: 10.1039/C7TC00038C.

(151) Po, R.; Bianchi, G.; Carbonera, C.; Pellegrino, A. "All That Glisters Is Not Gold": An Analysis of the Synthetic Complexity of Efficient Polymer Donors for Polymer Solar Cells. *Macromolecules* **2015**, *48* (3), 453–461 DOI: 10.1021/ma501894w.

(152) Pomerantz, M.; Amarasekara, A. S. Studies of Planar Poly(3,4-Disubstituted-Thiophenes). *Synth. Met.* **2003**, *135–136*, 257–258 DOI: 10.1016/S0379-6779(02)00670-7.

(153) Berrouard, P.; Dufresne, S.; Pron, A.; Veilleux, J.; Leclerc, M. Low-Cost Synthesis and Physical Characterization of Thieno[3,4-c]Pyrrole-4,6-Dione-Based Polymers. *J. Org. Chem.* **2012**, *77* (18), 8167–8173 DOI: 10.1021/jo301512e.

(154) Berrouard, P.; Najari, A.; Pron, A.; Gendron, D.; Morin, P.-O.; Pouliot, J.-R.; Veilleux, J.; Leclerc, M. Synthesis of 5-Alkyl[3,4-c]Thienopyrrole-4,6-Dione-Based Polymers by Direct Heteroarylation. *Angew. Chemie Int. Ed.* **2012**, *51* (9),

2068–2071 DOI: 10.1002/anie.201106411.

(155) Mercier, L. G.; Leclerc, M. Direct (Hetero)Arylation: A New Tool for Polymer Chemists. *Acc. Chem. Res.* **2013**, *46* (7), 1597–1605 DOI: 10.1021/ar3003305.

(156) Letizia, J. A.; Salata, M. R.; Tribout, C. M.; Facchetti, A.; Ratner, M. A.; Marks, T. J. N-Channel Polymers by Design: Optimizing the Interplay of Solubilizing Substituents, Crystal Packing, and Field-Effect Transistor Characteristics in Polymeric Bithiophene-Imide Semiconductors. *J. Am. Chem. Soc.* **2008**, *130* (30), 9679–9694 DOI: 10.1021/ja710815a.

(157) Guo, X.; Ortiz, R. P.; Zheng, Y.; Kim, M.; Zhang, S.; Hu, Y.; Lu, G.; Facchetti, A.; Marks, T. J. Thieno[3,4-c]Pyrrole-4,6-Dione-Based Polymer Semiconductors: Toward High-Performance, Air-Stable Organic Thin-Film Transistors. *J. Am. Chem. Soc.* **2011**, *133* (34), 13685–13697 DOI: 10.1021/ja205398u.

(158) Zhou, N.; Guo, X.; Ortiz, R. P.; Harschneck, T.; Manley, E. F.; Lou, S. J.; Hartnett, P. E.; Yu, X.; Horwitz, N. E.; Burrezo, P. M.; Aldrich, T. J.; López Navarrete, J. T.; Wasielewski, M. R.; Chen, L. X.; Chang, R. P. H.; Facchetti, A.; Marks, T. J. Marked Consequences of Systematic Oligothiophene Catenation in Thieno[3,4-c]Pyrrole-4,6-Dione and Bithiopheneimide Photovoltaic Copolymers. *J. Am. Chem. Soc.* **2015**, *137* (39), 12565–12579 DOI: 10.1021/jacs.5b06462.

(159) Guo, X.; Zhou, N.; Lou, S. J.; Smith, J.; Tice, D. B.; Hennek, J. W.; Ortiz, R. P.; Navarrete, J. T. L.; Li, S.; Strzalka, J.; Chen, L. X.; Chang, R. P. H.; Facchetti, A.; Marks, T. J. Polymer Solar Cells with Enhanced Fill Factors. *Nat. Photonics* **2013**, *7* (10), 825–833 DOI: 10.1038/nphoton.2013.207.

(160) Small, C. E.; Chen, S.; Subbiah, J.; Amb, C. M.; Tsang, S.; Lai, T.; Reynolds, J. R.; So, F. High-Efficiency Inverted Dithienogermole–thienopyrrolodione-Based Polymer Solar Cells. *Nat. Photonics* **2011**, *6* (2), 115–120 DOI: 10.1038/nphoton.2011.317.

(161) Jackson, N. E.; Savoie, B. M.; Kohlstedt, K. L.; Olvera de la Cruz, M.; Schatz, G. C.; Chen, L. X.; Ratner, M. A. Controlling Conformations of Conjugated Polymers and Small Molecules: The Role of Nonbonding Interactions. *J. Am. Chem. Soc.* **2013**, *135* (28), 10475–10483 DOI: 10.1021/ja403667s.

(162) Mei, J.; Bao, Z. Side Chain Engineering in Solution-Processable Conjugated Polymers. *Chem. Mater.* **2014**, *26* (1), 604–615 DOI: 10.1021/cm4020805.

(163) Ouattara, M. P.; Lenfant, S.; Vuillaume, D.; Pézolet, M.; Rioux-Dubé, J.-F.; Brisson, J.; Leclerc, M. Langmuir–Blodgett Films of Amphiphilic Thieno[3,4-c]Pyrrole-4,6-Dione-Based Alternating Copolymers. *Macromolecules* **2013**, *46* (16), 6408–6418 DOI: 10.1021/ma401030m.

(164) Kim, B.-G.; Ma, X.; Chen, C.; Ie, Y.; Coir, E. W.; Hashemi, H.; Aso, Y.; Green, P. F.; Kieffer, J.; Kim, J. SI: Energy Level Modulation of HOMO, LUMO, and Band-

Gap in Conjugated Polymers for Organic Photovoltaic Applications. *Adv. Funct. Mater.* **2013**, *23* (4), 439–445 DOI: 10.1002/adfm.201201385.

(165) Warnan, J.; Cabanetos, C.; Bude, R.; El Labban, A.; Li, L.; Beaujuge, P. M. Electron-Deficient N -Alkyloyl Derivatives of Thieno[3,4-c]Pyrrole-4,6-Dione Yield Efficient Polymer Solar Cells with Open-Circuit Voltages > 1 V. *Chem. Mater.* **2014**, *26* (9), 2829–2835 DOI: 10.1021/cm5002303.

(166) Beaupré, S.; Najari, A.; Leclerc, M. High Open-Circuit Voltage Solar Cells Using a New Thieno[3,4-c] Pyrrole-4,6-Dione Based Copolymer. *Synth. Met.* **2013**, *182*, 9–12 DOI: 10.1016/j.synthmet.2013.08.022.

(167) Grzybowski, M.; Gryko, D. T. Diketopyrrolopyrroles: Synthesis, Reactivity, and Optical Properties. *Adv. Opt. Mater.* **2015**, *3* (3), 280–320 DOI: 10.1002/adom.201400559.

(168) Wang, E.; Mammo, W.; Andersson, M. R. 25th Anniversary Article: Isoindigo-Based Polymers and Small Molecules for Bulk Heterojunction Solar Cells and Field Effect Transistors. *Adv. Mater.* **2014**, *26* (12), 1801–1826 DOI: 10.1002/adma.201304945.

(169) Graham, K. R.; Cabanetos, C.; Jahnke, J. P.; Idso, M. N.; El Labban, A.; Ngongang Ndjawa, G. O.; Heumüller, T.; Vandewal, K.; Salleo, A.; Chmelka, B. F.; Amassian, A.; Beaujuge, P. M.; McGehee, M. D. Importance of the Donor:Fullerene Intermolecular Arrangement for High-Efficiency Organic Photovoltaics. *J. Am. Chem. Soc.* **2014**, *136* (27), 9608–9618 DOI: 10.1021/ja502985g.

(170) Noyes, W. A.; Porter, P. K. Phthalimide. *Org. Synth.* **1922**, *2* (September), 75 DOI: 10.15227/orgsyn.002.0075.

(171) Sanger, M. J.; Danner, M. Aqueous Ammonia or Ammonium Hydroxide? Identifying a Base as Strong or Weak. *J. Chem. Educ.* **2010**, *87* (11), 1213–1216 DOI: 10.1021/ed100536n.

(172) Laurent, A. Ueber Naphthalinsäure Und Ihre Verbindungen. *Ann. der Pharm.* **1836**, *19* (1), 38–50 DOI: 10.1002/jlac.18360190108.

(173) Sice, J. Substituted Thenoic Acids. *J. Org. Chem.* **1954**, *19* (1), 70–73 DOI: 10.1021/jo01366a013.

(174) Durrwachter, J. R. Neutralization of a Toluene Waste Stream Containing Thionyl Chloride. *Org. Process Res. Dev.* **2017**, *21* (9), 1423–1426 DOI: 10.1021/acs.oprd.7b00195.

(175) Mercier, L. G.; Aïch, B. R.; Najari, A.; Beaupré, S.; Berrouard, P.; Pron, A.; Robitaille, A.; Tao, Y.; Leclerc, M. Direct Heteroarylation of β-Protected Dithienosilole and Dithienogermole Monomers with Thieno[3,4-c]Pyrrole-4,6-Dione and Furo[3,4-c]Pyrrole-4,6-Dione. *Polym. Chem.* **2013**, *4* (20), 5252 DOI:

10.1039/c3py21138j.

(176) Hernandez, J. L.; Deb, N.; Wolfe, R. M. W.; Lo, C. K.; Engmann, S.; Richter, L. J.; Reynolds, J. R. Simple Transfer from Spin Coating to Blade Coating through Processing Aggregated Solutions. *J. Mater. Chem. A* **2017**, *5* (39), 20687–20695 DOI: 10.1039/C7TA05214F.

(177) Griffini, G.; Douglas, J. D.; Piliego, C.; Holcombe, T. W.; Turri, S.; Fréchet, J. M. J.; Mynar, J. L. Long-Term Thermal Stability of High-Efficiency Polymer Solar Cells Based on Photocrosslinkable Donor-Acceptor Conjugated Polymers. *Adv. Mater.* **2011**, *23* (14), 1660–1664 DOI: 10.1002/adma.201004743.

(178) Beaupré, S.; Pron, A.; Drouin, S. H.; Najari, A.; Mercier, L. G.; Robitaille, A.; Leclerc, M. Thieno-, Furo-, and Selenopheno[3,4-c]Pyrrole-4,6-Dione Copolymers: Effect of the Heteroatom on the Electrooptical Properties. *Macromolecules* **2012**, *45* (17), 6906–6914 DOI: 10.1021/ma3011894.

(179) Anderson, A. I. The Dielectric Constant of Liquid Bromine. *Proc. Phys. Soc.* **1927**, *40* (1), 62–70 DOI: 10.1088/0959-5309/40/1/312.

(180) Mei, J.; Graham, K. R.; Stalder, R.; Reynolds, J. R. Synthesis of Isoindigo-Based Oligothiophenes for Molecular Bulk Heterojunction Solar Cells. *Org. Lett.* **2010**, *12* (4), 660–663 DOI: 10.1021/ol902512x.

(181) Van Pruissen, G. W. P.; Gholamrezaie, F.; Wienk, M. M.; Janssen, R. A. J. Synthesis and Properties of Small Band Gap Thienoisoindigo Based Conjugated Polymers. *J. Mater. Chem.* **2012**, *22* (38), 20387 DOI: 10.1039/c2jm34668k.

(182) *Crime Control Act of 1990. Pub. L. 101-647. 104 Stat. 4789. 29 November 1990.*

(183) Torabi, S.; Jahani, F.; Van Severen, I.; Kanimozhi, C.; Patil, S.; Havenith, R. W. A.; Chiechi, R. C.; Lutsen, L.; Vanderzande, D. J. M.; Cleij, T. J.; Hummelen, J. C.; Koster, L. J. A. Strategy for Enhancing the Dielectric Constant of Organic Semiconductors Without Sacrificing Charge Carrier Mobility and Solubility. *Adv. Funct. Mater.* **2015**, *25* (1), 150–157 DOI: 10.1002/adfm.201402244.

(184) Jahani, F.; Torabi, S.; Chiechi, R. C.; Koster, L. J. A.; Hummelen, J. C. Fullerene Derivatives with Increased Dielectric Constants. *Chem. Commun.* **2014**, *50* (73), 10645–10647 DOI: 10.1039/c4cc04366a.

(185) Jung, B. J.; Tremblay, N. J.; Yeh, M.-L.; Katz, H. E. Molecular Design and Synthetic Approaches to Electron-Transporting Organic Transistor Semiconductors. *Chem. Mater.* **2011**, *23* (3), 568–582 DOI: 10.1021/cm102296d.

(186) Takeda, Y.; Andrew, T. L.; Lobez, J. M.; Mork, A. J.; Swager, T. M. An Air-Stable Low-Bandgap n-Type Organic Polymer Semiconductor Exhibiting Selective Solubility in Perfluorinated Solvents. *Angew. Chemie Int. Ed.* **2012**, *51* (36), 9042–9046 DOI: 10.1002/anie.201204066.

(187) Cho, N.; Schlenker, C. W.; Knesting, K. M.; Koelsch, P.; Yip, H.-L.; Ginger, D. S.; Jen, A. K.-Y. K.-Y. High-Dielectric Constant Side-Chain Polymers Show Reduced Non-Geminate Recombination in Heterojunction Solar Cells. *Adv. Energy Mater.* **2014**, *4* (10), 1301857 DOI: 10.1002/aenm.201301857.

(188) Kim, H. J.; Han, A. R.; Cho, C. H.; Kang, H.; Cho, H. H.; Lee, M. Y.; Fréchet, J. M. J.; Oh, J. H.; Kim, B. J. Solvent-Resistant Organic Transistors and Thermally Stable Organic Photovoltaics Based on Cross-Linkable Conjugated Polymers. *Chem. Mater.* **2012**, *24* (1), 215–221 DOI: 10.1021/cm203058p.

(189) Jiang, H.; Taranekar, P.; Reynolds, J. R.; Schanze, K. S. Conjugated Polyelectrolytes: Synthesis, Photophysics, and Applications. *Angew. Chemie Int. Ed.* **2009**, *48* (24), 4300–4316 DOI: 10.1002/anie.200805456.

(190) Cutler, C. A.; Bouguettaya, M.; Reynolds, J. R. PEDOT Polyelectrolyte Based Electrochromic Films via Electrostatic Adsorption. *Adv. Mater.* **2002**, *14* (9), 684–688 DOI: 10.1002/1521-4095(20020503)14:9<684::AID-ADMA684>3.0.CO;2-7.

(191) Zhou, H.; Zhang, Y.; Mai, C.-K.; Collins, S. D.; Nguyen, T.-Q.; Bazan, G. C.; Heeger, A. J. Conductive Conjugated Polyelectrolyte as Hole-Transporting Layer for Organic Bulk Heterojunction Solar Cells. *Adv. Mater.* **2014**, *26* (5), 780–785 DOI: 10.1002/adma.201302845.

(192) Mai, C.-K.; Russ, B.; Fronk, S. L.; Hu, N.; Chan-Park, M. B.; Urban, J. J.; Segalman, R. A.; Chabinyc, M. L.; Bazan, G. C. Varying the Ionic Functionalities of Conjugated Polyelectrolytes Leads to Both *p*- and *n*-Type Carbon Nanotube Composites for Flexible Thermoelectrics. *Energy Environ. Sci.* **2015**, *8* (8), 2341–2346 DOI: 10.1039/C5EE00938C.

(193) Mei, J.; Kim, D. H.; Ayzner, A. L.; Toney, M. F.; Bao, Z. Siloxane-Terminated Solubilizing Side Chains: Bringing Conjugated Polymer Backbones Closer and Boosting Hole Mobilities in Thin-Film Transistors. *J. Am. Chem. Soc.* **2011**, *133* (50), 20130–20133 DOI: 10.1021/ja209328m.

(194) Anastas, P. T.; Warner, J. C. *Green Chemistry: Theory and Practice*; Oxford University Press: New York, 1998.

(195) Van Pruissen, G. W. P.; Gholamrezaie, F.; Wienk, M. M.; Janssen, R. A. J. Synthesis and Properties of Small Band Gap Thienoisoindigo Based Conjugated Polymers. *J. Mater. Chem.* **2012**, *22* (38), 20387 DOI: 10.1039/c2jm34668k.

(196) Piccinno, F.; Hischier, R.; Seeger, S.; Som, C. From Laboratory to Industrial Scale: A Scale-up Framework for Chemical Processes in Life Cycle Assessment Studies. *J. Clean. Prod.* **2016**, *135*, 1085–1097 DOI: 10.1016/j.jclepro.2016.06.164.

(197) Organisation for the Prohibition of Chemical Weapons. *Convention on the Prohibition of the Development, Production, Stockpiling, and Use of Chemical Weapons and on Their Destruction*; 2005.

(198) Leonard, N. J.; Wildman, W. C. Rearrangement of α-Aminoketones During Clemmensen Reduction. IV. Contraction of a Seven-Membered Ring in the Bicyclic Series. *J. Am. Chem. Soc.* **1949**, *71* (9), 3100–3102 DOI: 10.1021/ja01177a045.

(199) Da Ros, T.; Prato, M.; Lucchini, V. Additions of Azomethine Ylides to Fullerene C_{60} Assisted by a Removable Anchor. *J. Org. Chem.* **2000**, *65* (14), 4289–4297 DOI: 10.1021/jo000076d.

(200) Tamura, M.; Tamura, R.; Takeda, Y.; Nakagawa, Y.; Tomishige, K. Catalytic Hydrogenation of Amino Acids to Amino Alcohols with Complete Retention of Configuration. *Chem. Commun.* **2014**, *50* (50), 6656 DOI: 10.1039/c4cc02675f.

(201) Hedrera, M. E.; Perillo, I. A. 1H-4,5,6,7-Tetrahydro-1,3-Diazepines. Part I: Synthesis, Spectral and Chemical Properties of 1,2-Diaryl Derivatives. *J. Heterocycl. Chem.* **2000**, *37* (6), 1431–1438 DOI: 10.1002/jhet.5570370605.

(202) Saeki, A.; Yoshikawa, S.; Tsuji, M.; Koizumi, Y.; Ide, M.; Vijayakumar, C.; Seki, S. A Versatile Approach to Organic Photovoltaics Evaluation Using White Light Pulse and Microwave Conductivity. *J. Am. Chem. Soc.* **2012**, *134* (46), 19035–19042 DOI: 10.1021/ja309524f.

(203) Kohmoto, S.; Mori, E.; Kishikawa, K. SI: Room-Temperature Discotic Nematic Liquid Crystals over a Wide Temperature Range: Alkali-Metal-Ion-Induced Phase Transition from Discotic Nematic to Columnar Phases. *J. Am. Chem. Soc.* **2007**, *129* (44), 13364–13365 DOI: 10.1021/ja073962f.

(204) Wu, X.; Liu, X.; Zhao, G. Catalyzed Asymmetric Aryl Transfer Reactions to Aldehydes with Boroxines as Aryl Source. *Tetrahedron Asymmetry* **2005**, *16* (13), 2299–2305 DOI: 10.1016/j.tetasy.2005.06.010.

(205) Roncali, J.; Leriche, P.; Cravino, A. From One- to Three-Dimensional Organic Semiconductors: In Search of the Organic Silicon? *Adv. Mater.* **2007**, *19* (16), 2045–2060 DOI: 10.1002/adma.200700135.

(206) Maslak, P. Spiroconjugation: An Added Dimension in the Design of Organic Molecular Materials. *Adv. Mater.* **1994**, *6* (5), 405–407 DOI: 10.1002/adma.19940060515.

(207) Liu, T.; Troisi, A. What Makes Fullerene Acceptors Special as Electron Acceptors in Organic Solar Cells and How to Replace Them. *Adv. Mater.* **2013**, *25* (7), 1038–1041 DOI: 10.1002/adma.201203486.

(208) Distler, A.; Sauermann, T.; Egelhaaf, H.-J.; Rodman, S.; Waller, D.; Cheon, K.-S.; Lee, M.; Guldi, D. M. The Effect of PCBM Dimerization on the Performance of Bulk Heterojunction Solar Cells. *Adv. Energy Mater.* **2014**, *4* (1), 1300693 DOI: 10.1002/aenm.201300693.

(209) Liang, N.; Sun, K.; Zheng, Z.; Yao, H.; Gao, G.; Meng, X.; Wang, Z.; Ma, W.; Hou,

J. Perylene Diimide Trimers Based Bulk Heterojunction Organic Solar Cells with Efficiency over 7%. *Adv. Energy Mater.* **2016**, *6* (11), 1600060 DOI: 10.1002/aenm.201600060.

(210) Chen, W.; Yang, X.; Long, G.; Wan, X.; Chen, Y.; Zhang, Q. A Perylene Diimide (PDI)-Based Small Molecule with Tetrahedral Configuration as a Non-Fullerene Acceptor for Organic Solar Cells. *J. Mater. Chem. C* **2015**, *3* (18), 4698–4705 DOI: 10.1039/C5TC00865D.

(211) Liu, Y.; Lai, J. Y. L.; Chen, S.; Li, Y.; Jiang, K.; Zhao, J.; Li, Z.; Hu, H.; Ma, T.; Lin, H.; Liu, J.; Zhang, J.; Huang, F.; Yu, D.; Yan, H. Efficient Non-Fullerene Polymer Solar Cells Enabled by Tetrahedron-Shaped Core Based 3D-Structure Small-Molecular Electron Acceptors. *J. Mater. Chem. A* **2015**, *3* (26), 13632–13636 DOI: 10.1039/C5TA03093E.

(212) Zhan, C.; Yao, J. More than Conformational "Twisting" or "Coplanarity": Molecular Strategies for Designing High-Efficiency Nonfullerene Organic Solar Cells. *Chem. Mater.* **2016**, *28* (7), 1948–1964 DOI: 10.1021/acs.chemmater.5b04339.

(213) Liu, S. Y.; Wu, C. H.; Li, C. Z.; Liu, S. Q.; Wei, K. H.; Chen, H. Z.; Jen, A. K. Y. A Tetraperylene Diimides Based 3D Nonfullerene Acceptor for Efficient Organic Photovoltaics. *Adv. Sci.* **2015**, *2* (4), 1–7 DOI: 10.1002/advs.201500014.

(214) Liu, S.-Y.; Jung, J. W.; Li, C.-Z.; Huang, J.; Zhang, J.; Chen, H.; Jen, A. K.-Y. Three-Dimensional Molecular Donors Combined with Polymeric Acceptors for High Performance Fullerene-Free Organic Photovoltaic Devices. *J. Mater. Chem. A* **2015**, *3* (44), 22162–22169 DOI: 10.1039/C5TA06639E.

(215) Hawash, Z.; Ono, L. K.; Qi, Y. Recent Advances in Spiro-MeOTAD Hole Transport Material and Its Applications in Organic-Inorganic Halide Perovskite Solar Cells. *Adv. Mater. Interfaces* **2018**, *5* (1), 1700623 DOI: 10.1002/admi.201700623.

(216) Wu, X.-F.; Fu, W.-F.; Xu, Z.; Shi, M.; Liu, F.; Chen, H.-Z.; Wan, J.-H.; Russell, T. P. Spiro Linkage as an Alternative Strategy for Promising Nonfullerene Acceptors in Organic Solar Cells. *Adv. Funct. Mater.* **2015**, *25* (37), 5954–5966 DOI: 10.1002/adfm.201502413.

(217) Li, S.; Liu, W.; Shi, M.; Mai, J.; Lau, T.-K.; Wan, J.-H.; Lu, X.; Li, C.-Z.; Chen, H. A Spirobifluorene and Diketopyrrolopyrrole Moieties Based Non-Fullerene Acceptor for Efficient and Thermally Stable Polymer Solar Cells with High Open-Circuit Voltage. *Energy Environ. Sci.* **2015** DOI: 10.1039/C5EE03481G.

(218) Bulut, I.; Chávez, P.; Fall, S.; Méry, S.; Heinrich, B.; Rault-Berthelot, J.; Poriel, C.; Lévêque, P.; Leclerc, N. Incorporation of Spirobifluorene Regioisomers in Electron-Donating Molecular Systems for Organic Solar Cells. *RSC Adv.* **2016**, *6* (31), 25952–25959 DOI: 10.1039/C6RA02085B.

(219) Ma, S.; Zhang, H.; Zhao, N.; Cheng, Y.-B. Y.; Wang, M.; Shen, Y.; Tu, G. Spiro-Thiophene Derivatives as Hole-Transport Materials for Perovskite Solar Cells. *J. Mater. Chem. A* **2015**, *3* (23), 12139–12144 DOI: 10.1039/C5TA01155H.

(220) Franckevičius, M.; Mishra, A.; Kreuzer, F.; Luo, J.; Zakeeruddin, S. M.; Grätzel, M. A Dopant-Free Spirobi[Cyclopenta[2,1-b:3,4-b′]Dithiophene] Based Hole-Transport Material for Efficient Perovskite Solar Cells. *Mater. Horizons* **2015**, *2* (6), 613–618 DOI: 10.1039/C5MH00154D.

(221) Orlandi, S.; Pozzi, G.; Cavazzini, M.; Minudri, D.; Gervaldo, M.; Otero, L.; Fungo, F. Synthesis and Properties of an Electropolymer Obtained from a Dimeric Donor/Acceptor System with a 4,4′-Spirobi[Cyclopenta[2,1-b:3,4-b′]Dithiophene] Core. *Macromolecules* **2015**, *48* (13), 4364–4372 DOI: 10.1021/acs.macromol.5b00845.

(222) Ohshita, J.; Lee, K.-H.; Hamamoto, D.; Kunugi, Y.; Ikadai, J.; Kwak, Y.-W.; Kunai, A. Synthesis of Novel Spiro-Condensed Dithienosiloles and the Application to Organic FET. *Chem. Lett.* **2004**, *33* (7), 892–893 DOI: 10.1246/cl.2004.892.

(223) Lee, K.-H.; Ohshita, J.; Tanaka, D.; Tominaga, Y.; Kunai, A. Synthesis and Optical Properties of Spirobi(Dithienometallole)s and Spirobi(Dithienothiametalline)S. *J. Organomet. Chem.* **2012**, *710*, 53–58 DOI: 10.1016/j.jorganchem.2012.03.012.

(224) Ohshita, J.; Hayashi, Y.; Murakami, K.; Enoki, T.; Ooyama, Y. Single Oxygen Generation Sensitized by Spiro(Dipyridinogermole)(Dithienogermole)S. *Dalt. Trans.* **2016**, *45* (39), 15679–15683 DOI: 10.1039/C6DT02767A.

(225) Murakami, K.; Ooyama, Y.; Higashimura, H.; Ohshita, J. Synthesis, Properties, and Polymerization of Spiro[(Dipyridinogermole)(Dithienogermole)]. *Organometallics* **2016**, *35* (1), 20–26 DOI: 10.1021/acs.organomet.5b00817.

(226) Wright, I. A.; Kanibolotsky, A. L.; Cameron, J.; Tuttle, T.; Skabara, P. J.; Coles, S. J.; Howells, C. T.; Thomson, S. A. J.; Gambino, S.; Samuel, I. D. W. Oligothiophene Cruciform with a Germanium Spiro Center: A Promising Material for Organic Photovoltaics. *Angew. Chemie Int. Ed.* **2012**, *51* (19), 4562–4567 DOI: 10.1002/anie.201109074.

(227) Arumugam, S.; Wright, I. A.; Inigo, A. R.; Gambino, S.; Howells, C. T.; Kanibolotsky, A. L.; Skabara, P. J.; Samuel, I. D. W. Charge Transport in a Two-Dimensional Molecular Organic Semiconductor. *J. Mater. Chem. C* **2014**, *2* (1), 34 DOI: 10.1039/c3tc31670j.

(228) Gupta, V.; Lai, L. F.; Datt, R.; Chand, S.; Heeger, A. J.; Bazan, G. C.; Singh, S. P. Dithienogermole-Based Solution-Processed Molecular Solar Cells with Efficiency over 9%. *Chem. Commun.* **2016**, *52* (55), 8596–8599 DOI: 10.1039/C6CC03998G.

(229) Nakamura, M.; Ooyama, Y.; Hayakawa, S.; Nishino, M.; Ohshita, J. Synthesis of Poly(Dithienogermole)S. *Organometallics* **2016**, *35* (14), 2333–2338 DOI:

10.1021/acs.organomet.6b00263.

(230) Tanikawa, T.; Saito, M.; Guo, J. D.; Nagase, S.; Minoura, M. Synthesis, Structures, and Optical Properties of Heterasumanenes Containing Group 14 Elements and Their Related Compounds. *European J. Org. Chem.* **2012**, 7135–7142 DOI: 10.1002/ejoc.201201223.

(231) Gu, C.; Zhu, D.; Qiu, M.; Han, L.; Wen, S.; Li, Y.; Yang, R. Design, Synthesis and Optical Properties of Small Molecules Based on Dithieno[3,2-b:2′,3′-d]Stannole and Stannafluorene. *New J. Chem.* **2016**, *40* (9), 7787–7794 DOI: 10.1039/C6NJ01310D.

(232) Linshoeft, J.; Baum, E. J.; Hussain, A.; Gates, P. J.; Näther, C.; Staubitz, A. Highly Tin-Selective Stille Coupling: Synthesis of a Polymer Containing a Stannole in the Main Chain. *Angew. Chemie - Int. Ed.* **2014**, *53* (47), 12916–12920 DOI: 10.1002/anie.201407377.

(233) Urrego-Riveros, S.; Ramirez y Medina, I.-M.; Hoffmann, J.; Heitmann, A.; Staubitz, A. Syntheses and Properties of Tin-Containing Conjugated Heterocycles. *Chem. - A Eur. J.* **2018** DOI: 10.1002/chem.201703533.

(234) van Beelen, D. C.; Wolters, J.; van der Gen, A. Some Spectroscopic Properties of Cyclic Organolead Compounds I. *J. Organomet. Chem.* **1978**, *145* (3), 359–363 DOI: 10.1016/S0022-328X(00)81304-2.

(235) Wrackmeyer, B.; Horchler, K. Plumboles Bearing Organometallic Substituents. Their Synthesis and Reaction Mechanism, as Studied by Multinuclear Magnetic Resonance Spectroscopy. *J. Organomet. Chem.* **1990**, *399* (1–2), 1–10 DOI: 10.1016/0022-328X(90)80079-F.

(236) Zong, K.; Deininger, J. J.; Reynolds, J. R. Efficient Synthesis of Dithienogermole (DTG) Derivatives via Olefin Cross-Metathesis. *Org. Lett.* **2013**, *15* (5), 1032–1035 DOI: 10.1021/ol303529w.

(237) Ohshita, J.; Hwang, Y.; Mizumo, T.; Yoshida, H.; Ooyama, Y.; Harima, Y.; Kunugi, Y. Synthesis of Dithienogermole-Containing π-Conjugated Polymers and Applications to Photovoltaic Cells. *Organometallics* **2011**, *30* (12), 3233–3236 DOI: 10.1021/om200081b.

(238) Madhu, S.; Evans, H. A.; Doan-Nguyen, V. V. T.; Labram, J. G.; Wu, G.; Chabinyc, M. L.; Seshadri, R.; Wudl, F. Infinite Polyiodide Chains in the Pyrroloperylene-Iodine Complex: Insights into the Starch-Iodine and Perylene-Iodine Complexes. *Angew. Chemie Int. Ed.* **2016**, *55* (28), 8032–8035 DOI: 10.1002/anie.201601585.

(239) Dou, L.; Zheng, Y.; Shen, X.; Wu, G.; Fields, K.; Hsu, W.-C.; Zhou, H.; Yang, Y.; Wudl, F. Single-Crystal Linear Polymers Through Visible Light-Triggered Topochemical Quantitative Polymerization. *Science* **2014**, *343* (6168), 272–277 DOI: 10.1126/science.1245875.

(240) Facchetti, A.; Yoon, M.; Stern, C. L.; Hutchison, G. R.; Ratner, M. A.; Marks, T. J. Building Blocks for N-Type Molecular and Polymeric Electronics. Perfluoroalkyl- versus Alkyl-Functionalized Oligothiophenes (NTs; n = 2-6). Systematic Synthesis, Spectroscopy, Electrochemistry, and Solid-State Organization. *J. Am. Chem. Soc.* **2004**, *126* (41), 13480–13501 DOI: 10.1021/ja048988a.

(241) Shimizu, M.; Ryuse, D.; Kinoshita, T. Germanium-Bridged 2-Phenylbenzoheteroles as Luminophores Exhibiting Highly Efficient Solid-State Fluorescence. *Chem. - A Eur. J.* **2017**, *23* (58), 14623–14630 DOI: 10.1002/chem.201703235.

(242) Cardona, C. M.; Li, W.; Kaifer, A. E.; Stockdale, D.; Bazan, G. C. Electrochemical Considerations for Determining Absolute Frontier Orbital Energy Levels of Conjugated Polymers for Solar Cell Applications. *Adv. Mater.* **2011**, *23* (20), 2367–2371 DOI: 10.1002/adma.201004554.

(243) Bredas, J.-L. Mind the Gap! *Mater. Horiz.* **2014**, *1* (1), 17–19 DOI: 10.1039/C3MH00098B.

(244) Yokonuma, N.; Furukawa, Y.; Tasumi, M.; Kuroda, M.; Nakayama, J. Electronic Absorption and Raman Studies of BF_4^-Doped Polythiophene Based on the Spectra of the Radical Cation and Dication of α-Sexithiophene. *Chem. Phys. Lett.* **1996**, *255* (4–6), 431–436 DOI: 10.1016/0009-2614(96)00383-1.

(245) Connelly, N. G.; Geiger, W. E. Chemical Redox Agents for Organometallic Chemistry. *Chem. Rev.* **1996**, *96* (2), 877–910 DOI: 10.1021/cr940053x.

(246) Smith, M. B.; Michl, J. Singlet Fission. *Chem. Rev.* **2010**, *110* (11), 6891–6936 DOI: 10.1021/cr1002613.

(247) Smith, M. B.; Michl, J. Recent Advances in Singlet Fission. *Annu. Rev. Phys. Chem.* **2013**, *64*, 361–386 DOI: 10.1146/annurev-physchem-040412-110130.

(248) Busby, E.; Xia, J.; Wu, Q.; Low, J. Z.; Song, R.; Miller, J. R.; Zhu, X.; Campos, L. M.; Sfeir, M. Y. A Design Strategy for Intramolecular Singlet Fission Mediated by Charge-Transfer States in Donor–acceptor Organic Materials. *Nat. Mater.* **2015**, *14* (4), 426–433 DOI: 10.1038/nmat4175.

(249) Flood, E. A. Aliphatic Germanium Derivatives. II. Diethyldiphenylgermane, Diethylgermanium Oxide and Diethylgermanium Dibromide. *J. Am. Chem. Soc.* **1932**, *54* (4), 1663–1667 DOI: 10.1021/ja01343a065.

(250) Fei, Z.; Kim, J.-S. J. S.; Smith, J.; Domingo, E. B.; Anthopoulos, T. D.; Stingelin, N.; Watkins, S. E.; Heeney, M. A Low Band Gap Co-Polymer of Dithienogermole and 2,1,3-Benzothiadiazole by Suzuki Polycondensation and Its Application in Transistor and Photovoltaic Cells. *J. Mater. Chem.* **2011**, *21* (40), 16257 DOI: 10.1039/c1jm13628c.

(251) Getmanenko, Y. a; Tongwa, P.; Timofeeva, T. V; Marder, S. R. Base-Catalyzed

Halogen Dance Reaction and Oxidative Coupling Sequence as a Convenient Method for the Preparation of Dihalo-Bisheteroarenes. *Org. Lett.* **2010**, *12* (9), 2136–2139 DOI: 10.1021/ol1006423.

(252) Evenson, S. J.; Rasmussen, S. C. N-Acyldithieno[3,2-b:2',3'-d]Pyrroles: Second Generation Dithieno[3,2-b:2',3'-d]Pyrrole Building Blocks with Stabilized Energy Levels. *Org. Lett.* **2010**, *12* (18), 4054–4057 DOI: 10.1021/ol101647f.

(253) Yamada, S. Researches on Dichroism of Planar Complexes. II. The Color and the Structure of $[Pt(NH_3)_4][PtCl_4]$ and $[Pt(NH_3)_4][PtBr_4]$. *J. Am. Chem. Soc.* **1951**, *73* (4), 1579–1580 DOI: 10.1021/ja01148a048.

(254) Atkinson, L.; Day, P.; Williams, R. J. P. Semiconductivity of Magnus' Green Salt Analogues. *Nature* **1968**, *218* (5142), 668–669 DOI: 10.1038/218668a0.

(255) Zeller, H. R.; Brüesch, P. Band Structure of $K_2[Pt(CN)_4]Br_{0.30}\cdot 3H_2O$. *Phys. status solidi* **1974**, *65* (2), 537–542 DOI: 10.1002/pssb.2220650212.

(256) Kirtley, J. R.; Mannhart, J. When TTF Met TCNQ. *Nat. Mater.* **2008**, *7* (7), 520–521 DOI: 10.1038/nmat2211.

(257) Valade, L.; Legros, J.; Bousseau, M.; Cassoux, P.; Garbauskas, M.; Interrante, L. V. Molecular Structure and Solid-State Properties of the Two-Dimensional Conducting Mixed-Valence Complex $[NBu_4]_{0.29}[Ni(Dmit)_2]$ and the Neutral $[Ni(Dmit)_2]$(H_2dmit = 4,5-Dimercapto-1,3-Dithiole-2-Thione); Members of an Electron-Transfer Series. *J. Chem. Soc. Dalt. Trans.* **1985**, No. 4, 783 DOI: 10.1039/dt9850000783.

(258) Cassoux, P.; Valade, L.; Kobayashi, H.; Kobayashi, A.; Clark, R. A.; Underhill, A. E. Molecular Metals and Superconductors Derived from Metal Complexes of 1,3-Dithiol-2-Thione-4,5-Dithiolate (Dmit). *Coord. Chem. Rev.* **1991**, *110* (1), 115–160 DOI: 10.1016/0010-8545(91)80024-8.

(259) Delhaes, P. Design and Properties of Organic Metals. *Mol. Cryst. Liq. Cryst.* **1983**, *96* (1), 229–262 DOI: 10.1080/00268948308074708.

(260) Bechgaard, K.; Carneiro, K.; Rasmussen, F. B.; Olsen, M.; Rindorf, G.; Jacobsen, C. S.; Pedersen, H. J.; Scott, J. C. Superconductivity in an Organic Solid. Synthesis, Structure, and Conductivity of Bis(Tetramethyltetraselenafulvalenium) Perchlorate, $(TMTSF)_2ClO_4$. *J. Am. Chem. Soc.* **1981**, *103* (9), 2440–2442 DOI: 10.1021/ja00399a065.

(261) Wudl, F. Three-Dimensional Structure of the Superconductor $(TMTSF)_2AsF_6$ and the Spin-Charge Separation Hypothesis. *J. Am. Chem. Soc.* **1981**, *103* (24), 7064–7069 DOI: 10.1021/ja00414a007.

(262) Kobayashi, H.; Kobayashi, A.; Saito, G.; Enoki, T.; Inokuchi, H. Crystal Structure of a New Type of Two-Dimensional Organic Metal, $(C_{10}H_8S_8)_2(ClO_4)(C_2H_3Cl_3)_{0.5}$.

J. Am. Chem. Soc. **1983**, *105* (2), 297–298 DOI: 10.1021/ja00340a028.

(263) Parkin, S. S. P.; Engler, E. M.; Schumaker, R. R.; Lagier, R.; Lee, V. Y.; Scott, J. C.; Greene, R. L. Superconductivity in a New Family of Organic Conductors. *Phys. Rev. Lett.* **1983**, *50* (4), 270–273 DOI: 10.1103/PhysRevLett.50.270.

(264) Alvarez, S.; Vicente, R.; Hoffmann, R. Dimerization and Stacking in Transition-Metal Bisdithiolenes and Tetrathiolates. *J. Am. Chem. Soc.* **1985**, *107* (22), 6253–6277 DOI: 10.1021/ja00308a018.

(265) Reynolds, J. R.; Chien, J. C. W.; Lillya, C. P. Intrinsically Electrically Conducting Poly(Metal Tetrathiooxalates). *Macromolecules* **1987**, *20* (6), 1184–1191 DOI: 10.1021/ma00172a003.

(266) Svenstrup, N.; Becher, J. The Organic Chemistry of 1,3-Dithiole-2-Thione-4,5-Dithiolate (DMIT). *Synthesis (Stuttg).* **1995**, *1995* (03), 215–235 DOI: 10.1055/s-1995-3910.

(267) Liu, S.-G.; Liu, Y.; Zhu, D. Studies on Transition-Metal 4,5-Dimercapto-1,3-Dithiole-2-One (DMID) Complexes. Preparation and Characterization. *Synth. Met.* **1996**, *79* (1), 49–56 DOI: 10.1016/0379-6779(96)80130-5.

(268) Liu, S.-G.; Liu, Y.; Li, Y.; Zhu, D. Study on Transition Metal–4,5-Dimercapto-1,3-Dithiole-2-One Complexes and Related Compounds: Toward Structure–property Correlation. *Synth. Met.* **2000**, *114* (2), 139–146 DOI: 10.1016/S0379-6779(00)00241-1.

(269) Böttcher, B.; Lüttringhaus, A. Über Trithione. I. *Justus Liebigs Ann. Chem.* **1947**, *557* (1), 89–107 DOI: 10.1002/jlac.19475570107.

(270) Hartke, K.; Kissel, T.; Quante, J.; Matusch, R. Thion- Und Dithioester, XXIV. Synthese von Tetrathiooxalestern. *Chem. Ber.* **1980**, *113* (5), 1898–1906 DOI: 10.1002/cber.19801130525.

(271) Steimecke, G.; Sieler, H.-J.; Kirmse, R.; Hoyer, E. 1.3-Dithiol-2-Thion-4.5-Dithiolat Aus Schwefelkohlenstoff Und Alkalimetall. *Phosphorous Sulfur Relat. Elem.* **1979**, *7* (1), 49–55 DOI: 10.1080/03086647808069922.

(272) Wang, C.; Batsanov, A. S.; Bryce, M. R.; Howard, J. A. K. An Improved Large-Scale (90 g) Synthesis of Bis(Tetraethylammonium)Bis(1,3-Dithiole-2-Thione-4,5-Dithiol)Zincate: Synthesis and X-Ray Crystal Structures of Bicyclic and Tricyclic 1,4-Dithiocines Derived from 1,3-Dithiole-2-Thione-4,5-Dithiolate (DMIT). *Synthesis (Stuttg).* **1998**, *1998* (11), 1615–1618 DOI: 10.1055/s-1998-2197.

(273) Schumaker, R. R.; Engler, E. M. Thiapen Chemistry. 2. Synthesis of 1,3,4,6-Tetrathiapentalene-2,5-Dione. *J. Am. Chem. Soc.* **1977**, *99* (16), 5521–5522 DOI: 10.1021/ja00458a068.

(274) Givaja, G.; Amo-Ochoa, P.; Gómez-García, C. J.; Zamora, F. Electrical Conductive Coordination Polymers. *Chem. Soc. Rev.* **2012**, *41* (1), 115–147 DOI: 10.1039/C1CS15092H.

(275) Holdcroft, G. E.; Underhill, A. E. Preparation and Electrical Conduction Properties of Polymeric Transition Metal Complexes of 1,1,2,2-Ethenetetrathiolate Ligand. *Synth. Met.* **1985**, *10* (6), 427–434 DOI: 10.1016/0379-6779(85)90200-0.

(276) Vicente, R.; Ribas, J.; Cassoux, P.; Valade, L. Synthesis, Characterization and Properties of Highly Conducting Organometallic Polymers Derived from the Ethylene Tetrathiolate Anion. *Synth. Met.* **1986**, *13* (4), 265–280 DOI: 10.1016/0379-6779(86)90188-8.

(277) Dirk, C. W.; Bousseau, M.; Barrett, P. H.; Moraes, F.; Wudl, F.; Heeger, A. J. Metal Poly(Benzodithiolenes). *Macromolecules* **1986**, *19* (2), 266–269 DOI: 10.1021/ma00156a003.

(278) Matsuoka, R.; Sakamoto, R.; Kambe, T.; Takada, K.; Kusamoto, T.; Nishihara, H. Ordered Alignment of a One-Dimensional π-Conjugated Nickel Bis(Dithiolene) Complex Polymer Produced via Interfacial Reactions. *Chem. Commun.* **2014**, *50* (60), 8137–8139 DOI: 10.1039/C4CC02022G.

(279) Kambe, T.; Sakamoto, R.; Kusamoto, T.; Pal, T.; Fukui, N.; Hoshiko, K.; Shimojima, T.; Wang, Z.; Hirahara, T.; Ishizaka, K.; Hasegawa, S.; Liu, F.; Nishihara, H. Redox Control and High Conductivity of Nickel Bis(Dithiolene) Complex π-Nanosheet: A Potential Organic Two-Dimensional Topological Insulator. *J. Am. Chem. Soc.* **2014**, *136* (41), 14357–14360 DOI: 10.1021/ja507619d.

(280) Huang, X.; Sheng, P.; Tu, Z.; Zhang, F.; Wang, J.; Geng, H.; Zou, Y.; Di, C.; Yi, Y.; Sun, Y.; Xu, W.; Zhu, D. A Two-Dimensional π–d Conjugated Coordination Polymer with Extremely High Electrical Conductivity and Ambipolar Transport Behaviour. *Nat. Commun.* **2015**, *6* (May), 7408 DOI: 10.1038/ncomms8408.

(281) Tkachov, R.; Stepien, L.; Roch, A.; Komber, H.; Hennersdorf, F.; Weigand, J. J.; Bauer, I.; Kiriy, A.; Leyens, C. Facile Synthesis of Potassium Tetrathiooxalate – The "True" Monomer for the Preparation of Electron-Conductive Poly(Nickel-Ethylenetetrathiolate). *Tetrahedron* **2017**, *73* (16), 2250–2254 DOI: 10.1016/j.tet.2017.03.010.

(282) Piotraschke, J.; Pullen, A. E.; Abboud, K. A.; Reynolds, J. R. Extensively Conjugated Bimetallic (μ-Tetrathiooxalato)Copper(II) Complex $(Bu_4N)_2[(C_3S_5)CuC_2S_4Cu(C_3S_5)]$ for Electrically Conducting Charge Transfer Complexes. *Inorg. Chem.* **1995**, *34* (16), 4011–4012 DOI: 10.1021/ic00120a001.

(283) Pullen, A. E.; Zeltner, S.; Olk, R.-M.; Hoyer, E.; Abboud, K. A.; Reynolds, J. R. Extensively Conjugated Dianionic Tetrathiooxalate-Bridged Copper(II) Complexes for Synthetic Metals. *Inorg. Chem.* **1996**, *35* (15), 4420–4426 DOI:

10.1021/ic9601605.

(284) Pullen, A. E.; Olk, R.; Zeltner, S.; Hoyer, E.; Abboud, K. A.; Reynolds, J. R. A New Generation of Nickel−dmit-Based Molecular Conductors Based on Fully Conjugated Bimetallic Complexes. *Inorg. Chem.* **1997**, *36* (6), 958–959 DOI: 10.1021/ic9610389.

(285) Kubo, K.; Nakao, A.; Yamamoto, H. M.; Kato, R. Preparation and Characterization of Conducting Trimetallic Nickel−Dithiolene Complexes with Bridging Tetrathiooxalate Ligands. *J. Am. Chem. Soc.* **2006**, *128* (38), 12358–12359 DOI: 10.1021/ja0638004.

(286) Bai, J.; Zuo, J.; Shen, Z.; You, X.; Fun, H.; Chinnakali, K. A Convenient Route To Synthesize the Fully Conjugated Bimetallic Complex $(Bu_4N)_2\{tto[Ni(Dmit)_2]\}$ (tto = Tetrathiooxalate, $C_2S_4^{2-}$, and Dmit = 1,3-Dithiole-2-Thione-4,5-Dithiolate, $C_3S_5^{2-}$) and the Crystal Structure of a New Crystal Form. *Inorg. Chem.* **2000**, *39* (6), 1322–1324 DOI: 10.1021/ic9902875.

(287) Kroon, R.; Mengistie, D. A.; Kiefer, D.; Hynynen, J.; Ryan, J. D.; Yu, L.; Müller, C. Thermoelectric Plastics: From Design to Synthesis, Processing and Structure–property Relationships. *Chem. Soc. Rev.* **2016**, *45* (22), 6147–6164 DOI: 10.1039/C6CS00149A.

(288) Steimecke, G.; Kirmse, R.; Hoyer, E. Dimercapto-Isotrithion - Ein Neuer, Ungesättigter 1,2-Dithiolatligand. *Zeitschrift für Chemie* **1975**, *15* (1), 28–29 DOI: 10.1002/zfch.19750150117.

(289) Valade, L.; de Caro, D.; Faulmann, C.; Jacob, K. $TTF[Ni(Dmit)_2]_2$: From Single-Crystals to Thin Layers, Nanowires, and Nanoparticles. *Coord. Chem. Rev.* **2016**, *308*, 433–444 DOI: 10.1016/j.ccr.2015.05.014.

(290) Abashev, G. G.; Shklyaeva, E. V. Synthesis of 1,3-Dithiole-2-Thiones and Tetrathiafulvalenes Using Oligo-(1,3-Dithiole-2,4,5-Trithione). (Review). *Chem. Heterocycl. Compd.* **2006**, *42* (4), 423–439 DOI: 10.1007/s10593-006-0107-1.

(291) Olk, R.-M.; Dietzsch, W.; Kohler, K.; Kirmse, R.; Reinhold, J.; Hoyer, E.; Golic, L.; Olk, B. Zur Koordinationschemie Des 1,3-Dithiol-2-on-4,5-Dithiolats (Dmid) - Ein Vergleich Mit 1,3-Dithiol-2-Thion-4,5-Dithiolat (Dmit). Kristall- Und Molekulstruktur Des Tetrabutylammonium-Bis(1,3-Dithiol-2-on-4,5-Dithiolato)Nickelat(III), $(n\text{-}C_4H_9)_4N[Ni(Dmid)_2]$. *Zeitschrift fur Anorg. und Allg. Chemie* **1988**, *567* (1), 131–144 DOI: 10.1002/zaac.19885670115.

(292) Dietzsch, W.; Rauer, S.; Olk, R.-M.; Kirmse, R.; Köhler, K.; Golič, L.; Olk, B. Ligand Exchange Reactions between Metal(II) Chelates of Different Sulfur and Selenium Containing Ligands IX. Exchange Behavior of Chelates of 1,3-Dithiole-2-Thione-4,5-Dithiolate (Dmit) and 1,1-Dichalcogenolates. X-Ray Structure of $Bu_4N[Zn(dmit)(Et_2dtc)]$. *Inorganica Chim. Acta* **1990**, *169* (1), 55–62 DOI: 10.1016/S0020-1693(00)82036-8.

(293) Pokhodnya, K. I.; Faulmann, C.; Malfant, I.; Andreu-Solano, R.; Cassoux, P.; Mlayah, A.; Smirnov, D.; Leotin, J. Infrared and Raman Properties of [M(Dmit)$_2$] (M=Ni, Pd) Based Compounds. *Synth. Met.* **1999**, *103* (1–3), 2016–2019 DOI: 10.1016/S0379-6779(98)00287-2.

(294) Bigoli, F.; Cassoux, P.; Deplano, P.; Mercuri, M. L.; Pellinghelli, M. A.; Pintus, G.; Serpe, A.; Trogu, E. F. Synthesis, Structure and Properties of New Unsymmetrical Nickel Dithiolene Complexes Useful as near-Infrared Dyes. *J. Chem. Soc. Dalt. Trans.* **2000**, No. 24, 4639–4644 DOI: 10.1039/b006206p.

(295) Mulder, M. J. J.; Haasnoot, J. G.; Stufkens, D. J.; Tjeng, L. H.; Lin, H.-J.; Chen, C.-T.; Reedijk, J. A New Synthetic Strategy for Magnetic Metal Bis(Dithiolene) Based Conductors. *Eur. J. Inorg. Chem.* **2002**, *2002* (12), 3083–3086 DOI: 10.1002/1099-0682(200212)2002:12<3083::AID-EJIC3083>3.0.CO;2-O.

(296) Liu, G.; Fang, Q.; Xu, W.; Chen, H.; Wang, C. Vibration Assignment of Carbon–sulfur Bond in 2-Thione-1,3-Dithiole-4,5-Dithiolate Derivatives. *Spectrochim. Acta Part A Mol. Biomol. Spectrosc.* **2004**, *60* (3), 541–550 DOI: 10.1016/S1386-1425(03)00260-9.

(297) Sun, Y.; Sheng, P.; Di, C.; Jiao, F.; Xu, W.; Qiu, D.; Zhu, D. Organic Thermoelectric Materials and Devices Based on *p*- and *n*-Type Poly(Metal 1,1,2,2-Ethenetetrathiolate)s. *Adv. Mater.* **2012**, *24* (7), 932–937 DOI: 10.1002/adma.201104305.

(298) Sun, Y. Y.; Qiu, L.; Tang, L.; Geng, H.; Wang, H.; Zhang, F.; Huang, D.; Xu, W.; Yue, P.; Guan, Y. S.; Jiao, F.; Sun, Y. Y.; Tang, D.; Di, C. A.; Yi, Y.; Zhu, D. Flexible N-Type High-Performance Thermoelectric Thin Films of Poly(Nickel-Ethylenetetrathiolate) Prepared by an Electrochemical Method. *Adv. Mater.* **2016**, *28* (17), 3351–3358 DOI: 10.1002/adma.201505922.

(299) Jiao, F.; Di, C.-A.; Sun, Y.; Sheng, P.; Xu, W.; Zhu, D. Inkjet-Printed Flexible Organic Thin-Film Thermoelectric Devices Based on *p*- and *n*-Type Poly(Metal 1,1,2,2-Ethenetetrathiolate)s/Polymer Composites through Ball-Milling. *Philos. Trans. R. Soc. A Math. Phys. Eng. Sci.* **2014**, *372* (2013), 20130008–20130008 DOI: 10.1098/rsta.2013.0008.

(300) Menon, A. K. Development of Organic Thermoelectric Materials and Devices for Energy Harvesting, Georgia Institute of Technology, 2018.

(301) Menon, A. K.; Uzunlar, E.; Wolfe, R. M. W.; Reynolds, J. R.; Marder, S. R.; Yee, S. K. Metallo-Organic n-Type Thermoelectrics: Emphasizing Advances in Nickel-Ethenetetrathiolates. *J. Appl. Polym. Sci.* **2017**, *134* (3), 44402 DOI: 10.1002/app.44402.

(302) Schumaker, R. R.; Lee, V. Y.; Engler, E. M. Noncoupling Synthesis of Tetrathiafulvalenes. *J. Org. Chem.* **1984**, *49* (3), 564–566 DOI: 10.1021/jo00177a041.

(303) Rao, S. R. Chapter 2. Methods of Preparation and Purification. In *Xanthates and Related Compounds*; Marcel Dekker, INC.: New York, 1971; pp 7–9.

(304) Corey, E.; Chaykovsky, M. Methylenecyclohexane Oxide. *Org. Synth.* **1969**, *49* (September), 78 DOI: 10.15227/orgsyn.049.0078.

(305) Oshima, K.; Shiraishi, Y.; Toshima, N. Novel Nanodispersed Polymer Complex, Poly(Nickel 1,1,2,2-Ethenetetrathiolate): Preparation and Hybridization for n-Type of Organic Thermoelectric Materials. *Chem. Lett.* **2015**, *44* (9), 1185–1187 DOI: 10.1246/cl.150328.

(306) Toshima, N.; Oshima, K.; Anno, H.; Nishinaka, T.; Ichikawa, S.; Iwata, A.; Shiraishi, Y. Novel Hybrid Organic Thermoelectric Materials:Three-Component Hybrid Films Consisting of a Nanoparticle Polymer Complex, Carbon Nanotubes, and Vinyl Polymer. *Adv. Mater.* **2015**, *27* (13), 2246–2251 DOI: 10.1002/adma.201405463.

(307) Stickle, W. F.; Reynolds, J. R.; Jolly, C. A. Surface Characterization of Electrically Conducting Nickel Tetrathiooxalate/Poly(Vinyl Alcohol) Composites. *Langmuir* **1991**, *7* (11), 2460–2463 DOI: 10.1021/la00059a011.

(308) Lascelles, K.; Morgan, L. G.; Nicholls, D.; Beyersmann, D. Nickel Compounds. *Ullmann's Encycl. Ind. Chem.* **2005**, *1754* (1), 16 DOI: 10.1002/14356007.a17_235.pub2.

(309) Pray, A. R.; Heitmiller, R. F.; Strycker, S.; Aftandilian, V. D.; Muniyappan, T.; Choudhury, D.; Tamres, M. Anhydrous Metal Chlorides. In *Inorganic Syntheses: Reagents for Transition Metal Complex and Organometallic Syntheses, Volume 28*; 1990; Vol. 28, pp 321–323.

(310) Appendix B Data Tables, Table 11.2 Standard Reduction Potentials Ordered by Reduction Potential. In *Physical Chemistry*; Engel, T., Reid, P., Eds.; Pearson Education, Inc.: Upper Saddle River, NJ, 2010; p 1015.

(311) Yoshioka, N.; Nishide, H.; Inagaki, K.; Inagaki, K.; Tsuchida, E. Electrical Conductive and Magnetic Properties of Conjugated Tetrathiolate Nickel Polymers. *Polym. Bull.* **1990**, *23* (6), 631–636 DOI: 10.1007/BF01033109.

(312) Holdcroft, G. E.; Underhill, A. E. Synthesis and Physical Properties of Transition Metal Tetrathiolate Macromolecules. *Mol. Cryst. Liq. Cryst.* **1985**, *118* (1), 365–369 DOI: 10.1080/00268948508076242.

(313) Faulmann, C.; Chahine, J.; Jacob, K.; Coppel, Y.; Valade, L.; de Caro, D. Nickel Ethylene Tetrathiolate Polymers as Nanoparticles: A New Synthesis for Future Applications? *J. Nanoparticle Res.* **2013**, *15* (4), 1586 DOI: 10.1007/s11051-013-1586-5.

(314) Sheng, P.; Sun, Y.; Jiao, F.; Liu, C.; Xu, W.; Zhu, D. Optimization of the

Thermoelectric Properties of Poly[Cu_x(Cu-Ethylenetetrathiolate)]. *Synth. Met.* **2014**, *188*, 111–115 DOI: 10.1016/j.synthmet.2013.12.004.

(315) Schulz, R.; Schweig, A.; Hartke, K.; Koester, J. Theory and Application of Photoelectron Spectroscopy. 100. Variable-Temperature Photoelectron Spectral Study of 1,3-Dithiol-2-One and 4,5-Disubstituted 1,3-Dithiol-2-Ones. Thermal Generation of 1,2-Dithiete, 3,4-Disubstituted 1,2-Dithietes, and Dialkyl Te. *J. Am. Chem. Soc.* **1983**, *105* (14), 4519–4528 DOI: 10.1021/ja00352a004.

(316) Faulmann, C.; Cassoux, P.; Vicente, R.; Ribas, J.; Jolly, C. A.; Reynolds, J. R. Conductive Amorphous Metal-Tetrathiolato Polymers: Synthesis of a New Precursor $C_6O_2S_8$ and Its Derived Polymers and Laxs Structural Studies. *Synth. Met.* **1989**, *29* (1), 557–562 DOI: 10.1016/0379-6779(89)90349-4.

(317) Hwang, S. Toward the Practical-Use of Flexible Organic Thermoelectric Generators, Kyushu University, 2017.

(318) Larsen, J.; Bechgaard, K. 1,3,5,7-Tetrathia-s-Indacene-2,6-Dione Chemistry. Synthesis of New Multisulfur Donor Molecules and Nickel-Dithiolene Electron-Transfer Complexes. *J. Org. Chem.* **1987**, *52* (15), 3285–3288 DOI: 10.1021/jo00391a019.

(319) Burness, D. M. Methyl 3-Methyl-2-Furoate. *Org. Synth.* **1959**, *39* (September), 49 DOI: 10.15227/orgsyn.039.0049.

(320) Shao, M.; Dongare, P.; Dawe, L. N.; Thompson, D. W.; Zhao, Y. Biscrown-Annulated TTFAQ−Dianthracene Hybrid: Synthesis, Structure, and Metal Ion Sensing. *Org. Lett.* **2010**, *12* (13), 3050–3053 DOI: 10.1021/ol1010467.

(321) Kim, O.; Yoon, T. H.; McDermott, D. Electrical Conductivity of Polymeric Transition Metal Complexes Derived from 2,5-Diamino-1,4-Benzenedithiol. *J. Chem. Soc. Chem. Commun.* **1989**, No. 11, 740 DOI: 10.1039/c39890000740.

(322) Uzelac, E. J.; Rasmussen, S. C. Thiophene-Extended Nickel Thiazoledithiolene: π-Extended Fused-Ring Metal Dithiolenes with Stabilized Frontier Orbitals. *Eur. J. Inorg. Chem.* **2017**, *2017* (33), 3878–3883 DOI: 10.1002/ejic.201700702.

(323) Menon, A. K.; Wolfe, R. M. W.; Marder, S. R.; Reynolds, J. R.; Yee, S. K. Systematic Power Factor Enhancement in N-Type NiETT/PVDF Composite Films. *Adv. Funct. Mater.* **2018**, *28* (29), 1801620 DOI: 10.1002/adfm.201801620.

(324) Pan, Y.; Cheng, H. K. F.; Li, L.; Chan, S. H.; Zhao, J.; Juay, Y. K. Annealing Induced Electrical Conductivity Jump of Multi-Walled Carbon Nanotube/Polypropylene Composites and Influence of Molecular Weight of Polypropylene. *J. Polym. Sci. Part B Polym. Phys.* **2010**, *48* (21), 2238–2247 DOI: 10.1002/polb.22106.

(325) Jiang, F.; Zhang, L.; Jiang, Y.; Lu, Y.; Wang, W. Effect of Annealing Treatment on

the Structure and Properties of Polyurethane/Multiwalled Carbon Nanotube Nanocomposites. *J. Appl. Polym. Sci.* **2012**, *126* (3), 845–852 DOI: 10.1002/app.36955.

(326) Nandi, P. N.; Deshpande, D. A.; Kher, V. G. Thermogravimetric Analysis of Hexa- and Heptahydrate Crystals and Packed Powder of Nickel Sulfate. *Thermochim. Acta* **1979**, *32* (1–2), 143–149 DOI: 10.1016/0040-6031(79)85102-3.

(327) Hall, D. S.; Lockwood, D. J.; Bock, C.; MacDougall, B. R. Nickel Hydroxides and Related Materials: A Review of Their Structures, Synthesis and Properties. *Proc. R. Soc. A Math. Phys. Eng. Sci.* **2014**, *471* (2174), 20140792–20140792 DOI: 10.1098/rspa.2014.0792.

(328) Tomaszewicz, E.; Kotfica, M. Mechanism and Kinetics of Thermal Decomposition of Nickel(II) Sulfate(VI) Hexahydrate. *J. Therm. Anal. Calorim.* **2004**, *77* (1), 25–31 DOI: 10.1023/B:JTAN.0000033184.32714.7f.

(329) Meek, D. W.; Straub, D. K.; Drago, R. S. Transition Metal Ion Complexes of Dimethyl Sulfoxide. *J. Am. Chem. Soc.* **1960**, *82* (23), 6013–6016 DOI: 10.1021/ja01508a012.

(330) Wolfe, R. M. W.; Menon, A. K.; Fletcher, T.; Marder, S. R.; Reynolds, J. R.; Yee, S. K. Simultaneous Enhancement in Electrical Conductivity and Thermopower of N-Type NiETT/PVDF Composite Films by Annealing. *Adv. Funct. Mater.* **2018**.

(331) Jolly, C. A.; Reynolds, J. R. Semiconducting and Optically Polarizing Poly(Nickel Tetrathiooxalate)/Poly(Vinyl Alcohol) Composites. *Chem. Mater.* **1990**, *2* (5), 479–480 DOI: 10.1021/cm00011a001.

(332) Pyrasch, M.; Amirbeyki, D.; Tieke, B. Self-Assembled Poly(Metal Tetrathiooxalate) Films. *Colloids Surfaces A Physicochem. Eng. Asp.* **2002**, *198–200*, 425–431 DOI: 10.1016/S0927-7757(01)00954-2.

(333) Reynolds, J. R.; Jolly, C. A.; Krichene, S.; Cassoux, P.; Faulmann, C. Poly (Metal Tetrathiooxalates): A Structural and Charge-Transport Study. *Synth. Met.* **1989**, *31* (1), 109–126 DOI: 10.1016/0379-6779(89)90631-0.

(334) Breitzer, J. G.; Chou, J.; Rauchfuss, T. B. A New Synthesis of Tetrathiooxalate and Its Conversion to $C_3S_5^{2-}$ and $C_4S_6^{2-}$. *Inorg. Chem.* **1998**, *37* (8), 2080–2082 DOI: 10.1021/ic971327c.

(335) Engler, E. M.; Green, D. C.; Chambers, J. Q. Electrochemical Reduction of Carbon Diselenide and Preparation of 4,4′,5,5′-Tetra(Selenomethoxy)Tetraselenafulvalene. *J. Chem. Soc., Chem. Commun.* **1976**, *8* (4), 148–149 DOI: 10.1039/C39760000148.

(336) Popov, A. I.; Geske, D. H. Studies on the Chemistry of Halogen and of Polyhalides. XVI. Voltammetry of Bromine and Interhalogen Species in Acetonitrile. *J. Am. Chem. Soc.* **1958**, *80* (20), 5346–5349 DOI: 10.1021/ja01553a007.

(337) Kimura, M.; Ishiguro, H.; Tsukahara, K. Kinetics of Reduction of Iodine by Oxalate and Formate Ions in an Aqueous Solution: Difference in Mechanisms of the Reactions of Oxalate and Formate Ions with Iodine. *J. Phys. Chem.* **1990**, *94* (10), 4106–4110 DOI: 10.1021/j100373a041.

(338) Adler, S. J.; Noyes, R. M. The Mechanism of the Permanganate-Oxalate Reaction. *J. Am. Chem. Soc.* **1955**, *77* (8), 2036–2042 DOI: 10.1021/ja01613a002.

(339) Fetkenheuer, B.; Fetkenheuer, H.; Lecus, H. Über Die Einwirkung von Natriumamalgam Auf Schwefelkohlenstoff. *Berichte der Dtsch. Chem. Gesellschaft A B Ser.* **1927**, *60* (11), 2528–2537 DOI: 10.1002/cber.19270601120.

(340) Wawzonek, S.; Heilmann, S. M. Electrochemical Reduction of Carbon Disulfide in Dimethylformamide. *J. Org. Chem.* **1974**, *39* (4), 511–514 DOI: 10.1021/jo00918a021.

(341) Hartzler, H. D. Tetrathiooxalate Polymers and Their Preparation. 3,717,619, 1973.

(342) Liu, Z. J.; Kong, L. B.; Wang, L. M.; Zhou, Y. H.; Zhan, C. M. Poly (Tetrathiooxalic Acid) – Novel Cathode Active Material for Secondary Lithium Batteries. *J. New Mater. Electrochem. Syst.* **2005**, *8* (4), 269–272.

(343) Bacher, A. D.; Sens, I.; Müller, U. Ein Neuer Zugang Zu Tetrathiooxalaten. Die Kristallstruktur von $(NEt_4)_2[C_2S_4]$ / A Novel Access to Tetrathiooxalates. Crystal Structure of $(NEt_4)_2[C_2S_4]$. *Zeitschrift für Naturforsch. B* **1992**, *47* (5), 4–7 DOI: 10.1515/znb-1992-0516.

(344) Camp, C.; Cooper, O.; Andrez, J.; Pécaut, J.; Mazzanti, M. CS_2 Activation at Uranium(III) Siloxide Ate Complexes: The Effect of a Lewis Acidic Site. *Dalt. Trans.* **2015**, *44* (6), 2650–2656 DOI: 10.1039/C4DT02585G.

(345) Lund, H.; Hoyer, E.; Hazell, R. G. Tetrathiooxalate. Electrochemical Preparation and X-Ray Structure Determination of a Tetrathiooxalate. *Acta Chem. Scand.* **1982**, *36b*, 207–209 DOI: 10.3891/acta.chem.scand.36b-0207.

(346) Millar, S. Tips and Tricks for the Lab: Air-Sensitive Techniques (4). *ChemViews* **2013** DOI: 10.1002/chemv.201300043.